PHD

The Application of Enhanced Fluid Dynamic Gauging as a Fouling Sensor for Pressure Driven Membrane Separations in the Food Industry

Jones, Sarah

Award date:
2012

Awarding institution:
University of Bath

The Application of Enhanced Fluid Dynamic Gauging as a Fouling Sensor for Pressure Driven Membrane Separations in the Food Industry

Sarah Jones

A thesis submitted for the degree of Doctor of Philosophy

University of Bath

Department of Chemical Engineering

May 2012

Acknowledgements

Firstly, I would like thank my supervisor, Dr Mike Bird, who has always been extremely approachable, helpful and generous with his time throughout my studies here in Bath. I would also like to acknowledge the expert help and advice I received from Dr Ian Wilson, Dr Bill Patterson, and Dr John Chew of the University of Cambridge. They have been especially helpful throughout the project and have provided a very exciting working collaboration. Additional thanks goes to Dr Tim Mays for acting as my supervisor for 6 months and offering a different perspective to the project.

I would like to thank Dr Frank Lipnizki of *Alfa Laval* and John Jenson of *Nordzucker* for the generous donation of membranes, Spent Sulphite Liquor and molasses. I am also very grateful for the financial support provided by both companies and EPSRC. A huge thank you goes to Dr Arto Pihlajamäki for allowing me to visit Lappeenranta University of Technology, Finland, to perform numerous zeta potential experiments and FTIR measurements. Also for the many useful discussions throughout the course of the project.

I would also like to thank the technical support at the University of Bath, who have helped me enormously in all stages of the project, thank you too: Suzanne, John, Fernando, Robert, Richard, and Merv. I am also very grateful to the Paul Firth in the engineering workshop for his excellent workmanship.

I am also very grateful to my research group namely, Iain Argyle, Peter Bechervaise and Laura Head for their help, advice and interesting discussions. Special acknowledgement goes to my colleagues in postgraduate research, especially Iain Hitchcock, Hannah Leese and Kerry-Anne Young for their continual advice and support.

My final and most important thank you goes to my Dad, Mom, Grandparents and brother Craig for their constant moral support, encouragement and guidance throughout the years.

Abstract

The aim of this study was to further understand the fouling and cleaning mechanisms of synthetic membranes used to filter an industrially relevant feed. The main focus of this study was to understand the fouling layer properties during pressure driven filtration. A relatively new technique known as Fluid Dynamic Gauging (FDG) was applied to examine the fouling layer thickness. This work comprised of four main themes with overlapping objectives: (i) the optimisation of Spent Sulphite Liquor fouling and cleaning conditions, (ii) the optimisation of molasses fouling and cleaning conditions, (iii) the investigation of the effect of a simple pre-treatment upon the membrane separation performance, and (iv) the application of the FDG in the study of polymeric membranes.

An understanding of the mechanisms involved in fouling and cleaning of microfiltration and ultrafiltration membranes used to filter molasses and SSL has been attained. The variables affecting permeate flux and quality were optimised and mechanistic information concerning the synergistic effects between fouling and cleaning was gathered.

The application of a simple NaOH pre-treatment was found to affect both the type of foulant species attaching to the membrane surface, and resulted in an altered separation and cleaning performance. Zeta potential measurements, FTIR and AFM demonstrated that both in-pore and surface fouling was present. The data collected indicated that for both membranes evaluated, different fouling species were found to have attached, depending upon the pre-treatment protocol used. These findings are significant, as they offer support to the recommendations made by some polymeric membrane manufacturers that conditioning protocols should include a NaOH step. However, in the SSL system examined, the effect of NaOH pre-treatment resulted in an improvement in the subsequent performance only over the first two or three complete filtration cycles. It is therefore necessary to study membrane systems over multiple fouling and cleaning cycles before a recommendation can be made. An improved understanding of the interaction between the surface chemistry and surface physics during membrane filtration of complex food based material will benefit both membrane manufactures and food industry based users.

The technique of Fluid Dynamic Gauging was incorporated into an existing system and validated to monitor the development of cake layers over time. The FDG was also used to optimise conditions and track the thickness of the cake layer during multiple fouling cycles and its removal rate during cleaning, as an aid to understanding removal mechanisms. It has been shown that operating conditions have to be carefully chosen to minimise the effect of membrane fouling. The results show that FDG is a versatile and powerful technique for characterising the dynamics and mechanical behaviour of fouling layers on membrane surfaces. A particular advantage of the FDG technique is its ability to determine the thickness of fouling layers where other techniques would find difficulty. For example, the layers formed in this study were opaque, and consequently the determination of the development of deposit thickness with time would have been very challenging using conventional optical microscopy techniques.

Contents

List of Figures

List of Tables

Nomenclature

Roman Symbols

a	Channel height	m
A_m	Membrane surface area	m^2
b	Channel width	m
C	Volume of solid particle retained per unit filtrate volume	m^2
C_b	Feed solids concentration in bulk feed stream	wt.%
C_d	Discharge coefficient accounting for energy loss	-
C_g	Gel layer concentration	wt.%
C_M	Membrane surface concentration	wt.%
C_p	Feed solids concentration in permeate stream	wt.%
d	Inside diameter of gauge/channel	m
D	Diffusion coefficient	m^2s^{-1}
d_e	Equivalent diameter	m
d_g	Sauter diameter	m
d_h	Hydraulic diameter	m
d_i	Inside diameter of tube, i = 1 or 2	m
d_t	Inside diameter of nozzle throat	m
h	Clearance between the nozzle tip and gauging surface	m
h_k	Kozeny constant	-
h_0	Initial clearance between the nozzle tip and gauging surface	m
J	Overall membrane flux	ms^{-1}
J^*	Flux at “steady state”	$L\ h^{-1}m^{-2}$
J_c	Pure water flux after cleaning	$L\ h^{-1}m^{-2}$
J_F	Filtrate (Fouling) Flux	$L\ h^{-1}m^{-2}$
J_{lim}	Limiting flux	ms^{-1}
J_r	Flux recovery	%
J_V	Volumetric Permeate flux (steady state)	ms^{-1}
J_w	Pure water flux before fouling	$L\ h^{-1}m^{-2}$
k	Mass transfer coefficient	ms^{-1}
K	Fluid consistency index	-
L	Channel Length	m
l_{eff}	Equivalent length of the siphon tube	m
m	Mass flow rate	kgs^{-1}
m_{actual}	Actual mass flow rate	kgs^{-1}
m_{ideal}	Ideal mass flow rate	kgs^{-1}
n	Mechanism specific index	-
N	Number of channels	-
P	Pressure	Pa
Q	Volumetric flow rate	m^3s^{-1}
Q_0	Volumetric flow rate	m^3s^{-1}
R_a	Apparent rejection coefficient	-
R_a	Resistance due to adsorption on membrane surface	m^{-1}
R_A	Roughness	nm

R_{bl}	Boundary layer resistance	m^{-1}
R_C	Resistance due to cake layer	m^{-1}
R_{cp}	Resistance due to concentration polarisation	m^{-1}
Re	Reynolds number	-
R_F	Total fouling resistance	m^{-1}
R_g	Resistance due to gel layer	m^{-1}
R_I	Irreversible fouling resistance	m^{-1}
R_m	Virgin or cleaned membrane resistance	m^{-1}
R_{max}	Maximum true rejection coefficient	-
R_0	Total membrane resistance	m^{-1}
R_p	Resistance due to pore blocking	m^{-1}
R_R	Reversible fouling resistance	m^{-1}
R_s	Additional resistance	m^{-1}
R_T	Total fouling resistance	m^{-1}
R_{tube}	Inside radius of siphon tube	m
s	Mass fraction of solids in the cake	-
S_c	Schmidt number	-
S_h	Sherwood number	-
S_v	Particle surface area per unit volume	m^{-1}
t	Time	s
T	Temperature	^oC
T%	Transmission of solids	%
u	Average linear fluid velocity	ms^{-1}
u_0	Fluid linear velocity	ms^{-1}
V	Volume of fluid	m^3
w	Width of nozzle rim	m

Greek Symbols

α	Cake specific resistance	mkg^{-1}
δ	Deposit thickness	m
δ_m	Membrane thickness	m
ΔE	Steaming potential	mV
ΔP	Differential pressure	Pa
μ	Viscosity	$kg\ m^{-1}s^{-1}$
μ_P	Viscosity of the permeate	$kg\ m^{-1}s^{-1}$
ρ	Density of process fluid	$kg\ m^{-1}s^{-3}$
κ	Conductivity	ohm
ζ	Streaming potential	mV
γ_{lv}	Interfacial energies of the solid / vapour interface	Nm^{-1}
γ_{sv}	Interfacial energies of the solid / vapour interface	Nm^{-1}
γ_{sl}	Interfacial energies of the solid / liquid interface	Nm^{-1}
γ	Filtrate density	$kg\ m^{-3}$
Π	Osmotic pressure	bar
ε	Porosity	-
ε_0	Permittivity of a vacuum	$C^2N^{-1}m^{-2}$

ε_r	The relative dielectric constant of the electrolyte	-
ψ_0	Potential at the solid surface	mV
ψ_d	Potential at the surface of the diffuse layer	mV
ψ_i	Potential at the IHP	mV
σ_0	Charge densities at the solid surface	$\mu C\ cm^{-2}$
σ_i	Charge densities at the at the IHP	$\mu C\ cm^{-2}$
σ_d	Charge densities at the surface of the diffuse layer	$\mu C\ cm^{-2}$
σ	Area blocked membrane per unit filtrate volume	m^{-1}

Abbreviations

AFM	Atomic force microscopy
ATR	Attenuated Total Reflectance
CEB	Chemical enhanced backwash
CFD	Computational fluid dynamics
CFV	Cross flow velocity
CIP	Cleaning-in-place
COP	Cleaning-out-of-place
CP	Concentration polarisation
CW	Chemical wash
Da	Dalton (1000 Da – 1 kDa)
DOTM	Direct Observation Through the Membrane
DP	Differential pressure
DVO	Direct Visual Observation
FDG	Fluid Dynamic Gauging
FP	Fluoropolymer
FTIR	Fourier transform infrared spectroscopy
IHP	Inner Helmholtz plane
LS	Lignosulphonates
LVDT	Linear Variable Differential Transformer
MF	Microfiltration
MIR	Mid Infra Red
MRI	Magnetic resonance imaging
MW	Molecular weight (Da)
MWCO	Molecular weight cut Off (Da)
NaOH	Sodium hydroxide
NF	Nanofiltration
NMR	Nuclear Magnetic Resonance
OHP	Outer Helmholtz plane
P1	Protocol 1
P2	Protocol 2
PLC	Permeate line closed
PLO	Permeate line open
Psf	Polysulphone
PSU	Possible structural units
PWF	Pure water flux

RO	Reverse osmosis
SEM	Scanning electron microscopy
SFDG	Scanning Fluid Dynamic Gauging
SSL	Spent sulphite liquor
TMP	Transmembrane pressure
UDTR	Ultrasonic Time Domain Reflectometry
UF	Ultrafiltration
Wt. %	Weight percentage (%w/w)
ZP	Zeta potential

Chapter 1

Introduction

1.1. Membranes in Industry

Membrane separation technologies have gained a prominent place in the food, pharmaceutical and water treatment industries and are effective for a broad range of applications. Membrane technology has widespread applications in the food processing industries since their introduction in the 1960s. They provide a unique opportunity for accomplishing both the fractionation and concentration of components in liquid systems, while also retaining desirable physical and chemical characteristics of key food components (D'Souza and Mawson, 2005). They are beneficial for the recovery and re-use of both water and raw materials from process streams, thereby minimising waste disposal costs and reducing the process materials requirement. Correctly applied membrane processes can provide financial savings, conserve resources and are considered as very energy efficient compared to many separation processes (Smith and Petela, 1994).

1.2. The Fouling Issue

A major problem with membrane separation is the unwanted accumulation of material at the membrane surface, known as the fouling layer, which causes a reduction in flux and separation performance. This results in the need to clean the membrane, which is an expensive process. This is because the replacement or cleaning of membranes causes the following problems for the industry:

(i) *Production loss*. Revenue lost from the need to stop production during cleaning.
(ii) *Operating costs.* Process can be more labour intensive.
(iii) *Consumable costs.* Utilities are required for heating and cooling. Chemicals and water are required for detergent solutions.
(iv) *Energy costs*. Additional energy is required for heating, pumping, mixing etc.
(v) *Environmental Impact*. Effluent from cleaning processes can be detrimental to the environment unless it undergoes treatment.

Design to mitigate or minimise fouling and promote cleaning is complicated by the variety of fouling mechanisms that can occur. Therefore, a fundamental understanding of fouling mechanisms is of paramount importance. Therefore, the system as a whole should be studied, by looking at both the fouling and cleaning processes. Cleaning of membranes is inevitable, and the frequency of cleaning can be reduced due to advanced fouling knowledge. Although this area has received interest in the literature, there is a limited amount of resource on the actual fouling layer properties during membrane separation.

1.3. Membrane Characterisation

Membrane process optimisation requires a need to understand the basic phenomena occurring within the membrane, the polarization layer and the bulk fluid. Membrane surface characteristics such as hydrophobicity, charge, and roughness will affect the membrane separation characteristics. Modification of the membrane surface can lead to a decrease in the membrane fouling potential. Previous studies have shown that a membrane surface has a reduced fouling tendency if the surface is hydrophilic and charged similarly to the key fouling species in the filtrate solution (Capannelli *et al*., 1990; Jönsson and Jönsson, 1995; Vernhet and Moutounet, 2002; Väisänen, 2004). Fouled membrane surfaces can be characterised using a range of techniques such as: (i) Streaming potential measurements, (ii) Fourier Transform Infra-Red (FTIR) spectral peak height analysis, (iii) Scanning electron microscopy (SEM), (iv) Atomic force microscopy (AFM), and (v) Contact angle measurements.

1.4. Aims and Scope of this Study

The aim of this study is to further understand the fouling and cleaning mechanisms of an industrially relevant feed. An improved understanding of the interaction between the surface chemistry and surface physics during membrane filtration of complex food based material will benefit both membrane manufacture and food industry based users. The main focus being the understanding of the fouling layer properties during pressure driven filtration. It is proposed to use a relatively new technique, known as Fluid Dynamic Gauging, to measure the fouling layer thickness. The operational principles of this technique are explained in this study. The main objectives of this work are as follows:

- To evaluate the mechanisms involved in fouling and cleaning of microfiltration and ultrafiltration membranes and to investigate the variables affecting permeate flux and quality.
- To determine whether the application of a simple pre-treatment could affect both the type of foulant species attaching to the membrane surface, and result in an improved separation performance.
- To determine the synergistic effect between fouling and cleaning processes.
- To commission and validate an experimental system to incorporate the technique of Fluid Dynamic Gauging. The technique will be used to monitor the development of cake layers over time and investigate the influence of operational conditions.
- To use Fluid Dynamic Gauging to track the thickness of the cake layer during multiple fouling cycles and its removal rate during cleaning. This will give a greater understanding of the removal mechanisms.

1.4.1. Feed Selection

This study will focus on feed solutions that cause considerable fouling issues in industry. The feeds chosen are Spent Sulphite Liquor (SSL) and molasses. Both feeds are industrially relevant, and subject to severe fouling issues when membranes are used in their subsequent processing.

The SSL is a by-product of the chemical pulp production and contains mainly: (i) sulphonated lignins (Lignosulphonates), (ii) ash and (iii) various sugars (comprising of 70% pentose). The purpose of ultrafiltration with the SSL is to reduce the water content and concentrate the lignins (Lignosulphonates) from the sugars and salts to yield a high molar mass fraction of lignosulphonates in the retentate. The high molar mass fraction can be used to produce vanillin (Weis and Bird, 2001). Vanillin (V, 4-hydroxy-3-methoxybenzaldehyde) and its derivatives (ethylvanilin, vanillic acid, and acetovanillon) are used in the food and pharmaceutical industries, and in the production of polymers such as polyester (Hocking, 1997).

Molasses is a thick syrup by-product from the processing of sugar beet into sugar and contains mainly: (i) sugar, (ii) water and (iii) inorganic matter. The term ‘molasses’ is

applied to the final effluent obtained in the preparation of sugar by repeated crystallization. The purpose of membrane separation in this study is the clarification of molasses to protect the downstream process, e.g. precipitation, and chromatography. This requires the removal of calcium salts such as calcium sulphate, calcium oxalate, and calcium oxalate monohydrate. Microfiltration offers the possibility of separating the crystalline material (retained in the retentate) from the sugar and divalent ionic species (passed through to the permeate stream).

1.5. Thesis Structure

This thesis is divided into 7 chapters, which focus on the issues discussed above. A brief description of each chapter is given below:

Chapter 1: Introduction.

Chapter 2: Chapter 2 details the process and design considerations required for membrane fouling, monitoring and cleaning. A review of relevant literature aims to facilitate the understanding and interpretation of experimental results presented in subsequent chapters.

Chapter 3: Chapter 3 describes the experimental systems developed in this study and classifies the material and methods used. The relevant analytical techniques are also detailed.

Chapter 4: Chapter 4 presents the results concerning the fouling and cleaning properties of the ultrafiltration of SSL. The start of the chapter will focus on the optimisation of the fouling and cleaning of SSL filtration. This will include a discussion of the SSL filtration in terms of flux performance, resistance and rejection. The second part of the chapter will investigate the effect of pre-treatment cleaning on the filtration of SSL. The section explains the filtration process in further detail using various analysis techniques.

Chapter 5: Chapter 5 presents the results concerning the fouling and cleaning properties of the microfiltration of molasses. The start of the chapter will focus on the optimisation of the fouling and cleaning of molasses filtration. This will include a discussion of the molasses filtration in terms of flux performance, resistance and rejection. The second part will

investigate the effect of pre-treatment cleaning on the filtration of molasses. The section explains the filtration process in further detail using various analysis techniques.

Chapter 6: Chapter 6 presents the application of Fluid Dynamic Gauging in the investigation of synthetic membrane surface phenomena. The chapter is divided into approximately three parts: (i) dead-end dynamic gauging, (ii) cross flow filtration dynamic gauging and (iii) additional deposit analysis.

Chapter 7: Chapter 7 draws conclusions from the experimental work and makes recommendations and proposals for future work.

1.6. List of Publications arising from this Thesis

1.6.1. Refereed Journal Papers

S.A. Jones, Y.M.J. Chew, M.R. Bird, D.I. Wilson (2010). The Application of Fluid Dynamic Gauging in the Investigation of Synthetic Membrane Fouling Phenomena. *Food and Bioproduct Process*, 88, 409 – 418.

S.A. Jones, M.R. Bird, A. Pihlajamäki (2011). An Experimental Investigation into the Pre-Treatment of Synthetic Membranes using Sodium Hydroxide Solutions. *Journal of Food Engineering*, 105, 128 – 137.

S.A. Jones, D.I. Wilson, Y.M.J. Chew, M.R. Bird (2012). Fluid Dynamic Gauging of Microfiltration Membranes Fouled with Sugar Beet Molasses. *Journal of Food Engineering*, 108, 22 – 29.

S.A. Jones, A. Pihlajamäki, M.R. Bird (2012). The Role of Synthetic Membrane Pre-Treatment in influencing Performance over Multiple Operational Cycles. Accepted on 5/12/11, *Separation Science and Technology*.

1.6.2. Conference Proceedings

[1]S.A. Jones, M.R. Bird, Y.M.J. Chew, D.I. Wilson, W.R. Paterson (2008). The Application of Fluid Dynamic Gauging as a Fouling Sensor for Membrane Separations. *Engineering with Membranes*, ISBN 978-84-691-3670-6.

[2]S.A. Jones, Y.M.J. Chew, M.R. Bird, D.I. Wilson (2010). The Application of Fluid Dynamic Gauging in the Investigation of Synthetic Membrane Fouling Phenomena. *Fouling and Cleaning in Food Processing*, ISBN 978-0-09542483-2-1.

[3]S.A. Jones, M.R. Bird, A. Pihlajamäki (2010). The Effect of Pre-treatment Protocols upon the Fouling and Cleaning Characteristics of UF and MF Membranes. *Fouling and Cleaning in Food Processing*, ISBN 978-0-09542483-2-1.

[2]S.A. Jones (2010). The Application of Fluid Dynamic Gauging as a Fouling Sensor for Synthetic Membrane Separation. *Network Young Membrains 12* – Lappeenranta, June 7-9th.

[3]S.A. Jones, M.R. Bird, Y.M.J. Chew, D.I. Wilson (2011). Fluid Dynamic Gauging as a Tool in Understanding Synthetic Membrane Fouling. *Chemica 2011.*

[1] Presented as a poster by the candidate

[2] Presented orally by the candidate

[3] Presented orally by supervisor Dr M.R. Bird on behalf of the candidate

Chapter 2

Process and Design Considerations

2.1. Introduction

In this chapter, the literature is reviewed and the critical process and design parameters which influence membrane fouling and cleaning are identified. The two process fluids used in this study are discussed. This section also includes the current methods for monitoring fouling thickness and details the technique Fluid Dynamic Gauging that is being applied in this research.

2.2. Membrane Filtration

2.2.1. Introduction

Membrane separation is the use of a selective semipermeable barrier between two phases in solution or suspension. The material which passes through the membrane is called the permeate and the material which is retained by the selective barrier is called the retentate. Transport of species through a membrane takes place when a driving force (i.e. chemical or electrical potential) acts on the individual components in the system (Mulder, 2000). The fundamental principle behind the separation in this study is pressure driven, where a pressure gradient exists between the retentate and permeate side. This is used to concentrate or purify a dilute solution to varying extents depending on the structure of the membrane (Väisänen, 2004).

2.2.2. Different Filtration Classification

The different separations attained by membrane filtration are classified on the basis of their separation threshold (Table 2.1 and Figure 2.1). They are usually characterised by an effective pore-size or molecular weight cut-off (MWCO) and are divided into four distinct categories: microfiltration (MF), ultrafiltration (UF), nanofiltration (NF), and reverse osmosis (RO) (not shown in Table 2.1). The pore diameter of the membranes can vary between 10 μm for MF and 1 nm in the case of RO. MF, UF and NF, can be used for decolourisation and removal of other impurities. MF and UF are usually quite similar and act on the basis of sieving. This means the separation occurs mainly by size

and shape of the solutes relative to pore diameters. NF and RO separate by means of a different mechanism; using high pressure to curb higher resistance and osmotic pressure. They are used to isolate low molecular weight solutions or small organic molecules, which require denser membranes with a much higher hydrodynamic resistance.

Table 2.1: Comparison of Pressure Driven Membrane Processes (Adapted from Mulder, 2000)

	Microfiltration	Ultrafiltration	Nanofiltration
Membranes	(a)symmetric	asymmetric porous	asymmetric porous
Thickness	≈ 10 – 150 µm	≈ 150 µm	≈ 150 µm
Active layer	Asymmetric ≈ µm	≈ 0.1 – 1 µm	≈ 0.1 – 1 µm
Pore Size	≈ 0.05 – 10 µm	≈ 1 – 100 nm	≈ 0.5 – 2 nm
Driving Force	Pressure (0.1 - 2 bar)	Pressure (1 - 10 bar)	Pressure (5 - 10 bar)
Retentate	Particles (<0.1 mm)	Colloids, macrosoultes	Multivalent ions, organics
Permeate	All other species	Ions, organics	Low molecular organic

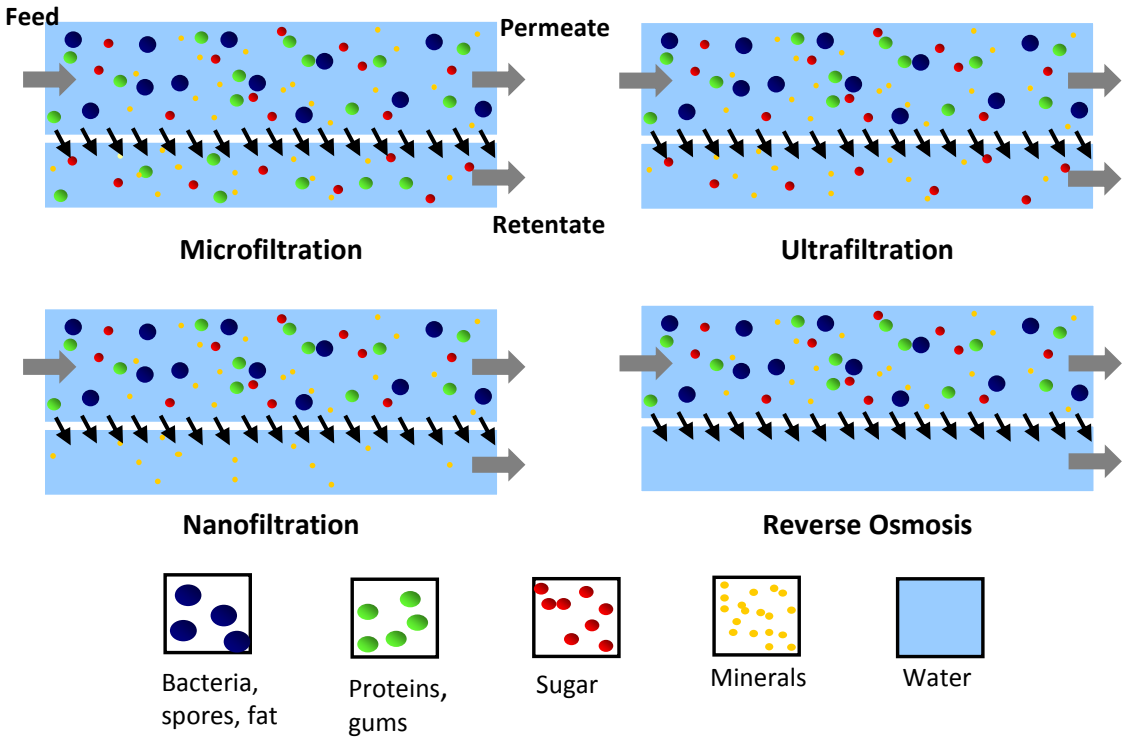

Figure 2.1: The different Membrane Processes (Adapted from Mulder, 2000).

2.2.2.1. Microfiltration

Microfiltration employs permeable membranes that separate particles in the micrometre size range with pore diameters between 0.05 µm and 10 µm. It is typically used for the concentration of colloid suspensions, bacteria, fat droplets, and yeast cells (Cheryan, 1998). MF membranes were first commercialised in the 1920s and were commonly used for bacteriological analysis of water. The number of successful MF applications grew rapidly after 1960, where it is now operated in fields such as biotechnological, automobile, electronics and the food industry (Huisman, 1998; Baker, 2004). It is usually operated at relatively low transmembrane pressures (0.1 to 3.0 bar) and high permeation fluxes (50 L m^{-2} hr^{-1} bar^{-1}), which distinguish MF from both RO and UF (Belfort *et al*., 1994). MF membranes are often vulnerable to intra-pore fouling.

2.2.2.2. Ultrafiltration

Ultrafiltration uses smaller pore membranes than MF, which are typically in the range of 0.01 µm and 0.10 µm. These membranes normally require larger applied pressures for separation. Salts, sugars, organic acids and smaller peptides are transmitted, while proteins, fats and polysaccharides are rejected. With UF membranes, it is standard to use the term "molecular weight cut off" (MWCO) instead of particle size. The definition of the MWCO is the nominal molecular weight (MW) of a solute for which 95 % of that solute is retained by the membrane (Coulson *et al*., 1997). The solutes retained by UF membranes are those with molecular weights of 1000 a.u or greater and depend on the nature of the membrane used. The UF membranes used in this study are of anisotropic structures. They have a finely porous surface layer supported on a much more open microporous substrate. The open microporous substrate provides mechanical strength, whereas the finely porous surface layer performs the separation (Baker, 2004). Recently, clarification and decolourisation by UF have gained importance. Moreover, its use in the food industry is of importance because of its low power consumption and simplicity of operation (Hamachi *et al*., 2003).

2.2.3. Filtration Modes

The arrangement of the membrane system is essential for optimal design. There are two conventional module operations used today, which are dead-end and crossflow filtration (Figure 2.2).

2.2.3.1. Dead-end Operation

In the dead-end mode, the feed flows towards the surface of the membrane, and is forced to pass through the membrane perpendicularly. This mode can be seen in Figure 2.2. Conventional filtration processes are typically operated in dead-end mode, where a sieving action occurs. It results in an accumulation of particles at the filter, which is referred to as a cake layer. The quality of the permeate will decrease with time as a result of the increase in the concentration of rejected components in the feed. This is discussed in more detail below. Dead-end membrane filtration is not of practical interest for most filtration applications due to the instantaneous flux decline that results. However, it is effectively used for specific separations such as pilot-scale tests. Absence of an axial shear rate distinguishes the dead-end filtration from the cross flow filtration during the cake build-up on the membrane surface (Mulder, 2000; Koltuniewicz *et al*., 1995). Dead-end filtration is only suitable for dilute suspensions. As for unstirred dead-end filtration the cake continues to grow until the process is stopped (Belfort *et al*., 1994). Kim and Hoek (2002) reported that the pressure dependent cake volume fraction was found to be highly dependent on initial flux, particle size, bulk solution ionic strength, and weakly dependent on the particle surface (zeta) potential.

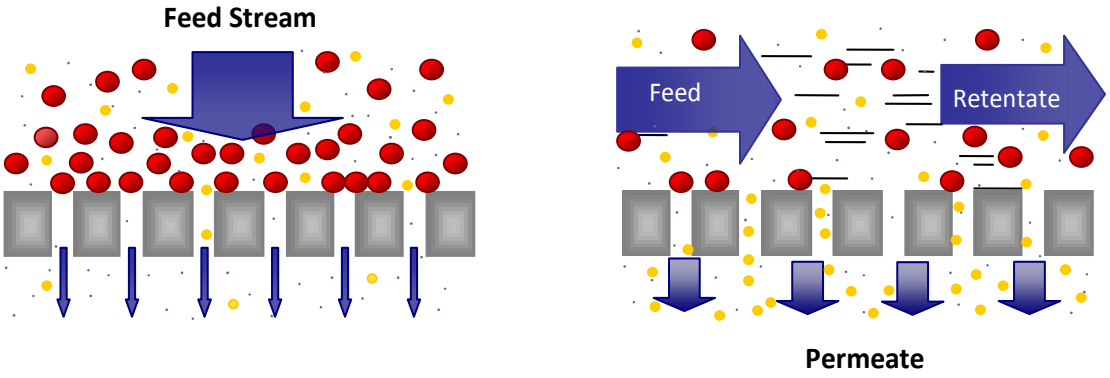

Figure 2.2: Dead-end (left) and Cross flow Filtration (right).

2.2.3.2. Cross flow Operation

In cross flow filtration, the feed flows parallel to the membrane surface with the inlet feed stream separating into the permeate and the retentate (Figure 2.2). The composition of the feed is a function of distance along the module. Cross flow filtration provides significant built-in advantages over dead-end filtration. The movement of the retentate

passing tangential to the surface of the membrane can act as a washing action removing some of the cake layer build up and reduces the flux decline. In practice, the permeation rate falls with time due to concentration polarisation (accumulation of retained solute on the surface of the membrane) and membrane fouling (Mulder, 2000). The flux can be optimised by modifying certain parameters across the membrane during cross flow filtration, such as transmembrane pressure and shear rate. These will be discussed in section 2.3.10. Cross flow is widely used in virtually all commercial large-scale pressure driven membrane plants (Belfort *et al*., 1994).

2.2.3.3. Membrane Configuration

There are four types of modules used in cross flow operation, which are flat sheet, spiral wound, hollow fibre and tubular (Figure 2.3). The advantages and disadvantages are summarised in Table 2.2. The *Plate and frame* (flat sheet) module configuration is the simplest. It contains sets of flat sheet membranes with spacers sandwiched between to allow permeate out. The disadvantage of plate and frame modules is that they have a high capital cost and average running costs, though the membranes can be easily replaced like tubular modules. *Spiral wound* modules consist of several flat sheet membranes separated by turbulence promoting mesh separators, which are formed into a roll similar to a 'Swiss roll'. The feed flows into the module inside the feed spacer, and the permeate flows into the central tube of the module through the permeate spacer. Permeate spirals toward the perforated central tube for collection. The spiral wound module system is usually the cheapest to install and operate. However, they are extremely vulnerable to fouling. The *hollow fibre* module consists of bundles of fine tubes or fibres (0.1 to 2.0 mm in diameter) of filter material bundled together inside a tubular housing. The hollow fibre (wide fibre) system requires the largest capital plant investment. However, the fouling tendency and cleanability of the membrane is low. With the *tubular* module, the membrane is cast on the inside of a porous support tube, which is housed within a perforated stainless steel pipe. The more expensive tubular module requires high plant investment, high running costs and occupies a large volume (Coulson *et al*., 1997).

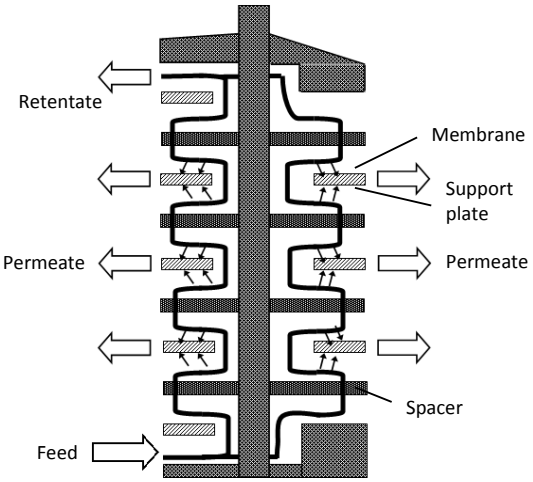

(a) Plate and Frame

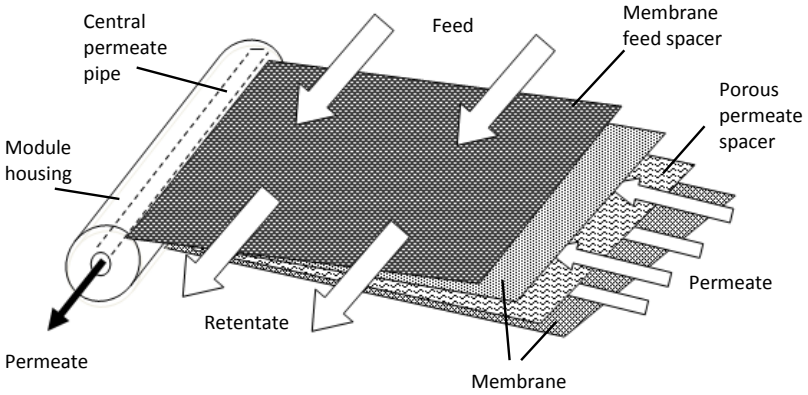

(b) Spiral Wound

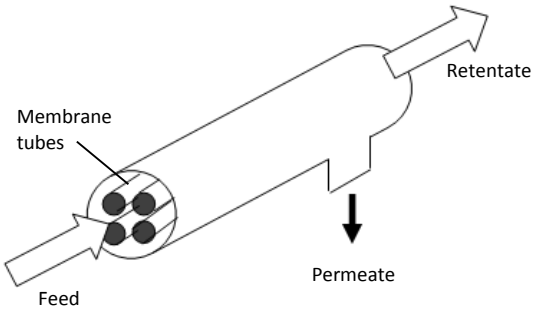

(c) Tubular

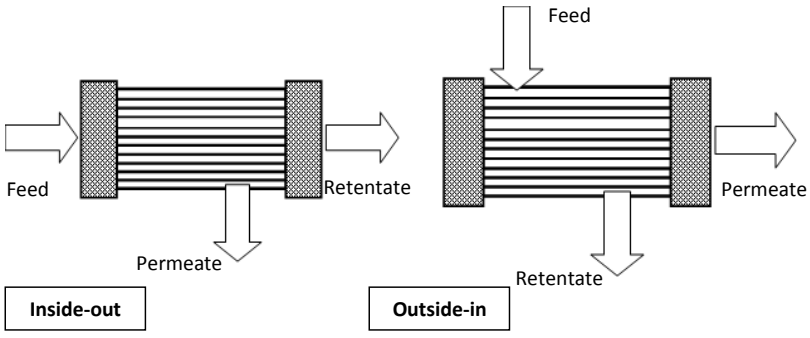

(d) Hollow Fibre

Figure 2.3: Diagrams showing different cross flow membrane module designs (Adapted from Mulder, 2000).

2.2.3.4. Modules appropriate for Spent Sulphite Liquor and Molasses Filtration

The Spent Sulphite Liquor (SSL) contains fibres. Therefore, it is essential that the arrangement is constructed to avoid clogging. Table 2.2 shows that tubular and plate and frame modules are the most appropriate choice. This is because they are not as sensitive to solid particles and have been used with SSL previously (Claussen, 1978; Tsapiuk *et al*., 1989; Weis, 2004).

Molasses is a highly viscous mixture made up of high molecular mass components. Thus, fouling tendencies are high. Plate and frame modules and tubular modules are typically used in the sugar industry (Lipnizki *et al*., 2006). However, membrane technology is not a recognized technology as a standard unit of operation in the sugar industry. For this study, only flat sheet will be investigated for both feeds. This is due to the need to have access and inspect the fouling layer on the membrane, which will be discussed further below.

Table 2.2: Comparison of Standard Membrane Modules (Adapted from Mulder, 2000)

	Flat Plate	Tubular	Spiral-Wound	Hollow-Fibre
Packing Density	Moderate	Low	High	High
Investment	High	Low – high	Low	Medium – High
Energy	Low – moderate	High	Moderate	Low
Variable Costs	Average	Low – high	Low	Low – average
Fouling Tendency	Average	Low	Average	Low – High
Cleanability	Good	Good	Difficult	Good
Replacement	Sheet	Tubes	Element	Element
Manufacture	Simple	Simple	Complex	Moderate

2.2.4. Membrane Material

Membranes can be constructed of natural or synthetic materials such as porous polymers, ceramics or metals. The different techniques that are available to prepare porous polymeric membranes are sintering, stretching, track etching, phase separation, sol-gel process, vapour deposition and solution coating (Wagner, 2001; Weis, 2004). The phase inversion techniques are commonly used to make the majority of the organic polymeric membranes. These processes rely on the phase separation of polymer solutions producing porous polymer membranes. The membrane structure is the result of the combination of the phase separation and mass transfer. Most membranes used in

the industry have an asymmetric structure, whereby the membrane consists of two layers. The top layer is a very thin dense layer (also called the top skin layer), and the bottom layer is a porous sub layer. The top dense layer governs the performance (permeation properties) of the membrane while the porous sub layer provides the membranes mechanical strength (Khulbe *et al*., 2008). Ideally, membranes should have high porosity to ensure high fluxes, and a narrow pore size distribution to ensure good selectivity (Shorrock, 1999).

According to Cheryan (1998) membrane filtration does not affect the chemical structure or thermal stability of the materials used. Hydrophobic membranes, such as polysulphone, polypropylene, polyvinyldienefluoride and polytetrafluorethylene, absorb more protein compared with hydrophilic membranes (e.g. cellulose acetate, poly-acrylonitrile) (Makardij *et al*., 1999). In general, hydrophilic membranes have superior properties in regard to fouling, but hydrophobic membranes are still commonly used in UF (Jönsson and Jönsson, 1995). The charge on the membrane surface is important. If the membrane surface and the foulant (e.g. colloidal material) have the same charge, it means adhesion of material to the membrane is reduced. This helps to inhibit membrane fouling. Many colloidal materials have a slight negative charge from acid groups, such carboxylic and sulphonic acids. If the charges are different, the effect is the reverse (Baker, 2004). However, hydrophobic membranes are expensive, and need to be prevented from drying out once wetted. To overcome the drying, all commercial membranes are coated in a hydrophilic agent, e.g. glycerine during manufacturing. This preservative needs to be removed before a membrane can be measured for performance (conditioning).

2.3. Membrane Fouling

2.3.1. Introduction

The membrane process is measured by the flux (throughput), and ideally there should be 100 % transmission of the desired component. In practice this is impossible due to the effects of fouling. Fouling is defined as the unwanted deposition (or growth) of suspended, dissolved, or chemically generated species from process fluids on to a surfaces. Membrane fouling is a complex phenomenon. As soon as a separation of

dissolved matter occurs, spontaneous accumulation of substances i.e. concentration polarisation (formation of a concentration boundary layer) and fouling appears on the membrane. This then causes a decrease in pore size and porosity of the membrane (Väisänen, 2004). Concentration polarisation is discussed further in section 2.3.8. The formation of a deposit on a membrane surface can occur due to several mechanisms:

(i) *Particulate fouling* – due to the accumulation of particulate material originally suspended in the feed.
(ii) *Chemical precipitation* – occurs when the feed stream becomes more concentrated and the solubility of some components are exceeded.
(iii) *Reaction fouling* – is when foulants are formed by chemical reaction either in the bulk fluid or on/with the membrane surface (Adsorption).
(iv) *Colloidal fouling* – causes the material to be deposited due to colloidal charge or size characteristics.
(v) *Biological fouling* – occurs when micro-organisms attach to the membrane.

If the filtration feed is of a complex nature multiple mechanisms can occur simultaneously or synergistically (Evans, 2008). Membrane fouling is influenced by the hydrodynamics of the filtration process, the interactions between the membrane and foulants in the feed stream and between the fouling layer and foulants (Marshall *et al*., 1993; Doyen *et al*., 1996). It has been recognized that electrostatic interactions and hydrophobic/hydrophilic interactions between the membrane and the fouling material(s) have a significant bearing on fouling. Concentration polarisation in MF is different from that in UF as the fouling can be caused by particles as well as solutes. Factors effecting fouling in pressure driven membrane are discussed in section 2.3.10. A number of models correlating the flux to operating parameters exist in the literature. These are based on three models; (i) the resistance in series theory, (ii) film theory and (iii) the osmotic pressure theory.

2.3.2. Membrane Flux

Flux through a membrane is defined as the volume of fluid *V*, permeating the membrane in a given time *t*, through a known membrane area, A_m. The volume flux can be characterised by Equation 2.1.

$$J_v = \frac{\Delta V}{\Delta t A_m} \quad 2.1$$

The convective flux through a porous membrane is restricted by three factors (Equation 2.2).

$$J_v = \frac{\text{Driving Force}}{(\text{Viscosity})(\text{Total Resistance})} \quad 2.2$$

For a solution where the solvent is freely transferable the convective flux through the membrane can be described by Equation 2.3.

$$J_v = \frac{\Delta P - \Delta \pi}{\mu(R_T)} \quad 2.3$$

where ΔP is the hydrostatic or transmembrane pressure, $\Delta \pi$ is the osmotic pressure, μ is the viscosity of the feed solution, R_T is the total hydraulic resistance including the membrane resistance R_m and any additional resistances (R_s) caused by the interaction of the solute with the membrane. The osmotic pressure of most solutes is affected by temperature and concentration and can be considered negligible when encountered in MF and UF. When no fouling or concentration polarisation occurs the pure water flux can then be expressed by Equation 2.4.

$$J_v = \frac{\Delta P}{\mu_m R_m} \quad 2.4$$

where μ_m is the viscosity of pure water. R_m can be determined experimentally at fixed pressure, temperature and cross flow velocity (CFV), assuming the physical properties of the membrane remains unchanged throughout. R_m is a constant.

Fouling leads to flux decline and loss of selectivity (Aimar *et al*., 1994; Field *et al*., 1995). For dilute mixtures comprising of a solvent and a solute, the selectivity is usually expressed in terms of retention, R_a, towards the solute. The solute is partly or

completely retained while the solvent moves freely through the membrane (Equation 2.5).

$$R_a = \frac{C_b - C_p}{C_b} = 1 - \left(\frac{C_p}{C_b} \right) \qquad 2.5$$

where C_b is the solute concentration in the feed and C_p is the solute concentration in the permeate. The retention of solutes is an important parameter that provides information about the progress of fouling and the quality of product flux after cleaning. Brans *et al*. (2004) reviewed the effects of fouling on selectivity, where depth fouling led to smaller effective pores and to different retention characteristics. The cake layer formation was found to lead to different retention behaviour, as the cake retains small particles that should pass the membrane. When the selectivity is affected the product quality is compromised. This can have a greater consequence than low production rates (Shorrock, 1999). The cake layer above the membrane can act as a secondary membrane, often with greater selectivity than the membrane itself; consequentially MF can act as UF.

2.3.3. Membrane Flux Decline

In MF and UF the flux decline can be very severe, causing a change in the membrane properties. Figure 2.4 displays an example filtration graph which details a typical fouling and cleaning experiment. Some of the fouling is permanent and a pure water flux can be a measure of the membrane behaviour taken at constant conditions (Stage A in Figure 2.4). Fouling can be reversible or irreversible. Reversible fouling can be removed by flushing the membrane with pure water after the fouling filtration (Stage C). Pore blocking and cake formation are considered short-time reversible fouling. This means fouling takes place on a small time scale and can be avoided or removed by the correct choice of process conditions, e.g. high cross flow velocity or black flushing (Brans *et al*. 2004; Väisänen, 2004). Brans *et al*. (2004) define long-time reversible fouling as ‘a slow flux decrease in time (hours) and can be removed by stopping the production process and applying a cleaning procedure’. Concentration polarisation is the only fully reversible mechanism. Irreversible fouling cannot be

removed with water flushing, and in some cases chemical cleaning (Stage D) is also inadequate. Irreversible fouling is usually caused by adsorption and pore constriction.

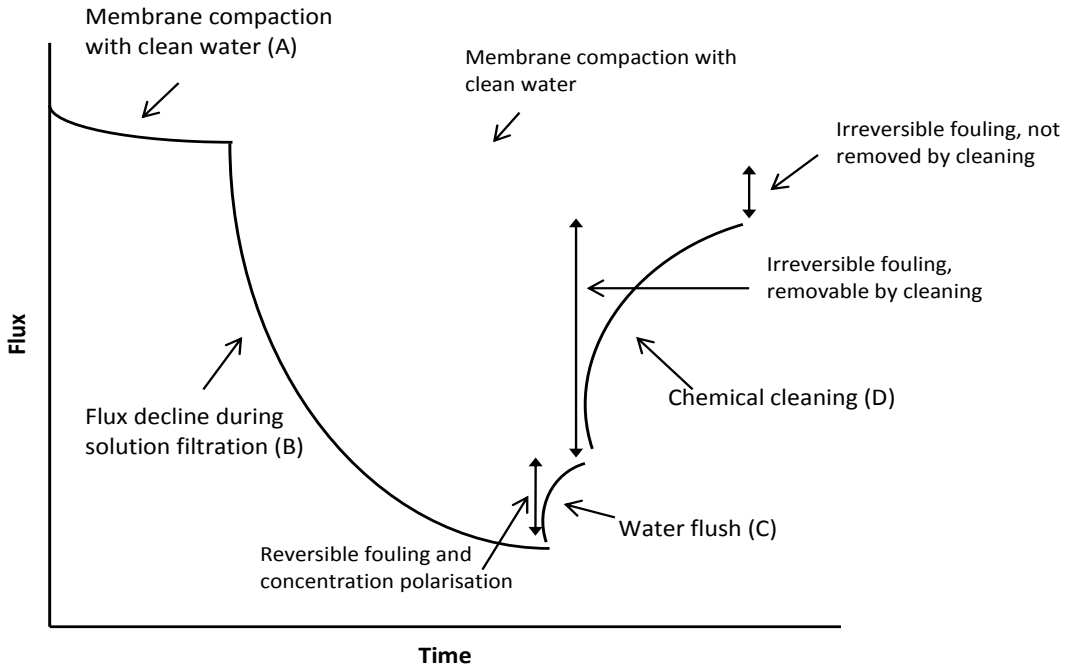

Figure 2.4: Schematic illustration of the filtration procedure (Adapted from Väisänen, 2004).

The flux decline can be caused by several increases in resistances that are summarised in Figure 2.5. Membrane fouling can be divided into four categories; (i) adsorptive fouling, (ii) pore blocking, (iii) cake layer formation, and (iv) gel layer formation. Adsorption consists of three processes: transport of foulant by diffusion or convection towards the membrane internal pore wall, followed by attachment to the surface and conformational changes on the surface (Metsämuuronen, 2003). This causes pore constriction, which obstructs the movement of other material. Pore blocking/plugging occurs once the foulants completely obstruct the transportation of solvent or solute through a pore. Cake layer formation is a special case of concentration polarisation, whereby the concentration at the boundary layer increases to a maximum forming a solid deposited layer. A gel layer may also be formed at the membrane surface due to a high concentration and pressure.

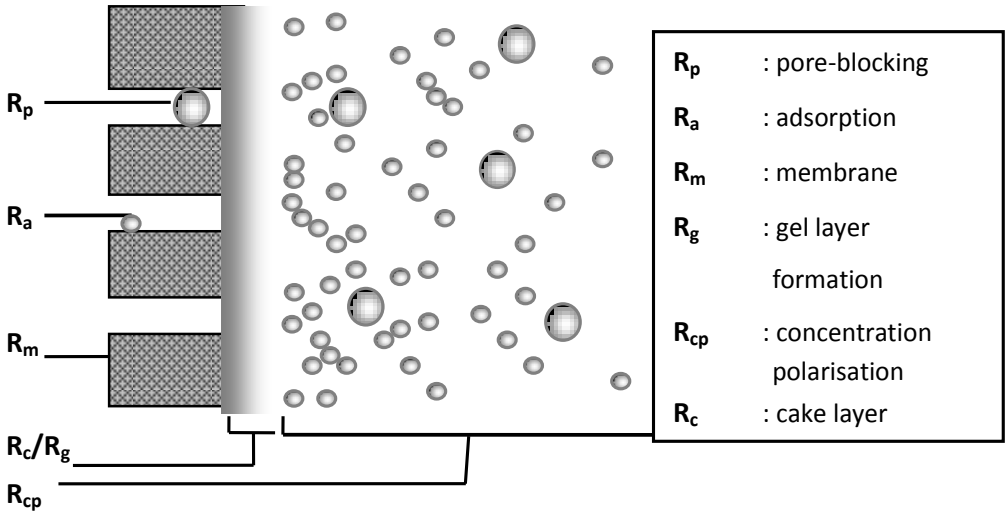

Figure 2.5: Overview of various types of resistance towards mass transport across a membrane (After Mulder, 2000).

2.3.4. Resistance in Series Model

The resistance in series model is derived from the governing equation for pressure driven membrane flux. Membrane resistance is the product of pore size, pore density, pore depth, the materials wettability, and the hydrodynamic resistance of the device holding the membrane. The interaction forces between solute, solvent, and membrane material play an important role as well (Fane and Fell, 1987). The resistances shown in Figure 2.5 are used in the resistance in series model to equate a total fouling resistance (R_T), shown in Equation 2.6.

$$R_T = R_m + R_p + R_a + R_{cp} + R_g + R_c \qquad 2.6$$

A fouling resistance (R_F) can be determined using Equation 2.7.

$$R_F = R_p + R_a + R_g + R_c \qquad 2.7$$

This results in the total hydraulic resistance shown in Equation 2.8.

$$R_T = R_m + R_F + R_{cp} \qquad 2.8$$

The cake resistance, R_c can be calculated using the Carman-Kozeny Equation if the cakes porosity, ε, and the cake layer thickness, δ_c are known (Equation 2.9).

$$R_c = \frac{h_k S_v^2 (1-\varepsilon)^2}{\varepsilon^3} \delta_c \qquad 2.9$$

where h_k is the Kozeny constant, generally assumed to be 5 (Okamoto *et al*., 2001) and S_v is the particle surface area per unit volume.

2.3.5. Gel Layer Model (Limiting Flux)

The gel layer model assumes that a cake gel layer is formed on the membrane surface. The model can be used to describe the occurrence of limiting flux (flux independence of TMP). The model is based on a thin film model in a highly polarised system. A gel layer (R_g) can be formed at the membrane surface instead of a cake layer due to a high concentration and pressure (where concentration polarisation is very severe). In the gel layer region the flux can be described by Equation 2.10. The model assumes that the solute is fully retained and the concentration at the membrane surface is constant. The convective force of solute towards the membrane surface is balanced by the diffusivity of solute back to the bulk solution. The gel layer concentration depends on the size, shape and chemical structure, but is independent of the bulk concentration (Mulder, 2000).

$$J_{\lim} = \frac{\Delta P}{\mu (R_m + R_g)} = k \ln\left(\frac{C_g}{C_b}\right) \qquad 2.10$$

Three regions exist for the flux-TMP relationship (Figure 2.6): (i) pressure controlled region, (ii) transition region, and (iii) mass-transfer controlled region. Here, the mass-transfer controlled region flux is independent of TMP (Limiting Flux). The flux can also decrease with increasing TMP (dashed line in Figure 2.6), as shown by Jönsson (1984) and later discussed by Metsämuuronen (2003). This occurs as the pressure continues to increase and there is no further increase in concentration. Instead the layer becomes more compacted resulting in a hydrodynamic resistance and a decrease in the permeate flux.

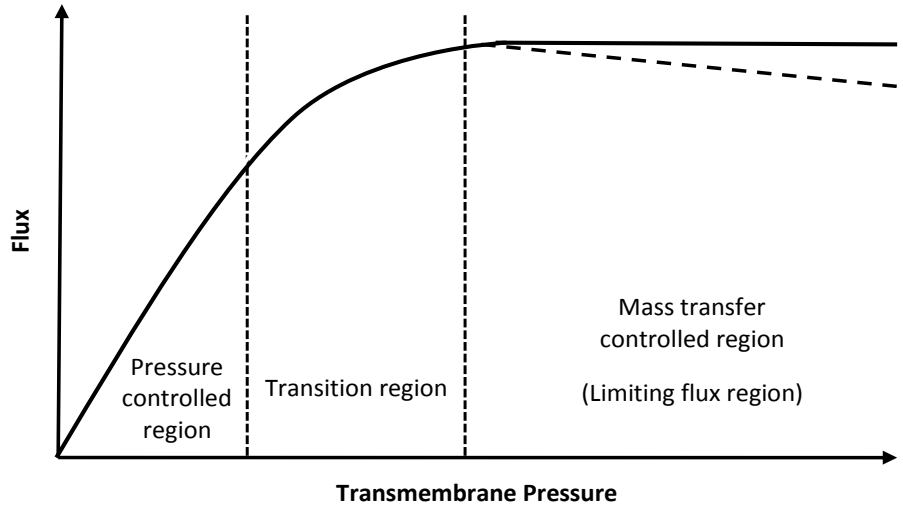

Figure 2.6: Graph to show permeate flux dependence on the TMP in different regions.

2.3.6. Osmotic Pressure Model

In typical UF feed concentrations, the osmotic pressure of macro solutes is negligible, and is therefore often ignored (Jönsson and Trägårdh, 1990). An osmotic pressure model has been developed and it assumes the osmotic pressure is generated by the retained macromolecules and the low molecular weight components permeate through freely. The main contributions to the osmotic pressure of a solution are from low molecular weight solutions except for high flux operations. For high flux values, high rejection and low mass transfer values, the concentration of the macromolecule solutes cannot be neglected (Elimelech and Bhattacharjee, 1998; Mulder, 2000). The model is based on a combination of the resistance in series method and the particle transport approach. The driving force through the membrane is given by the transmembrane pressure minus the osmotic pressure difference across the membrane, $\Delta\pi$ (Equation 2.11).

$$J = \frac{\Delta P - \Delta\pi}{\mu R_m} \qquad 2.11$$

Aimar and Sanchez (1986) applied the osmotic model with the limiting flux conditions, assuming total solute rejection the results obtained were in good agreement with experimental data. Opong and Zydney (1991) also successfully demonstrated the use of the osmotic pressure model for the UF of bovine albumin solutions. However, in the crossflow MF of particle suspensions the increase in osmotic pressure at the membrane

surface is only a minor part of the flux decrease. The formation of a cake layer of a gel layer is the major part of the flux decrease, which is not accounted for in the osmotic pressure model (Huisman, 1998).

2.3.7. Boundary Layer Model

Concentration polarisation leads to an increase of the solute concentration at the membrane surface. This exerts a hydrodynamic resistance on the permeating solvent molecules. This happens if the solute molecules are completely retained by the membrane. If the system is at steady state conditions, the convective flow of the solute molecules towards the membrane surface will be equal to the diffusive flow back to the bulk of the feed. The solvent flux can then be described by the membrane resistance (R_m) and the boundary layer resistance (R_{bl}), (Equation 2.12).

$$J = \frac{\Delta P}{\mu\left(R_m + R_{bl}\right)} \qquad 2.12$$

In this model it is assumed that no gelation or limiting flux can occur. Wijmans *et al*. (1985) showed that the osmotic pressure model and the boundary layer model are equal in both theory and experimental data. Cheng and Wu (2001) compared the flux values predicted by the osmotic pressure and the boundary layer model. The predicted fluxes from the boundary layer model were higher than the osmotic pressure model and even greater than the experimental data.

2.3.8. Concentration Polarisation

Permeate flux over time reveals a rapid initial decline followed by a more gradual long-term decline. The initial decline is attributed to concentration polarisation, a rapid build-up of solute particle concentration near the membrane surface (Figure 2.7), while the long-term decline is attributed to various modes of membrane fouling (Chen *et al*., 2004a). The retained solutes, which cannot pass through the membrane, accumulate at the membrane surface and the amount gradually increases (Figure 2.7). This concentration build-up generates a diffusive flow back to the bulk of the feed (Fick's first law). After a given period of time, steady-state conditions are achieved. Mulder (2000) best describes the phenomenon: 'The convective solute flow to the membrane surface is balanced by the solute flux through the membrane plus the diffusive flow

from the membrane surface to the bulk'. This concentration polarisation reduces the permeating components concentration difference across the membrane, thereby lowering its flux and the membrane selectivity (Baker, 2004).

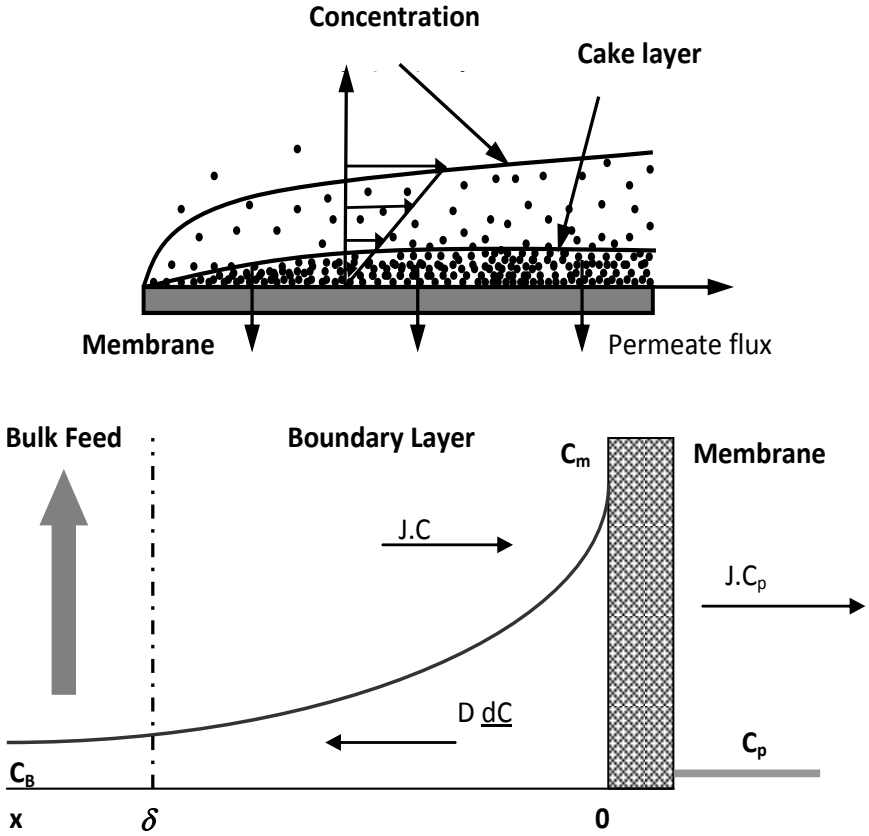

Figure 2.7: Top - Schematic description of concentration polarisation and cake formation over a membrane surface in cross flow filtration (Adapted from Chen *et al.*, 2004a). Bottom - Concentration polarisation: concentration profile under steady state conditions (Adapted from Mulder, 2000).

Performing a mass balance such that the convective transport of solute to the membrane is equal to the sum of the permeate flow plus the diffusive back transport of the solute (based on the concentration profile in Figure 2.7, Equation 2.13 is derived).

$$J.C = D\frac{dC}{dx} + J.C_P \qquad 2.13$$

where the boundary conditions are:

$x = 0 \rightarrow C = C_M$

$x = \delta \rightarrow C = C_B$

Rearrangement, integration and substitution of the above boundary conditions becomes Equation 2.14.

$$\ln\left[\frac{C_M - C_P}{C_B - C_P}\right] = \left(\frac{J_V \delta}{D}\right) \qquad 2.14$$

The ratio of the diffusion coefficient, *D*, and the thickness of the boundary layer,δ, are termed the mass transfer coefficient, Equation 2.15.

$$k = \frac{D}{\delta} \qquad 2.15$$

As discussed by Mulder (2000), concentration polarisation can affect the separation performance by causing a lower flux and a change in retention behaviour. A high flux membrane suffers from higher concentration polarisation compared to lower flux membranes (Metsämuuronen, 2003). There are conflicting opinions about the explanations for permeate flow resistance in the concentration polarisation boundary layer. Some authors suggest that the gel polarisation model is correct, whereas others prefer the osmotic pressure model (Bowen *et al*., 1996; Field and Aimar, 1993). Another explanation by some authors is the increased concentration and compression of the boundary layer which causes increased viscosity, decreased diffusivity and increased solute-solute interactions (Aimar and Field, 1992; Saksena and Zydney, 1997).

2.3.9. Mechanism of Membrane Fouling

The decline of flux in MF and UF of a solution or suspension is attributed to concentration polarisation and fouling phenomena (e.g. adsorption, pore blocking, long term and irreversible process), (Bhattacharjee and Bhattacharya, 1993). According to Tracey and Davis (1994) there are two sorts of membrane fouling, which are external and internal (Figure 2.8). External Fouling is when adsorption/desorption takes place on the external surface of the membrane and both hydraulic permeability and solute transmission characteristics are altered due to: (i) increase in the effective membrane thickness, (ii) blockage of pore entrances, and (iii) constriction of entrances. Internal fouling is when the adsorption or desorption takes place within the pores, the hydraulic

permeability and solute transmission characteristics are altered due to: (i) internal blockage of pore and (ii) internal constriction of pore.

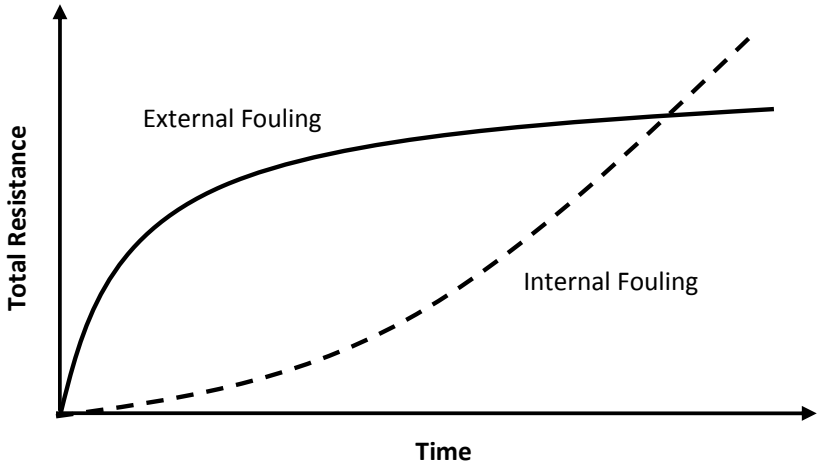

Figure 2.8: Graph to illustrate the internal and external fouling (Adapted from Tracey and Davis, 1994).

2.3.9.1. Pore Blocking

Constant pressure blocking filtration laws were developed in their recognised form by Shirato *et al*. (1979) and later expanded by Hermia (1982) to include an intermediate blocking law. Bowen *et al*. (1995) explained the fouling of MF membranes in terms of successive or simultaneous presence of the following stages (Figure 2.9).

a) *Complete Blocking* - the smallest pores are blocked by particles arriving at the membrane surface and no further material can pass through the pores.
b) *Standard Blocking* - the inner surface of the bigger pores are covered, a result of direct adsorption of particles, which leads to reduction of pore volume.
c) *Intermediate Blocking* - some particles arriving at the membrane cover particles already deposited while others directly block some of the pores.
d) *Cake Filtration* - a cake build up occurs due to the accumulation and agglomeration of particles absorbed onto the membrane surface.

The laws allow a prediction of the type of blocking occurring at a given instance during fouling flux decline. Hermia (1982) derived an empirical fouling model for non-

Newtonian fluids in dead-end filtration. All blocking laws have the same general form (Equation 2.16).

$$\frac{d^2t}{dV^2} = K\left(\frac{dt}{dV}\right)^n \qquad 2.16$$

where V is the volume of permeate collected in time t, K and n are constants depending upon the mechanisms involved. K is a system specific decay constant called the fluid consistency index, and n is a mechanism specific index. The constants are summarised in Table 2.3 for the given blocking laws.

Table 2.3: Parameters of the blocking filtration laws (After Hermia, 1982)

Blocking Law	***K***	***n***
Cake Filtration (Figure 2.9d)	$K_c = \frac{\alpha \gamma s}{A R_o Q_o (1-ms)}$	0
Intermediate Blocking (Figure 2.9c)	$K_i = \frac{\sigma}{A}$	1
Standard Blocking (Figure 2.9b)	$K_s = \frac{2C}{\delta_m A} Q_o^{1/2}$	1.5
Complete Blocking (Figure 2.9a)	$K_c = u_o \sigma$	2

where α is cake specific resistance (m kg^{-1}), γ is the filtrate density (kg m^{-3}), s is the mass fraction of solids in the cake, A is membrane surface area (m^2), R_0 is total membrane resistance (m^{-1}), Q_0 is the volumetric flow rate (m^3 s^{-1}), m is the mass ratio of wet cake to dry cake, σ is the area of blocked membrane per unit filtrate volume (m^{-1}), C is the volume of solid particles retained per unit filtrate volume, δ_m is the membrane thickness (m) and u_0 is the fluid linear velocity (ms^{-1}).

More recently Field *et al*. (1995) extended these blocking laws to describe crossflow filtration by inclusion of a back diffusion term (Equation 2.17).

$$-\frac{dJ}{dt} = K\left(J - J^*\right)J^{(2-n)} \qquad 2.17$$

where J^* is the flux at steady state. Curve fitting of Equation 2.12 to experimental data will give an indication of the fouling mechanism occurring. The knowledge of the position and extent of deposition on the membrane can aid the implementation of the correct cleaning procedure.

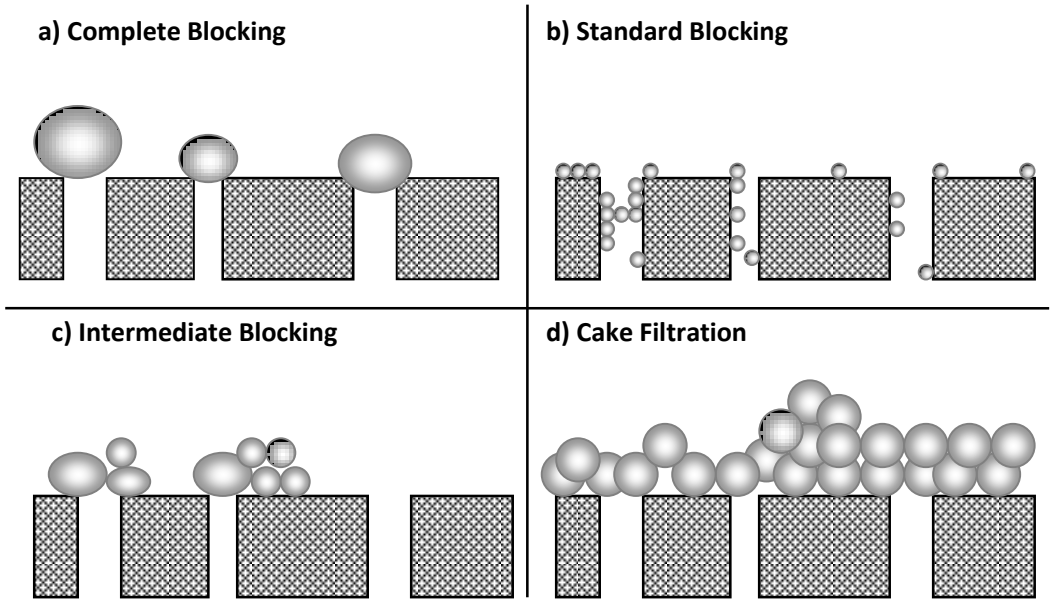

Figure 2.9: Pore Blocking Model (After Bowen *et al*., 1995).

2.3.10. Effect of Fouling Operating Parameters

There are many ways to prevent or minimise fouling and concentration polarisation. These include adjusting the filtration process parameters such as shear force, pressure, pH, salt concentration, feed concentration and temperature or flow rate (Väisänen *et al*., 2002).

2.3.10.1. Temperature

Temperature has an effect on the mass transfer coefficient values as well as the viscosity of the solution. As the temperature increases so does the permeate flux. This is due to a decrease in viscosity and increase in diffusivity of the feed (Marshall *et al*., 1993). Vigneswaran and Kiat (1988) observed that the effect of increasing temperature on fouling flux was minor for lower cut-off UF membranes. The temperature capability of a membrane system is, in most cases, not dictated by the temperature limitation of the membrane, but primarily by the membrane configurations and other components in the membrane system. Energy consumption to pre-heat the feeds must be taken into consideration when deciding upon conditions.

2.3.10.2. Cross Flow Velocity

In industry, turbulent flow conditions are normally selected as cross flow is effective in removal of accumulated substances at the membrane surface, often due to shear rate (Wu and Bird, 2007). Shear rate is a function of the velocity at which the filtrate is passed across the surface of the membrane. This shear acts to sweep away particles which accumulate at the membrane surface (Kumar, 2009). This can lead to a thinning of the concentration polarisation layer (Belfort *et al*., 1994). A reduction in concentration polarisation can be achieved by increasing the mass transfer away from the membrane (Bartlett, 1998; Bian *et al*., 2000). The mass transfer coefficient, *k*, is related to the Sherwood number (*Sh*), Equation 2.18.

$$Sh = \frac{k\,d_h}{D} = a\,\mathrm{Re}^{b}\,Sc^{c} \qquad 2.18$$

where *Re* is the Reynolds number, *Sc* the Schmidt number, and *a*, *b*, and *c* are constants. The Lévêque solution is most widely used for laminar flow (Equation 2.19). Here, the parabolic velocity profile is assumed to be developed at the channel entrance (Coulson *et al*., 1997).

$$Sh = 1.62\left(\frac{d_h}{L}\,\mathrm{Re}\,Sc\right)^{1/3} \qquad 2.19$$

where *L* is the duct length. Equation 2.20 is used for turbulent flow which is the Dittus-Boelter correlation (Coulson *et al*., 1997).

$$Sh = 0.023\,\mathrm{Re}^{0.8}\,Sc^{0.33} \qquad 2.20$$

These equations assume fully developed flow, negligible pressure drop and solute loss in the axial direction. The increased energy consumption as a result of increased cross flow velocity must be considered in the efficiency of the whole process.

2.3.10.3. Transmembrane Pressure

Transmembrane pressure (TMP) is the difference in pressure between the filtrate side of the membrane and the permeate side of the membrane and is the driving force of the membrane separation. The effect of TMP has been observed by numerous researchers (Field *et al*., 1995; Kalhoinen *et al*., 2007; Mikulasek, 1994). It has been observed that as the TMP increases so does the permeate flux, with a linear relationship until a certain pressure where the permeate flux levels off and reaches a limiting value. This has been discussed further in section 2.3.5. Jönsson (1984) found that when ultra-filtering 9.1 wt. % whey protein solutions the flux values decreased with increased TMP once a maximum was reached. Barros *et al*. (2003) found that flux variations in UF of pineapple juice were independent of TMP variation, and the flux remained constant as pressure increases. This suggested that they were operating within the limiting flux region. Whereas Laorko *et al*. (2010) observed flux increasing linearly as TMP increased under low pressure (TMP < 0.4 bar). However, the results showed that TMP did not have significant effect on the phytochemical properties of clarified pineapple juice. Blanpain *et al*. (1993) found whilst filtering beer using MF membranes the retention increased significantly as TMP was increased. When the TMP was decreased again the rejection decreased significantly. Evans (2008) also observed an increase in solids retention as the TMP increased during the UF of tea.

All membranes are sensitive to pressure. Kallioinen *et al*. (2007) discussed that under high pressure on a polymeric membrane, compaction can occur. This left a more dense structure with smaller pores and lower membrane flux. It can also affect the retention of the membrane, where membrane compaction causes a decrease in pore size or deformation of the pore geometry. According to Wagner (2001) it is important to correctly support the membrane to prevent pressure squeezing the membrane into the support material.

2.3.11. Prevention of Membrane fouling

Methods to prevent fouling should be highlighted before cleaning is considered. Important considerations are feed pre-treatment, membrane pre-treatment and system hydraulics. Muthukumaran *et al*. (2005) discussed the various methods that have been used to reduce the negative effects of concentration polarisation and fouling. The

techniques that have been shown to be effective are turbulence promoters, pulsatile flow, vortex mixing, unsteady jet, gas sparged membrane filtration and two-phase gas liquid flow. Also, methods known as 'assisted filtration' are used to prevent membrane fouling. This is when electrical and sonic forces are used to modify the filtration performance. Muthukumaran *et al*. (2007) found that ultrasound increases the flux by increasing the mass transfer coefficient within the concentration polarisation layer. It also leads to a less compressed fouling cake.

2.3.11.1. Effect of Feed Pre-treatment

Pre-treatment of the feed solution can cause great differences in flux and transmission. Methods employed include heat treatment, pH adjustment, chlorination, chemical clarification, and pre-filtration (Mulder, 2000; Shorrock, 1999). Altering the pH of a solution can control fouling as it can affect the solubility, conformation of macromolecules, and the flux via charge modification (Väisänen, 2004). Lee and Merson (1976) found that adjusting the ionic strength and pH of a fluid improved flux by up to 70 %. Lee and Merson (1976) also used pre-filtration; which involves removing any suspended particles that could adhere to a membrane surface. Fan *et al*. (2008) found that pre-filtration using a 1.5 μm glass-fibre filters enhanced the permeate flux for MF by removing particulates but had limited effect for the UF of sludge-lagoon effluent. Daufin *et al*. (1991) and Gesan *et al*. (1995) used chemical clarification to reduce the fouling potential in the MF of whey. The pre-treatment consisted of a physicochemical process comprising increased ionic calcium and constant pH accompanied by heat (55 ºC) to cause aggregation of complex lipid-calcium phosphate particles, which are then separated by MF. Almécija *et al*. (2009) proposed eliminating fouling agents using physiochemical treatments to enhance flux values in the UF of acid whey. A protocol comprising of salt addition, pH and temperature modification, and centrifugation was used to remove the main fouling agents calcium and phosphate salts from acid whey without altering the profile of the desired proteins.

2.3.11.2. Effect of Membrane Pre-treatment

The membrane surface can be modified to make it less prone to fouling. The membrane properties can influence the structure of the initial fouling layer. Membrane chemistry can affect the adsorption rate of the first few layers of the deposited material (Barros *et al*., 2003). Modification of the surface can be made by using surfactants, chemical

modification, electron irradiation, UV irradiation, plasma treatment, blending, coating and grafting (Väisänen, 2004; Rana *et al*., 2005). Kulkarni *et al*. (1994) found that when the surface of a polyamide composite membrane chemically reacts with a strong hydrofluoric acid solution, the top polyamide layer becomes slightly thinner. This resulted in a considerable flux increase and a similar or improved rejection.

Plasma polymerization is when a porous substrate membrane is placed in plasma, and the surface of the membrane is subjected to various changes corresponding to the property of plasma. The substrate surface can be etched and/or chemically active sites can be introduced to the surface (Kulkarni *et al*., 1994). Bryjak *et al*. (2000) found that the plasma modification method was able to obtain a membrane with a requested pore diameter. The use of plasma on porous membranes resulted in an increase of pore diameter, deposition of polymer layer and/or rebuilding of surface functional groups.

Maartens *et al*. (2000) used surfactant precoating on Polysulphone UF membranes to prevent fouling when purifying natural brown water. The membranes were treated with commercial non-ionic surfactants Triton X-100 and Pluronic F108. The precoating produced varied results; the Triton X-100 coated membranes were more susceptible to foulants adsorption, whereas the Pluronic F108 coated membrane significantly reduced the foulant adsorption. Graft polymerization can control the adhesion of particles and macromolecules onto the substrate surfaces. Wang *et al*. (2000) used ozone treatment followed by graft-polymerization with hydroxyethyl methacrylate (HEMA) for the hydrophilic surface modification of a Polypropylene membrane. An improvement in flux recovery was achieved with the grafted Polypropylene MF membranes, suggesting that the modified membranes had a high reversibility of the fouling layer. Hilal *et al*. (2003) used photo-induced grafting copolymerisation to modify membrane surfaces to lower fouling properties. The modified membranes displayed lower fouling properties than the non-modified membranes. According to Hilal *et al*. (2005) the disadvantages of the coating and grafting techniques include the erosion of the coated layer on the modified surface which can lead to substandard reliability and durability.

In certain membrane systems it may also be possible to selectively adsorb key foulants to the filter surface, leading to the generation of a beneficial fouling layer. Such a layer

can lead to improvements in permeate flux and selectivity for the system concerned (Evans and Bird, 2010; Wu and Bird, 2007).

2.3.12. Critical Flux Concept

This concept was first developed by Field *et al*. (1995), whereby a hypothesis for critical flux in MF was proposed: 'On start up there exists a flux below which a decline of flux with time does not occur; above it fouling is observed.' The correlation between flux and transmembrane pressure can be seen in Figure 2.10. If the critical flux is exceeded then reducing TMP does not restore the original flux producing hysteresis at a lower flux. The correct selection of initial TMP can reduce the rate of fouling providing a critical flux is not exceeded, ideally a constant-flux, rather than constant-pressure operating mode is to be preferred (Field *et al*., 1995). The strong form of the critical flux is the point where the TMP corresponding to a set flux starts to deviate from that for pure water (Figure 2.10). The weak form critical flux is when the TMP required is greater than for the pure water, but the TMP still increases linearly with the flux until a point.

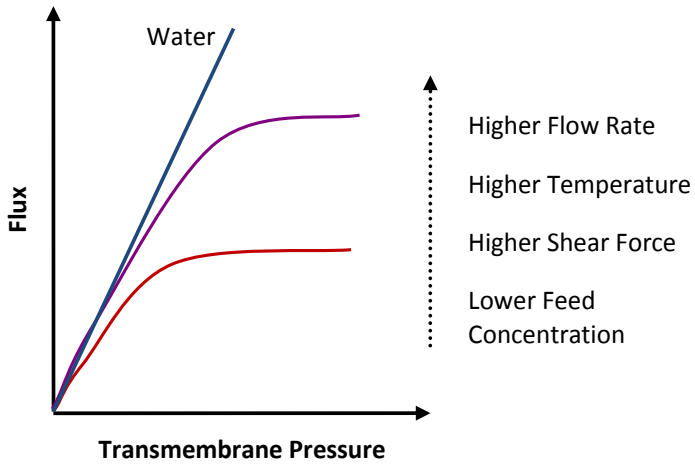

Figure 2.10: Correlation between flux and transmembrane pressure. Purple line – strong critical flux, red line – weak critical flux (Adapted from Väisänen, 2004).

Wu *et al*. (1999) investigated the critical flux measurements for model colloids; the experimental data supported the 'strong form' of critical flux for the filtration of X30 silica suspension, whereas a 0.15 % HT50 silica suspension exhibited a weak form of the critical flux. Wu *et al*. (1999) also observed that with increasing membrane pore sizes the critical fluxes decreased, which was explained by the possible adsorption within pore walls which could affect the critical flux. Whilst Chen (1998) found that the critical flux increased with increasing pore size in the MF of 0.1 – 1.0 wt. % Bovine

Serum Albumin (BSA). It was also found that the critical flux decreased with increasing concentration. Metsämuuronen *et al*. (2002) determined the critical fluxes by constant flux UF of myoglobin solutions and baker's yeast. The critical flux was found to increase with increasing CFV and decreasing solute concentration. The highest critical flux was obtained in the presence of repulsive electrostatic forces between molecules at pH 8. Bacchin *et al*. (2006) recommends that for industrial streams (complex feeds) the sustainable flux should be considered. Sustainable flux takes into account a low rate of fouling rather than zero fouling, as zero fouling can be unfeasible. The sustainable flux is dependent on optimised hydrodynamic conditions, feed conditions and process time; above this the rate of fouling is economically and environmentally unsustainable.

2.4. Membrane Cleaning

2.4.1. Introduction

Cleaning is one of the most important steps for maintaining membrane performance, such as permeability and selectivity (Makardij *et al*., 1999). All membranes will foul during operation involving liquid, causing the membrane performance flux and/or selectivity to drop to below acceptable levels. Although operational conditions and methods should be studied first to reduce the fouling process, cleaning of the membrane is inevitable. Trägårdh (1989) defined membrane cleaning as 'a process where the membrane is relieved of materials which are not an integral part of the membrane'. Cleaning can be summarised into four distinct methods: i) Hydraulic ii) Mechanical iii) Electrical and iv) Chemical. These methods are discussed in the following sections.

2.4.1.1. Hydraulic Cleaning

Hydraulic cleaning includes methods such as removing deposits using turbulence or reversal of TMP (only possible on tubular or hollow fibre membranes). These methods include: back flushing (flow reversal), back pulsing (backpressure is applied at rapid pulses), rotating disks and secondary vortex flows. These hydraulic cleaning techniques rarely restore maximum membrane flux (Shorrock and Bird, 1998; Field *et al*., 1995). Gabrus *et al*. (2008) observed an increase in filtration efficiency when back-flushing was implemented in the MF of yeast suspensions through ceramic membranes. Flat sheet modules do not have the mechanical strength to be compatible with back flushing.

2.4.1.2. Mechanical Cleaning

Mechanical cleaning involves scouring fouled surfaces with an abrasive material. It is very limited due to the mechanical strength and accessibility of the membrane surface (Scott and Hughes, 1996). Mulder (2000) discusses that mechanical cleaning is limited to tubular systems, where cleaning can be applied using oversized sponge balls at high velocity. Maartens *et al*. (2002) combined the use of mechanical and chemical cleaning in the UF of E-stage pulp mill effluent using Poly (ether sulphone) (PES) tubular membranes. The flux through the fouled membranes was successfully restored by cleaning with the non-ionic detergent Triton® X-100 and sponge balls. Although, re-adsorption of foulants during subsequent contact with the effluent could not be prevented.

2.4.1.3. Electric Cleaning

Electric cleaning is performed by applying an electric field across the membrane so that charged particles or molecules will migrate in the direction of the electric field. The membranes must be sufficiently conductive and special module designs are required, however an advantage is that the process can be *in situ* and therefore continuous. Bowen *et al*. (1989) describes that voltage applied across the membrane causes the formation of micro-bubbles at the membrane surface which drive foulant material out into the bulk feed and removed by the flowing stream. Tarazaga *et al*. (2006) used space distributions of electric field in the range between 40 and 180 V/m in low frequency pulse produced by half wave rectified, 50 Hz ac, in order to achieve an UF continuous process with a minimum operation cost. This cleaning method does not need to interrupt the work cycle of the membrane.

2.4.1.4. Chemical Cleaning

Polymeric membrane module configurations (flat sheet and spiral wound) do not readily facilitate back flushing. Therefore chemical cleaning remains the membrane regeneration technique of choice. Chemical cleaning is the most commonly used cleaning procedure in industry and is the type that will be used in this study. It can be performed by various methods: (i) cleaning-in-place (CIP): the fouled membrane is directly immersed in the chemical solution, (ii) cleaning-out-of-place (COP): soaking the membrane in a separate tank usually with a higher concentration cleaning chemical, (iii) chemical wash (CW): adding chemicals directly in the feed stream, or (iv) chemical

enhanced backwash (CEB): chemical cleaning in conjunction with a physical cleaning stage (Lin *et al*., 2010). It is usually performed by CIP through filling the retentate channel with a cleaning solution from a separate tank. The details of chemical cleaning will be discussed further in this section.

2.4.2. Chemical Cleaning Agents

Cleaning is a heterogeneous interaction between the detergent solution, the fouled layer and the surface. Optimisation of a cleaning regime is required for each membrane and feed. This requires knowledge of how the chemical, thermal and hydraulic operating conditions affect cleaning. This means variation of concentration, temperature, flowrate and transmembrane pressure. The key issue to understand membrane fouling and cleaning is to understand interactions: (i) between the fouling materials and membranes, (ii) between the cleaning chemicals and fouling material, (iii) between the cleaning chemicals and membrane, and (iv) among the fouling materials (Zuh and Nystrom, 1998).

A cleaning agent can affect fouling material present on a membrane surface in three ways: (i) the foulants may be removed by chemical and / or hydraulic interaction, (ii) the morphology of the foulants may be changed (e.g. by swelling or compaction) or (iii) the surface chemistry of the deposit may be altered so that the hydrophobicity or charge is modified (Weis *et al*., 2003). According to Bird and Fryer (1992) and Lin *et al*. (2010) the chemical cleaning processes at the membrane surface can be divided into six stages:

(i) bulk reactions,
(ii) the transport of the detergent to the interface,
(iii) the transport of the detergent into the foulant layer,
(iv) a cleaning reaction in the fouling layer,
(v) the transport of the cleaning reaction products back to the interface,
(vi) the transport of the product to the bulk solution

Chemicals commonly used for cleaning MF and UF membranes are summarized in Table 2.4. While single component cleaners can be used (mainly in academic research studies), most commonly, several chemicals are incorporated into built/formulated

cleaning solutions for industrial usage (D'Souza and Mawson, 2005). In this study only single component cleaning agents will be tested. This is so the component that is causing the interaction on the membrane is known. With the different feed requirements, both alkalis and acid agents will be used.

- **Alkalis –** solubilise carbonates, bind ion salts, regulate pH, emulsify fat and peptise proteins. Caustic can increase solubility of solutes by hydrolysis and solubilisation.
- **Acid –** mineral and organic acids are effective at removing inorganic salts formed by calcium or metal films.

Table 2.4: Major categories of membrane cleaning chemicals (Liu *et al*., 2000)

Category	Major Functions	Typical Chemicals
Caustic	Hydrolysis, solubilisation	NaOH
Oxidants/Disinfectants	Oxidation, disinfection	NaOCl, H_2O_2
Acids	Solubilisation	Citric Acid, nitric acid
Chelating Agents	Chelation	Citric Acid, EDTA
Surfactants	Emulsifying, dispersion	Surfactants, detergents

The cleaning ability of the cleaning agent is only one of the factors when choosing the appropriate solution. According to Kane and Middlemass (1985) the following factors should also be considered: good solubility, moderate foam levels, good chemical stability, cost and safety.

2.4.3. Cleaning Operating Parameters

Membrane cleaning is conducted through the chemical reactions between cleaning chemicals and fouling materials. The factors that affect the mass transfer, chemical reactions and subsequently the cleaning efficiency are the concentration, temperature, length of cleaning period, and the hydrodynamic conditions (Liu *et al*., 2000). Chen *et al*. (2003) successfully used a factorial design approach to identify the key factors and interaction in cleaning of UF and RO membranes in municipal wastewater reclamation. It was found that temperature and concentration of high pH cleaning solutions played important roles. Bird and Bartlett (2002) also discovered that the chemical cleaning temperature and concentration has the greatest effect upon flux recovery, and that both

have an optimal value that can maximise cleaning performance. Increasing the cleaning temperature increases the cleaning efficiency until a certain point; after this point the detergent can become decomposed or the vapour pressure of the cleaning solution hindered (Bartlett, 1998).

The concentration of cleaning chemicals not only needs to maintain a reasonable reaction rate, but also needs to overcome the mass transfer's barrier imposed by the fouling layer (Liu *et al*., 2000). The effect of increasing concentration on flux recovery is not always continuously linear. There is a concentration beyond which no further increase in flux recovery is observed. Bansal *et al*. (2006), Bird and Bartlett (2002), Nigam *et al*. (2008), Popović *et al*. (2009) found that an increase in concentration of NaOH solution did not always increase flux recovery. Nigam *et al*. (2008) postulated that the higher concentration solutions enhanced the swelling of the deposits which caused additional pore blockage. Popović *et al*. (2009) also observed re-fouling in the later stages of cleaning after whey protein filtration using ceramic tubular membranes. The deposits remained either unchanged or increased in size. This swelling in the pores was found to decrease the pore diameter to approximately one-half of its nominal value. Popović *et al*. (2009) suggested shortening the cleaning stage of the cycle which could lower the effects of re-fouling/swelling and also save time.

Bartlett *et al*. (1995) optimised the cleaning of whey protein deposits from stainless steel and ceramic MF membranes. The noticeable results were the minimal increase in flux with increasing cross flow velocity and the decrease in cleaning performance with increasing transmembrane pressure. Cleaning at zero bar TMP can cause an increased and maximum flux recovery (Kim *et al*., 1993).

2.4.4. Measurement of Cleaning Efficiency

Membrane cleaning efficiency is a function of multiple parameters such as hydrodynamic conditions, concentration and temperature of the cleaning solution (Liu *et al*., 2000; Chen *et al*., 2003). The cleaning conditions were optimised by varying concentration, TMP and temperature. The cleaning efficiency was evaluated by the ratio of the PWF after cleaning (J_c) to the PWF measured before fouling (J_w) for each cleaning stage. The percentage flux recovery ($\%J_r$) was calculated using Equation 2.21.

$$\%J_r = \left(\frac{J_c}{J_w}\right) \times 100 \qquad 2.21$$

Visual inspection of cleaned membrane surfaces can also give a good indication of their state of cleanliness.

2.4.5. Fouling and Cleaning Synergy

It is important that fouling and cleaning processes are investigated synergistically, considering the whole process over multiple operational cycles. Bartlett (1998), Shorrock (1999), Wallberg *et al*. (2001), and Weis (2004) all recommend that the performance of the system should be judged on how the membrane responds after fouling and cleaning, i.e. how quickly the membrane re-fouls. Blanpain-Avet *et al*. (2004) investigated the effect of multiple fouling and cleaning cycles upon the membrane performance of a 0.1 μm tubular ceramic membrane when fouled with a whey protein concentrate. Blanpain-Avet *et al*. (2004) suggests that achieving a stable steady state which suffers no further flux decline is more important than recovering the membrane to its original state. Weis *et al*. (2005) observed during multiple fouling and cleaning cycles of SSL filtration that fluxes measured were often high following cleaning. The FTIR and Zeta potential results though showed that the cleaning regime didn't return the membrane surfaces to a pristine state with increasing cycle. Evans (2008) performed multiple fouling and cleaning cycles using a 30 kDa Fluoropolymer membrane for the filtration of black tea. The pure water fluxes after cleaning increased initially for the first few cycles, and then decreased to 91 % of the initial virgin membrane flux by cycle 17. Evans (2008) also found that the charges on the membrane pore wall were less negative with increasing fouling cycle.

2.5. Studying the Nature of Membrane Surfaces

Flux is not always a reliable parameter from which conclusions on fouling cleaning efficiency can be drawn (Weis, 2004; Delaunay *et al*. 2006). Membrane surface characteristics such as hydrophobicity, charge, and roughness will affect the membrane separation characteristics. Fouled and cleaned membrane surfaces can be characterised using the following techniques: (i) contact angle measurements, (ii) streaming potential measurements, (iii) Atomic force microscopy (AFM), and (iv) Fourier Transform Infra-

Red (FTIR) spectral peak height analysis. These techniques can be used on virgin, conditioned, fouled and cleaned surfaces as a diagnostic tool for fouling and cleaning potential.

2.5.1. Membrane Hydrophobicity

One way to estimate membrane hydrophobicity is to measure the contact angle (Gekas *et al*., 1992). Hydrophobic interaction can be described as "like attracts likes". That is, there is a natural tendency of attraction between membranes and solutes with similar chemical structures. Hydrophobic attraction results from van der Waals force between molecules. Contact angle measurement at the membrane surface can be used to identify its hydrophobicity. The greater the contact angle, the more hydrophobic of a membrane medium is. The contact angle measurement is used for control of cleaning process success, investigation and control of adhesion, film formation, and surface treatments (Väisänen, 2004). For hydrophobic membranes the contact angle will be larger than 90º and for hydrophilic membranes the contact angle will be less than 90º tending toward 0º as shown in Figure 2.11.

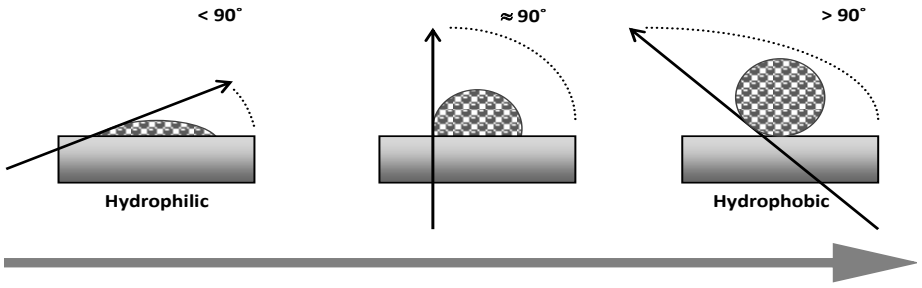

Figure 2.11: Classification for contact angles of liquid droplets on membrane surfaces using the sessile drop method.

The contact angle measurement can also be considered in terms of the thermodynamics of the materials involved. Equilibrium contact angles can be calculated from the Young equation (Equation 2.22) which is valid only for smooth, rigid and homogeneous surfaces. This analysis involves the interfacial free energies between the three phases; a solid surface, a liquid and a vapour phase (Figure 2.12).

$$\gamma_{LV}\cos\theta = \gamma_{SV} - \gamma_{SL} \qquad 2.22$$

where γ_{LV}, γ_{SV}, and γ_{SL} refer to the interfacial energies of the liquid / vapour (surface tension), solid / vapour and solid / liquid interfaces respectively; θ is the contact angle specific to the system.

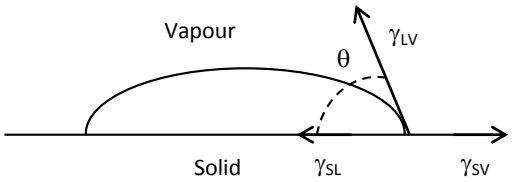

Figure 2.12: Principle of the sessile drop method.

The measurement of water contact angle is affected by many factors including material, manufacturing process, roughness of the membrane surface, the purity of water, and even the techniques used by individual investigators. There are a number of methods in which the contact angle can be measured, these include; the sessile drop method, the captive bubble method and the Wilhelmy plate method. The sessile drop method involves measuring the angle of a drop of water on the membrane surface. The captive bubble method is where the profile of a small bubble of air is measured that has been placed into contact with the membrane immersed into a liquid. The Wilhelmy plate method involves the immersing and withdrawing of a membrane in and out of a liquid whilst measuring the advancing and receding contact angles.

2.5.2. Zeta Potential and Surface Charge

The surface charge on membranes has a significant influence on its filtration and fouling tendencies. The surface charge of a porous membrane is related to the zeta potential of the membrane, which is usually evaluated from electro kinetic experiments. When ions are present in a system that contains an interface, there will be a variation in the ion density near the interface which is described by a profile (Figure 2.13). The presence of a surface charge leads to ions in the solution of an opposite charge being attracted towards the surface. This leads to a greater concentration of counter ions close to the surface than in the bulk of the liquid, concentration that falls off with increasing distance from the surface (Weis, 2004). The charge on the surface is balanced by excess counter-ions in the liquid thus neutrality is maintained which produced a variation in the electrical potential between the solid surface and the bulk solution (Hunter, 1981). The

bound layer of the counter ion adsorbed on the surface is the Stern layer and the remainder of the counter ions are dispersed in the diffuse layer. The thickness of the Stern layer depends on the radius on the specifically adsorbed counter-ions. The potential of the solid surface with respect to the bulk liquid is represented by ψ_0 in Figure 2.13, and is called the surface potential. The diffuse double layer theory assumes that there exists a certain stationary plane inside of the double layer. The solvent molecules near the solid surface remains stationary due to electric field of the solid surface while rest of the diffuse double layer moves along with the flow (Hiemenz, 1997). This specific plane is called the surface of shear, which is situated between the bound layer and the diffusive layer. The potential difference between the plane of shear and the bulk solution is the zeta potential. This can be determined by measurements of electro osmosis or streaming potential (Hunter, 1981; Hiemenz, 1997).

The streaming potential method has been proven to be the best method to characterise the surface charge densities of different membranes (Nyström *et al.*, 1994). Streaming potential is the potential induced when an electrolyte solution flows across a stationary, charged surface. It arises when a pressure difference is applied across a membrane that causes the double layer to shear. The flow of fluid displaces the electric charge of the diffusive part of the double layer which generates a potential in the opposite direction to the movement of the charges. This hinders further dislocation of ions to achieve a steady state. It is the resulting stable potential difference that is the streaming potential (Weis, 2004). From streaming potential measurements the zeta potential can be calculated using the Helmholtz-Smoluchowski equation. Further details on the Helmholtz-Smoluchowski are given in section 3.7.1.

Nyström *et al*. (1994) developed a new apparatus where simultaneous streaming potential and flux could be measured. This allowed the adsorption of a solute on an UF membrane to be tracked and the flux reduction with membrane charge correlated. Nyström and Zhu (1997) then used simultaneous streaming potential and flux measurements on virgin, precleaned, fouled and cleaned membranes. It was established that the charge characterisation method could be a useful tool for determining if the fouling is situated in the pores of the membrane or on the membrane surface.

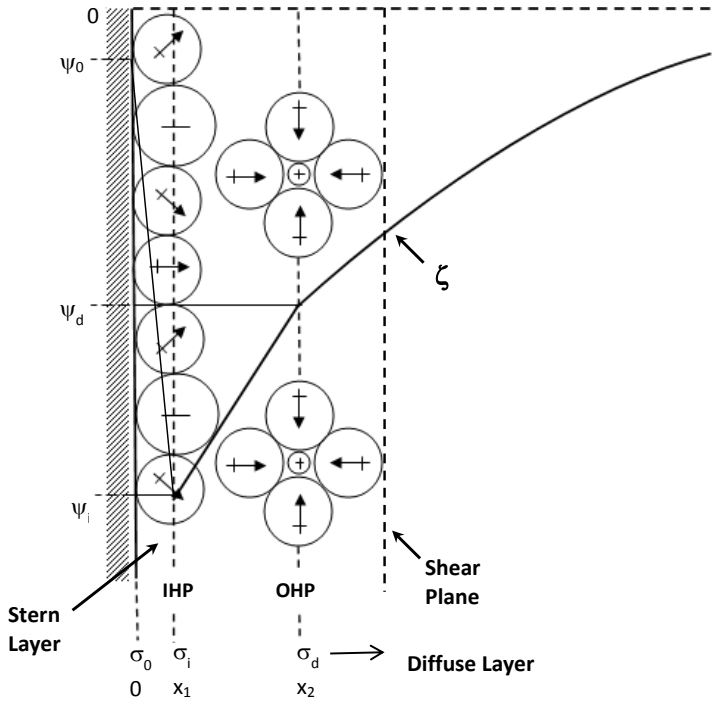

Figure 2.13: A model of the electrical double layer in aqueous solution (Adapted from Hunter, 1981). IHP is the Inner Helmholtz Plane and OHP is the Outer Helmholtz plane. ψ_0 is the potential at the solid surface, ψ_d is the potential at the surface of the diffuse layer, ψ_i is the potential at the IHP. σ_0, σ_i, and σ_d are the charge densities at the solid surface, at the IHP and at the surface of the diffuse layer. x is the distance from the solid surface inside the double layer.

2.5.3. Membrane Surface Morphology

Atomic force microscopy (AFM) is primarily used to probe surface topography and interactions on the atomic-molecular scale (Chan and Chen, 2004). The AFM technique requires only minimal sample preparation and can generate three-dimensional information concerning the topography of the surface such as quantitative surface roughness. The surface roughness is estimated by the arithmetic average of the absolute values of the surface height deviations measured from the centre plane based on AFM images (Hobbs *et al.*, 2006).

The AFM consists of a cantilever with a sharp tip (probe) at its end that is used to scan the specimen surface (Figure 2.14). A laser beam is deflected off the attached cantilever into a dual element photodiode as the tip scans the surface of the sample, moving up and down with the contour of the surface. The topography of the surface is derived from the plot of laser reflection versus the tip position on the sample surface. The AFM is capable of nanoscopic movements with high precision.

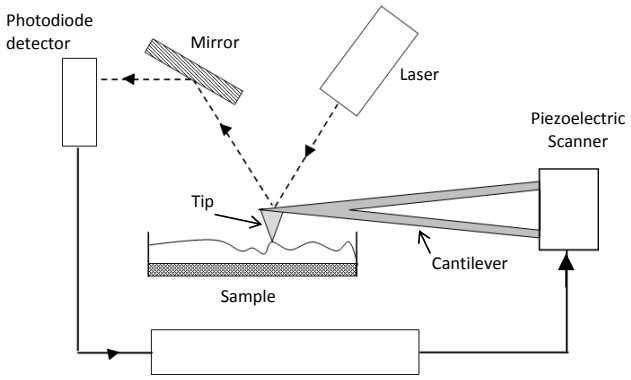

Figure 2.14: Schematic illustrating AFM characterisation (Chan and Chen, 2004).

There are three modes of measurements; contact, non-contact, and intermittent-contact mode. In the contact mode the tip comes into direct contact of the surface while the cantilever moves across. This enables high scanning speeds and atomic resolution images to be made. In the non-contact mode the tip does not physically touch the surface; the cantilever oscillates slightly above the surface. It responds only to the forces between the tip and the surface. This method is advantageous when soft and elastic materials are to be tested. The intermittent-contact (tapping) mode is similar to the non-contact mode although the probe is moved close to the sample. It involves making the cantilever perform constant vertical oscillations across the sample surface, 'tapping' it with a specified force (Chan and Chen, 2004). The advantages of this method are a higher lateral resolution on most samples, lower forces and less damage to soft samples (Väisänen, 2004). Tapping mode is operated for most AFM's today. Riedl *et al*. (1998a) and Riedl *et al*. (1998b) observed during the MF of apple juice that, membrane morphology was very important in the structure on the surface and flux resistance of the fouling layer. They found that smoother membranes produce a much thinner, denser fouling layer that has a higher flux resistance and forms more rapidly than the looser fouling layer observed on the rough membrane surfaces. Weis *et al.*, (2005) investigated the fouling of polyethersulphone and regenerated cellulose UF membranes with Spent Sulphite Liquor over multiple fouling and cleaning cycles. It was found that the rougher RC membranes, despite being more hydrophilic, had a greater tendency to resist adhesion over smoother yet more hydrophobic PES membranes.

2.5.4. Chemical Nature (ATR-FTIR)

Attenuated total reflection-Fourier transform infrared spectroscopy (ATR-FTIR) is generally used to understand the nature of the adhered deposits on a membrane surface and their structures. To comprehend the types of chemical bonds or functional groups present on a membrane surface. In this technique the infrared beam reflects inside of the internal reflection elements (IRE), which can be made of e.g. zinc selenide, KRS-5, diamond or germanium. The sample is pressed against an IRE surface and the infrared light penetrates to the surface. The beam of infrared light passes through the ATR crystal in such a way that it reflects several times and travels through the whole crystal creating a standing wave of reflections, known as an evanescent wave. With each reflection, certain wavelengths are absorbed by the sample. The analyses are thus based on the interaction between the evanescent wave and any adsorbed species. The angle and dimensions define the number of reflections of the IRE. The intensity of the spectrum is proportional to the number of reflections (Chan and Chen, 2004; Väisänen, 2004; Weis, 2004). A schematic diagram of the pathway through the crystal is shown in Figure 2.15.

The ATR-FTIR is a versatile and non-destructive technique that requires minimal sample preparation. It can give information on which functional groups appear and which disappear after fouling and cleaning on the membrane surface. Fontyn *et al*. (1991) used difference spectra of virgin and fouled membranes to identify foulants. Pihlajamäki *et al*. (1996) demonstrated that FTIR is a useful tool in analysing membrane material variation and surface porosity. The materials used in the manufacturing of Polysulphone UF membranes of different pore sizes were identified. The membranes of different pore sizes were found to be different, though conclusions could not be made based merely using the FTIR technique.

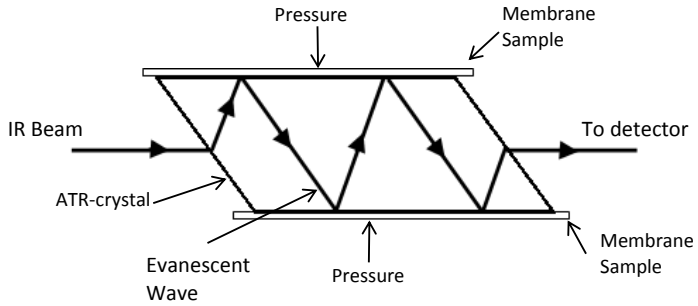

Figure 2.15: A schematic diagram of an ATR accessory (After Weis, 2004).

Väisänen *et al*. (2002) used FTIR spectra to reveal the foulants that were present and the changes in the foulant composition after cleaning (i.e. new peaks in the spectrum) when fouled with wood mill circulation water. For complex fouling mixtures analysing the data can be difficult. Some bonds and functional groups absorb at the same frequency, which can cause overlapping of spectra peaks. Nystrom *et al*. (1994) had difficulties identifying the foulants when ultra-filtering a mixture of lactoferrin and BSA with a 100 kDa MWCO regenerated cellulose membrane. The difficulties transpired as the membrane contained OH groups that showed peaks in the same wavenumber ranges as protein peaks.

2.5.5. Summary

Zhu and Nyström (1998) demonstrated that the use of a number of tools should be used to obtain a clear representation on the fouling and cleaning mechanisms during filtration. The influence of chemical cleaning on protein fouled UF was investigated and the results were characterised by flux, streaming potential and FTIR measurements. Väisänen *et al*. (2002) also demonstrated that a combination of techniques; flux recovery, SEM, FTIR and AFM can provide a complete description of fouling and cleaning mechanisms. These studies showed that rather than using one characterisation technique, a combination of several is much more effective.

2.6. Current Characterisation of Fouling on Membranes

The phenomenon of membrane fouling has been studied extensively by many authors using a variety of techniques to try and understand the following three regions; (i) the membrane, (ii) the fluid boundary layer and (iii) the bulk fluid in the membrane module (Chen *et al*., 2004b). Design to mitigate or minimise fouling and promote cleaning is complicated by the variety of fouling mechanisms that can arise. Therefore, a fundamental understanding of fouling mechanisms is of paramount importance. *In situ* methods are preferable because they allow deposition or blockage to be monitored without moving the sample from its original position. Chen *et al*. (2004a, 2004b) reviewed progress on methods for *in situ* observation of membrane processes classified these into two categories: optical techniques and non-optical probes. The former provides real-time observation of membrane fouling at the surface using high magnification cameras and provide information that can be used to identify suitable

design parameters. Optical methods include; DOTM (Direct observation through membrane), Laser triangulometry, Optical shadowgraph, Refractometry techniques, Photo-interrupt sensors, and Fluorescence techniques. Non-optical probes are used to investigate angstromic, micron, and macro level. These include ultrasonic reflectometry, laser sheets and magnetic resonance imaging (MRI). Details of some of these techniques are described in the following sections.

2.6.1. Direct observation techniques

The simplest method to directly observe particle deposition is visualisation by an optical microscope. The direct observation through the membrane (DOTM) technique was first developed to observe particle deposition during the crossflow MF process. DOTM is a powerful technique for the study of fundamentals of particle deposition and interactions between the particles and the membrane. A DOTM set up includes an optical microscope with both transmitted and reflected light source options. With the selected magnification of the microscope and CCTV video camera attached to the microscope with the transmitted light source (Chen *et al*., 2004b). This enables particles larger than 1 μm to be identified. Li *et al*. (1998) first published the DOTM technique, whereby a microscope and video camera assembled above a cross flow filtration test cell, in which the permeate flowed upwards through a transparent alumina membrane. This allowed fouling to be viewed from the underside of the membrane. Li *et al*. (1998) observed that it is more likely for particles to deposit on the membrane surface where other particles had deposited; that the particles in the cake layer are smaller at higher crossflow velocities. This work was extended by Li *et al*. (2000) where DOTM was used to observe the deposition of super micron particles (3 – 12 μm) on MF membranes and to identify the critical fluxes for cake formation as a function of crossflow. The observed critical fluxes were compared with various prediction models. According to Chen *et al*., (2004a, 2004b) the major disadvantages of the DOTM technique described above are the need to use a relatively transparent membrane and the requirement of a relatively clear feed solution. This confines the use of the technique to only a limited number of MF inorganic porous membranes. Another limitation is the positioning of the microscope objective below the membrane at the permeate side and does not allow the observation of particle accumulation beyond a monolayer.

Zhang *et al*. (2010) developed an improved method combining the mass balance and the DOTM technique. The mass balance equation was modified to enable the estimation of the critical flux using the rate of surface coverage obtained from the DOTM images. The critical fluxes obtained using this method were independent of the operation time as the deposition rates were always zero, and therefore were more accurate than the 'standard' DOTM measurements which typically include uncertainties due to the finite flux steps.

2.6.2. Laser Triangulometry

Throughout membrane filtration, laser triangulometry can be used to track the growth of a particle cake layer and to measure the thickness of the cake layer. The principle of the technique is based on the reflection of laser light shone towards the membrane surface through a window in the feed side of a crossflow membrane module. The reflection of the laser beam off the surface is captured by a CCD camera. With the build-up of a cake layer, the reflection of the laser light from the cake layer is deflected from the central position (reflection of the laser light on the clean membrane); the distance of the reflected light shift on the imaging plane can be used to estimate the thickness of the cake layer (Chen *et al*., 2004a, 2004b; Altmann and Ripperger, 1997). Altmann and Ripperger (1997) applied a laser triangulometer to measure the cake layer height *in situ* under various filtration conditions. They used a commercial laser triangulometer during the crossflow MF of diatomaceous earth and silica particles. The study provided valuable information on polarisation profiles and cake thickness, but little information on the phenomena occurring at the membrane solution interface as particles deposit.

Hamachi and Mietton-Peuchot (1999, 2001) developed a different technique whereby a laser device was used to measure deposit thickness of a bentonite suspension. It is based on a He-Ne laser beam and an optical captor, which relies on the absorption of light by the deposit. Where the formation of the deposit on the membrane surface translates into absorption of light, the image of the focal point is picked up on a photomultiplier; this allows an immediate measurement of the signal. The deposit thickness is a direct correspondence to the variation of the intensity of the signal. This method is limited by the concentration of the suspension and the pixel resolution of the CCD sensor and zoom lens capability which affects the measurement resolution (Güell *et al*., 2009).

2.6.3. Refractometry Techniques

Refractometry is, in principle, similar to shadowgraphy in that the refractive index gradient within the cell causes deflection of light, which is related to the concentration gradient in the polarized layer (Chen *et al*., 2004a). A number of Refractometry techniques have been developed to measure concentration polarisation of dissolved species near a membrane surface. These include using a laser based differential refractometric method (Gowman and Ethier, 1997).

2.6.4. Ultrasonic Time-domain Reflectometry

Ultrasonic time-domain reflectometry (UTDR) is a technique that uses sound waves to measure the location of a moving or stationary interface and can provide information on the physical characteristics of the media through which the waves travel (Chen *et al*., 2004a). Bond *et al*. (1995) first described use of UTDR to study membrane fouling and compaction with high-frequency transducers. This technique was then applied by Mairal *et al*. (1999) for *in situ* measurement of membrane fouling during reverse osmosis of calcium sulphate solutions. This technique was then further investigated by Li *et al*. and colleagues for the detection of fouling layers on flat sheet surfaces (Li *et al*., 2002, 2003; Sanderson *et al*., 2002). Li *et al*. (2003) utilized the UTDR technique to monitor fouling during UF of paper mill effluent. The results showed a good correlation between the ultrasonic response signals and the development of the fouling layer on the membrane surface. More recent reports of this group's work have described the ability of real time UTDR for detection of the fouling layers on hollow fibre membranes (Li *et al*., 2006) and tubular UF membranes (Li *et al*., 2006). Silalahi *et al*. (2009) also used UTDR to explain the mechanism of fouling which occurs during crossflow MF due to the effect of particle size. The study demonstrated that the UTDR technique can be used to show the effect of emulsion size on fouling mechanisms observed during membrane filtration of water containing oil emulsions. Silalahi *et al*. (2009) observed that the cake layer formation followed by adsorption dominated when the particle size distribution was above the nominal membrane pore size, whereas adsorption and compaction occurred in the range below and above the membrane pore size. The UTDR technique is one of the limited non-invasive methods that could be applied to commercial-scale modules (Chen *et al*., 2004b). However, the drawback of the UTDR technique is that

the implementation is complex, and relies on a number of assumptions about the properties of both the foulant and the medium.

2.6.5. Nuclear Magnetic Resonance Imaging

Airey *et al*. (1998) used nuclear magnetic resonance (NMR) micro-imaging to investigate the concentration polarisation phenomena in membrane filtration of colloidal silica suspensions using a single tubular MF membrane. Phase sensitive NMR flow imaging was used to map the 1D distribution of the feedstock crossflow on the lumen side of the membrane as well as measuring the axial flow profile within the concentration polarisation layer itself. The polarisation layer was observed to be highly asymmetric, being much thicker at the bottom of the module than at the top. NMR imaging can be used for flow profiles, cake deposition, and the local concentration can theoretically be determined from calibrated relaxation times. The applications of the NMR technique in membrane systems are limited by the size restrictions or "field of view" provided by conventional imaging apparatus, another disadvantage if the equipment itself is very costly and energy intensive (Chen *et al*., 2004b).

2.6.6. Summary

The optical techniques provide real-time observations using high magnification cameras to record membrane fouling at the surface providing information that can be used for suitable design parameters. A disadvantage of these methods is that they require a specially designed membrane cell and are restricted to specific membranes. Industrial applications for non-invasive probes for membrane processes require fast data analysis and ease for on-line monitoring, whilst research applications often require high resolution and quantitative answers. These methods also are expensive and require skilled operators. It is therefore difficult to use these methods in a larger-scale experimental setup (Chen *et al*., 2004a, 2004b). A simple, low-cost and reliable technique for *in situ* detection of the layer thickness is still desirable (Lister *et al*., 2011). A possible solution is the use of a technique known as Fluid Dynamic Gauging, which is the focus of this study and discussed in detail in section 2.7.

2.7. Fluid Dynamic Gauging (FDG)

2.7.1. Introduction

Fluid Dynamic Gauging (FDG) is a technique that has application in the measurement of the thickness and deformation behaviour of soft fouling layers deposited on a substrate, such as whey proteins, food fats, crude oil and bio films. It was pioneered by Tuladhar *et al*. (2000), where a theoretical model of performance was developed and its validity demonstrated. The inspiration of the gauge came from pneumatic gauging (Gale, 1995). Pneumatic gauging features an air jet moving outwards from a nozzle fixed perpendicular to the surface to be gauged. As the nozzle approaches the surface the pressure profile is altered by the presence of the surface and this can be used to detect the distance, as the location of the 'clean' surface is known. Bridge *et al*. (2001) reported that pneumatic gauging was unsuitable for measuring fragile deposits, especially for deposits that might shrink or slump if they are removed from their liquid environment. The gauge was therefore modified by having the process fluid sucked into the nozzle and imposing a fixed pressure drop while measuring the mass flow rate, now known as Fluid Dynamic Gauging. This results in the following features (Tuladhar *et al*., 2000):

(i) Thickness determined simply by measuring discharge flow rate ,
(ii) Easy to install and operate,
(iii) Sophisticated equipment not required and can be built cheaply,
(iv) Avoids introduction of foreign matter due to siphon effect,
(v) Data generated rapidly,
(vi) Can be used as a sampling device.

The work in this study is a further extension of this technique developed by the research group at Cambridge University. A summary of the previous FDG research is presented in Table 2.5. Further details of the different configurations of the FDG can be found in section 2.7.3.

Table 2.5: Summary of FDG work performed since invention. Selected publications

Year	Study	Researcher
1997	Initial development of Fluid Dynamic Gauging	Tuladhar *et al.*
2000	Development of a novel non-contact proximity gauging for thickness measurement of soft deposits and its application in fouling studies	Tuladhar *et al*.
2002	Thermal conductivity of whey protein films undergoing swelling – measurement by dynamic gauging	Tuladhar *et al*.
2003	Dynamic Gauging in duct flows	Tuladhar *et al*.
2004	Computational fluid dynamics studies of dynamic gauging	Chew *et al*.
2004	Fluid Dynamic Gauging for measuring the strength of soft solid deposits	Chew *et al*.
2006	Solvent-based cleaning of emulsion polymerization reactors	Chew *et al*.
2006	Development of a novel micro-scale technique for monitoring food proteins undergoing cleaning	Hooper *et al*.
2007	Swelling and its suppression in the cleaning of polymer fouling layers	Saikhwan *et al*.
2007	Fluid Dynamic Gauging: A new tool to study deposition on porous surfaces	Chew *et al*.
2009	Experimental and CFD studies of Fluid Dynamic Gauging in annular flows	Gu *et al*.
2010	The application of the Fluid Dynamic Gauging in the investigation of synthetic membrane fouling phenomena	Jones *et al*.
2010	A scanning Fluid Dynamic Gauging technique for probing surface layers	Gordon *et al*.
2011	Fluid Dynamic Gauging applied to the annular test apparatuses for fouling and cleaning	Gu *et al*.
2011	Pressure mode Fluid Dynamic Gauging for studying cake build-up in crossflow microfiltration	Lister *et al*.
2011	An analytical method for selecting the optimal nozzle external geometry for Fluid Dynamic Gauging	Peralta *et al*.
2012	Fluid Dynamic Gauging of microfiltration membranes fouled with sugar beet molasses	Jones *et al*.

2.7.2. Principles and Theory

Using FDG measurements can be made *in situ* and in real time. The principle of the device is shown schematically in Figure 2.16. The detailed theoretical development can be found in Tuladhar *et al*. (2000), here an outline of the device will be given. The technique features a fully submerged gauging nozzle, held normal to the gauging surface at clearance, *h*. The technique exploits the flow characteristics of the liquid as it is drawn by suction from the surrounding reservoir (1) through the nozzle and hence

through the tube (4). A pressure difference, ΔP_{14}, is set up between the liquid near the surface and the discharge end of the gauge, so that the fluid flows into the nozzle. For a *fixed suction pressure*, the mass flow rate of the process fluid, *m*, flowing into the nozzle is strongly dependent on *h* (Tuladhar *et al*., 2000). By measuring the mass flow rate of gauge discharge, the distance between the nozzle and the deposit layer, *h*, can be calculated. For a *fixed gauging flow* rate the pressure drop across the nozzle is sensitive to the distance between the nozzle and the surface, *h*, so that *h* may be obtained from knowledge of this pressure difference and the flow rate. By combining this with a suitable displacement measurement to gauge the location of the underlying membrane surface, h_o, the deposit layer thickness, δ, can be determined from Equation 2.23. Any changes in the deposit layer thickness resulting from cleaning or further deposition are monitored.

$$\delta = h_0 - h \qquad 2.23$$

The total pressure drop across the nozzle and the tube can be seen in Equation 2.24.

$$\Delta P_{14} = \rho g H = \Delta P_{12} + \Delta P_{23} + \Delta P_{34} \qquad 2.24$$

Assuming that the flow through the siphon tube is fully developed, the pressure drop in the tube is governed by the Hagen-Poiseuille, Equation 2.25.

$$\Delta P_{34} = \frac{32 \mu \upsilon_c l_{eff}}{d^2} \quad = \frac{128 l_{eff} \mu m}{\rho \pi d^4} \qquad 2.25$$

The effective length, l_{eff}, is defined as the length of a hypothetical straight tube which would support the same pressure drop as the actual tube when subjected to the same flow rate. The effective length is determined by separate experiments, for which the nozzle had been removed from the tube, performed at high values of *h*. The equation for l_{eff} is Equation 2.26.

$$l_{eff} = \frac{\rho^2 gH\pi d^4}{128\mu m} \qquad 2.26$$

In the gauging experiment, when the nozzle approaches the surface the gauged surface has an effect on the flow pattern. Therefore the clearance (ΔP_{12}) and nozzle (ΔP_{23}) pressure drops are grouped together as ΔP_{13}, Equation 2.27.

$$\Delta P_{13} = \Delta P_{12} + \Delta P_{23} = \rho gH - \Delta P_{34} \qquad 2.27$$

For a small clearance, the flow pattern through the nozzle is complex and affected by the proximity of the gauging surface, described by the discharge coefficient, C_d (Chew, 2004). For design purposes the discharge coefficient is used to quantify the performance of the nozzle. C_d accounts for the energy losses due to the flow near the nozzle entrance, and is defined as the ratio of the actual to ideal mass flow rate through the nozzle, *viz*, defined by Equation 2.28.

$$C_d = \frac{m_{actual}}{m_{ideal}} = \frac{m}{\frac{\pi d_t^2}{4}\sqrt{2\rho\Delta P_{13}}} \qquad 2.28$$

where:

$$\Delta P_{13} = \Delta P_{14} - \Delta P_{34} = \rho gH - \frac{128\mu m l_{eff}}{\pi d^4 \rho} \qquad 2.29$$

When the distance between the stiff surface and the gauging nozzle, *h*, is small, such that h/d_t is less than 0.25, the mass flow rate through the nozzle, *m*, is very sensitive to the value of *h* and the measurement of *m* may therefore be used to locate the position of the surface in space (Chew *et al*., 2004a). An example of how to calculate the thickness deposit can be seen in Appendix C5. A nozzle size of 5 mm gives cake thickness measurements with an accuracy of ± 50 μm. A geometrically similar nozzle, with d_t = 1 mm (the size used in this project), has been shown to give an accuracy of ± 10 μm (Chew *et al*., 2007).

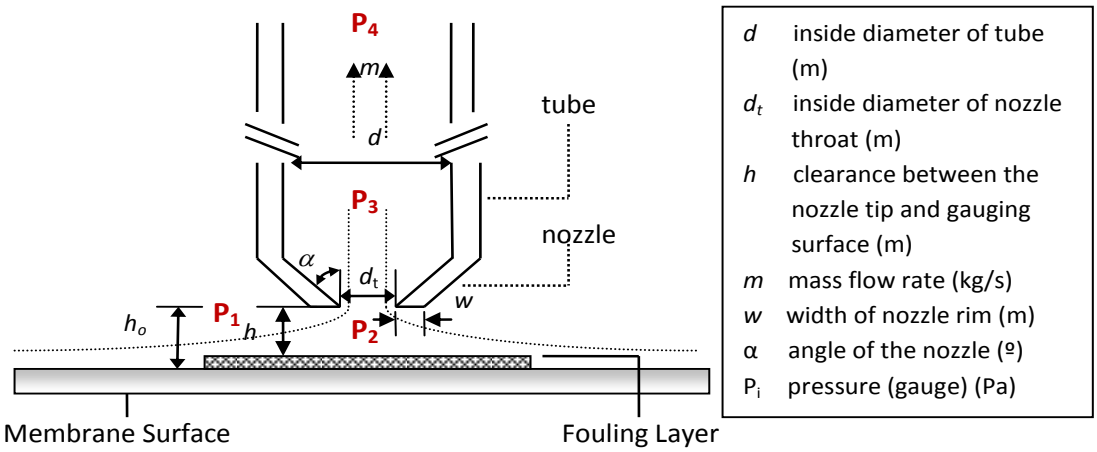

Figure 2.16: Schematic of a typical gauging nozzle showing dimensions (after Chew *et al*., 2007).

2.7.3. Fluid dynamic systems

FDG was developed by Tuladhar *et al*. (2000, 2002a), where the gauge was operated in quasi-stagnant mode and within a duct system. Since its invention the FDG has been advanced to a series of studies which are summarised in Table 2.5 and discussed in section 2.7.3.1 to 2.7.3.3.

2.7.3.1. Quasi-stagnant Gauging

A typical apparatus for quasi-stagnant gauging can be found in Chapter 3.5, Figure 3.7. In the quasi-stagnant mode the gauging flow maintained by a siphon effect is the only significant fluid movement. This mode of gauging was first employed by Tuladhar *et al*. (2000), which was then developed for a number of applications. Chew *et al*. (2004a) applied the dynamic gauging technique to measure the thickness of soft solid deposits (dried tomato paste) on surfaces *in situ* and to quantify the removal behaviour of these materials. The extent of removal was deduced from the thickness calculations, and the shearing yield strength from CFD simulations. The results demonstrate the potential of this technique in determining the stresses required to remove deposits from surfaces, providing valuable information on the mechanical properties of the deposit in fouling and cleaning studies (Chew *et al*., 2004a, 2004b). Chew *et al*. (2005a) used the same FDG rig to study the adhesion of calcium sulphate scales on roughened stainless steel plates and reported the expected increase in adhesion with roughness. Saikhwan *et al*. (2006) varied this work investigating the effect of surface modification of stainless steel on the removal of baked tomato paste; both the surface morphology and energy were

characterized and related to FDG studies. Hooper *et al*. (2006b) used a more compact version of the device used by (Chew *et al*., 2004a) to determine the strength and deformation behaviour of soft-solid fouling layers on hard surfaces immersed in liquid. The FDG techniques and micromanipulation were related directly in parallel studies of removal of baked tomato puree deposits from stainless steel surfaces. Hooper *et al*. (2006a) then reported the benefit of using the FDG as a sampling device: where the liquid withdrawn through the gauge can be taken from the 'boundary layer' of fluid above the deposit layer. This enabled them to track the evolution of solubilised protein over time.

A FDG rig was specially designed for processing solvents (Chew *et al*., 2005b, 2006). FDG has been applied successfully to study the fouling and cleaning mechanisms in the cleaning of emulsion polymerization reactors (Chew *et al*., 2005b). Chew *et al*. (2006) then used FDG on various solid surfaces to study the kinetics of the cleaning, of polymer layers representative of polymerization reactor foulants on laboratory test sections and in an industrial pilot plant. Saikhwan *et al*. (2007) advanced these works into a more detailed study investigating the swelling and cleaning behaviour of layers of a non-cross-linked acrylate-styrene copolymer, simulating fouling layers found in emulsion polymerization reactors, in aqueous NaOH. The findings from cleaning of composite layers can provide useful guidance for solvent selection, reactor operation and cleaning scheduling (Chew *et al*., 2006).

Chew *et al*. (2007) adapted the previous rigs used by Chew *et al*. (2004a) and Hooper *et al*. (2006b) to allow the measurement of particle fouling during dead-end filtration. The FDG apparatus generated thickness information of the filtration cake and the permeate flux simultaneously. This initial study into using FDG on permeable surfaces demonstrated the potential for FDG to generate useful data in membrane systems. This has led to this study on the application of FDG in the investigation of dead-end and crossflow filtration for MF membranes and further studies by Chew *et al*. research group (Chew *et al*., 2010; Lister *et al*. 2011).

Gordon *et al*. (2010a, 2010b) further adapted the quasi-stagnant systems to include a scanning mode. An automated, scanning FDG probe (sFDG) was developed which

allows the thickness of a sample layer to be monitored at several points during an experiment. Gordon *et al*. (2010a) demonstrated the performance of the sFDG using gelatine, PVA and baked tomato purée deposits. Gordon *et al*. (2010b) studied the cleaning kinetics of model gelatine fouling layers when contacted with aqueous solutions at different pH and temperatures. Thickness-time profiles were collected for several points in the surface over the course of a single experiment. The sFDG holds great advantages to the future development of FDG as more information is gathered, therefore reducing the number of experiments needed to be performed.

2.7.3.2. Duct Flow Gauging

Tuladhar *et al*. (2002a) first published the application of FDG in duct flow; where the behaviour of layers of soft material undergoing cleaning in flowing liquids, *in situ* and in real time was investigated. The technique was used to study the swelling and removal of whey protein films related to cleaning-in-place of dairy heat exchanger fouling deposits. Tuladhar *et al*. (2002b) also combined the techniques of FDG with heat flux sensors to monitor the process of swelling and removal of whey protein deposits by alkaline cleaning in place (CIP). The thickness measurements provided by the gauging technique allowed the swelling behaviour and thermal conductivity of the protein deposits and gels to be measured directly. Hooper *et al*. (2006a) advanced these studies to compare whey protein model foulants for studying cleaning of milk fouling deposits. A duct flow system with resistance measurements was used and compared to results in quasi-stagnant conditions. Gu *et al*. (2009a) was then able to use computational fluid dynamics to simulate FDG in a duct flow system for steady, incompressible, laminar flows. CFD simulations predicted the stresses beneath the nozzle and confirmed the practical working range of the gauge ($0.10 < h/d_t < 0.25$).

The work of Gu *et al*. (2009a) led to the development of a FDG technique for application to annular flow sections for studying fouling and cleaning in heat exchangers (Gu *et al*., 2009b, 2011a, 2011b). Gu *et al*. (2009b) demonstrated that the technique of FDG can work effectively for a curved surface (inner convex surface of an annulus). Experiments in the turbulent regime revealed three characteristic zones instead of the typical two, namely ‘‘curvature,’’ ‘‘incremental,’’ and ‘‘asymptotic,’’ of which the ‘‘curvature’’ zone is new to the current (curved) geometry (Gu *et al*., 2009b). This work was extended by Gu *et al*. (2011a) to include results in the laminar and

transitional annular flow regimes. FDG was successfully applied for different annular geometries and for a heated surface at various wall temperatures. Gu *et al*. (2011b) then compared this work with the results gathered using the *fixed gauging flow* method (discussed in section 2.7.3.3). This new mode of measurement was shown to perform similarly well. Gu *et al*. (2011a, 2011b) found that the calibrations obtained for a heated surface, at various wall temperatures, confirmed that FDG can be used with a heated surface as employed in fouling test systems.

2.7.3.3. Pressure-mode FDG

In the duct flow gauging discussed above there are two pressure driving mechanisms operating: (i) a fixed hydrostatic suction head and (ii) a pressure associated with flow in the duct. These establish a pressure difference which induces fluid into the nozzle (known as *fixed suction pressure* mode). In this study a new mode of operation is employed (*fixed gauging flow*) where the gauging flow (m) is fixed and the gauging pressure (ΔP_{14}) measured. The new mode has also been demonstrated by Lister *et al*. (2011) for a duct flow system and Gu *et al*. (2011b) for an annular system. Lister *et al.* (2011) reported the successful use of FDG to investigate particulate deposition of glass ballotini onto cellulose ester MF membranes at low TMP. CFD simulations were performed and showed good agreement with experimental data.

This new mode of operation is advantageous as the amount of liquid withdrawn from the bulk system can be controlled by a valve so it doesn't affect the filtration process. Controlling the gauging flow also allows for higher working pressures and improved control of the applied shear stress on the fouling layer.

2.8. Spent Sulphite Liquor

Spent Sulphite Liquor (SSL) is a by-product of chemical pulp production and contains mainly sulphonated lignin (called lignosulphonates), cooking chemicals (such as magnesium sulphate) and various sugars (such as pentose). Phenols, like humic acids, are also important foulants in water purification (Weis *et al*., 2003). Lignin in wood is a randomly cross-linked sheet-like polymer, encrusting the cellulose fibres (Myrvold, 2008). This separation process was selected for study, as the University of Bath have experience dealing with this feed and the phenolic compounds present are relatively

well understood. SSL has always been a major concern to the paper industry for its disposal and any sort of recovery of its constituents. The paper industry is a major consumer of water and consumes around 0.1 million tons of water per ton of finished paper (Bhattacharya *et al*., 2005).

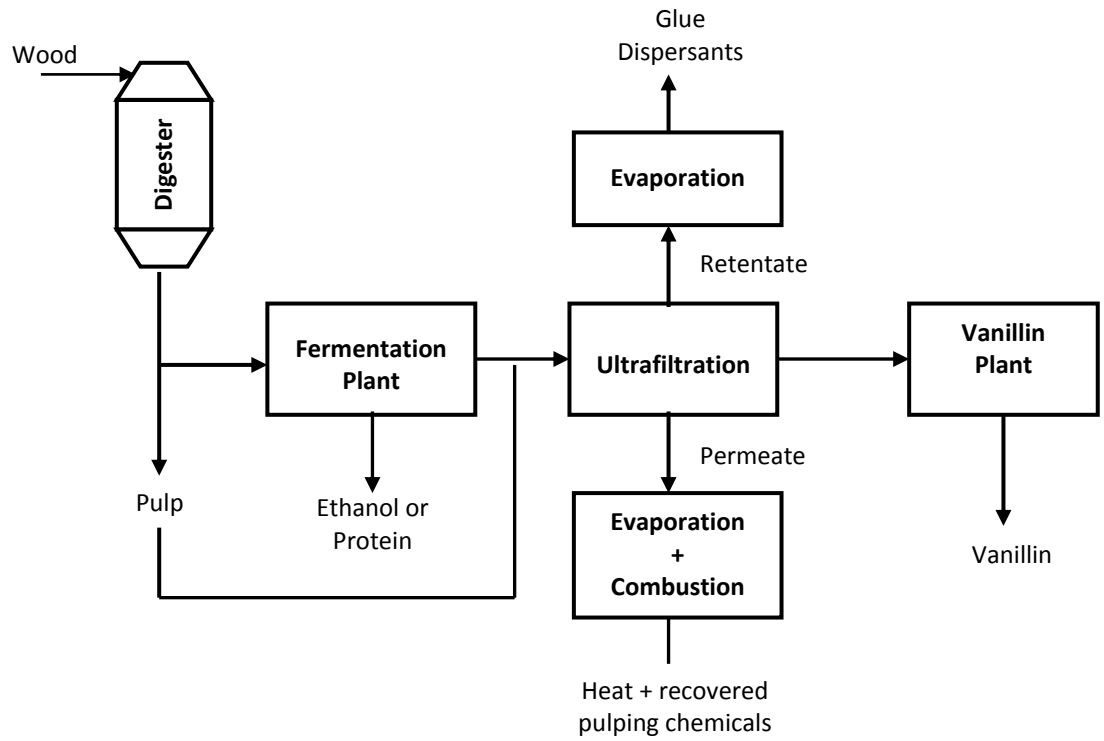

Figure 2.17: Processing of wood pulp (After Weis, 2004).

The steps for processing lignosulphonates are shown in Figure 2.17. The first stage of the wood pulp processing is the grinding of the tree trunks in the digester to make wood chips. The chips are boiled under pressure with an aqueous solution of magnesium sulphite to purify the cellulose contained in the wood by elimination of the matter that impregnates with the aim to extract the lignin between the cell walls and bring into the water-soluble form. In the process here this is done by the sulphite pulping process to produce lignosulphonates not the "Kraft" pulping process, which produces the Kraft-Lignin. After this cooking stage the cellulose can be removed through sedimentation and the remaining liquor can be fermented. The monosaccharide is ultra-filtered to recover the lignosulphonates (Casey, 1980; Britt, 1995). Lignosulphonates can then be used for the synthesis of Vanillin, which is one of the most important commercial flavours (Bjørsvik, 1999).

2.8.1. Membrane Separation with SSL

The use of membranes in the pulp and paper industry can be divided into three main sectors: (i) use of separation of valuable chemicals from effluent streams, (ii) pollution control and waste management, and (iii) resource saving e.g. energy, water (Weis, 2004). Fractionation of cooking liquor from sulphite pulp mills by UF has been studied since the 1970s (Claussen, 1978; Bar-Sinai and Wayman, 1976; Tsapiuk *et al*., 1989; Wallberg *et al*., 2001). The use of pressure-driven membrane filtration processes for applications such as the clarification of solids, protein isolation and sterilization has become a well-established technology. Claussen (1978) discussed the potential of effectively and economically using UF in the manufacture of lignosulphonates products from SSL. The pilot tests showed that the SSL filtration could operate at 80 ºC continuously for months with only slightly modified separation performance. Jönsson and Wimmerstedt (1985) then found that the total solids of SSL could be concentrated from 6 % to 12 % with a flux of 40 L $hr^{-1}m^{-2}$ by RO, and the membrane lifetime of more than a year was obtained with efficient membrane cleaning two to six times a week.

The optimal membrane cut-off during fractionation of SSL is not obvious due to the molecular weight composition of lignosulphonates (LS) being a polydispersed system with a wide range of MWs from 200 to 100,000 Da (Tsapiuk *et al*., 1989; Bhattacharya *et al*., 2005). Bhattacharya *et al*. (2005) observed that 80 % of LS present in SSL have molecular weights more than or equal to 100 kDa. The structure of LS can be seen in Figure 2.18; when a membrane with a tight cut-off is used, the lignin in the retentate has a greater purity, due to an increase in the fraction of the low molecular-weight compounds passing through the membrane. Though more low molecular-weight lignin compounds are lost in the permeate (Wallberg *et al*., 2003). Tsapiuk *et al*. (1989) found that when lignosulphonates filtration concentration and pressure are low the fractionation process yields LS fractions with a narrow molecular weight distribution. In contrast, when these values are high, the fractionation ability does not depend on the membrane properties, but is determined primarily by the self-retention properties of the gel layer formed from the high molecular weight fractions. When producing lignosulphonates from SSL, membranes with a MWCO of 20 kDa are typically used (Wallberg *et al*., 2003).

Weis and Bird (2001) and Weis *et al*. (2003, 2005) investigated the long term performance of UF membranes fouled with SSL. Weis *et al*. (2003) found that over the short term, the membrane material, its porosity, and surface roughness, were the dominant factors in determining the cleaning performance. Whereas, over the long-term, the surface became irreversibly fouled, and the physico-chemical interactions between cleaning agent and foulant were dominant, and the influence of the membrane material itself becomes less significant. Weis *et al*. (2005) demonstrated the importance of examining membrane performance over multiple fouling and cleaning cycles.

Recently Restolha *et al*. (2009) investigated the application of UF, NF and RO to filter the thin SSL generated in a Portuguese pulp and paper mill that uses acidic magnesium based sulphite pulping of *E. globulus*, for the separation of the lignosulphonates from the sugars. They found most of the UF/NF/RO membranes tested couldn't fractionate the lignosulphonates or even separate them from the sugars due to the overlap of the molecular weights of LS and sugars.

2.8.2. Purpose of using a Membrane Separation Process in this Project

The purpose of using membrane separations with SSL is to reduce the water content and concentrate the lignin (Lignosulphonates) from the sugars and salts to yield a high molecular weight fraction of lignosulphonates in the retentate. The high molecular weight fraction can be used to produce vanillin, stabilizers, detergents etc. (Weis and Bird, 2001). Many of the mechanisms that take place at the membrane surface and inside the pore structure during the separation are not fully understood, therefore further investigation is required. There is also a particular industrial interest in the effect of multiple fouling and cleaning cycle operations. The SSL feed will also be used to investigate the synergy of fouling and cleaning cycles.

2.8.3. Analysis of SSL at *Industria de Celulose S.A. Constância*, Portugal

The chemical composition of SSL from acidic magnesium-based sulphite pulping of *E. globulus* wood has been studied by the University of Aveiro for the specific feedstock used in this study (Evtuguin *et al*., 2008; Marques *et al*., 2009a; Marques *et al*., 2009b). Marques *et al*. (2009a) studied the three major groups of non-volatile liquor components (inorganics, lignosulphonates, and sugars) and extractives. Lignosulphonates were found to be the most abundant organic fraction of spent liquor (*ca.* 50 % of liquor dry

matter). Three main classes of low molecular weight extractives were detected and characterized: phenolic, fatty acids, and sterols. The SSL used contains a high proportion of carbohydrates (*ca.* 30 % of dry solids), which were mainly pentose sugar (more than 70 % of total sugars content). Approximately 70 % of xylose in SSL was present as monomeric sugars and *ca.* 30 % as xylo-oligosaccharides (Evtuguin *et al.*, 2008; Marques *et al*., 2009a).

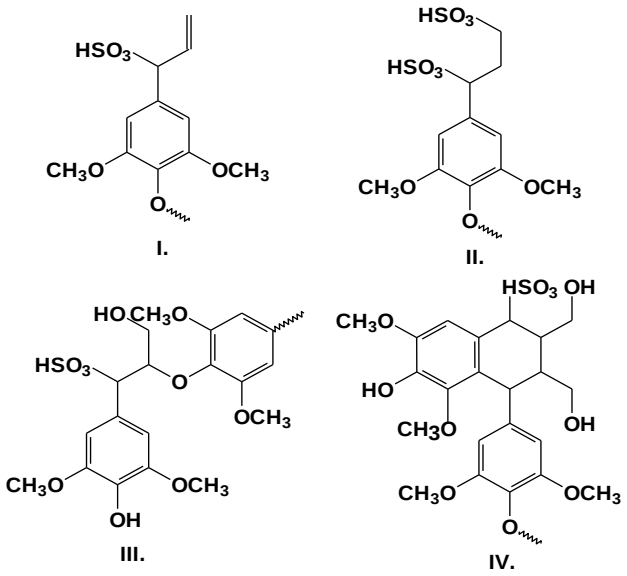

Figure 2.18: Structures detected in lignosulphonates (Evtuguin *et al*., 2008).

Weis (2004) discussed the role of lignosulphonates in the fouling process. The lignosulphonates were found to cause the majority of the fouling problems. It is therefore important to understand the chemistry and structure of lignosulphonates. Marques *et al*. (2009b) studied the structure of lignosulphonates. Four of the structures detected in lignosulphonates are presented in Figure 2.18. Marques *et al*. (2009b) identified more than ten types of lignosulphonates structures derived from different lignin structural units.

2.9. Molasses

Molasses is a thick syrup by-product from the processing of the sugarcane or sugar beet into sugar. The word molasses comes from the Portuguese word melaço, which comes from the Greek mellas, "honey" (McNulty, 1997). The molasses that is of interest here comes from sugar beet, which is different to that from cane molasses. Sugar was first

produced using sugar beets in the mid-1700s after a German chemist Andreas Marggraf discovered the presence of sugar in the vegetable. The process was perfected in 1793 by another German, Franz Karl Achard, and the first beet sugar factory was opened in the Prussian province of Silesia in 1802. By the end of 1813 there were 334 French sugar beet plantations. In the United States it was not until the end of the nineteenth centenary that it turned a profit with 30 beet sugar processing plants (Baikow, 1967; Curtin, 1983; McNulty, 1997).

In the sugar beet process (Figure 2.19), the beet roots are loaded into a flume where they are separated and washed. In the next stage the beets are sliced and loaded into cylindrical diffusers where the beet juice is washed away with hot water. This juice is clarified by adding milk of lime and carbon dioxide, heated and mixed with lime. The juice is then filtered, creating a mud like substance (carb juice). This carb juice is heated and clarified, causing the clear juice to rise and the mud to settle. The mud is filtered out, leaving a pale yellow liquid (thin juice). The juice is pumped into an evaporator which extracts the water until only syrup remains. This syrup is then concentrated through several stages of vacuum boiling (Lipnizki *et al*., 2006; Hinková *et al*., 2002; McNulty, 1997).

Molasses is only the syrup left from the final crystallisation stage; intermediate syrups are referred to as high green and low green. Any liquid feed ingredient that contains in excess of 43 % sugars is termed molasses (Curtin, 1983). Molasses typically contains 20 % water, 8 % inorganic matters, 72 % sugar and non-sugar organic substances such as organic acids, lipids and inorganic salts, invert sugar, macromolecules of high molecular weight (Kaur *et al*., 2002; Toğrul and Arslan, 2004). Molasses has traditionally been used as a major component in compound feeds and livestock feeds due to its physical and chemical properties. However, it is now also being more widely used in various industrial processes. Molasses is used in various industries, including food and drinks manufacture, fuels, rubber, printing, chemical and construction industries, alongside the traditional agricultural uses.

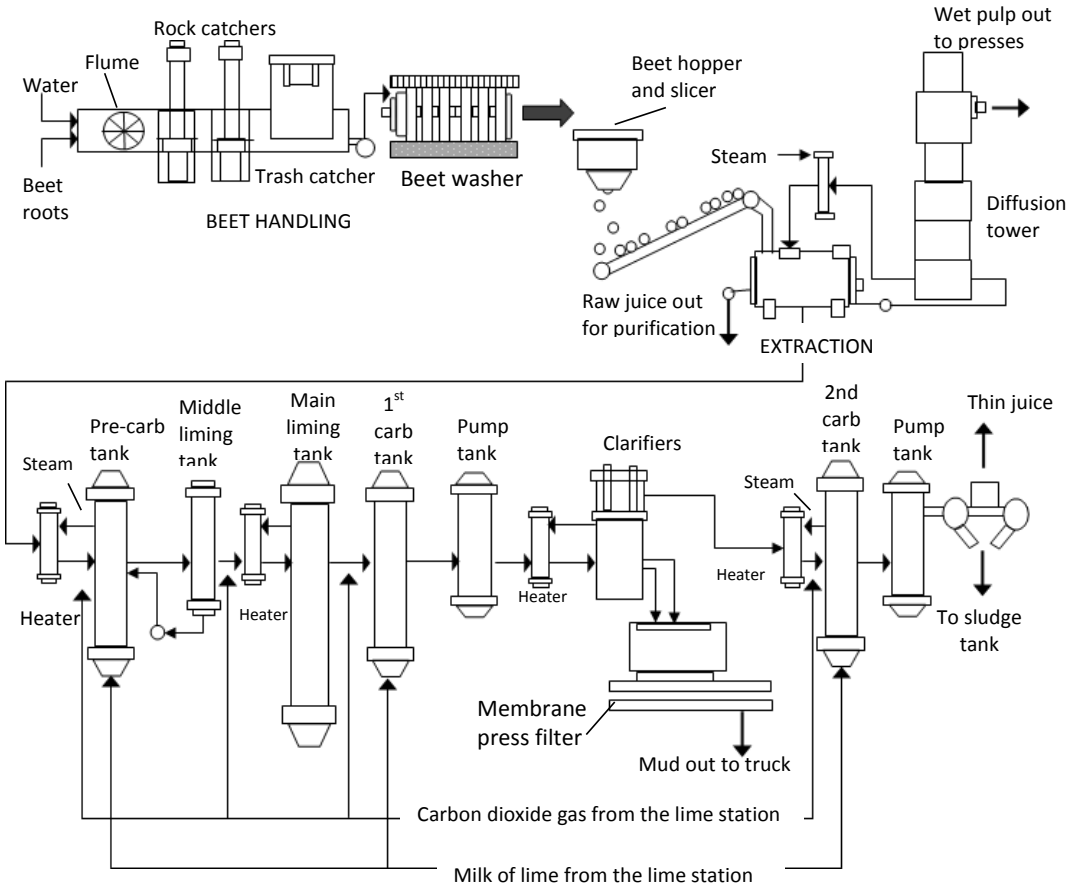

Figure 2.19: Molasses Manufacture (After McNulty, 1997).

2.9.1. Membrane Separation with Sugar and Molasses

Trägårdh and Gekas (1988) first reviewed and discussed the application of membrane technology in the sugar industry due to the development of newer membrane materials. Lipnizki *et al*. (2006) then reviewed more recent developments in the application of membrane processes in the beet and cane sugar productions. They discussed that while there are some successes; membrane technology has not established itself as a standard unit of operation in the sugar industry. There are currently limited studies on application of membrane process in the clarification of molasses. These studies are discussed in this section.

Non-sucrose compounds tend to build into the sucrose crystals during the crystallization. Removing the undesired compounds is one of the severe problems in sugar technology. The environmental pollution needs to be addressed as well, since energy consumption of sugar production is high (200 – 300 kW/h beet) (Ŝereŝ *et al*., 2006). A membrane separation technique could be inserted in the existing technology

process of sugar production to combat these issues. Saska and Lataillade (1994) reported on the concentration and decolourisation of dilute products from cane molasses desugarisation using RO and NF membranes. Vercellotti *et al*. (1998) investigated the effect of the clarification processes for cane sugar and molasses using synthetic organic membranes, ceramic colloidal and ultrafilters. They studied the colloidal chemistry of the molasses retentate which indicated that the affinity of the natural components producing very high molecular weight aggregates. These aggregates are implicated in membrane fouling and decrease in flux and throughout.

Decloux *et al*. (2000) found that the filtration of raw cane sugar syrup and diluted molasses through 20 kDa membrane removes 91 % of the turbidity and 40 % of colour. MF (between 0.1 μm and 1.4 μm pore size) achieved good clarification but poor decolourisation of the permeate. Decloux *et al*. (2000) also demonstrated that in order to obtain reliable decolourisation using UF, precautions must be exercised in colour analysis and in application of operating conditions. They concluded that temperature was the most important factor and best decolourisation was obtained at 60 ºC, with a 3 bar TMP and 2.5 ms^{-1} CFV using 15 kDa MWCO. Hamachi *et al*. (2003) found the opposite, that temperature actually does not have any appreciable effect on decolourisation, but only the permeate flux increased with the increase of temperature. It was also found that for a given membrane pore diameter, the changes of TMP and the cross flow velocity values do not have appreciable effect on the colour removal. This indicates that the removal of colour components is simply a pore size exclusion effect. The application of UF and NF in the sugar industry is to a great extent hindered by the occurrence of membrane fouling and concentration polarisation caused by non-sucrose compounds. The composition and the amount of non-sucrose compounds depend on sugar-beet quality and the technology involved (Gyura *et al*., 2005).

Mousavi and Moghadam (2009) used UF and NF membranes to filter diluted molasses. The ultrafilters were found to be unsuitable for the desugarisation of molasses but decolourisation did occur. The NF membranes were more successful in terms of sugar rejection and decolourisation. Steindl and Rackemann (2010) concluded that membranes can remove polysaccharides, turbidity and colloidal impurities. This caused a lowering in the molasses viscosity (Steindl, 2001). Steindl and Rackemann (2010)

then assessed the operation and performance of two membrane plants utilising a range of UF and MF membranes. The membrane filtration of clarified juice led to improvements in downstream processes including an increase in crystal growth rate of 15 to 23 % resulting from the reduction in viscosity of the syrup by 15 to 20 %. The lower viscosity and higher growth rates of the syrups also result in the production of sugar of lower colour (~ 40 %), reduced ash levels (~ 35 %) and higher filterability (~ 17 %).

2.9.2. Purpose of using a Membrane Separation Process in this Project

Molasses is a thick syrup by-product from the processing of sugar beet into sugar and contains mainly: (i) sugar, (ii) water and (iii) inorganic matter (crystalline and dissolved calcium sulphate, calcium oxalate monohydrate and calcium oxalate dihydrate). The purpose of membrane separation in this study was the clarification of molasses to protect the downstream process, e.g. precipitation, and chromatography. This required the removal of the crystals, calcium sulphate, calcium oxalate, and calcium oxalate monohydrate. MF offers the possibility of separating the crystalline material (retained in the retentate) from the sugar and divalent ionic species (passed through to the permeate stream). This is of commercial relevance, as the clarification of molasses protects downstream processes such as precipitation and chromatography. The presence of undesired compounds is one of the most severe problems in the sugar industry (Šereš *et al*., 2006).

The molasses should be used at as low a dilution rate and as high a temperature as possible. The molasses can be experimented on to temperatures as high as 80 ºC without any changes to the properties. The molasses cannot be used in delivered form as the viscosity is too high for pumping around the circuit and for effective separation.

2.9.3. Analysis of Molasses by Nordzucker (2008)

An investigation was made by Nordzucker (2008), *Nakskov*, Denmark, to identify the composition of insoluble solids in the molasses used in this study. The investigation showed that the insoluble solids in the molasses comprised of calcium salts of oxalate, sulphate, citrate and phosphate. The crystals in the molasses feed (Figure 2.20) were judged as calcium sulphate; in the photo they can be seen to be 1 - 6 µm wide and 5 – 20 µm long. The crystals judged as calcium oxalate dihydrate are 1 - 2 µm square,

calcium oxalate monohydrate are 1 - 2 µm wide and 5 - 6 µm long. In the retentate there is an absence of calcium sulphate.

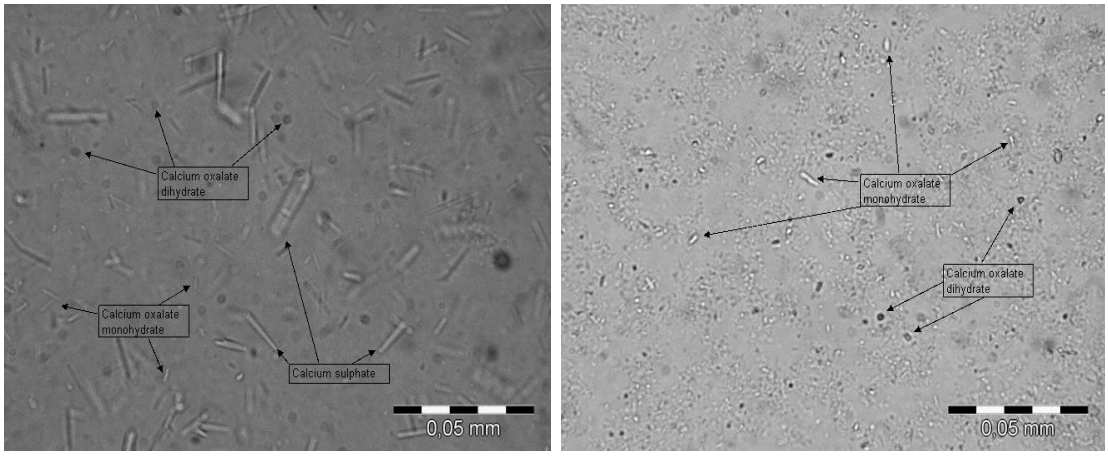

Figure 2.20: Microscope photo of particles in 78 °Brix molasses feed (left), 50 °Brix sediment from molasses retentate (Right).

2.9.4. Viscosity of Molasses

Knowledge of the rheological behaviour of molasses is important as it provides information on its physical properties and assists in understanding the fundamental mechanisms of momentum and heat transfer (Kaur *et al*., 2002). Kaur *et al*. (2002) found that the viscosity of molasses varies with the nature and amount of non-sucrose present in it, that the viscosity of molasses increases with the increase in total solids. Kaur *et al*. (2002) also found starch to be one of the constituents of molasses that result of deterioration as it comes under the category of complex organic non-sugar of high molecular weight.

The rheological behaviour of molasses was studied by Toğrul and Arslan (2004), and it was found that molasses showed pseudo plastic characteristic (shear-thinning), where there was a high linear correlation coefficient for the dependence of viscosity on temperature. Toledo (1991) also indicated a shear thinning behaviour of molasses, which can exhibit non-Newtonian and Newtonian behaviour. Toğrul and Arslan (2004) also developed mathematical models for the prediction of the apparent viscosity of molasses containing ethanol as a function of ethanol concentration and temperature. These models can be useful for designing equipment for engineering applications concerning molasses.

2.10. Summary

This chapter dealt with the process and design considerations which occur when studying the fouling and cleaning of synthetic membranes with industrially relevant feeds. The basic principles of membrane separation processes have been discussed and the consideration of the available literature has identified the key parameters. It has been recognised that changing one fouling parameter can require several of the additional parameters to be altered in order to reduce fouling (Vigneswaran and Kiat, 1988; Väisänen, 2004). The chemical, thermal and physical resistance of membranes were identified as the limiting factors in both the filtration process and the cleaning process.

It is difficult to separate the effects of filtration and cleaning upon the membrane life expectancy. Fouled membrane surfaces can be characterised using the following techniques: (i) streaming potential measurements, (ii) Fourier Transform Infra-Red (FTIR) spectral peak height analysis, (iii) Scanning electron microscopy (SEM), (iv) Atomic force microscopy (AFM), and (v) contact angle measurements.

A fundamental understanding of fouling mechanisms is of paramount importance. *In situ* methods are preferable because they allow deposition or blockage to be monitored without moving the sample from its original position. Fluid Dynamic Gauging is a measurement technique that can be used to determine the thickness and deformation behaviour of soft-solid fouling layers deposited on a membrane.

Chapter 3

Material and Methods

3.1. Introduction

This chapter presents the experimental systems for the fouling and cleaning of the ultrafiltration of Spent Sulphite Liquor (SSL) and the microfiltration of molasses. It contains the details of all the experimental equipment; (i) standard cross flow filtration rig, (ii) dead-end Fluid Dynamic Gauging membrane separation rig, (iii) cross flow Fluid Dynamic Gauging membrane separation rig, and (iv) the analysis techniques. The material properties of the systems have been identified and discussed.

3.2. Raw Materials

3.2.1. Spent Sulphite Liquor

The liquid SSL was supplied by *Industria de Celulose S.A.*, Constância, Portugal. The SSL was diluted to the required final mixture with reverse osmosis (RO) water at ambient temperature. The chemical composition of SSL can be seen in Table 3.1.

Table 3.1: SSL composition (After Marques *et al*., 2009a)

	SSL
pH	2.90
d, g/cm^3	1.18
Dry solids %	17.80
Ash %	2.80
Furfural %	<0.10
Methanol %	<0.10
Acetic Acid %	0.80
Extractives, %	0.07
LS, %	5.90
Sugars, %	
Rhamnose	0.10
Arabinose	0.10
Xylose	2.10
Mannose	0.10
Galactose	0.20
Glucose	0.60

3.2.2. Molasses

The liquid molasses was supplied by *Nordzucker*, Nakskov, Denmark. The molasses was diluted to the required final mixture with RO water at ambient temperature. The chemical composition of molasses can be seen in Table 3.2.

Table 3.2: Molasses composition (Nordzucker, 2008)

Analyses	Molasses Feed
Brix (°)	45.0
Ash (%)	8.3
mg/kg	
Potassium	49591
Sodium	9615
Calcium	4458
Magnesium	661
Chloride	2735
Sulphate	8227
Phosphate	522
Nitrate	1518
Oxalic Acid	377
Malic Acid	4722
Citric Acid	1391
Formic Acid	2547
Acetic Acid	7162
Oxalate Acid	317
Citrate Solids	200
Formate Solids	2201
Acetate Solids	832

3.2.3. Reverse Osmosis (RO) Water

RO treated water was used in all experiments except for the calibration experiments for the dead-end FDG rig, where standard tap water was used. The RO unit (*Elga Ltd*, Intercept RO-S) produces water of a low salt content having a measured conductivity of 5 – 10 μS cm^{-1} and a consistent hardness of below 5 °e (≈ 70 mgL^{-1} $CaCO_3$).

3.2.4. Chemical Cleaning Agent

The SSL fouled membranes were only cleaned with Sodium Hydroxide (NaOH); using a similar protocol to that performed by Weis (2004). NaOH was chosen due to its relatively low cost, common industrial use and past application to a number of deposits. NaOH of technical grade from *Fisher Scientific* (Loughborough, UK) was used. The solutions were made by adding the desired mass of powder to the required mass of RO

water at a desired temperature (0.10, 0.25, 0.50 wt. %). The molasses feed were cleaned using varying concentrations of citric acid (0.10, 0.25, 0.50 wt. %) and NaOH (0.10, 0.25, 0.50 wt. %) (both supplied by *Fisher Scientific*).

3.3. Membranes

3.3.1. Polymeric Membranes

The polymeric flat sheet membranes tested were (i) 20 kg mol^{-1} molar mass cut-off (MMCO) Fluoropolymer (FP); *Alfa Laval* FS61PP, (ii) 20 kg mol^{-1} MMCO Polysulphone (Ps*f*); *Alfa Laval* GR61PP, (iii) 0.5 μm pore size Ps*f*; *Alfa Laval* GRMRT5, (iv) 0.9 μm pore size Ps*f*; *Alfa Laval* PSURTI and (v) 1.5 μm pore size Polysulphone; *Alfa Laval* GRTRT8. The recommended operating limits can be seen in Appendix B1. All materials are commercially available and supplied by *Alfa Laval*, Nakskov, Denmark.

3.3.2. Microweaves

The Microweaves that were tested were Twilled Dutch Weaves (Figure 3.1). Twilled Dutch Weaves were produced by weaving with thicker warp stainless steel wires alternately over and under a large number of thinner stainless steel weft wires. They were ideal due to the strength of material and the high mesh density. The effective pore sizes of 5 μm and 10 μm were tested in the dead end filtration rig.

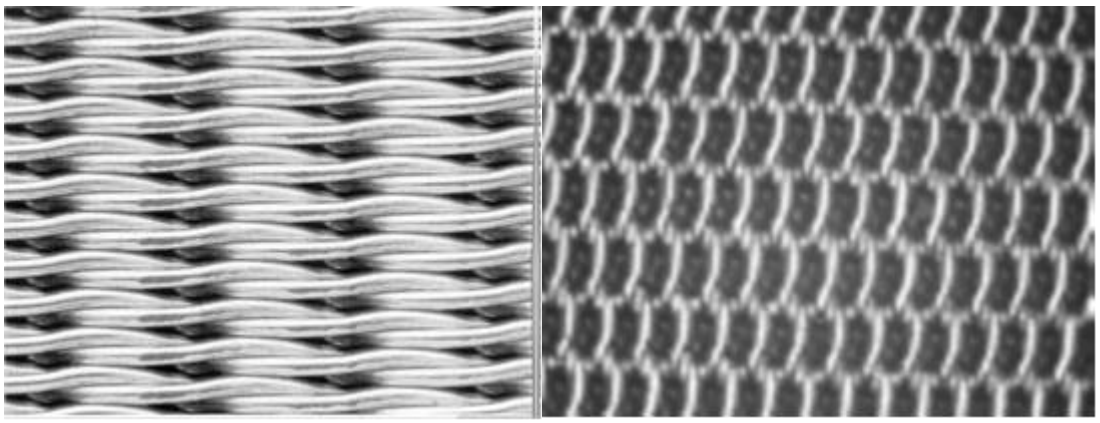

Figure 3.1: Top view of the Dutch Twill Microweaves.

3.4. Standard Cleaning and Fouling Rig

The standard cleaning and fouling rig was used for all cross flow filtration of both SSL and molasses. This experimental rig was designed by Weis (2004) to achieve easy and fast operation, flexibility, and delivery of reliable results. This rig was then adapted in this study for the cross flow FDG experiments (section 3.6).

3.4.1. Cross flow Filtration Rig

The materials used for the rig were plastic or stainless steel (type 316). The rig can be seen in Figure 3.2. It contained three polyethylene holding tanks (50 litres) that held both fouling solutions, both cleaning solutions and pure water. The pump used was a six stage centrifugal pump from *Lovara* (SV2-11T15M), where the liquid was passed through a 9 plate heat exchanger, with an exchange area of 0.3 m^2. The desired temperature was achieved with a counter-current of heat-transfer oil, which was pumped from an external heater (Conair) through the plates. The liquid was then passed either through the main pipe or the bypass, which returned the surplus of flow through a flexible hose back to the tank, while the main pipe travelled to the membrane module. The liquid in the main pipe before entering the module passed through a needle valve to regulate the flow, measured using a magnetic flow meter. The transmembrane pressure over the module was controlled by a needle valve immediately after the module. The module consisted of two outputs, the retentate that returned directly to the corresponding tank and permeate, which was collected in a beaker positioned on a balance which was connected to a computer, where the software (*LabView* 2008) translated into permeate output per time.

In the rig design, there were several shared lines, to ensure these are not contaminated from previous solutions; the lines were thoroughly drained, before taking a new solution. This was achieved by the bypass and return lines being constructed as flexible hoses, where they were placed over the drains and the pipe work emptied entirely. All pipes after the pump were constructed of 0.5” (12, 27 mm) o.d. 316 stainless steel. The connectors and valves (*Swagelok Ltd*) were of 316 stainless steel and rated to 10 bar pressure.

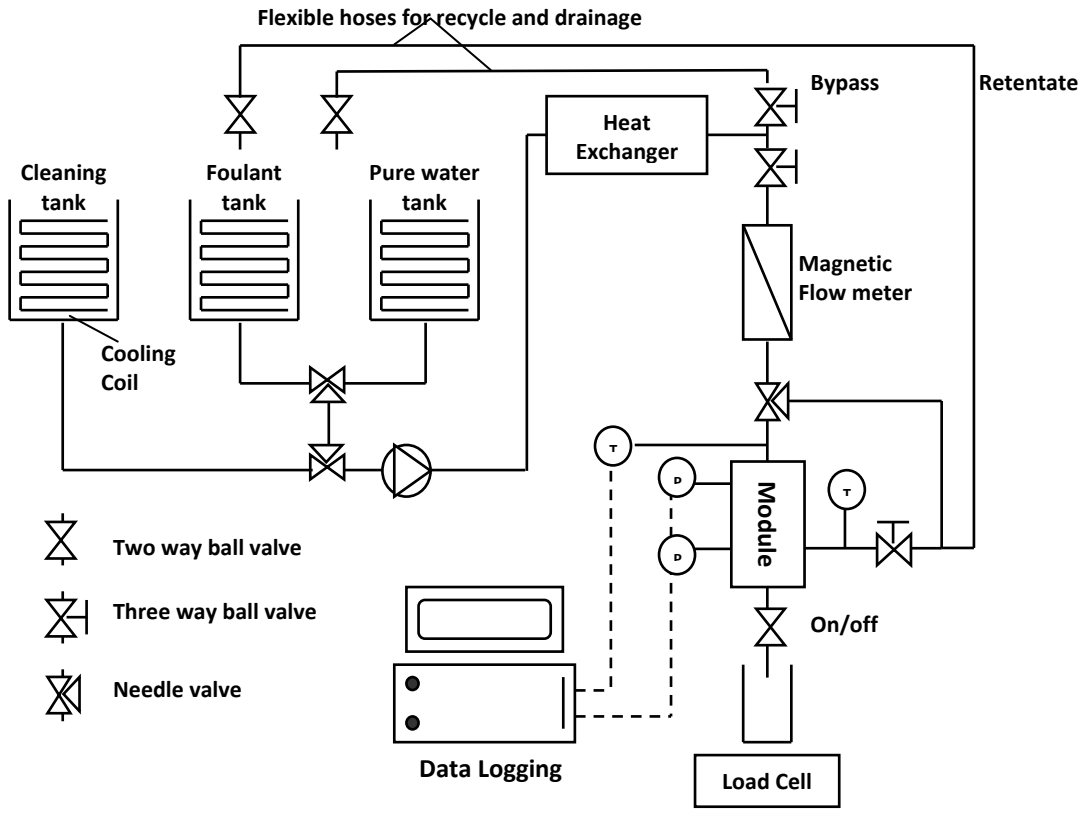

Figure 3.2: Schematic diagram for the cross flow filtration rig.

3.4.2. The Module

The selection criteria for the membrane module design were (i) industrial relevance, (ii) ease of membrane removal, and (iii) accessibility. Flat sheet modules allow variation of insert geometry and can easily be adapted for the use of the FDG. The membranes also required to be used for ex situ tests, e.g. SEM, AFM. The relative advantages and disadvantages of all the module configurations are discussed in Chapter 2.2.3.3. The membrane module selected was a flat-sheet module constructed out of stainless steel. The module included a double o-ring set up which ensured sealing, with a support section made of polypropylene with pores of 1 μm. The module also contained removable Perspex inserts, which allowed for channel geometry changes. The lid and base of the membrane module were sealed together with fourteen bolts; this can be seen in the Figure 3.3 to Figure 3.5. Care was taken when replacing and tightening the module lid due to risk of membrane rupture, which can result, from over-tightening and uneven distribution of force.

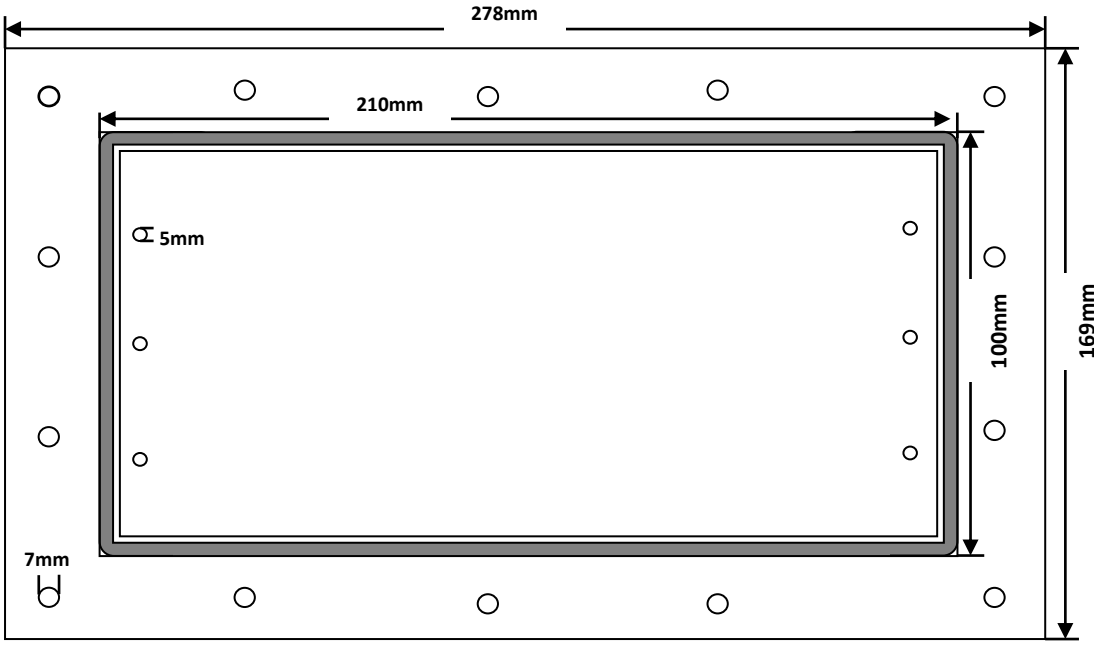

Figure 3.3: Diagram of the top stainless plate of the flat sheet module (not drawn to scale).

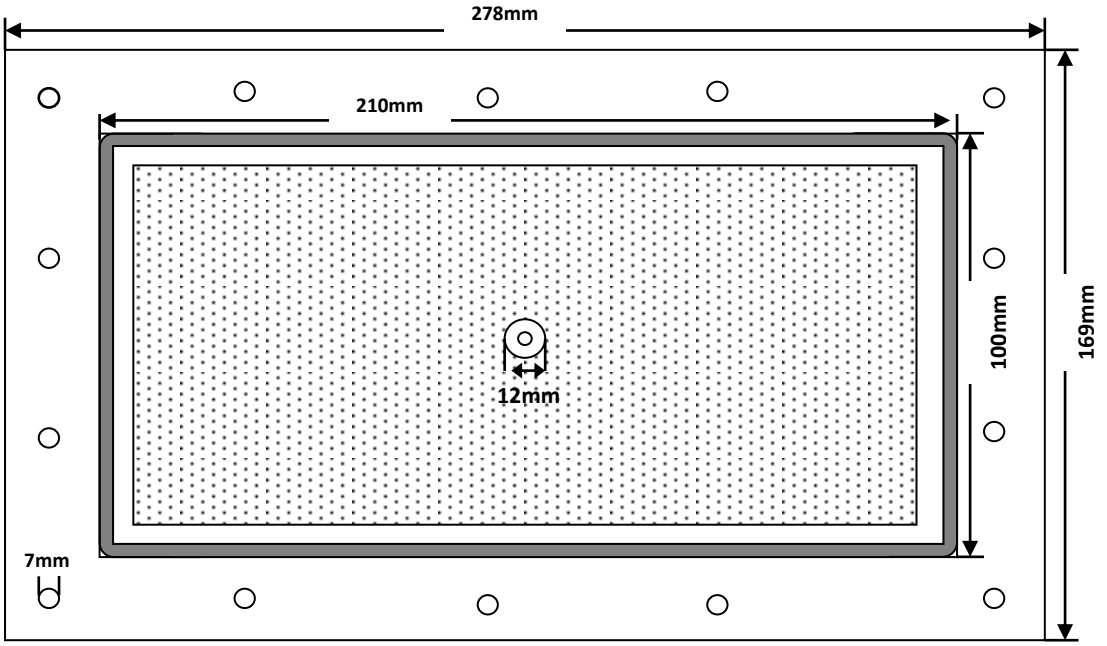

Figure 3.4: Diagram of the bottom stainless steel plate of the flat sheet module (not drawn to scale).

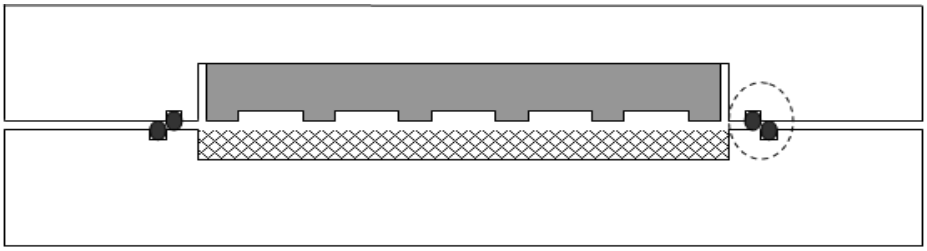

Figure 3.5: Diagram of the single flat-sheet membrane module (not drawn to scale).

Two different types of replaceable *Perspex* (poly (methyl methacrylate)) inserts were used in this study. The first insert was used for the standard filtration with SSL and molasses (Chapters 4 and 5). This insert was designed and verified by Weis (2004) and provided 7 channels of 7 mm width, 1 mm height and 191 mm in length providing a filtration area of 0.0095 m^2. The second insert was for use in the FDG experiments (Chapter 6). It was designed to ensure equal flow through the channels and allow enough room for the gauge to take measurements (Figure 3.6). The FDG insert provided 5 channels of 10 mm width, 5 mm height and 191 mm in length; this provides a filtration area of 96 cm^2. Both inserts contained a mixing channel; this ensured that the feed is fully mixed before entering the channels, with equal flow, breaking up the jet stream of the incoming solution. It was found that the fouling layers were evenly distributed over the entire membrane sheet when doing filtration experiments.

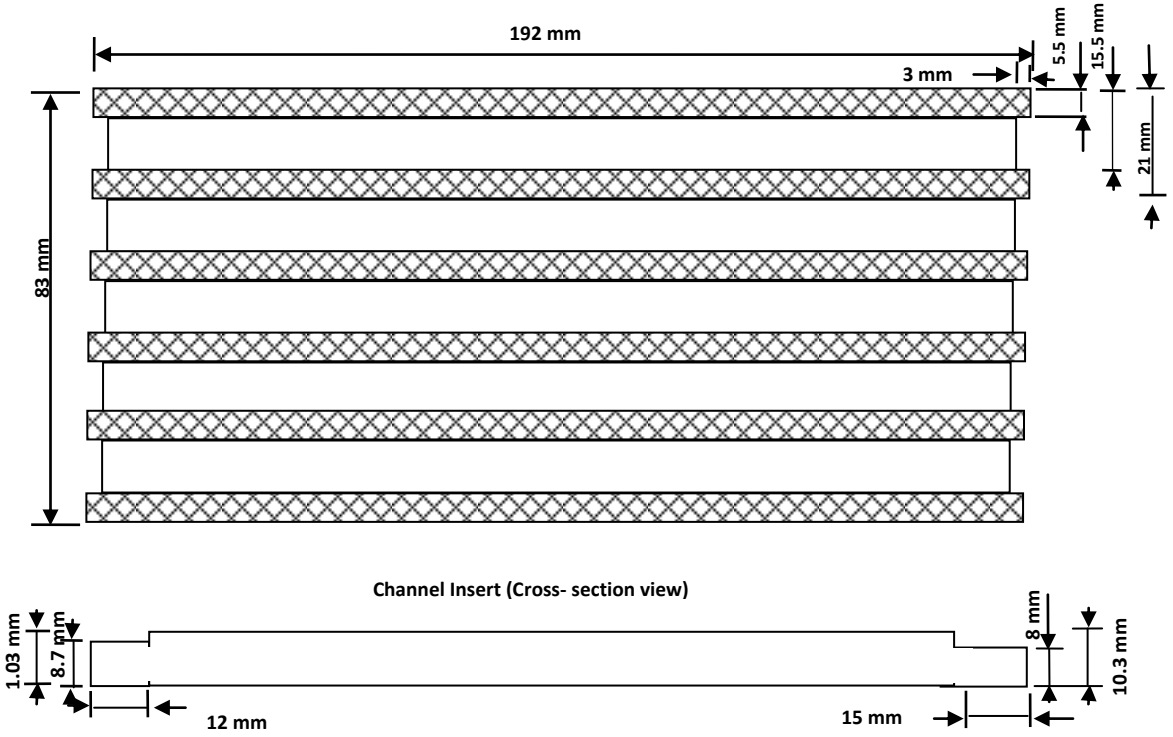

Figure 3.6: FDG five channel insert (not drawn to scale). Top view and cross-section view.

3.4.3. Experimental Procedure

A comprehensive commissioning programme was carried out with the aim of formulating and optimising experimental protocols. The programme involved a trial and error approach to improving experimental methods to increase reproducibility. Some of the operational parameters were fixed, since they were not of direct importance for the

outcome of the study. These parameters were cross flow velocity (CFV) and time, though the selection of these parameters still has some significance for the overall meaning of the results. Decloux *et al.* (2000) recommended that the optimal flux set point should first be established with experiments of constant pressure at the maximal velocity to characterise the pseudo-stabilised flux. Runs can then be performed around this set point and a little lower. The CFV was kept the same for all parts of the cycle. Turbulent conditions were chosen as these are used in industry and the high cross flow is effective in reducing concentration polarisation at the membrane surface. The selections of length of time for each part of the cycle are discussed next.

3.4.3.1. Membrane Conditioning

Pure water was used to condition the membranes, removing the glycerine preservative which new membranes are coated with during manufacture. Weis *et al*. (2005) found that a temperature of 60 ºC was hot enough to reduce the viscosity of the glycerine sufficiently to facilitate its removal from polymeric membrane surfaces. The work of Weis *et al*. (2005) has been extended in this study. The conditioning methods used were: (i) conditioning with water at 60 ºC, a transmembrane pressure (TMP) of 1.0 bar, a CFV of 1.89 ms^{-1}, and a feed volume of 25 litres for 90 minutes, and (ii) conditioning with water at 60 ºC (conditions as method 1) followed by cleaning with 0.50 wt. % NaOH at 50 ºC, 1.0 bar TMP, CFV of 1.89 ms^{-1}, and a feed volume of 25 litres for 30 minutes. One objective of this study was to determine whether the application of a NaOH pre-treatment could affect both the type of foulant species attaching to the membrane surface, and result in an improved separation performance.

3.4.3.2. Pure Water Flux Measurements

Pure water flux (PWF) measurements were taken before fouling, after fouling and after cleaning cycles. The conditions for PWF measurements were a temperature of 22 ºC, a TMP of 1.0 bar, a CFV of 1.89 ms^{-1}, and a feed volume of 25 litres for 10 minutes. The PWF measurements were used to investigate the various fouling resistances.

3.4.3.3. Fouling Conditions

The effects of operating conditions for both feeds were investigated by varying fouling TMP, concentration, and temperature at a constant CFV of 1.89 ms^{-1}. Flux

measurements were recorded and permeate samples taken throughout the duration of the experiment. A constant feed concentration was maintained, with the exception of the small samples taken for analysis. This minimises the retentate concentration effects during the filtration. TMPs of 0.5, 1.0, 1.5, 2.0, 2.5, 3.0, 3.5, and 4.0 bar were tested where the mass transfer information was investigated. Temperatures of 22 ºC, 40 ºC, 50 ºC, 60 ºC and 70 ºC were varied. The length of the fouling process was typically 90 minutes. Using the work performed by Bowen *et al*. (1995), this was deemed long enough for steady state to be reached under the conditions shown in Equation 3.1.

$$\frac{J_F(t-\Delta t)-J_F(t)}{J_F(t)} < 0.05 \qquad 3.1$$

3.4.3.4. Rinsing Conditions

The role of rinsing for preparing the membrane for the subsequent chemical cleaning is extremely important, as the removal of as much of the possible deposited layer during rinsing can maximise the efficiency of the cleaning process in terms of time and cleaning agent consumption (Matzinos and Álvarez, 2002). Water alone was found to be incapable of cleaning the fouled deposits; it was therefore considered wasteful of energy to use temperatures higher than ambient. Rinsing time was set to 15 minutes as it represents an industrial standard (Weis, 2004).

3.4.3.5. Chemical Cleaning Conditions

The cleaning operating conditions were optimised for each membrane and feed. The CFV was set for all stages of the cleaning cycle. The TMP, temperature, concentration, and time were all optimised for cleaning of both feeds. The cleaning cycles after fouling were carried out using NaOH for the SSL feeds. The molasses feeds were cleaned using a combination of NaOH and citric acid. The alkali and acid cleaning was evaluated in terms of the observed flux recovery. The cleaning efficiency was evaluated by the ratio of the pure water flux after cleaning (J_c) to the PWF measured before fouling (J_w) for each cleaning stage. The percentage flux recovery ($\%J_r$) was defined as Equation 3.2.

$$\%J_r = \left(\frac{J_c}{J_w}\right)\times 100 \qquad 3.2$$

The molasses filtration process was also optimised in terms of chemical cleaning sequences. Twelve treatment protocols were evaluated, comprising of (i) alkali then acid, (ii) acid then alkali and (iii) alkali / acid / alkali steps. Concentrations of 0.10 and 0.25 wt. % were tested for both NaOH and citric acid cleaning agents.

3.4.4. The Optimal Cleaning and Fouling Protocol

The conditions mentioned above have all been investigated in this study (see results Chapter 4 and 5) and the optimum standard conditions summarising the fouling and cleaning cycles are shown in Table 3.3. These steps are one complete cycle, except for conditioning which is an additional step for the virgin membrane. The optimum conditions for both SSL and molasses were found to be similar.

Table 3.3: Details a summary of the fouling/cleaning cycles. (* Varied during experiments)

Stage	Fluid	Protocol
Conditioning	Reverse osmosis water	60 ^{o}C, 120 min, 1.0 bar, 1.89 ms^{-1}
PWF Measurements	Reverse osmosis water	22 ^{o}C, 10 min, 1.0 bar, 1.89 ms^{-1}
Fouling	SSL/Molasses	60 ^{o}C*, 90 min*, 3.0 bar*, 1.89 ms^{-1}
PWF after fouling	Reverse osmosis water	22 ^{o}C, 10 min, 1.0 bar, 1.89 ms^{-1}
Rinsing	Reverse osmosis water	22 ^{o}C, 15 min, 1.0 bar, 1.89 ms^{-1}
PWF after rinsing	Reverse osmosis water	22 ^{o}C, 10 min, 1.0 bar, 1.89 ms^{-1}
Cleaning	NaOH/Citric acid (Conc. varied)	50 ^{o}C*, 30 min*, 1.0 bar*, 1.89 ms^{-1}
PWF after cleaning	Reverse osmosis water	22 ^{o}C, 10 min, 1.0 bar, 1.89 ms^{-1}

3.5. Dead-end Membrane Filtration Rig

A dead-end membrane filtration rig was first used to ascertain if the membranes and feeds in this study were suitable for use with the FDG. The rig was borrowed from the University of Cambridge, and the works of Chew (2004) were used as a comparison.

3.5.1. Dead-end Dynamic Gauging Rig

The experimental set up for the calibration and filtration experiments is shown in Figure 3.7. The apparatus consists of a Perspex tank (300 mm × 300 mm × 250 mm). A nozzle

of throat diameter, d_t, was connected to a straight tube of inner diameter, d_1. This section was connected to a curved pipe (shown as a straight pipe in Figure 3.7) with a diameter d_2. The dimensions of the nozzle schematic are d_t = 5 mm, d_1 = 20 mm, d_2 = 12 mm, w = 2.5 mm, λ = 0.5 mm and α = 45º (Figure 3.7). A constant hydrostatic head (the suction flow into the nozzle) is achieved by the siphon tube arrangement, with a continuous supply of tap water feeding into the tank (weir). The spindle of the micrometer M1 (*Mitutoyo*, Japan) controls the vertical movements of the gauge, which sets the clearance, h, relative to the gauged surface. In the tank, there is a Perspex filtration cell containing the membrane that is clamped on a metal grid (for support) beneath the nozzle. This separates the feed side and the permeate (liquid below the membrane). The diameter of the membrane available for flow is 41 mm. This can be seen in Figure 3.8. There are three ports on the box (reservoir side); this is to control different conditions required. These ports are controlled by rubber bungs and can be opened and closed. During the filtration experiment, a dead-end filtration system is simulated; a Perspex column is placed on the box with length 100 mm, diameter 83 mm and a thickness of 3 mm, where the feed is fed. The driving force of the permeate flow is maintained by a fixed hydrostatic difference, F. The mass of permeate is measured continuously using an electric balance (*Mettler* PB3001-L) and connected to a computer. A second balance is used to collect and weigh the mass of gauging fluid. The error in measuring the mass is less than ± 0.005 g.

3.5.2. Effective Length Calculations

The effective length of the siphon tube is used to compensate for the frictional losses in the siphon tube caused by the bends. Bends in the tube disturb the normal streamline and cause extra frictional losses. These losses are taken into account in the pressure drop across the tube by finding the effective length. The actual length of the siphon tube, without the nozzle tip, is 0.42 m and the curved pipe is 0.95 m. The effective length of the curved tube was determined by exploiting the siphon effect, by placing the tube in the tank with the nozzle removed, and at a high clearance from the surface (greater than 20 mm). The detailed method is described in Appendix C4.

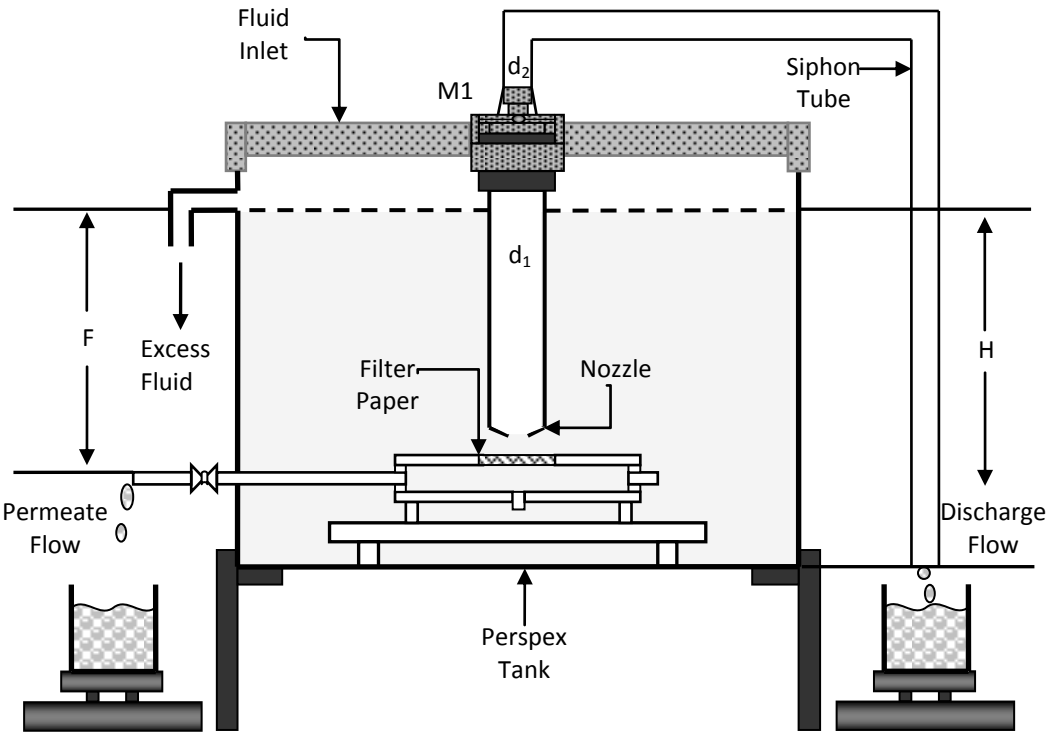

Figure 3.7: Schematic of dead-end FDG apparatus. In reality, section d_2 is a curved pipe.

3.5.3. Materials

In the calibration experiments, the gauging fluid was tap water at 22 ± 0.5 ºC. In the filtration experiments only diluted molasses was used. The membranes used for separation were 0.5 μm, 0.9 μm, and 1.5 μm Ps*f*. The Microweaves used were 5 μm and 10 μm effective pore size.

3.5.4. Calibration Experiment

In the calibration experiment, the nozzle was fully immersed in a liquid (tap water), and positioned close to the gauged surface. The clearance, *h*, was varied using the micrometre, where the tip of the nozzle touching the surface indicated the zero point ($h = 0$).

The hydrostatic head, *H*, was kept constant by a weir arrangement and was the principle driving force for the gauging fluid. The nozzle approached the gauging surface in advancing mode, i.e. starting from $h/d_t < 1$. The discharge liquid was then collected and weighed. The discharge mass flow rate (m) is sensitive to the nozzle clearance ratio h/d_t. The calibration experiments were performed by repeating the permeate system

conditions from Chew *et al.* (2007), here the two ports (B1 and B2) were closed and permeate (B3) was opened and collected. This resulted in two opposing flows, the upward gauging flow and the downward permeate flow.

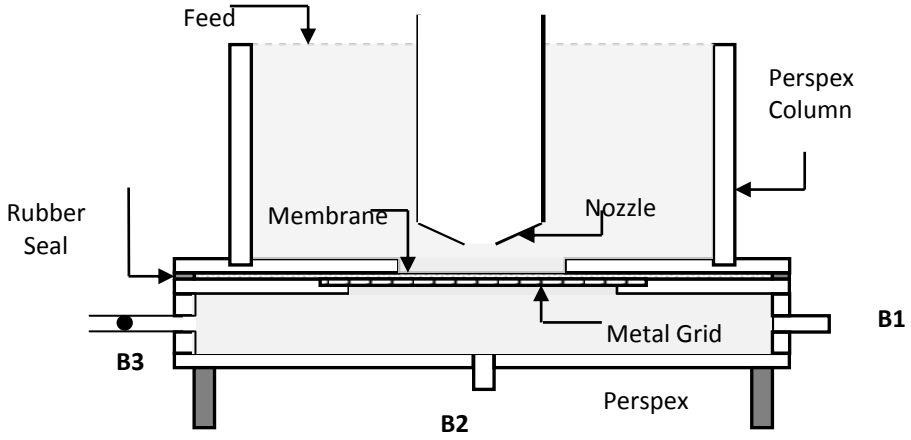

Figure 3.8: Arrangement of membrane in filtration mode.

3.5.5. Thickness Experiment

In the thickness experiments, the gauging and permeate flows were established prior to starting the feed, which was continuously fed into the Perspex column. The zero point of the gauge was first measured, using H = 20 mm (i.e. as low as possible so that the cake formation is not disrupted). The permeate flow was collected and measured using a balance connected to a computer. The gauge must be within the working range of $h/d_t \leq 0.25$. The thickness measurements were performed at intervals of approximately 60 seconds and each measurement took about 10 seconds. When no measurements were made, the gauge was moved far from the membrane to minimise the suction effect of gauging flows on the build-up of cake process.

3.6. Fluid Dynamic Gauging Cross Flow Membrane Rig

A second identical module to that described in section 3.4 was adapted by the addition of the FDG.

3.6.1. Cross flow Dynamic Gauging Rig

A schematic diagram of the FDG apparatus is shown in Figure 3.9; the module is positioned in the crossflow rig as detailed in section 3.4 (Figure 3.2). The RO water and

the molasses were circulated through the system using a six stage centrifugal pump (*Lovara* SV2-11T15M). A nozzle similar to that shown in Figure 2.16 and used by Tuladhar *et al*. (2003) (d_t = 1 mm; d = 4 mm, 45º nozzle angle) was mounted in the central duct (10 mm x 5 mm) of a 5-channel Perspex insert (adapted from the cross flow filtration rig) on the feed side of the membrane. The stainless steel membrane test cell was also adapted to allow the FDG to be mounted (Figure 3.10). The five channels were identical, giving a filtration area of 0.0096 m^2. A second insert was also used for the initial verification of the FDG in the cross flow filtration rig. The one channel insert gave a filtration area of 0.0019 m^2. The position of the nozzle above the membrane was controlled using a linear guide rail (*THK*-KR15, positioning accuracy 20 µm, repeatability ± 3 µm) and an accurate stepper motor (*Nanotec* 0.9°, 0.67 A). A Linear variable differential transformer (± 1 mm stroke, *RS-Components*) was also used as a secondary measurement of position. A differential pressure (DP) cell (error ± 0.8 %) was connected between tapings near the gauge nozzle and another at the top of the gauge to measure the pressure drop across the nozzle. The nozzle pressure drop is labelled ΔP_N, (equivalent to ΔP_{14}) to differentiate it from the transmembrane pressure drop, TMP. The discharge mass flow rate from the gauging probe was controlled using a fine needle valve; the gauging mass flow rate and transmembrane permeate flow rate were both measured using *Sartorius* balances connected to a data logging PC. By repeating gauging experiments, an overall global experimental error estimate in dynamic gauging measurements of ± 3.4 % has been determined using apparatus 2.

3.6.2. Materials

This system was calibrated using RO water and fouling experiments were conducted using diluted molasses. The molasses feed were cleaned using citric acid and NaOH.

3.6.3. Calibration Experiment

During the calibration experiments, the zero point of the gauge in relation to the membrane surface was first measured. RO water was recirculated through the duct at varying cross flow velocities, from 0.70 to 2.78 ms^{-1} (corresponding to a duct Reynolds number, Re_D, of 4000 – 18520), transmembrane pressure (TMP, 0.35 to 2.0 bar) and temperature (22 to 60 ºC). During a calibration test, m was maintained constant for each condition investigated. The nozzle approached the membrane in advancing mode, with

h/d_t changing from 1 to 0. Both ΔP_N and permeate flux were recorded at regular distances from the membrane surface.

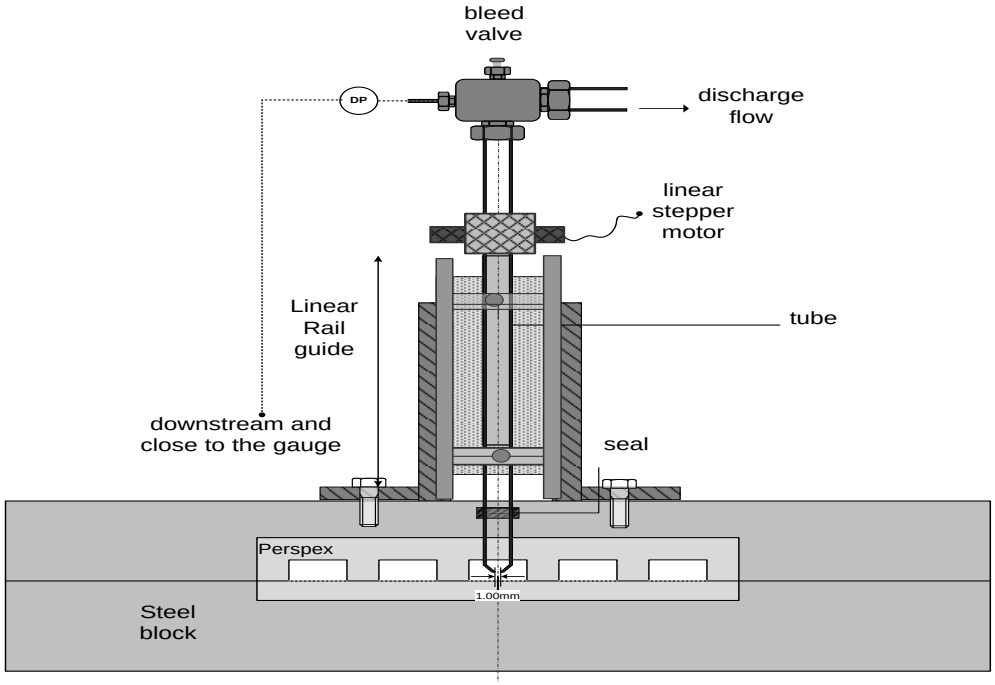

Figure 3.9: Schematic cross-section of membrane test cell showing the FDG configuration (not drawn to scale).

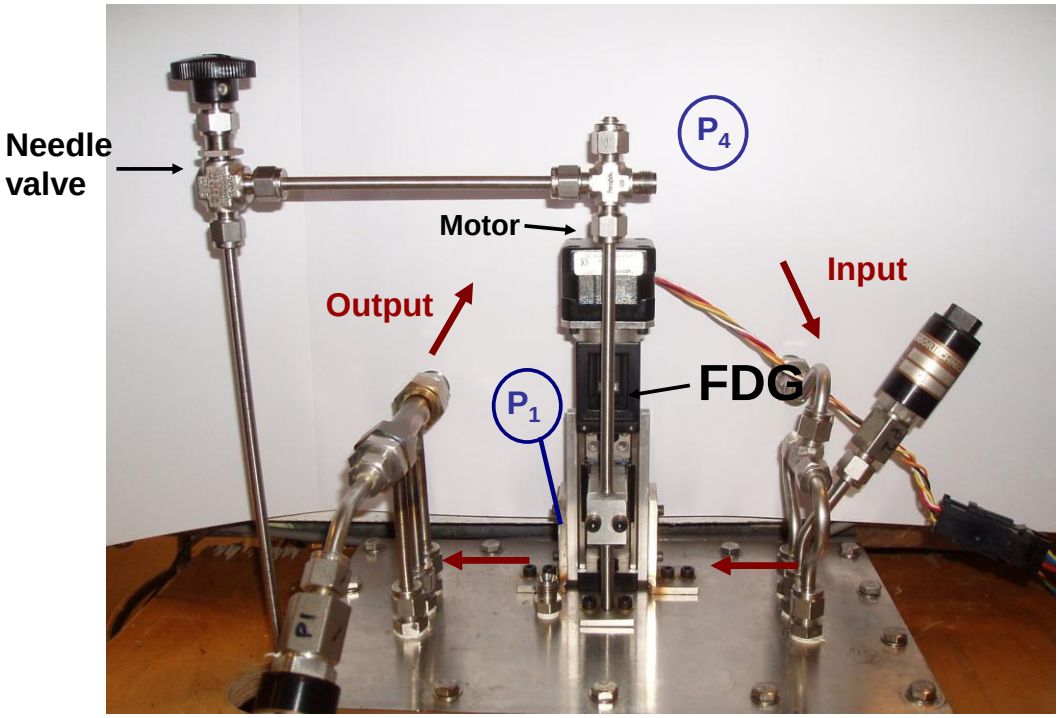

Figure 3.10: Picture of the FDG apparatus disconnected from the full cross flow equipment.

3.6.4. Thickness Experiment

The process fluid for the filtration experiments was molasses diluted to the required final mixture with RO water at ambient temperature. A feed volume of 35 litres was heated to the desired temperature. The polymeric microfiltration membranes tested were Polysulphone sheets with pore sizes of 0.5 μm, 0.9 μm, and 1.5 μm. During the filtration experiments, the molasses solution was recycled through the rig at varying values of CFV (0.70 to 2.78 ms^{-1}), TMP (0.35 to 2.00 bar), temperature (22, 40, 60 ± 0.5 ºC) and concentration (35, 45, 55 ºBrix). The permeate flow was collected and plotted versus time. The thickness of a cake layer was determined by measuring ΔP_N at a fixed value of *m*: this, with the corresponding calibration chart yields the new *h* value. The gauge must be within the working range, $h/d_t \leq 0.25$, for the gauge to detect the surface reliably. The thickness measurements were performed at intervals of approximately 100 seconds and each measurement took about 10 seconds. When no measurements were made, the gauge was withdrawn from the channel, and the gauging flow stopped to minimize the effect of suction upon the build-up of the cake layer.

3.6.5. Cake Layer Removal

FDG was used to track the thickness of the 45 ºBrix molasses fouling deposit (cake layer) during fouling and its removal rate during rinsing and cleaning. It was used as an aid to understanding the removal mechanisms. The experiments were performed as section 3.6.4, whereby the removal of the cake layer was also monitored during the subsequent rinsing and cleaning stages. Two possible methods of FDG operation during chemical cleaning were considered: (i) Method 1 - permeate side open with recycle back to the feed tank, and (ii) Method 2 (also with recycle to the feed tank) - permeate side closed during the first part of the protocol. Method 1 generates information concerning the change of membrane resistance during the full cleaning cycle. Method 2 records only the data at the end of the cleaning cycle (final 15 minutes) and the overall flux recovery.

3.7. Surface Analysis Techniques

The following techniques were used (i) Streaming potential measured through the pores, (ii) ATR-FTIR, (iii) SEM, (iv) AFM and (v) Contact angle measurement.

3.7.1. Streaming Potential through Pores

The surface charge on membranes has a significant influence on its filtration and fouling tendencies. The surface charge of a porous membrane is related to the zeta potential of the membrane, which is usually evaluated from electrokinetic experiments, such as streaming potential using saline solution (Evans, 2008). The streaming potential technique is an attractive way to determine the ζ-potential of membrane (Fievet *et al*., 2006). Streaming potential is the potential induced when an electrolyte solution flows across a stationary, charged surface. It quantifies an electrokinetic effect which reflects the properties of the surface, the flow characteristics, and the chemistry and thermodynamics of the electrolyte solution in the experiment (Huisman *et al*., 2000).

The streaming potential of the membrane samples were carried out at the Lappeenranta University of Technology, Finland. Simultaneous measurements of flux and streaming potential through the pores were obtained using a cross-flow membrane module designed for flat sheet membranes with an area of 10.4 cm^2. The module was equipped with two sets of Ag/AgCl electrodes, one on the feed side of the membrane and one on the permeate side enabling the measurement of the streaming potential developed across the membrane (zeta-potential in the pores). The membrane was inserted into the module, compacted and stabilised at a constant pressure and flow rate. The streaming potential measurements were performed with a 0.001 (10^{-3} M) KCl solution. An approximate pH range of 3.7 – 7.0 was covered. At each pH examined, the pressure was varied and the flow rate kept constant in order to calculate the zeta potential based on the Helmholtz-Smoluchowski equation (Equation 3.3) without corrections at a temperature 25 ºC (Nyström *et al*., 1994). The data was collected using acquisition software programmed with MS® quickBASIC version 4.5 and using ADDA 14 interface card.

$$\zeta = \frac{\Delta E}{\Delta P}\frac{\mu\kappa}{\varepsilon_0\varepsilon_r} \qquad 3.3$$

where ΔE is the streaming potential, ΔP the TMP drop, μ the viscosity of the solution, κ the conductivity of electrolyte in the pores (approximated as bulk conductivity), ε_0 the permittivity of a vacuum and ε_r the dielectric constant of pure water at 25 ºC. Equation

3.3 is valid only as long as the Debye length of the solution is small compared to the radius of the pores (Huisman *et al*.. 1998; Christoforou *et al*., 1985). This condition is fulfilled for the microfiltration and ultrafiltration membranes and ionic strengths considered in this study.

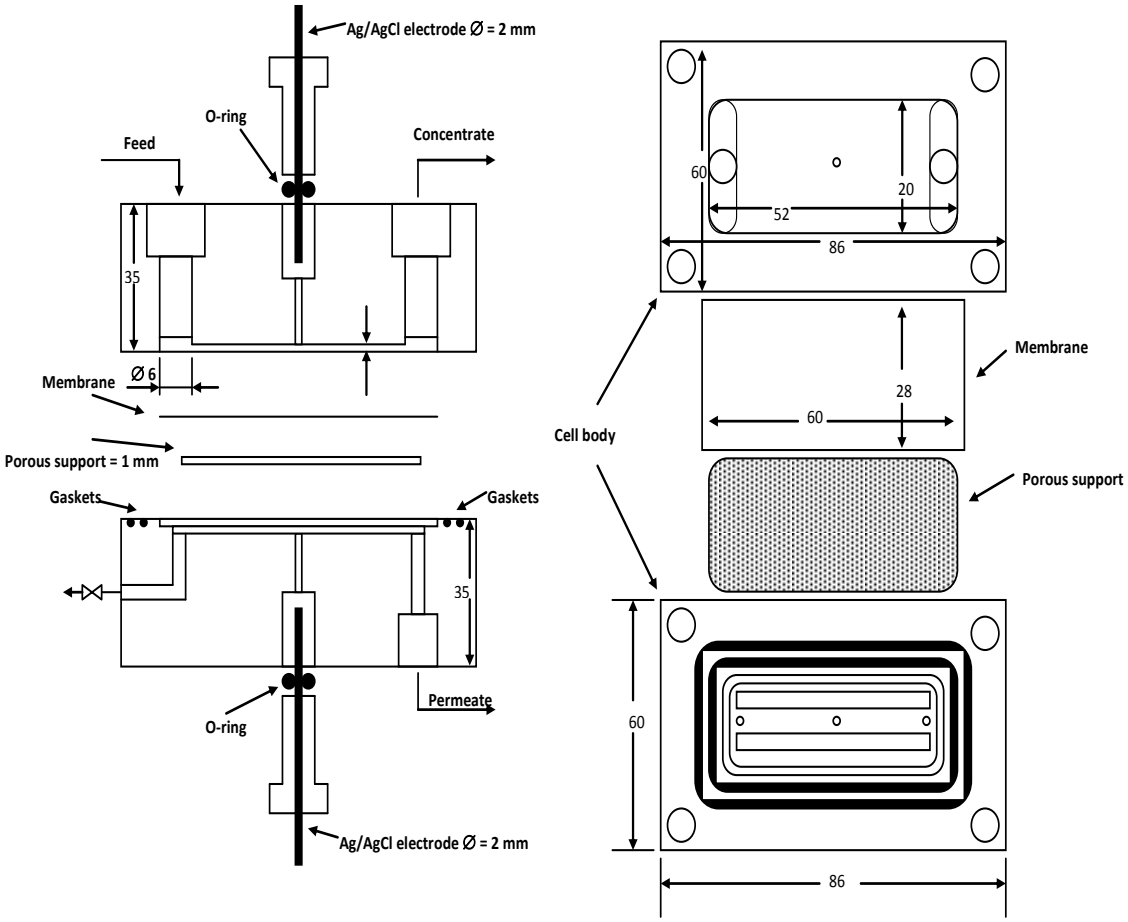

Figure 3.11: Module for the measurements of streaming potential through the pores of flat sheet membranes of area approximately 10.4 cm^2 (After Pihlajamäki, 1998).

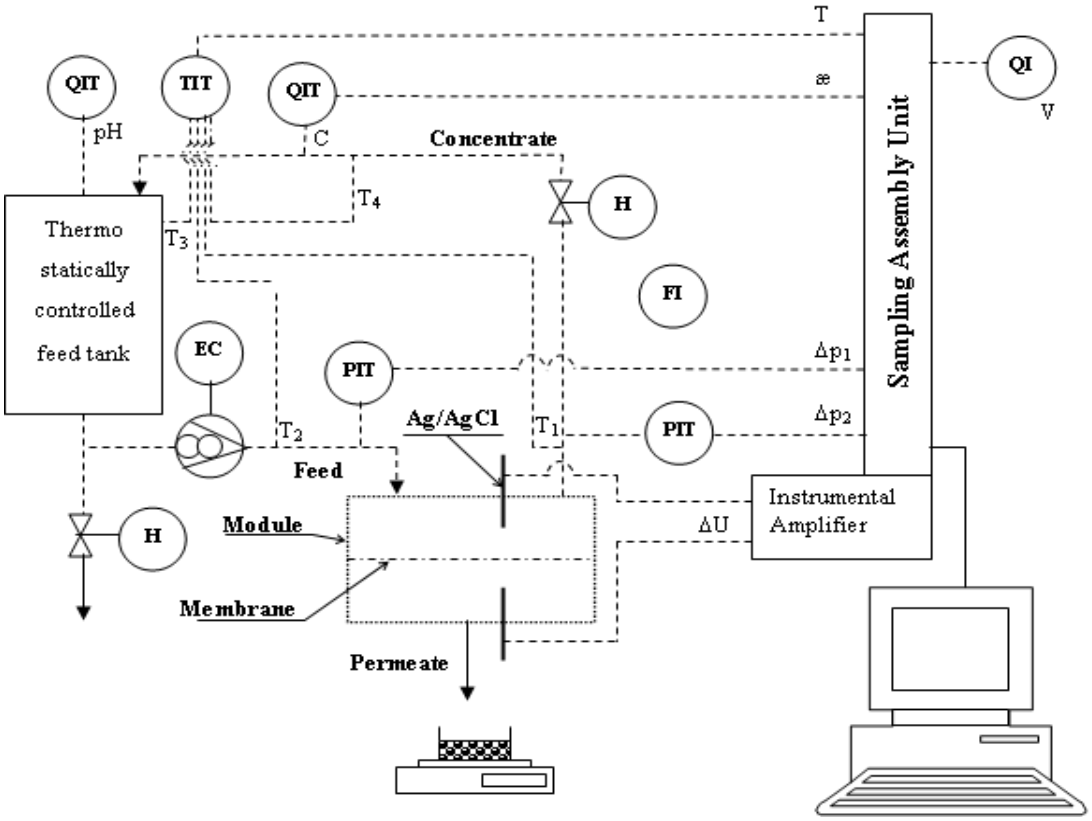

Figure 3.12: The apparatus for streaming-potential measurements (After Pihlajamäki, 1998).

3.7.2. ATR-FTIR

A *Perkin-Elmer* 2000 FTIR apparatus and Attenuated Total Reflection (ATR) method was used to record IR-spectra at Mid Infra-Red (MIR) region. ATR-FTIR was used to understand the nature of the adhered deposits and their structures. It was provided with a HeNe laser as a radiation source (unpolarized IR radiation), triglycine sulphate (TGS) as a detector and optical kBr as a beam splitter. The resolution of the FTIR apparatus was adjusted to 2.0 cm^{-1}, the optical path difference (OPD) velocity to 0.2 cm^{-1} and the data-collecting internal to 1.0. A KRS-5 crystal (thallium bromide iodine) was used as an internal reflection element (45º, 17 reflections), (Pihlajamäki *et al*., 1996). Each spectrum was made of 100 co-added scans. The membrane samples were dried for 24 hours at room temperature prior to use. This PE 2000 also includes a search program that suggests possible structural units (PSUs) of a spectrum.

3.7.3. Scanning Electron Microscopy (SEM)

Scanning electron microscopy (SEM) was applied to observe the state of membrane surface after different fouling processes and subsequent cleaning. Air and vacuum-dried

membranes were stuck to SEM stubs with conductive paste, followed by coating with a thin layer of gold. Afterwards, the specimens were viewed with a *JSM* 6310 SEM in combination with a microanalysis system, *LINK* AN10000. An X-ray Diffractometer was used to identify and characterise any minerals on the membrane surface.

3.7.4. Atomic Force Microscopy (AFM)

Atomic force microscopy (AFM) also known as scanning force microscopy is primarily used to probe surface topography and interactions on the atomic-molecular scale. The AFM used was a *Dimension 3100* tip-scanning instrument with a Nanoseope IV controller (*Vecco* USA). The cantilevers used in intermittent contact mode were standard tapping mode tips (*Olympus*). A small piece of the membrane was stuck on a metal disc using double sided sticky tape and placed on the AFM stage. Images were scanned at a rate of 1 Hz. Surface statistics were calculated with the instruments software. R_A (the mean roughness) was calculated as an average value of that calculated from each scan line for the 5 x 5 μm images.

3.7.5. Contact Angle Measurement

Contact angle measurement of the membrane surface can be used to characterise hydrophobicity. For hydrophobic membranes the contact angle will be larger than 90º and for hydrophilic membranes the contact angle will be less than 90º tending toward 0º as shown in Figure 2.11. The contact angle measurements were made using the sessile drop method using a KSV CAM 101 instrument goniometer (*KSV Instruments Ltd*). A drop of water was placed with a syringe on a porous surface and the contact angle measured. This procedure was repeated 8 times at different points on the membrane with measurements taken from both sides of the drop producing a total of 16 measurements, which are then averaged (Evans and Bird, 2006).

3.7.6. Mass Analyses of SSL and Molasses Fractions

Due to the nature of the processes in the production in both SSL and molasses analysis is required to investigate different components in the feeds.

3.7.6.1. Water Content and Dry Weight

The feed and permeate samples were analysed for solid concentration by drying in an oven. The water determination was based on evaporating free water at temperatures above 100 ºC (SSL) and 65 ºC (Molasses) for 48 hr, weighing the samples before and after the evaporation process. The transmission of total solids was calculated using Equation 3.4.

$$T\% = \left(\frac{C_p}{C_b} \right) \mathrm{X}\, 100 \qquad 3.4$$

where C_p is the total solid concentration in the permeate stream and C_b is the total solid concentration in the bulk feed solution (calculated as a wt. % of the total stream).

3.7.6.2. Brix

Brix is a term originally used for pure sucrose solutions to indicate the percentage of sucrose in the solution on a weight basis. However, in addition to sucrose, molasses contains glucose, fructose, raffinose, and numerous non-sugar organic materials. Consequently, a Brix value for molasses will often differ dramatically from actual sugar or total solid content. The relationship between refractive index and the amount of sucrose on a dry basis is well known for sucrose.

The Brix value is gathered using an ABBÉ ‘60’ refractometer. The instrument employs the critical angle effect marked by a demarcation line (border line) between light and dark portions of the telescope field. The rays from the prism fall on a mirror where they are reflected into the field telescope of the instrument. The mirror is positioned to bring the borderline into coincidence with the telescope cross wires, which is observed in the scale telescope. The scale is a direct function of the refractive index. A small sample (between 1 and 2 mm diameter) of molasses is placed on the microscope covering the whole slide (fixed prism). The feed spreads out to cover the interface and a reading is taken. This refractive index value is then converted to a corresponding brix value.

3.7.7. Viscosity Measurements

Rheology experiments were performed in a Bohlin CVOR 200 rheometer. The rheometer was set up in with a cone and plate configuration. The test solution was pipetted onto the flat bottom plate. The upper plate (4º cone) was then lowered into position. The cone is then rotated in the desired manner and the resulting response is measured by the lower plate. The temperature was regulated using either a water bath or the temperature control unit (TCU). The various viscosities for selected solutions in this study are shown in Appendix B.

3.8. Summary

This chapter described the experimental systems used in this study for the fouling and cleaning of the ultrafiltration of SSL and the microfiltration of molasses. It contained the details of all the experimental equipment; (i) standard cross flow filtration rig, (ii) dead-end FDG membrane separation rig, (iii) cross flow FDG membrane separation rig, and (iv) the analysis techniques.

Chapter 4

The Influence of Fouling and Cleaning Conditions upon Performance of Ultrafiltration for Processing Spent Sulphite Liquor

4.1. Introduction

This chapter details the experimental results concerning the filtration of Spent Sulphite Liquor (SSL). The membrane samples have been compared and described both quantitatively and qualitatively, in terms of flux performance and surface characteristics of the membrane. SSL was studied in the cross flow rig with two different materials; Polysulphone (Ps*f*) and Fluoropolymer (FP) membranes. The majority of the experiments were performed with the 20 kDa molecular weight cut-off (MWCO) FP membrane. This chapter is split into two sections; (i) the fouling and cleaning optimisation of SSL filtration, and (ii) the effect of pre-treatment cleaning on the filtration of SSL. The first section discusses the SSL filtration in terms of flux performance, resistances and rejection. The second section explains the filtration process in further detail using various analytic techniques.

4.2. Conditioning

Conditioning was required to remove glycerine from the membrane surfaces before further experiments could be performed; it was achieved using the protocol developed by Weis *et al*. (2005), with reverse osmosis (RO) water at 60 ºC, 1.0 bar transmembrane pressure (TMP), and 1.89 ms^{-1} cross flow velocity (CFV) for 120 min. The RO water was changed frequently to ensure the removed glycerine didn't re-foul the membrane surface. These conditions were found to be sufficient to remove the glycerine coatings. A flux decline was seen for the 20 kDa Ps*f* from 920 L m^{-2} hr^{-1} to an average of 575 L m^{-2} hr^{-1} after 120 min. A flux decline was seen for the 20 kDa FP from 865 L m^{-2} hr^{-1} to an average of 600 L m^{-2} hr^{-1} after 120 min. The Ps*f* and FP membranes exhibited slightly different flux trends but with a general slight decline. To ensure the reliability of the experimental data multiple measurements were performed at each stage. This resulted in an error of ± 6 %; this is acceptable for the study of membrane

fouling. Further experiments were performed on the effects of this conditioning step. These results are presented in section 4.6 and 4.7.

4.3. Ultrafiltration of SSL – Fouling Conditions Optimisation

The purpose of membrane separation with the SSL was to reduce the water content and concentrate the lignin (Lignosulphonates) from the sugars and salts to yield a high molar mass fraction of lignosulphonates in the retentate. The high molar mass fraction can be used to produce vanillin (Weis and Bird, 2001). Vanillin (V, 4-hydroxy-3-methoxybenzaldehyde) and its derivatives (ethylvanilin, vanillic acid, acetovanillon) are used in the food and pharmaceutical industries, and in the production of polymers such as polyester (Hocking, 1997). Wallberg *et al*. (2003) recommended the use of 20 kDa membranes when filtering SSL to produce lignosulphonates.

4.3.1. Fouling Conditions

The fouling conditions have been optimised by varying temperature and TMP. The SSL was filtered in its delivered form of 17.80 wt. % dry solids. The following equations have been used, throughout this chapter, to optimise the fouling conditions in the filtration of SSL.

Once a membrane is fouled it displays numerous resistances, which can be characterised by the resistance in the series model as shown in Equations 4.1 and 4.2 (Ousman and Bennasar, 1995; Jiraratananon and Chanachai, 1996).

$$J_F = \frac{\Delta P}{\mu_p R_T} = \frac{\Delta P}{\mu_p \left(R_m + R_{cp} + R_F \right)} \qquad 4.1$$

$$R_F = R_I + R_R \qquad 4.2$$

where J_F is the permeate flux, μ_p is the viscosity of the permeate, ΔP is the transmembrane pressure, R_m is the intrinsic membrane resistance, R_T is the total fouling resistance, R_{cp} is the resistance in the concentration polarisation region, R_F is the fouling resistance term, R_I is the irreversible fouling resistance and R_R is the rinsable fouling resistance. R_m is calculated by measuring the flux of RO quality water through a

conditioned virgin or cleaned membrane. R_F is determined from the initial flux of RO water after fouling has finished. R_I is calculated by noting the increase in flux when flushed with RO water for 10 minutes after fouling has finished. R_R is then determined from $R_R = R_F - R_I$. Rinsable fouling is defined here as that which is removed by rinsing at 1.0 bar TMP and 1.89 ms^{-1} CFV to remove any loosely bound particulates. Irreversible fouling is defined as not being removed by rinsing, i.e., material binding to pores or adhering to the membrane surface. These terms are relative and depend on the rinsing conditions used (which are constant to allow comparison) (Evans and Bird, 2006; Shorrock and Bird, 1998). Knowing R_m, R_F and R_T gives an estimate of R_{cp} using Equation 4.1.

The apparent (observed) rejection was used to compare the operating conditions. The permeate concentration (C_p) was correlated to the bulk concentration (C_b) of retentate (Equation 4.3). The rejection of SSL solids was measured by the collection of permeate and retentate samples at steady state flux. The dry mass of each sample was recorded in triplicate and an average and standard deviation was calculated.

$$R_a = 1 - \left(\frac{C_p}{C_b} \right) \qquad 4.3$$

with the conditions, that $R_a \leq 1$.

4.3.1.1. Temperature

The fouling temperature was varied maintaining a constant TMP of 3.0 bar, CFV of 1.89 ms^{-1} for 90 min where standard rinsing and cleaning conditions were used. RO pure water fluxes (PWF) were maintained constant before and after fouling and after cleaning (22 ºC, 1.0 bar, and 1.89 ms^{-1}). Room temperature (22 ºC), 60 ºC and 70 ºC were studied as a comparison. Figure 4.1 displays the fouling flux data for the Ps*f* and FP membranes. It shows the first, last and average flux values in the fouling section of the cycle. The last fouling point indicates when the flux has reached steady state. The initial fluxes increased as the feed temperature was raised. Filtering at 22 ºC produced steady state fluxes of 25 L m^{-2} hr^{-1} (Ps*f*) and 26 L m^{-2} hr^{-1} (FP) respectively; which was not viable for this process. As the fouling cycles reached steady state, the final fouling fluxes showed similar values for the 60 ºC and 70 ºC feed temperatures. The changes in

viscosity of SSL did not affect the fouling process at the higher temperatures. The phenolic compounds are thought to contribute most to the fouling problem during the lignosulphonates separation (Weis *et al*., 2005). The causes of the fouling problems are discussed in more detail in section 4.6 and 4.7. The FP membrane resulted in superior fouling flux performance over the Ps*f* membrane (*ca.*12 % enhanced steady state flux) when filtering at 60 ºC. The optimal fouling temperature for filtering SSL was found to be 60 ºC.

Figure 4.2 shows the breakdown of the different resistive layers present at steady state fouling versus SSL temperature. As the change in viscosity due to temperature changes has already been incorporated into the fouling resistance calculation, the differences are associated with other factors. The increases in R_R and R_{cp} resistances for the 22 ºC fouled membranes were responsible for the increases in the total resistance over the higher temperatures of 60 ºC and 70 ºC. The R_I decreased slightly from 3.13 x 10^{12} m^{-1} for the Ps*f* 60 ºC fouled membrane to 2.67 x 10^{12} m^{-1} for 22 ºC fouled Ps*f* membrane (FP membrane: 3.00 x 10^{12} m^{-1} to 2.65 x 10^{12} m^{-1}). This irreversible fouling resistance value is when rinsed with RO water only; it does not take into account the use of a cleaning agent. Hence, the lower filtration temperature can reduce the irreversible fouling resistance and increase both rinsable and concentration polarisation resistances. The resistance breakdown shows that the R_R and R_{cp} were responsible for the increased resistance on the Ps*f* membrane over the FP membrane. Figure 4.3 displays the membrane resistance after fouling and cleaning compared to the membrane resistance before fouling. It shows that the membrane fouled at 22 ºC had the least membrane resistance after cleaning. As the fouling temperature increased so did the membrane resistance after cleaning. This could be due to the result of the fouled material on the 22 ºC fouled membrane was more easily removed, as the foulants could have reacted less with the membrane surface at this temperature. The foulants at the higher temperatures of 60 ºC and 70 ºC could have caused greater adhesion to the membrane surface. The fouling that occurred at the higher temperatures also had additional solids passing through the membrane; this could have caused more fouling adhesion on the pore walls than at 22 ºC. The membrane resistance after fouling and cleaning values for both Ps*f* and FP membranes show that the cleaning regime removed most of the fouling

resistance. The FP membranes had a greater degree of cleanability under the conditions applied.

Figure 4.4 shows the apparent solids rejection data versus fouling temperature for the Ps*f* and FP membranes. Increasing the temperature from 22 – 60 ºC decreased the rejection from 0.44 to 0.37 (Ps*f*) and 0.42 to 0.33 (FP) respectively. The rejection coefficient is further decreased to 0.36 (Ps*f*) and 0.30 (FP) at 70 ºC. This decrease could be due to increased flux going through the membrane forcing more solids through and the membranes therefore becoming less selective at the higher temperatures. The Ps*f* membrane rejected more solids than the FP membrane due to the increased flux values for the FP membrane. The properties of the Ps*f* membrane could also be more selective preventing certain solids from passing through. Internal fouling such as pore blocking may also have occurred more in the Ps*f* membrane, stopping the larger particles in passing through the membrane in turn increasing the solids rejection (Blanpain *et al*., 1993).

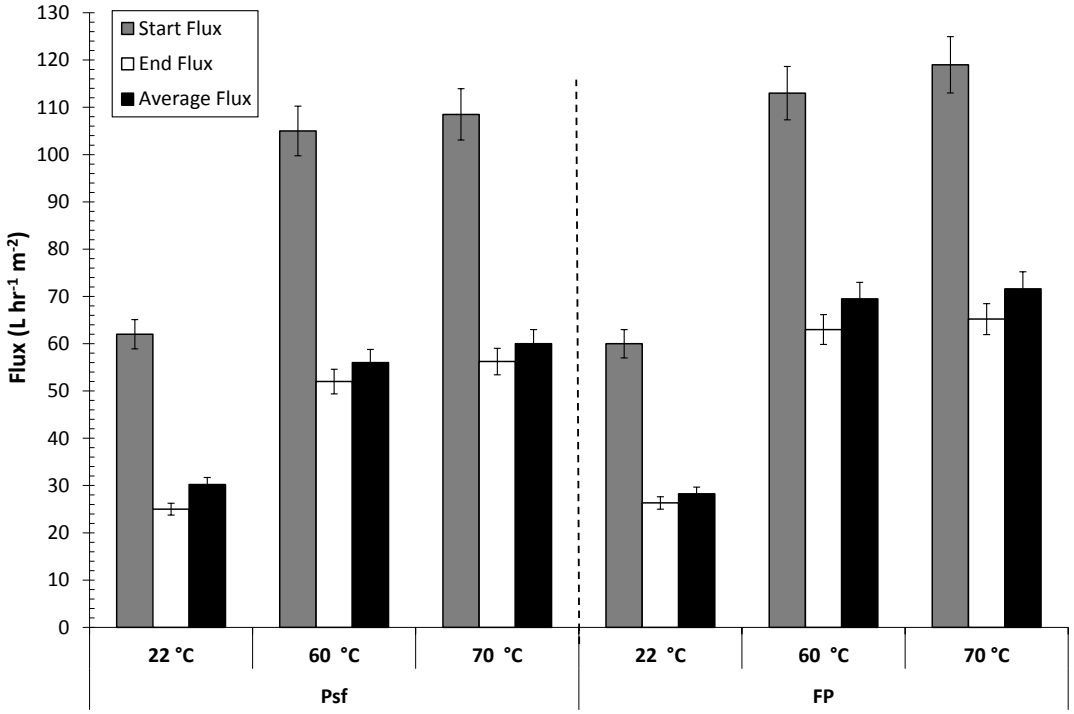

Figure 4.1: Graph to show fouling flux data as a function of fouling temperature on Ps*f* and FP membranes when fouled with SSL (3.0 bar TMP, 1.89 ms^{-1} CFV) for 90min.

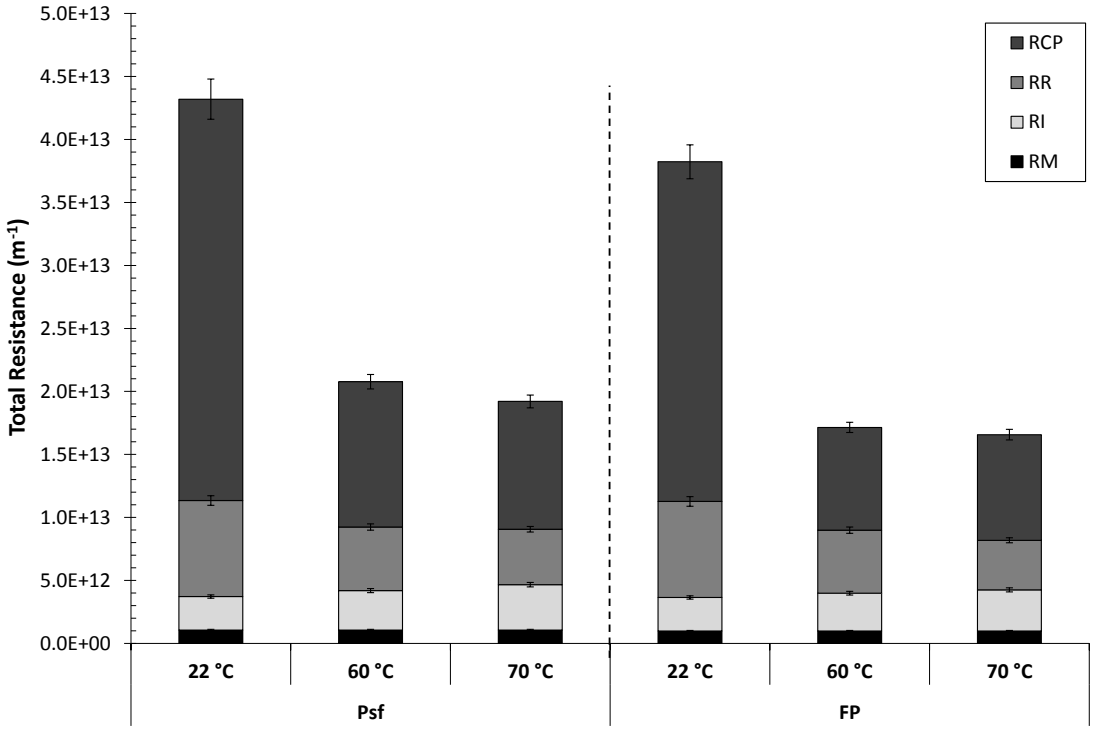

Figure 4.2: Graph to show fouling resistance data as a function of fouling temperature on Ps*f* and FP membranes when fouled with SSL (3.0 bar TMP, 1.89 ms^{-1} CFV) for 90 min.

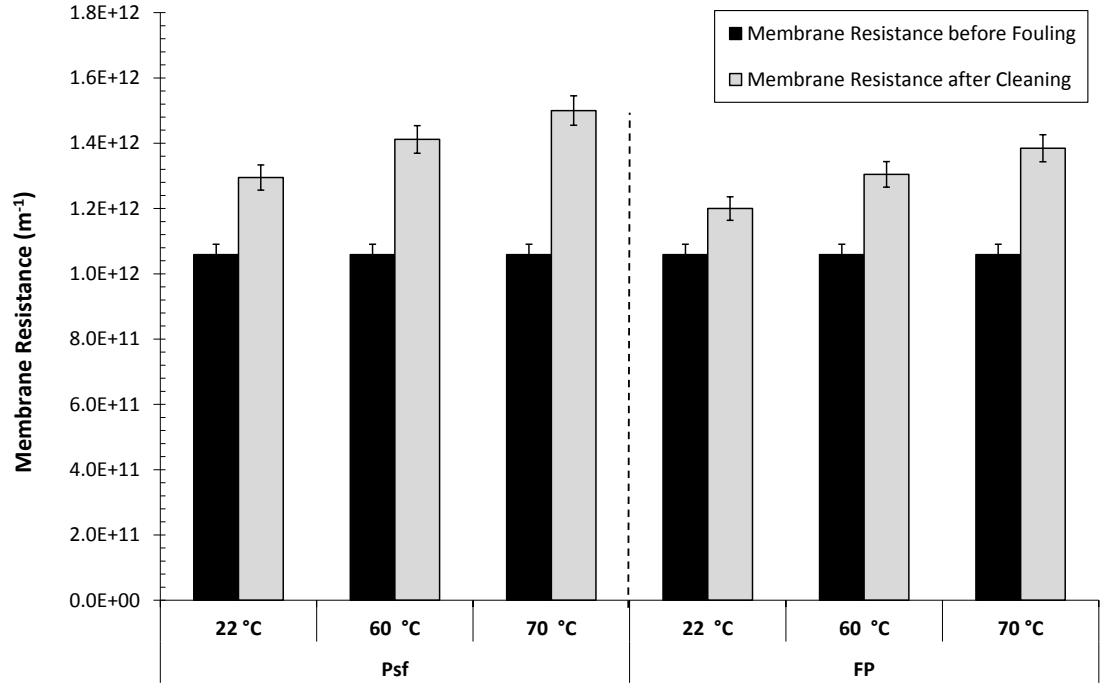

Figure 4.3: Graph to show pure water membrane resistances after cleaning vs. fouling temperature variation on Ps*f* and FP membranes when fouled with SSL (3.0 bar TMP, 1.89 ms^{-1} CFV) for 90 min. All cleaning conditions maintained at 0.10 wt. %, 1.0 bar, 1.89 ms^{-1} and 50 ºC.

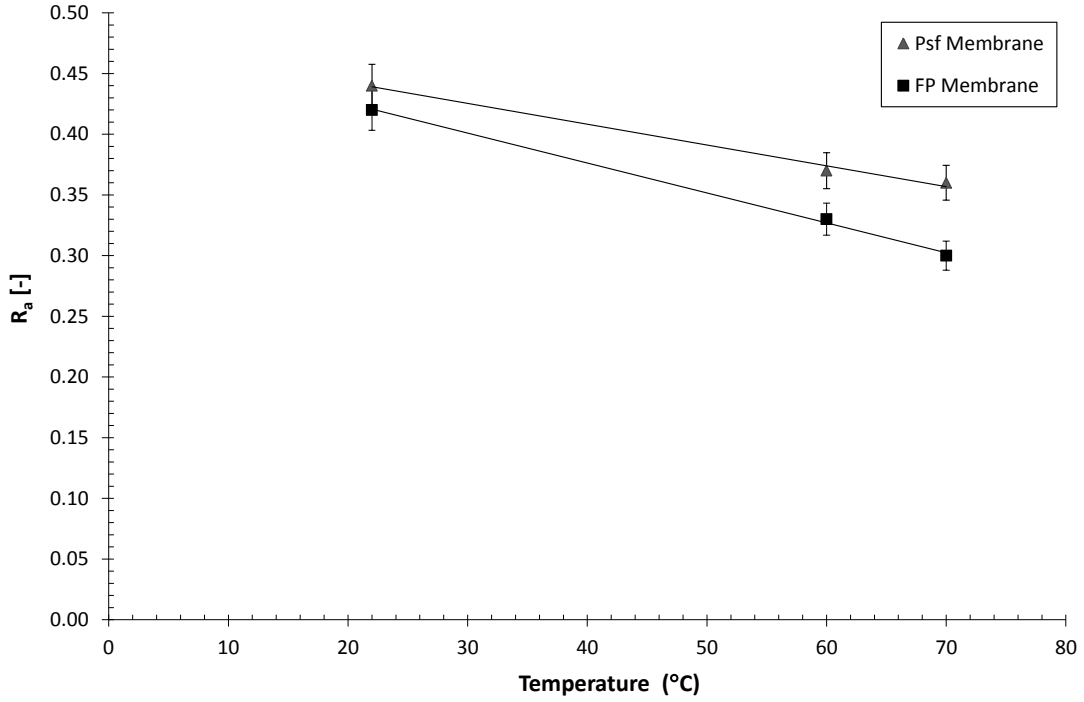

Figure 4.4: Graph to show the apparent rejection coefficient as a function of fouling temperature variation through Ps*f* and FP membranes when fouled with SSL (3.0 bar TMP, 1.89 ms^{-1} CFV) for 90 min.

4.3.1.2. Transmembrane Pressure

The fouling TMP was varied from 1.0 to 4.0 bar whilst maintaining a constant CFV of 1.89 ms^{-1} and a temperature of 60 ºC for 90 min where standard rinsing and cleaning conditions were used. RO pure water fluxes (22 ºC, 1.0 bar, and 1.89 ms^{-1}) were maintained constant before and after fouling and after cleaning. Figure 4.5 shows the first, last and average flux values in the fouling section of the cycle. The data shows that increasing the TMP increased the fouling flux until 3.0 bar TMP for the FP membrane and 4.0 bar for the Ps*f* membrane where no further increase in flux is seen regardless of the increased TMP. Bhattacharya *et al*. (2005) also observed that the rate of increase of flux with pressure becomes less as the pressure increases gradually to a high value; this is known as the limiting flux. The limiting flux is when a maximum concentration is reached at the membrane surface where a gel layer is possibly formed (Song, 1998). The Ps*f* and FP membranes limiting fluxes at 1.89 ms^{-1} when steady state flux was observed was at 52 L m^{-2} hr^{-1} (Ps*f*) and 63 L m^{-2} hr^{-1} (FP) respectively. The limiting flux in relation to varying CFVs of the FP membrane has been discussed further in the mass transfer section 4.3.2.

Figure 4.6 shows a breakdown of the different resistive layers present at steady state versus TMP. The resistance breakdown shows that the resistances due to concentration polarisation (R_{cp}) were responsible for the increased resistance on the Ps*f* membrane over the FP membrane. The higher pressures lead to an increase in R_{cp} and hence a higher rejecting membrane (Figure 4.8). For the Ps*f* membrane, R_{cp} was 35 % of the total resistance at 1.0 bar and 57 % of the total resistance at 4.0 bar, whereas for the FP membrane R_{cp} was 33 % of the total resistance at 1.0 bar and 51 % of the total resistance at 4.0 bar. This indicates that there was slightly more back diffusion occurring on the Ps*f* membranes. R_R remains approximately constant for all TMPs. The R_I increases from 2.40 x 10^{12} m^{-1} for 1.0 bar TMP to 3.60 x 10^{12} m^{-1} at 4.0 bar TMP for the Ps*f* fouled membranes. There was also a slight increase in R_I for the FP fouled membrane (2.32 x 10^{12} m^{-1} to 3.20 x 10^{12} m^{-1}). This increase in irreversible resistance could be explained by an increase in a compressed fouling layer on the membranes surface at the higher pressures which couldn't be completely removed without the use of a cleaning agent. Figure 4.7 shows that for both membranes the membrane resistance after fouling and cleaning increases as the fouling TMP increases. When fouling at higher TMPs, an increased fouling layer was formed which was increasingly difficult to remove. Concentration polarisation and cake layer formation are classed as reversible, though the associated high concentrations at the membrane surface increases the probability of irreversible fouling after rinsing and cleaning (Shorrock and Bird, 1998). This indicated that the lower fouling pressures had a higher degree of cleanability.

Figure 4.8 displays the apparent solids rejection data versus fouling TMP for the Ps*f* and FP membranes. Increasing the TMP from 1.0 bar to 2.0 bar increased the rejection coefficient from 0.24 to 0.35 (Ps*f*) and 0.20 to 0.31 (FP). The rejection coefficient was further increased to 0.37 (Ps*f*) and 0.33 (FP) at 3.0 bar. This increase in solids rejection was assumed to be due to either a simply sieving mechanism or hindrance in the solute transport. The increase in pressure caused an increase in the polarised layer thickness which acted as a secondary membrane (Bhattacharya *et al*., 2005; Blainpain *et al*., 1993). This increased pressure can also cause compaction of the fouling layer meaning the pore sizes are decreased, hindering the transport of the larger particles (Kallioinen *et al*., 2007). The FP membranes produced additional flux values compared to the Ps*f*

membranes, and hence more solid transmission due to additional solids being dragged through the membrane.

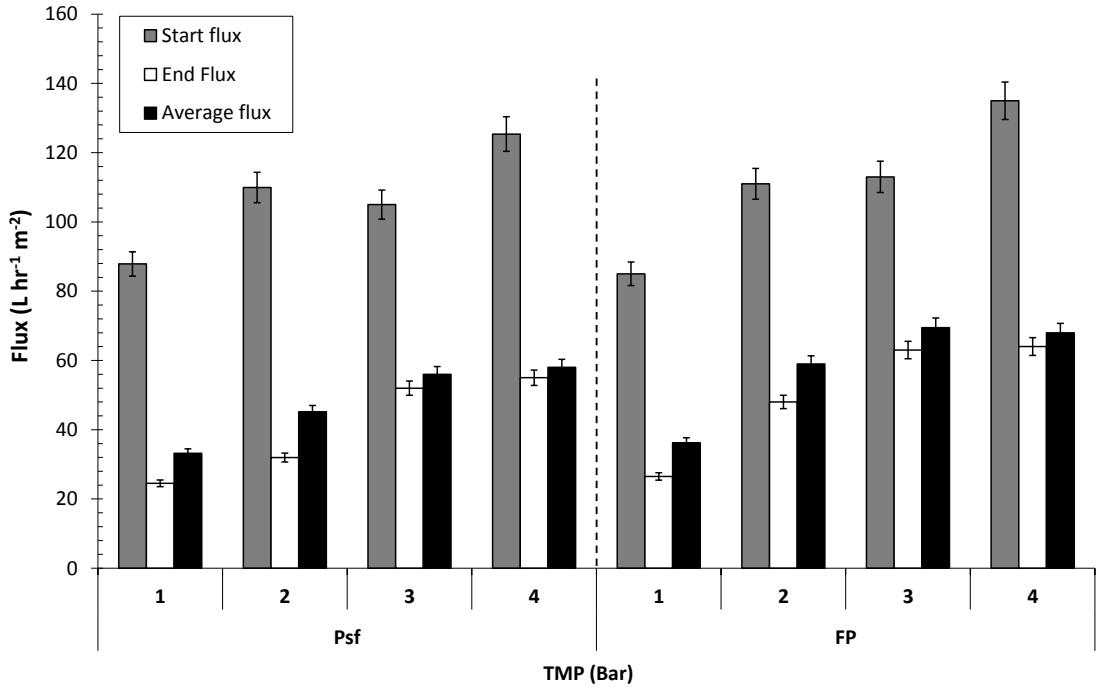

Figure 4.5: Graph to show variation of fouling flux data as a function of fouling TMP on Ps*f* and FP membranes when fouled with SSL (60 ºC, 1.89 ms^{-1} CFV) for 90min.

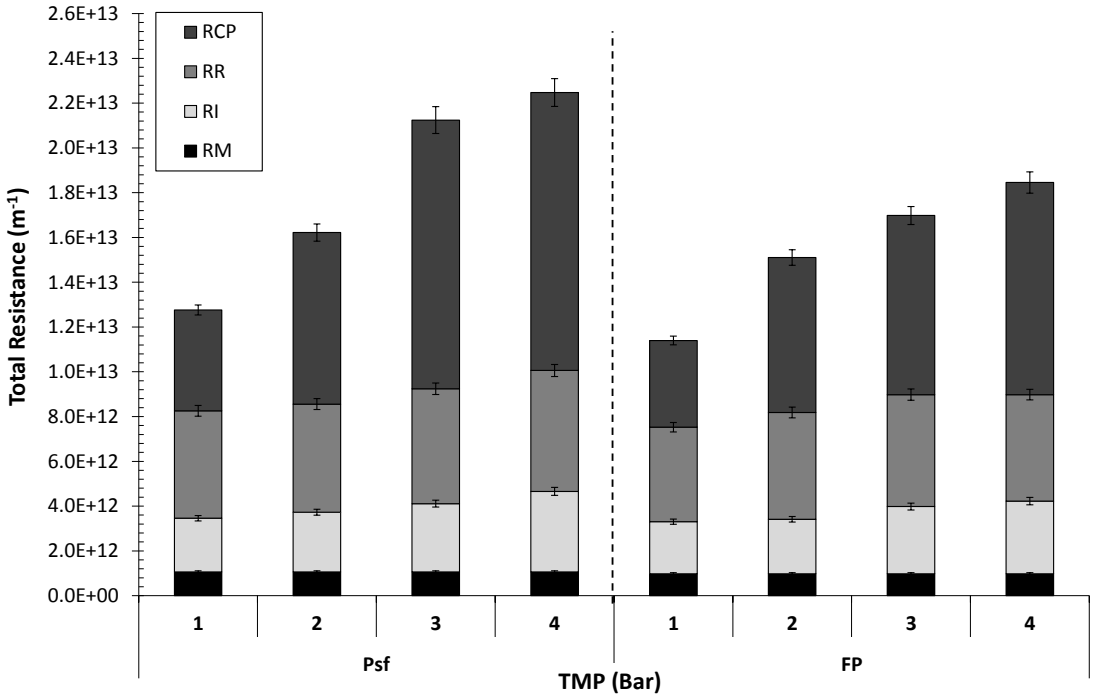

Figure 4.6: Graph to show fouling resistance data as a function of TMP on Ps*f* and FP membranes when fouled with SSL (60 ºC, 1.89 ms^{-1} CFV) for 90 min.

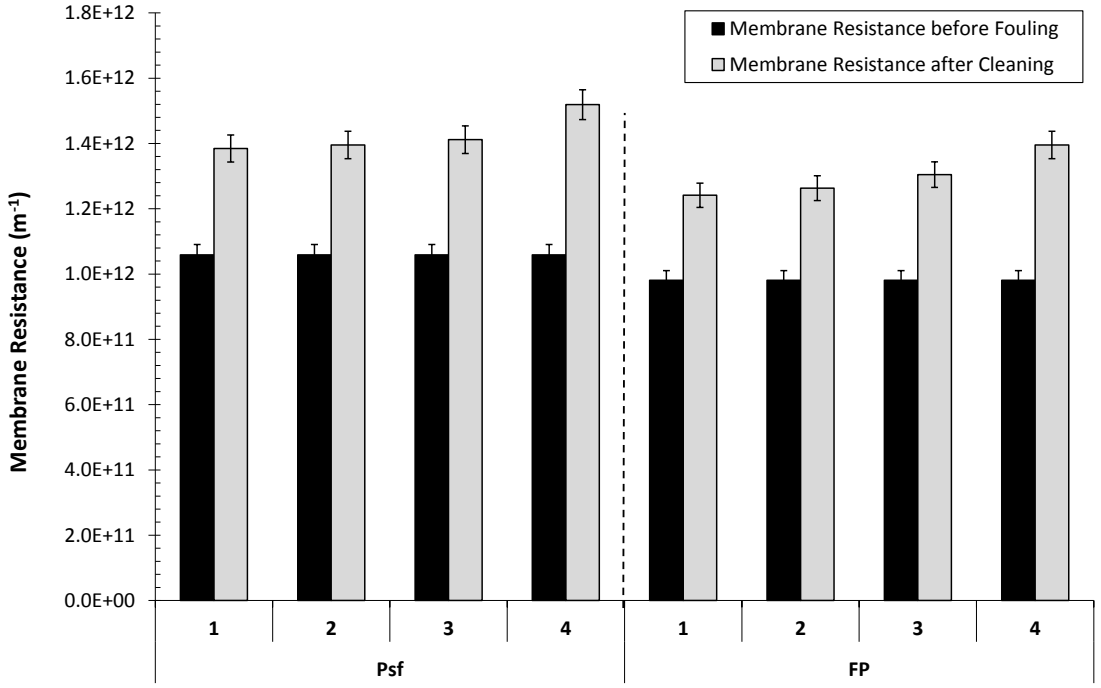

Figure 4.7: Graph to show pure water membrane resistances after cleaning vs. TMP variation on Ps*f* and FP membranes when fouled with SSL (60 ºC, 1.89 ms^{-1} CFV) for 90 min. All cleaning conditions maintained at 0.10 wt. %, 1.0 bar, 1.89 ms^{-1} and 50 ºC.

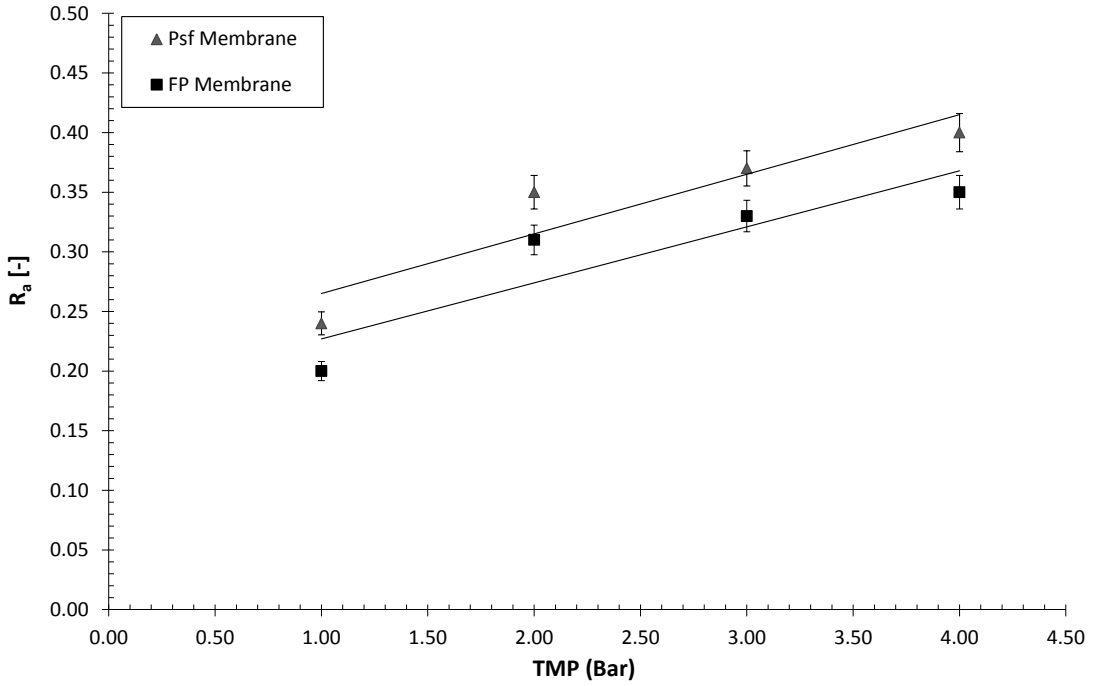

Figure 4.8: Graph to show the apparent rejection coefficient as a function of TMP variation through Ps*f* and FP membranes when fouled with SSL (60 ºC, 1.89 ms^{-1} CFV) for 90 min.

4.3.2. Mass Transfer Information

A knowledge of the mass transport coefficient (k) is necessary for design purposes and to predict the behaviour of a membrane with respect to the permeate flux (Todisco *et al*., 2002). The mass transfer coefficient for a solution can be determined by the velocity variation technique. The velocity variation method is based on the variation in apparent rejection when cross-flow velocities are changed. The rejection of solids can be studied by the so called film layer model based on the diffusion model of the Fick's first law (Bird *et al*., 1960). The theory assumes formation of a thin layer of thickness (δ) inside the retentate phase on the membrane surface where the concentration decreases from C_m on the surface to C_b in the bulk. The integration of the mass balance equation in which convective and diffusive transport is equilibrated with the mass flux in the permeate leads to Equation 4.4 (Práddanos *et al*., 1995; Todisco *et al*., 2002). In this simple model, concentration polarisation is the only fouling mechanism considered.

$$J_v = k \,\mathrm{In}\left(\frac{C_m - C_p}{C_b - C_p}\right) \qquad 4.4$$

where, k is the mass transfer coefficient ($k = D/\delta$). The apparent (observed) rejection coefficient was calculated using Equation 4.3. The maximum concentration at the membrane surface (a true rejection coefficient) can be defined as Equation 4.5.

$$R_{\max} = 1 - \left(\frac{C_p}{C_m}\right) \qquad 4.5$$

When dealing with high pressures there is a high degree of concentration polarisation slowly increasing at the membrane surface, C_m, such that the resulting high fluxes should be approximately independent of TMP (Limiting Flux). Based on the assumptions of the traditional film-layer theory the solute transport through the membrane would be mainly convective, leading to a virtually constant ratio C_p/C_m and a maximum true retention coefficient, R_{max}. If Equation 4.3 and 4.5 are substituted into Equation 4.4, Equation 4.6 is produced. A plot of $\ln[(1-R_a)/R_a]$ against J_v, yields a straight line with a slope 1/k and intercept of $\ln[(1-R_{max})/R_{max}]$.

$$\mathrm{In}\left(\frac{1-R_a}{R_a}\right)=\mathrm{In}\left(\frac{1-R_{\max}}{R_{\max}}\right)+\frac{J_v}{k} \qquad 4.6$$

Figure 4.9 displays the fouling flux data as a function of TMP (0.5 to 4.0 bar) and CFV (0.28 to 1.89 ms^{-1}) for the 20 kDa FP membrane. The limiting flux is the maximum stationary flux obtained when increasing TMP. The TMPs where the limiting flux occurred for all CFVs was 2.5 bar to 3.0 bar. Figure 4.10 displays the apparent solids rejection data as a function of fouling TMP and CFV for the 20 kDa FP membrane. The apparent rejection coefficient slightly increased linearly with increasing TMP, whereas it decreased with increasing CFV. This behaviour has also been observed in the ultrafiltration of tea (Todisco *et al*., 2002). The higher surface shear associated with increased CFV could have resulted in the decreasing R_a. Concentration polarisation occurs because of the convective transport of foulants to the membrane surface. Thereby increasing the shear rate causes greater back diffusion and transportation of foulants to the bulk solution which decreases the accumulation at the membrane surface (Bian *et al*., 2000). The flux values decreased somewhat in certain cases after 3.0 bar, though the R_a values continued to increase. This could be attributed to the fact that SSL is a polydispersed system with a wide range of molecular weights which might have partially blocked some pores. Similarly as the pressure increases, convective flux continues to increase, forming a continuous polarised layer on the membrane surface (Sridhar and Bhattacharya, 1991).

The limiting region of 2.5 bar to 4.0 bar has been used in Equation 4.6 to plot Figure 4.11. The plots of $\ln[(1-R_a)/R_a]$ against flux for CFVs of 1.11, 1.36, 1.63 and 1.98 ms^{-1} (Re = 4000 – 7000) were used for the estimation of the mass transfer coefficients. As shown in Figure 4.11, all the experimental data are well fitted by straight lines with a slope which varied with CFV. Extrapolation of the y-axis of the lines connecting the flux rejection data can be seen. The lines converge towards a similar y-axis intercept of -1.06, which corresponds to a true (actual) rejection coefficient of approximately 0.74 (74 % solids rejected). This actual rejection value is useful as an insight into the degree of concentration polarisation occurring. This actual rejection converts to an estimated membrane surface concentration (C_m). The concentration on the surface, C_m for the highest CFV of 1.89 ms^{-1} (Re = 7000) and 3.0 bar was 46 wt. %. The concentration

difference compared to the bulk concentration, C_b of 17.8 wt. % was large. This implies that there is a high degree of concentration polarisation occurring. The intercept of the data in the laminar region (results not shown) was slightly different, where the intercept of -1.53 corresponds to an actual rejection coefficient of approximately 0.82 (82 % solids rejected).

The gradients of the lines in Figure 4.11 have been used calculate the mass transfer coefficients and are displayed in Figure 4.12. The membrane filtered at 1.89 ms^{-1} (Re = 7000) had a mass transfer number of 1.06 x 10^{-5} ms^{-1}. The two regions of flow (laminar and turbulent) have been fitted with a straight line and the gradients studied. The transition from developed laminar flow to turbulent flow takes place at Re = 2200. The progression from the laminar to turbulent regime is clearly shown. The gradients show that the turbulent regime has a slightly promoted mass transfer relationship.

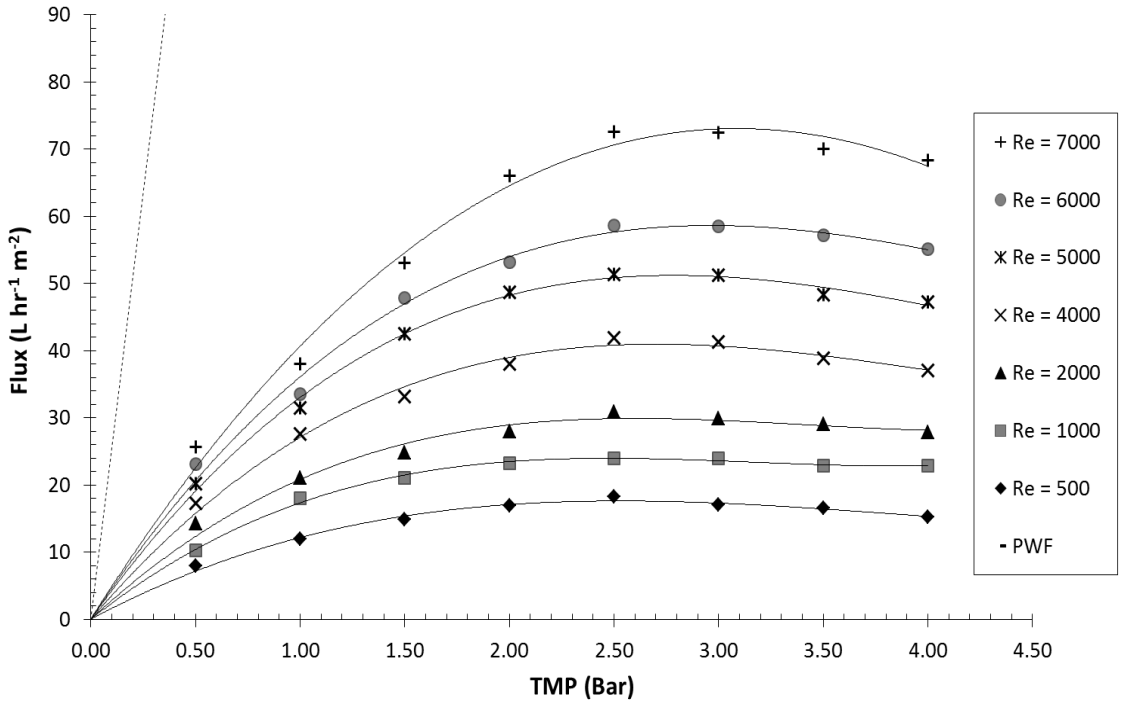

Figure 4.9: Graph to show fouling flux data as a function of TMP on FP membranes when fouled with SSL (60 ºC) at different Reynolds numbers (CFV) for 90 min.

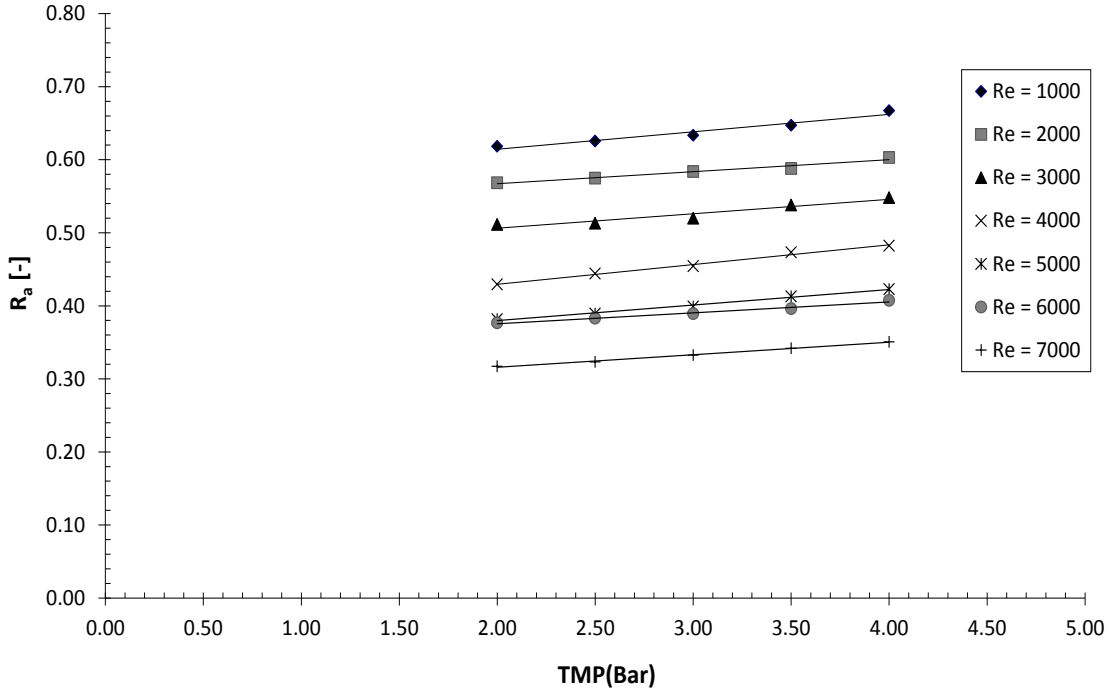

Figure 4.10: Graph to show the apparent rejection coefficient as a function of applied TMP on FP membranes when fouled with SSL (60 ºC) at different Reynolds numbers (CFV) for 90 min.

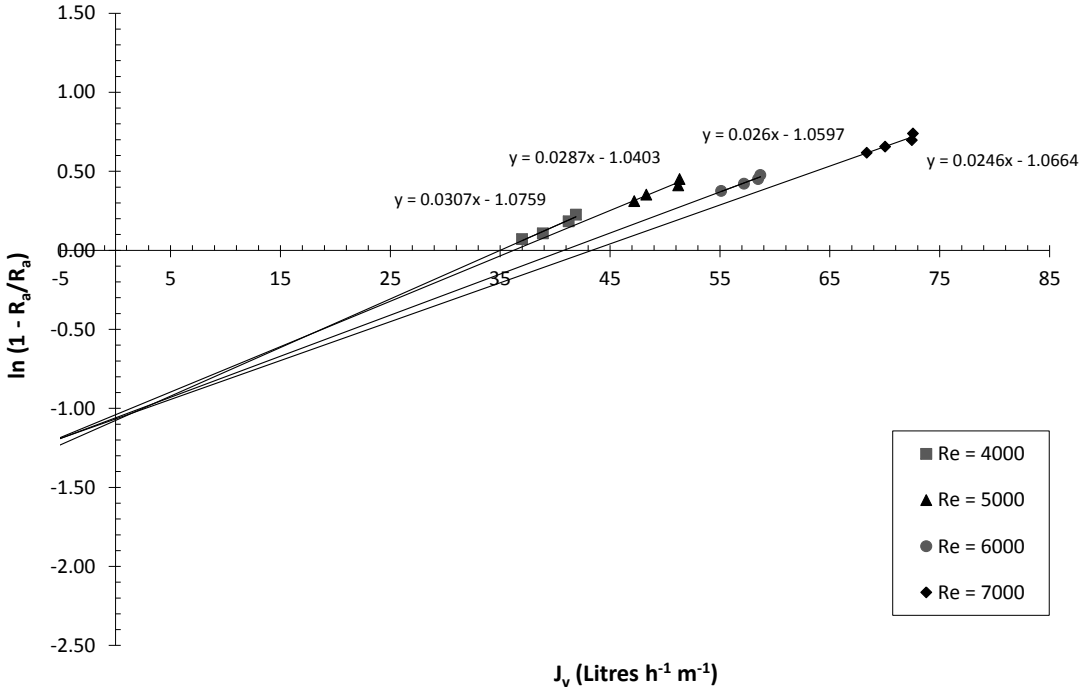

Figure 4.11: Linearised plot of the concentration polarisation equation for various CFVs with trend lines extrapolated to meet the y-axis. Constant temperature (60 ºC), varied Re: 4000, 5000, 6000 and 7000 and TMP: 2.5, 3.0, 3.5, 4.0 bar.

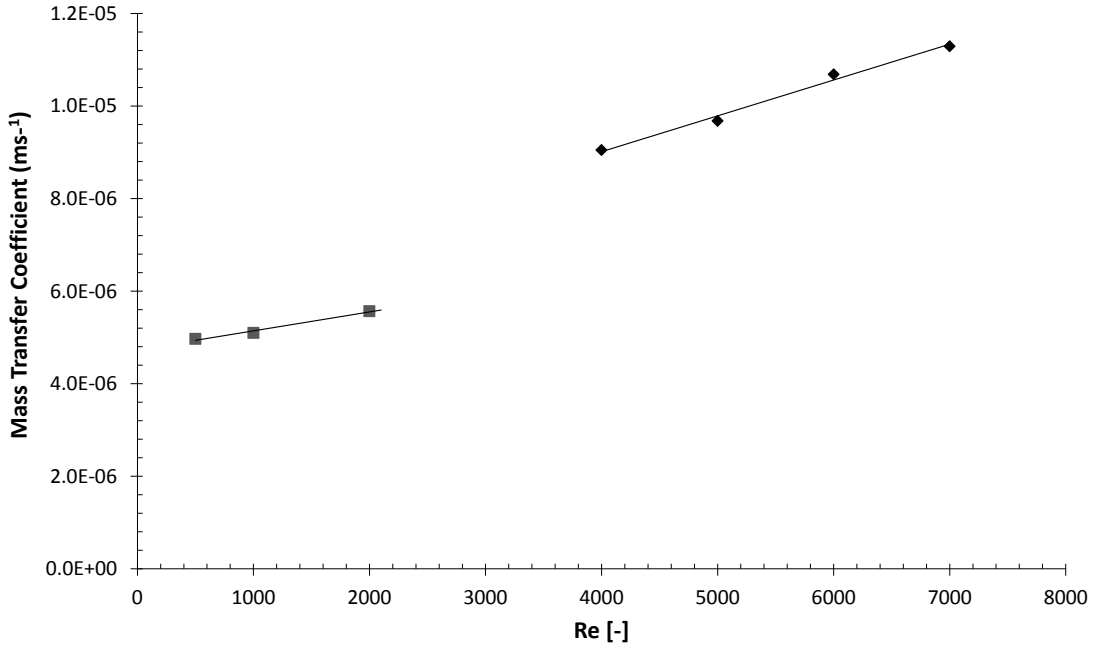

Figure 4.12: Mass transfer coefficient variation for laminar and turbulent flow regimes during SSL filtration.

4.4. Ultrafiltration of SSL – Cleaning Conditions Optimisation

The 20 kDa Ps*f* and FP membranes were fouled by filtering SSL under the same operating conditions (60 ºC, 3.0 bar, and 1.89 ms^{-1}). For all cleaning experiments, the SSL feed was filtered until it reached the same steady state flux (Error ± 6 %). The steady state flux was approximately 16 % of the initial PWF value. The rinsing stage before cleaning was necessary to remove as much of the foulant as possible. If the cleaning agent is added and there is still a high degree of fouling in the system, a lot of the cleaning agent is consumed in the bulk and is not available for cleaning (Trägårdh, 1989). The rinsing stage was performed at 22 ºC, 1.0 bar TMP, and 1.89 ms^{-1} CFV for 15 min; this removed the majority of the loosely bound particulates.

4.4.1. Effect of Cleaning Operating Conditions

Membrane cleaning efficiency is a function of multiple parameters such as hydrodynamic conditions, concentration and temperature of the cleaning solution (Liu *et al*., 2000; Chen *et al*., 2003). The cleaning conditions were optimised by varying concentration, TMP and temperature. The cleaning efficiency was evaluated by the ratio of the PWF after cleaning (J_c) to the PWF measured before fouling (J_w) for each cleaning stage. The percentage flux recovery ($\%J_r$) was calculated using Equation 4.7.

$$\%J_r = \left(\frac{J_c}{J_w}\right) \times 100 \quad 4.7$$

4.4.1.1. Cleaning Agent Concentration

The NaOH concentration was varied whilst maintaining a constant TMP of 1.0 bar, CFV of 1.89 ms^{-1}, and temperature of 50 ºC for 30 min. Three concentrations were chosen; 0.10 wt. %, 0.25 wt. % and 0.50 wt. %. Figure 4.13 compares the flux data for NaOH concentration variation on Ps*f* and FP membranes. It shows the first, last and average flux values in the cleaning section of the cycle. The cleaning flux trend for both membranes was similar. The pH of the cleaning solution becomes higher as NaOH increases and the manufacturing limits of the membrane become an issue, here 0.50 wt. % was the highest concentration tested. Figure 4.14 shows the effect of NaOH concentration on the product (fouling) flux after the first cycle of fouling and cleaning. It compares the PWF after cycle 1 to the fouling, cleaning and PWF after cycle 2. The cycle 2 fouling fluxes had no statistically relevant differences when varying the cleaning concentration. The highest PWFs after 2 cycles was 0.25 wt. % for the Ps*f* membrane (240 L m^{-2} hr^{-1}), whereas the lowest concentration of 0.10 wt. % was superior for the FP membrane (245 L m^{-2} hr^{-1}). Figure 4.15 shows the effect of NaOH concentration on the PWF recovery after fouling and cleaning for two cycles. The gel layer was largely removed by the chemical cleaning agent and large changes in PWF recovery were seen after the first cleaning stage. The PWF recovery after cycle 2 sees a decrease in recovery of 15 % for the Ps*f* membrane and 21 % for the FP membrane when cleaning with 0.10 wt. % NaOH. The PWF fluxes after cleaning did not vary significantly with NaOH concentration, except the higher concentration of 0.50 wt. % where the flux recovery decreased. Bansal *et al*. (2006), Bird and Bartlett (2002), Popović *et al*. (2009) also found that an increase in concentration of NaOH solution did not always increase flux recovery. The increasing concentration of the NaOH solution could cause the lower flux recovery by; (i) the increasing concentration sealing the surface and preventing the removal of the deposit and/or (ii) a chemical induced gelation could have occurred when the cleaning solution was introduced (Bansal *et al*., 2006; Fryer, 1997; Mercadé-Prieto and Chen, 2005). A lower concentration is therefore often better both environmentally and economically. An optimal NaOH concentration of 0.10 wt. %

produced a flux recovery of 80 % (± 3 %) for the Ps*f* membrane and 85 % (± 3 %) for the FP membrane after one cycle.

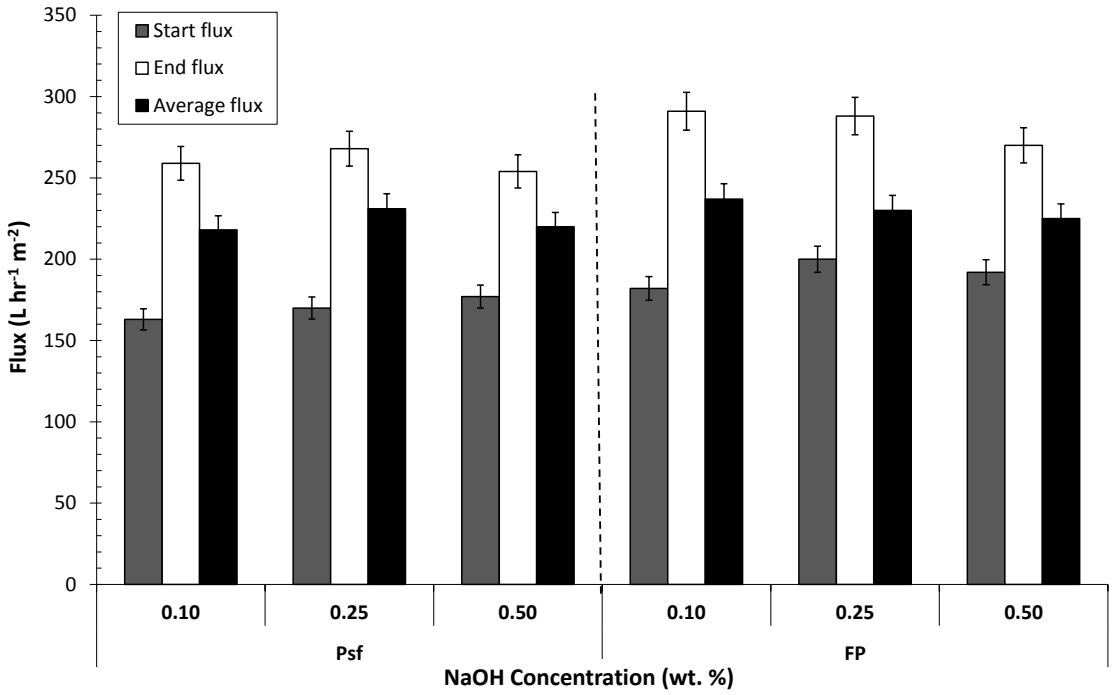

Figure 4.13: Graph to show NaOH cleaning flux as a function of cleaning concentration variation on Ps*f* and FP membranes when fouled with SSL (3.0 bar, 60 ºC, 1.89 ms^{-1}) for 90 min. All cleaning conditions maintained at 1.0 bar, 1.89 ms^{-1} and 50 ºC.

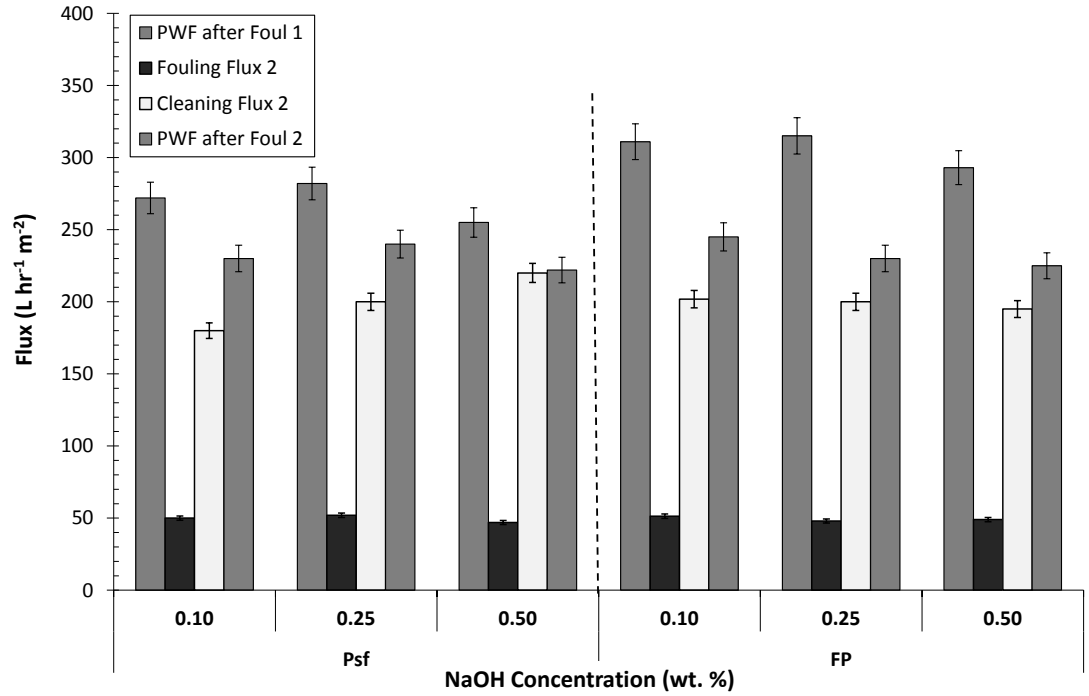

Figure 4.14: Graph to show the PWFs, fouling fluxes and cleaning fluxes for twice fouled membranes vs. cleaning TMP variation on 20 kDa Ps*f* and FP membranes when fouled with SSL (3.0 bar TMP, 60 ºC, 1.89 ms^{-1}) for 90 min. All cleaning conditions maintained at 1.0 bar, 1.89 ms^{-1} and 50 ºC.

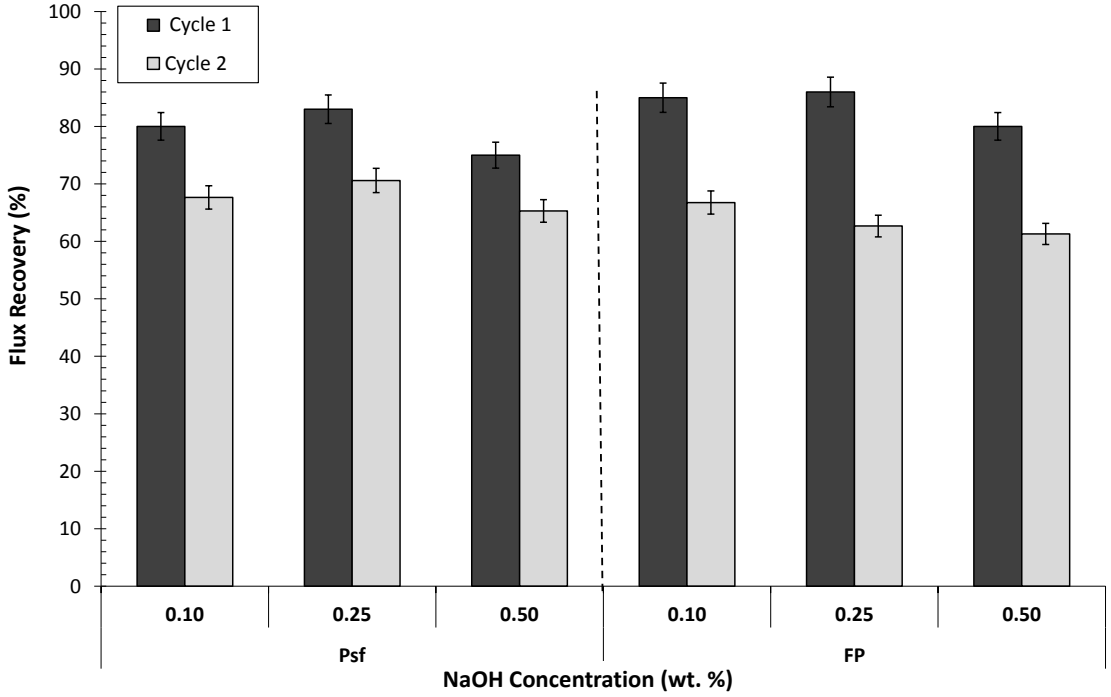

Figure 4.15: Graph to show flux recovery as a function of cleaning concentration variation on Ps*f* and FP membranes when fouled with SSL (3.0 bar TMP, 60 ºC, 1.89 ms^{-1}) for 90 min. All cleaning conditions maintained at 1.0 bar, 1.89 ms^{-1} and 50 ºC.

4.4.1.2. Transmembrane Pressure

The TMP was varied while maintaining a constant NaOH concentration of 0.10 wt. %, CFV of 1.89 ms^{-1}, and temperature of 50 ºC for 30 min. Figure 4.16 compares the flux data for cleaning TMP variation on Ps*f* and FP membranes. It shows the first, last and average flux values in the cleaning section of the cycle. The cleaning fluxes increased with increased TMP to 1.0 bar, due to the extra forces being imposed on both the membrane surfaces. There was a slight decrease in cleaning fluxes at 2.0 bar for both membranes. Figure 4.17 shows the effect of TMP on the product (fouling) flux after the first cycle of fouling and cleaning. It compares the PWF after cycle 1 to the fouling, cleaning and PWF after cycle 2. The cycle 2 fouling fluxes which had been cleaned at 2.0 bar were lower than the two other cleaning TMPs. This could be explained by the decreased flux recovery after the first cleaning cycle. The highest PWFs after 2 cycles was 0.5 bar for the Ps*f* membrane (235 L m^{-2} hr^{-1}), whereas 1.0 bar was slightly improved for the FP membrane (245 L m^{-2} hr^{-1}). The PWF values for the 0.5 bar and 1.0 bar were comparable. Figure 4.18 shows the effect of TMP variation on the PWF recovery after fouling and cleaning for two cycles. The optimal cleaning TMP for flux recovery was 1.0 bar, as operating at 0.5 bar and 2.0 bar affected the flux recovery. The

cleaning at 0.5 bar didn't generate sufficient forces on the membrane surface to remove an adequate amount of the fouling material. Whereas, the higher TMP of 2.0 bar could have caused compaction of the membrane, triggering some of the fouling or cleaning material to cause pore blocking (Jönsson and Trägårdh, 1990). The cleaning regime of the FP membrane had an increased effect compared to the Ps*f*, whereas after cycle 2, the PWF flux after cleaning showed that the Ps*f* membrane had a slightly better flux recovery than the FP membrane.

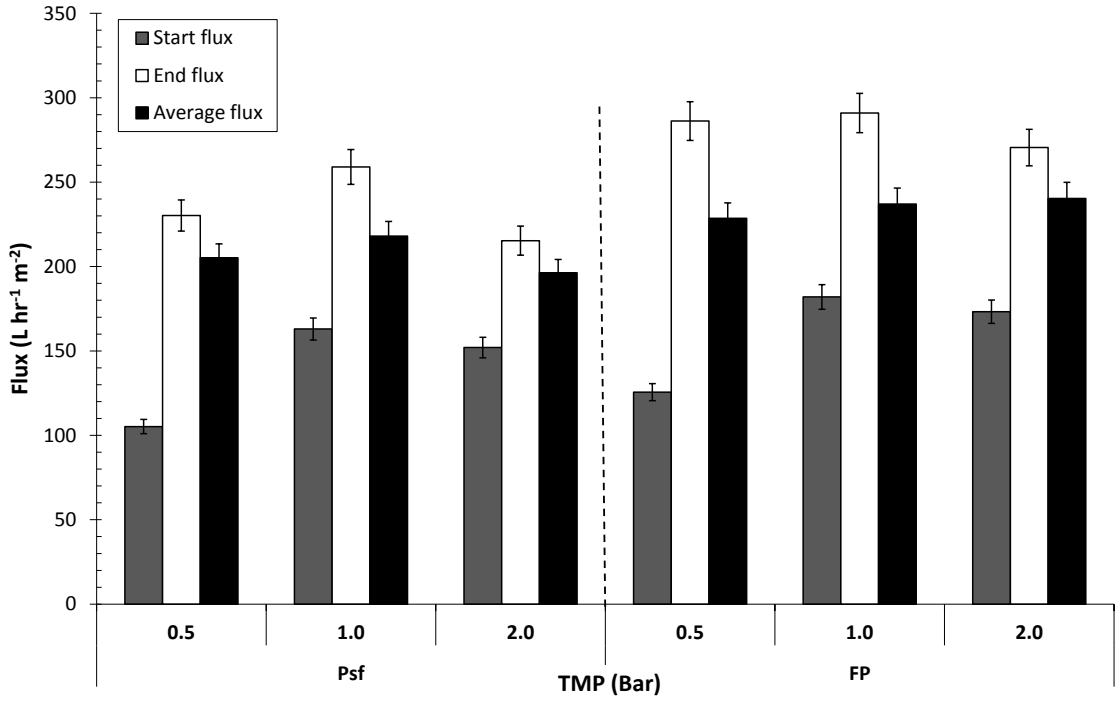

Figure 4.16: Graph to show NaOH cleaning flux as a function of cleaning TMP variation on Ps*f* and FP membranes when fouled with SSL (3.0 bar, 60 ºC, 1.89 ms^{-1}) for 90 min. All cleaning conditions maintained at 0.10 wt. % NaOH, 1.89 ms^{-1} and 50 ºC.

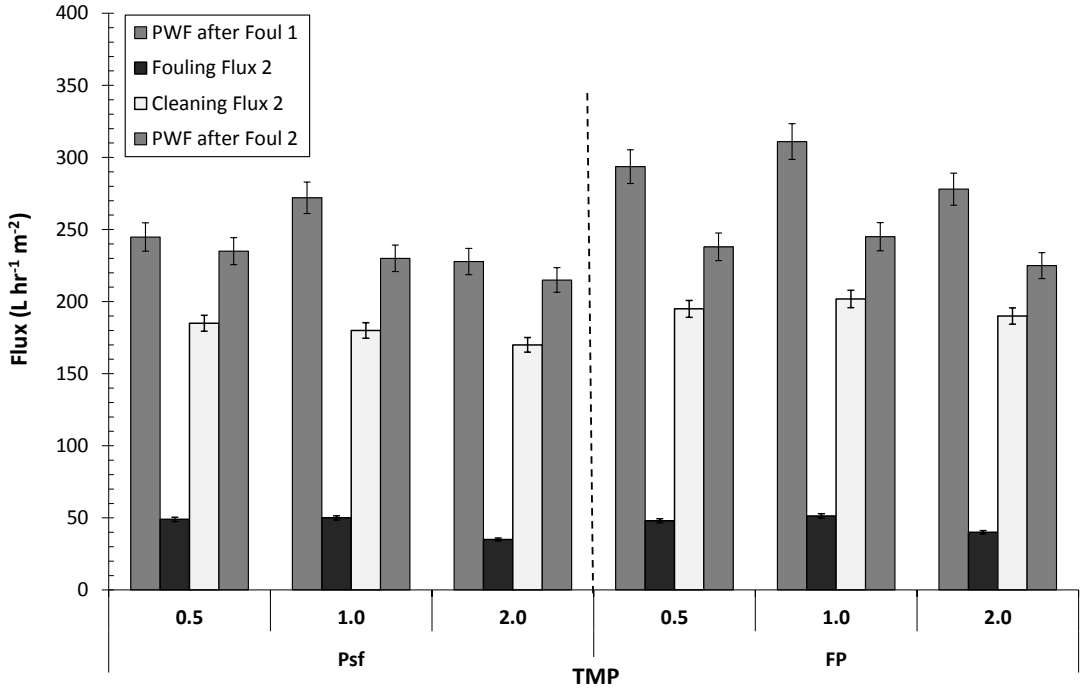

Figure 4.17: Graph to show the PWFs, fouling fluxes and cleaning fluxes for twice fouled membranes vs. cleaning TMP variation on 20 kDa Ps*f* and FP membranes when fouled with SSL (3.0 bar TMP, 60 ºC, 1.89 ms^{-1}) for 90 min. All cleaning conditions maintained at 0.10 wt. % NaOH, 1.89 ms^{-1} and 50 ºC.

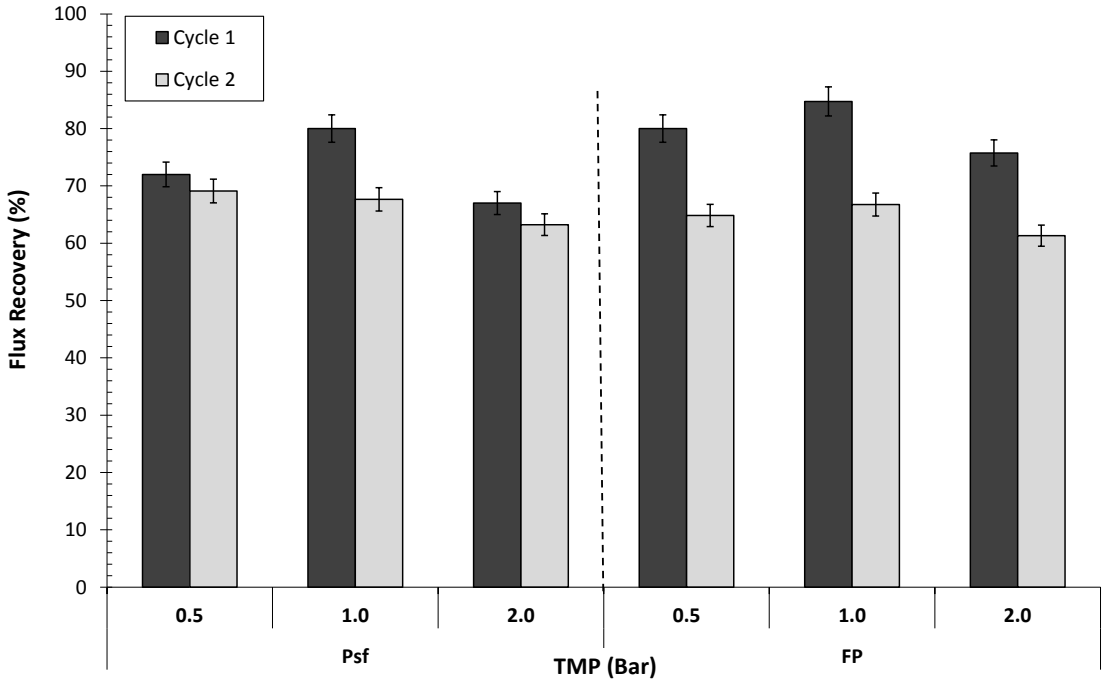

Figure 4.18: Graph to show flux recovery as a function of cleaning TMP variation on Ps*f* and FP membranes when fouled with SSL (3.0 bar TMP, 60 ºC, 1.89 ms^{-1}) for 90 min.

4.4.1.3. Temperature

The temperature was varied while maintaining a constant NaOH concentration of 0.10 wt. %, CFV of 1.89 ms^{-1}, and TMP of 1.0 bar for 30 min. Figure 4.19 compares the flux data for cleaning temperature variation on Ps*f* and FP membranes. It shows the first, last and average flux values in the cleaning section of the cycle. Three cleaning temperatures were chosen, 22 ºC, 50 ºC and 60 ºC. These temperatures were chosen as many previous authors have found that 50 ºC is the ideal temperature for cleaning and room temperature is used as a comparison (Weis, 2004; Evans, 2008). The cleaning fluxes increased with increased temperature fairly dramatically for both membranes till 50 ºC (Figure 4.19). This is perhaps due to the decreased viscosity, and increased reaction rates of the cleaning solution when the temperature is raised. Figure 4.20 shows the effect of TMP on the product (fouling) flux after the first cycle of fouling and cleaning. It compares the PWF after cycle 1 to the fouling, cleaning and PWF after cycle 2. The higher temperatures of 50 ºC and 60 ºC produced similar values of PWF after two fouling and cleaning cycles. At 22 ºC the flux recovery after cycle 1 for the Ps*f* membrane was only 35 % and the FP membrane was 33 % respectively (Figure 4.21). At this temperature, the membrane would probably still have foulants on the surface and in the pores. This is shown in the fouling data after the first cleaning, where the flux values decreased by 38 % (Ps*f*) and 52 % (FP) from the first cycle. PWF flux shows that the FP membrane has slightly better flux recovery than the Ps*f* membrane. The cleaning regime at 22 ºC showed that the FP and Ps*f* membranes had remarkably similar results, though the flux recovery of the Ps*f* membrane had slightly better results. The cleaning regime of the FP membrane after cycle 1 had an increased effect compared to the Ps*f* membrane at 50 ºC. After two cycles, the flux recovery values were not significantly different. These experiments seem slightly inconclusive in respect to the different membranes, but do show that cleaning at a higher temperature of 50 ºC is optimal. Raising the temperature of NaOH to 60 ºC slightly decreases the flux after fouling and cleaning. This increase in temperature could help the sodium ions to react with the lignosulphonates which causes the fouling layer to become more compressed (Weis, 2004).

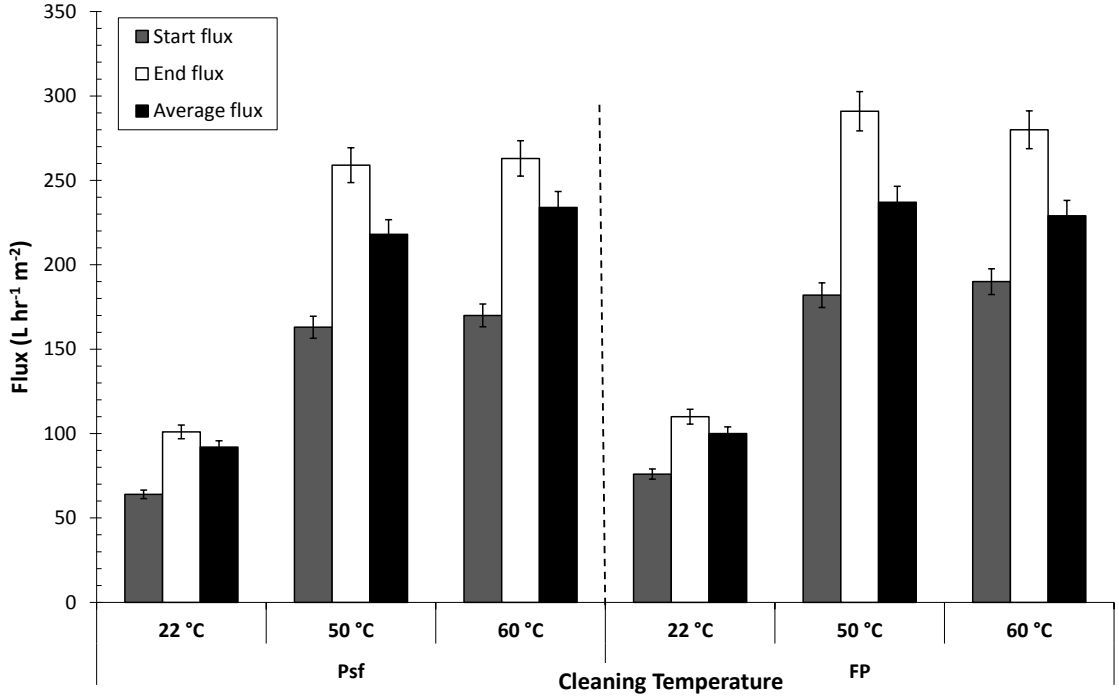

Figure 4.19: Graph to show NaOH cleaning flux as a function of cleaning temp variation on Ps*f* and FP membranes when fouled with SSL (60 ºC, 3.0 bar, 1.89 ms^{-1}) for 90 min. All cleaning conditions maintained at 0.10 wt. % NaOH, 1.89 ms^{-1} and 1.0 bar TMP .

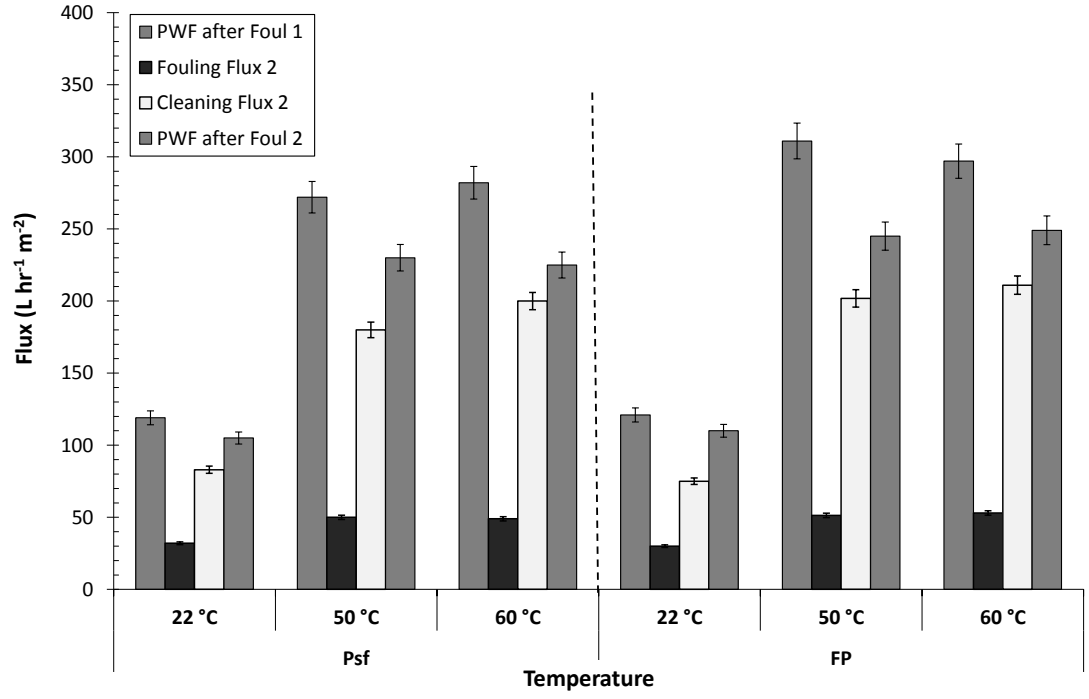

Figure 4.20: Graph to show the PWFs, fouling fluxes and cleaning fluxes for twice fouled membranes vs. cleaning temp variation on 20 kDa Ps*f* and FP membranes when fouled with SSL (3.0 bar TMP, 60 ºC, 1.89 ms^{-1}) for 90 min. All cleaning conditions maintained at 0.10 wt. % NaOH, 1.89 ms^{-1} and 1.0 bar TMP.

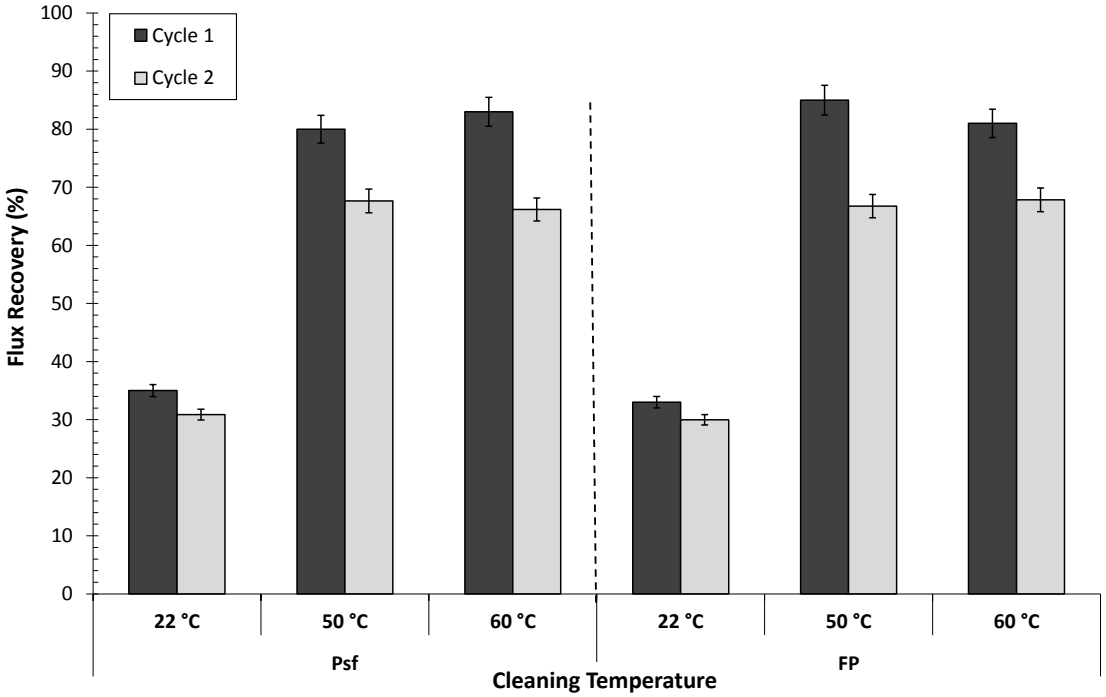

Figure 4.21: Graph to show flux recovery as a function of cleaning temp variation on Ps*f* and FP membranes when fouled with SSL (3.0 bar TMP, 1.89 ms^{-1}) for 90 min.

4.4.2. Membrane Contact Angle

The contact angle of a surface against water reflects its wettability. When water wets the surface, i.e., shows a small contact angle, the surface has the ability to interact with water molecules (dipoles). Dissociable groups on a surface help it to interact with water molecules and to make the surface more hydrophilic (Mänttäri *et al*., 2006). For hydrophobic membranes, the contact angle will be larger than 90º and for hydrophilic membranes the contact angle will be less than 90º tending toward 0º. The measurement of water contact angle is affected by many factors including material, manufacturing process, roughness of the membrane surface, the purity of water, and even the techniques used by individual investigators.

The hydrophobicity of the membranes was characterised by recording contact angle measurements (Table 4.1). The two types of membranes tested were both considered to be moderately hydrophilic as the contact angles measured were less than 90º. The FP membrane showed a slightly more hydrophilic nature compared to the Ps*f* membrane. After fouling and cleaning cycles, both membrane surfaces had a contact angle between that of a virgin and a fouled surface (Ps*f*: 62º, FP: 60º).

Table 4.1: Contact angle of water drops made with membrane surfaces

Membrane	Contact Angle (°)			
	Unconditioned	Conditioned	Fouled	After Cleaning
Fluoropolymer	64 ± 2	62 ± 2	45 ± 3	60 ± 2
Polysulphone	57 ± 3	67 ± 3	49 ± 2	62 ± 2

4.5. Optimal SSL Fouling and Cleaning Filtration Conditions

The fouling conditions have been optimised by varying CFV, TMP and temperature. The FP membrane overall had a superior performance over the Ps*f* membrane. The optimised conditions were found to be: a TMP of 3.0 bar, a CFV of 1.89 ms^{-1} and a temperature of 60 ºC for 90 min. The standard rinsing and cleaning conditions were also optimised. A summary of all the conditions can be found in Table 4.2. These conditions were used for all other experiments concerning the filtration of SSL.

Table 4.2: Summary of the filtration cycle conditions

Stage	Fluid	Protocol
Conditioning	Reverse osmosis water	60 °C, 120 min, 1.0 bar, 1.89 ms^{-1}
PWF Measurements	Reverse osmosis water	22 °C, 10 min, 1.0 bar, 1.89 ms^{-1}
Fouling	SSL	60 °C, 90 min, 3.0 bar, 1.89 ms^{-1}
PWF after fouling	Reverse osmosis water	22 °C, 10 min, 1.0 bar, 1.89 ms^{-1}
Rinsing	Reverse osmosis water	22 °C, 15 min, 1.0 bar, 1.89 ms^{-1}
PWF after rinsing	Reverse osmosis water	22 °C, 10 min, 1.0 bar, 1.89 ms^{-1}
Cleaning	NaOH (0.10 wt. %)	50 °C, 30 min, 1.0 bar, 1.89 ms^{-1}
PWF after cleaning	Reverse osmosis water	22 °C, 10 min, 1.0 bar, 1.89 ms^{-1}

4.6. Pre-Treatment of 20 kDa FP Membranes – Single Cycle

The objective of this part of the study was to determine whether the application of a simple NaOH pre-treatment could affect both the type of foulant species attaching to the membrane surface, and improve the separation performance. Manufacturers have recommended that a pre-cleaning treatment consisting of a NaOH solution should be applied to some classes of flat sheet polymeric membrane before feeds are filtered (Alfa Laval, 2009). Whilst this is recommended, it is not commonly practiced. Jönsson and

Trägårdh (1990) found that a membrane that has been cleaned before use has quite a different performance than membranes that have not been cleaned. Nyström and Zhu (1997), and Zhu and Nyström (1998) also found that cleaning the membrane before filtration can modify the separation process and the types of foulants subsequently attaching to the surface. Jeżowska *et al*. (2006) likewise observed that a simple pre-treatment using a standard membrane cleaner gave a significant improvement in the permeate flux though it did not result in an improvement in the retention. In certain membrane systems, it may be possible to selectively adsorb key foulants to the membrane surface as an anti-fouling pre-treatment, leading to the generation of a beneficial fouling layer. Such a layer can lead to improvements in permeate flux and selectivity for the system concerned (Evans and Bird, 2010; Wu and Bird, 2007). Here, the effect of two pre-treatment methods for the filtration of SSL (17.8 wt. % dry solids) using a 20 kDa MWCO FP membrane has been compared. The pre-treatment methods used in this study involved: (i) conditioning with water at 60 ºC only; and (ii) conditioning with water at 60 ºC followed by cleaning with NaOH. Membrane surface characteristics such as hydrophobicity, charge, and roughness will affect the membrane separation characteristics. Fouled membrane surfaces were subsequently characterised using: (i) Streaming potential measurements, (ii) Fourier Transform Infra-Red (FTIR) spectral peak height analysis, (iii) Scanning electron microscopy (SEM), (iv) Atomic force microscopy (AFM) and (v) Contact angle measurements.

4.6.1. Conditioning Flux Data for SSL with 20 kDa FP Membranes

Conditioning was required to remove glycerine from the membrane surfaces; it was performed using the protocol developed in Weis *et al*. (2005), with RO water at 60 ºC, 1.0 bar TMP, and 1.89 ms^{-1} CFV for 120 min. These conditions were found sufficient to remove glycerine coatings. The real flux data for the 20 kDa FP membranes are shown in Figure 4.22. All the membranes displayed a slight flux decline but varying flux regions, therefore, a normalised flux was used to compare the other samples (results not shown). The concentration of NaOH used in Protocol 2 was tested with regard to PWF before fouling, fouling flux and PWF after fouling and cleaning. Figure 4.23 compares four concentrations of NaOH cleaning before fouling (0.10, 0.25, 0.40 and 0.50 wt. %). The membrane was also treated with 0.75 wt. % NaOH, but the membrane was deformed when taken out of the filtration module. It is believed the concentration was

too high for the FP membranes, as it produced a pH of 13.3. The other concentrations of NaOH had similar fluxes before fouling and fouling fluxes. The fluxes after fouling and cleaning showed the main differences, where the 0.50 wt. % NaOH was the preferred choice with the greatest flux recovery.

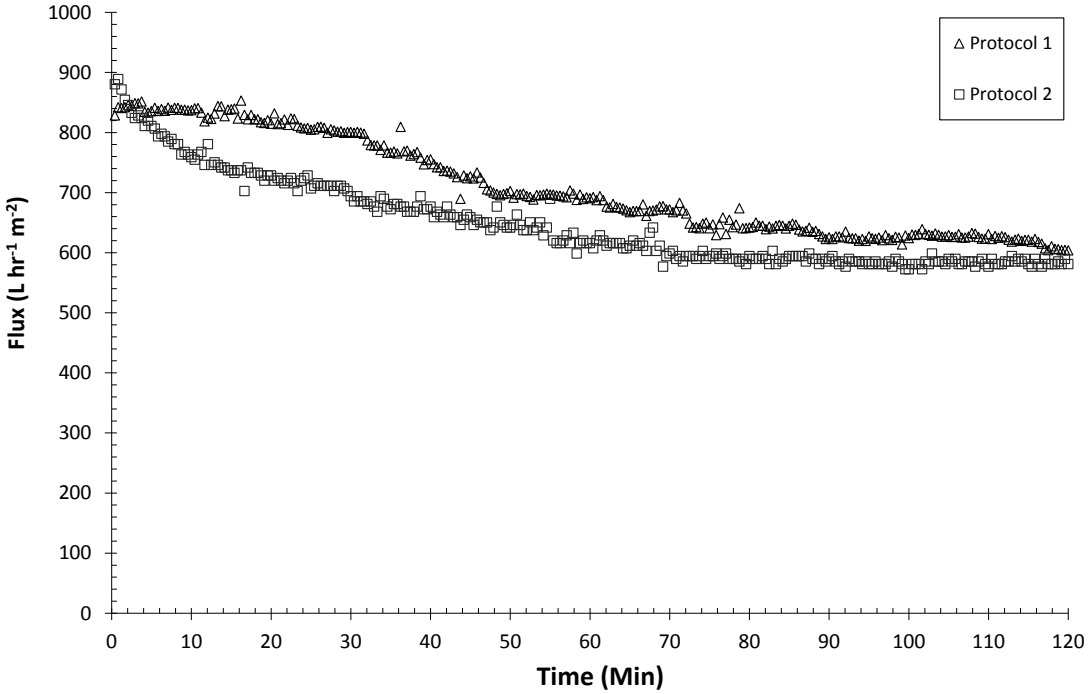

Figure 4.22: Graph to show the average effect of conditioning on flux for Protocol 1 and Protocol 2 treated 20 kDa FP membranes. Graph shows the conditioning with 60 ºC water for 120 min. The cleaning with NaOH on Protocol 2 membranes was performed after this stage.

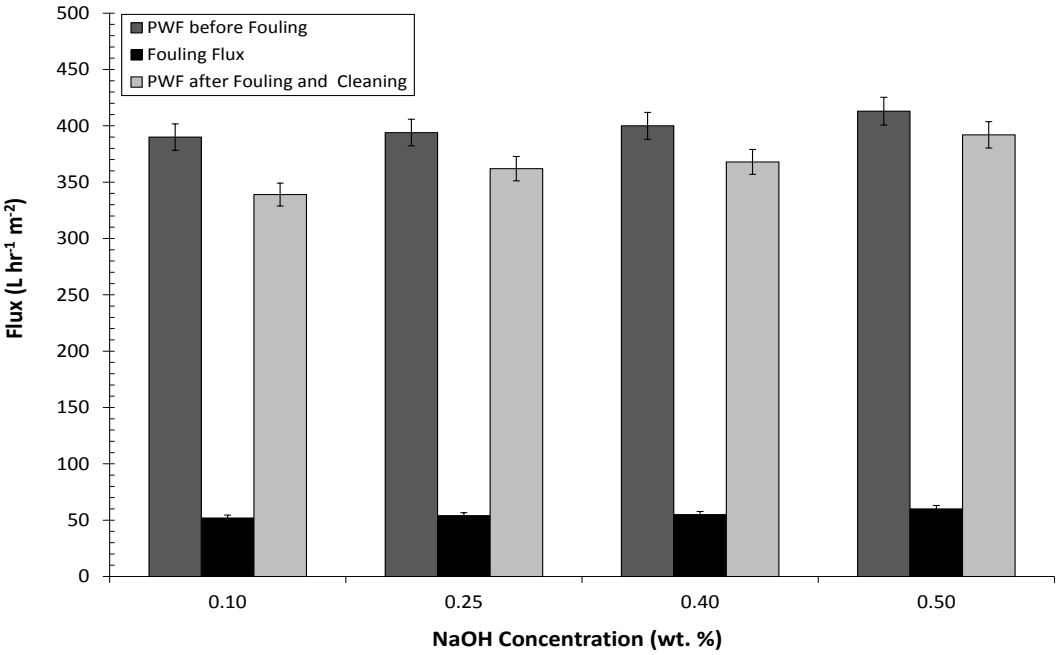

Figure 4.23: Graph to show the average effect of NaOH concentration cleaning before fouling, during fouling and after cleaning on flux values for Protocol 2 treated 20 kDa FP membranes.

4.6.2. Flux Data for SSL with 20 kDa FP Membranes

The fouling conditions have been optimised previously by CFV, TMP and temperature. The fouling TMP was maintained at a constant TMP of 3.0 bar, CFV of 1.89 ms^{-1} and a temperature of 60 ºC for 90 min where standard rinsing and cleaning conditions were used. RO pure water fluxes (22 ºC, 1.0 bar, and 1.89 ms^{-1}) were maintained constant before and after fouling and after cleaning. Cleaning after fouling maintained a constant NaOH concentration of 0.10 wt. %, CFV of 1.89 ms^{-1}, temperature of 50 ºC for 30 min.

The flux data has been normalised; with the initial PWF taken as 1.0, and the other data scaled accordingly for each Protocol. The initial flux for the Protocol 1 treated membrane was 451 L m^{-2} hr^{-1} and that for the Protocol 2 membrane was 405 L m^{-2} hr^{-1}. These values refer to the PWF recorded after the corresponding conditioning Protocol. These values were taken rather than those for the virgin membrane; otherwise a false comparison of the cleaning of the membrane over time would be made. The two pre-treatment conditioning methods displayed similar flux trends, which are shown in Figures 4.24. A rapid decline in fouling flux is shown which develops into a much lower steady state flux. This trend is expected for pressure driven membrane separation (Hinková *et al*., 2000). The decline of flux in the UF membrane can be attributed to concentration polarisation and various adhesion fouling phenomena (such as adsorption, pore blocking and deposition of solidified solutes). The lignosulphonates represent a polydispersed system with a wide range of molecular weight distribution from 200 to 15,000 Da. Pore blocking and adsorption would occur when separating with a 20 kDa membrane (Bhattacharya *et al*., 2005). The phenolic compounds are thought to contribute significantly to the fouling problem during lignosulphonates separation (Weis *et al*., 2005). Weis *et al*. (2005) also found that the acids in the SSL are also major foulants, and are partially responsible for the flux decline appearing during the ultrafiltration. Jönsson and Jönsson (1995) found that the fatty acids in SSL can reduce membrane flux severely, typically due to adsorption. Protocol 1 results in a slightly superior fouling flux performance than Protocol 2 (3.6 % enhanced flux). However, this is not statistically significant. As Protocol 1 produced an error of ± 4 % and Protocol 2 had an error value of ± 5 %. Protocol 1 continues to outperform Protocol 2 during the first 25 minutes of cleaning. However, after 30 minutes the positions are reversed, and Protocol 2 provides a flux recovery of 95 % (± 1), compared to 87 % (± 1) seen for

Protocol 1. It is hypothesised that these differences in flux recovery could be due to a charge modification of the membrane when pre-treated with Protocol 2, as shown by the zeta potential results in section 4.6.4. This modification of the surface results in different species being attached to the membrane (section 4.6.7). It appears that these species are more easily removed than the foulant species deposited following the application of Protocol 1. Figure 4.24 demonstrates that whilst neither cleaning treatments were able to return the membrane to a pristine condition for the cleaning times selected, Protocol 2 offered the promise of a greater recovery for a longer cleaning cycle.

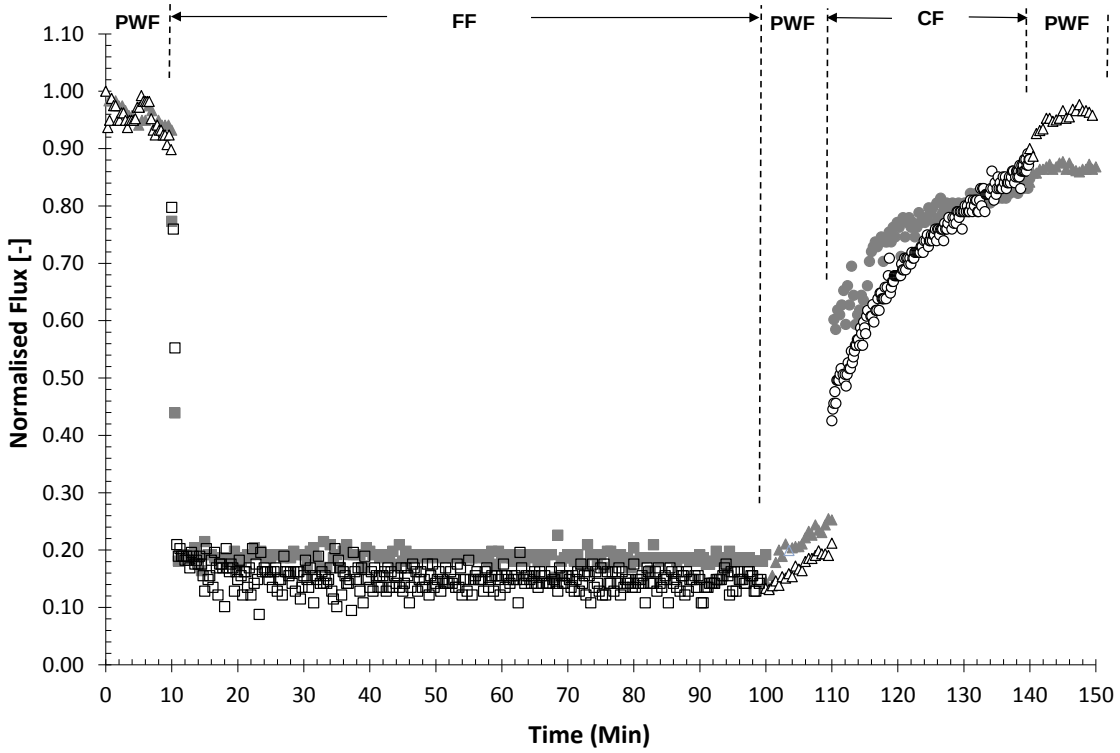

Figure 4.24: UF of SSL using 20 kDa FP membranes: Graph to show normalised PWF, fouling flux and cleaning flux vs. Time. Symbols: ▲ – PWF, ■ – fouling flux (FF), ● – cleaning flux (CF); solid symbols – P1, open symbols P2. Average initial flux; P1: 451 L m^{-2} hr^{-1}, P2: 405 L m^{-2} hr^{1}. Average final flux; P1: 392 L m^{-2} hr^{-1}, P2: 385 L m^{-2} hr^{1}.

4.6.3. Resistances

Figure 4.25 displays the magnitude of the resistances, under steady state conditions for the SSL fouled membranes. The membrane resistance before fouling for the Protocol 1 membrane was 8.88 x 10^{11} m^{-1} and 9.53 x 10^{11} m^{-1} for Protocol 2 membrane. The difference in these values are due to the initial PWF fluxes for Protocol 1 and Protocol 2 membranes being 451 L m^{-2} hr^{-1} and 405 L m^{-2} hr^{-1} respectively. Figure 4.25 shows that

the application of Protocol 2 (1.92 x 10^{13} m^{-1}) leads to an increase in the total resistance over Protocol 1 (1.25 x 10^{13} m^{-1}). The resistance breakdown shows that the R_{cp} is principally responsible for the increased resistance when applying Protocol 2 (P1: 6.09 x 10^{12} m^{-1}, P2:1.11 x 10^{13} m^{-1}). R_R remains approximately constant for both protocols (P1: 2.34 x 10^{12} m^{-1}, P2: 2.66 x 10^{12} m^{-1}). The R_I increases from 3.16 x 10^{12} m^{-1} for Protocol 1 to 4.50 x 10^{12} m^{-1} for Protocol 2 treated membranes. This irreversible fouling resistance value is when rinsed with RO water only; it does not take into account the use of a cleaning agent. The membrane resistance after fouling and cleaning values (P1: 9.23 x 10^{11} and P2: 9.76 x 10^{11} m^{-1}) show that the cleaning regime removes most of the fouling resistance (Figure 4.26). There is no statistical difference in the resistances recorded for membranes treated with the two Protocols either before fouling or after cleaning.

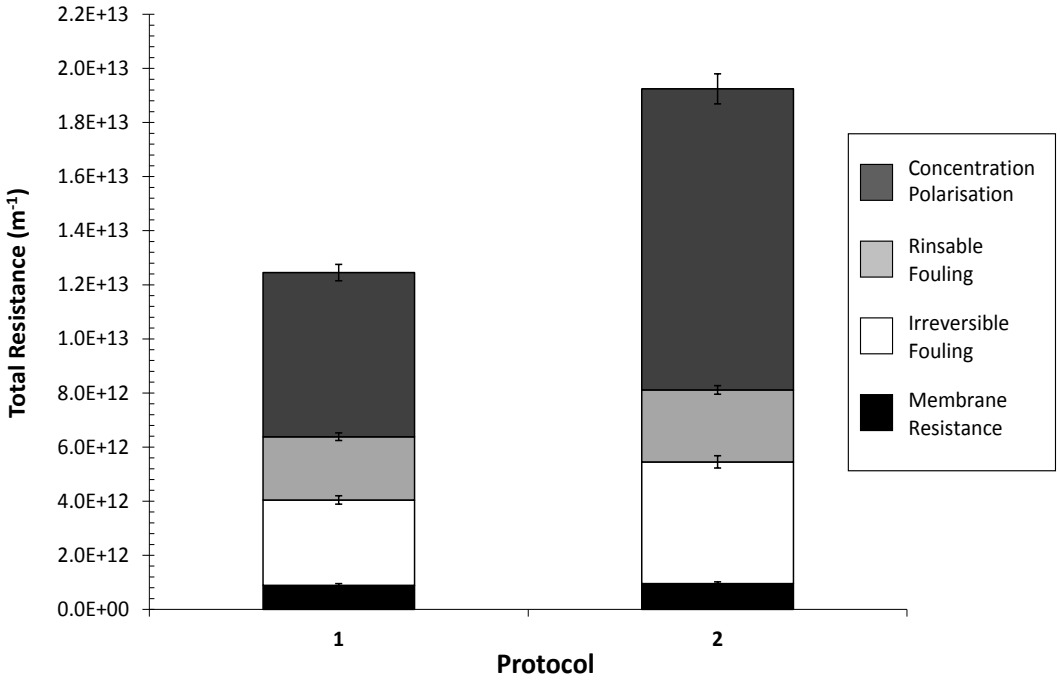

Figure 4.25: Graph to show breakdown of fouling resistance at steady state (after 90 min) when pre-treatment Protocol is varied for 20 kDa FP membranes during the filtration of SSL.

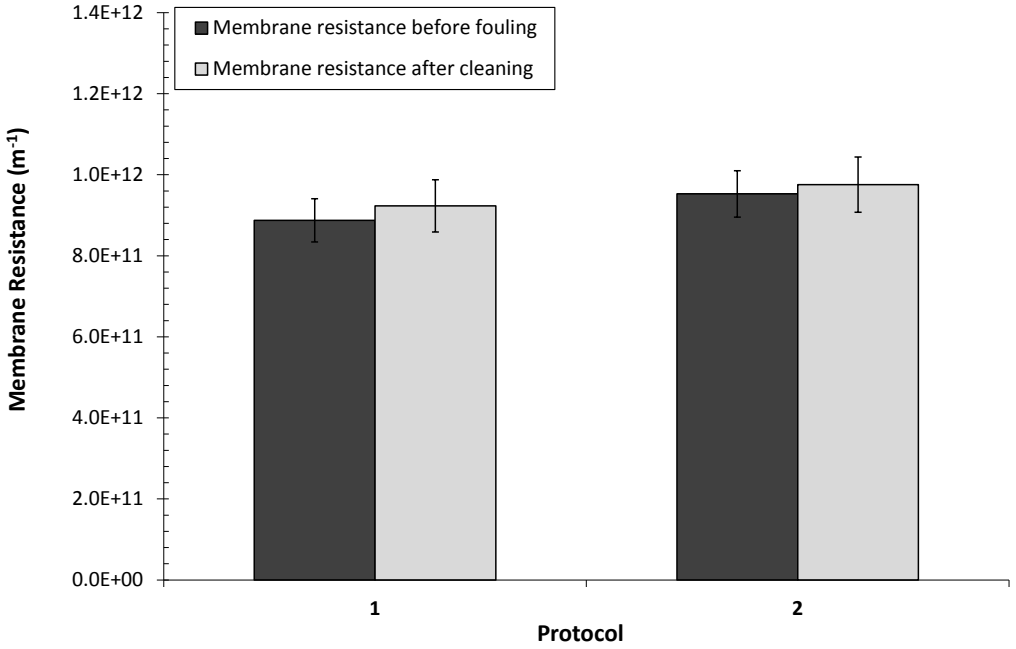

Figure 4.26: Graph to show pure water membrane resistances after fouling and cleaning vs. pure water membrane resistance before fouling when the pre-treatment Protocol is varied for 20 kDa FP membranes during the filtration of SSL.

4.6.4. Streaming Potential through Pores

Previous studies have shown that a membrane surface has a reduced fouling tendency if the surface is hydrophilic and charged similarly to the key fouling species in the filtrate solution (Pihlajamäki, 1998). The high charge densities keep the molecules away from each other and from the surface of the membrane. In addition retention is usually increased. The variation of apparent zeta potential (ZP) on the pore walls has been determined from streaming potential measurements for the FP 20 kDa membrane. Over the pH range examined (3.7 – 7.0) all the membranes displayed a negative charge, with the charge becoming increasingly negative as the pH value increased.

4.6.5. Zeta-potential Measurements for Conditioned Membranes

Figure 4.27 shows the apparent zeta potential on the pore walls of the two pre-treatment methods. Over the pH range examined (3.7 – 7.0), the Protocol 1 treated FP membrane displayed a highly negative charge (-1.30 to -4.70 mV), with the charge becoming more negative as the pH increases. The FP membrane that was treated with water and NaOH (Protocol 2) showed similar trends to the membrane treated with only water but had a more positive charge (-0.40 to -3.61 mV). This increased value could suggest the attachment of Na^+ ions to the negative functional groups, modifying the surface.

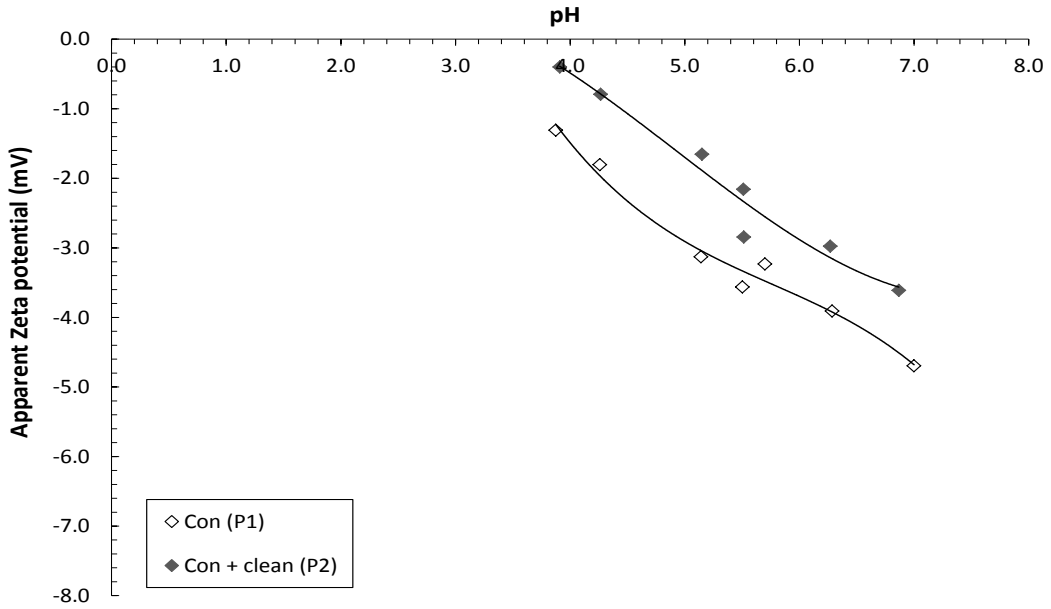

Figure 4.27: Apparent zeta-potential on the pore walls of conditioned 20 kDa FP membranes at different pH values. Temperature, 25 ^{o}C; pH adjustments were made with 0.001 M KCl.

4.6.6. ZP Measurements for SSL Fouled and Cleaned Membranes

The zeta potential depends upon the nature of the ions present in the solution along with the properties of the solid surface itself. The variations of the apparent zeta potentials on the pore walls determined from streaming potential with the FP 20 kDa membrane are given in Figures 4.28 and 4.29. Over the pH range examined (3.7 – 7.0) all the FP membranes displayed a negative charge, where the charge becomes more negative with increasing pH. Figures 4.28 and 4.29 show that once the membrane has become fouled, it becomes more negatively charged regardless of the pre-treatment method. This suggested that there were negatively charged foulants adhering to the pore wall surfaces. The main types of foulants were thought to be the lignosulphonates, fatty acids and resin acids (Weis *et al*., 2003). Figure 4.28 suggests that the fouling was possibly lignosulphonates based, as the zeta-potential remains constant over the pH range studied (from 4.0 to 7.0). Fouling was carried out at a pH of 2.9, that of the SSL. At this pH, extrapolation of the experimental data indicates that the FP membranes would display a weak positive charge, or no charge at all (i.e. values are close to that of the isoelectric point). Under these conditions, adsorption would most likely be driven by hydrodynamic forces and hydrophobic interactions occurring between the foulants and the membrane surface.

The zeta potential data shows that once the membrane is cleaned the zeta potential values are between those of the conditioned membrane and the fouled membrane. This means that the zeta potential was not totally restored after the fouling and cleaning procedures. This suggests either: (i) that the cleaning protocols were not entirely removing the fouling, or (ii) the neutralizing effects of the metal cations in the cleaning agent (e.g. the attachment of Na^+ ions to the negative functional groups) have changed the properties of the membrane and/or those of the remaining foulants.

Figure 4.29 does show that the membrane sample subjected to Protocol 2 had a slightly less negative charge than that prepared using Protocol 1 (Figure 4.28). This was possibly due to the adhesion of metal cations from the caustic cleaning agent to the negatively charged fouled surface. Interestingly, this reduced surface charge was linked to an initial reduction in fouling flux performance when compared to a water conditioned membrane (Figure 4.24). However, it also seemed to result in an increased flux recovery during cleaning that is seen in the superior performance of the Protocol 2 treated membrane at the end of the cleaning process (35 minutes of cleaning, Figure 4.24). Moreover, the sustained increase in cleaning flux for the Protocol 2 treated membranes indicated that the relative improvement over the Protocol 1 treated membranes was likely to be maintained for longer cleaning times.

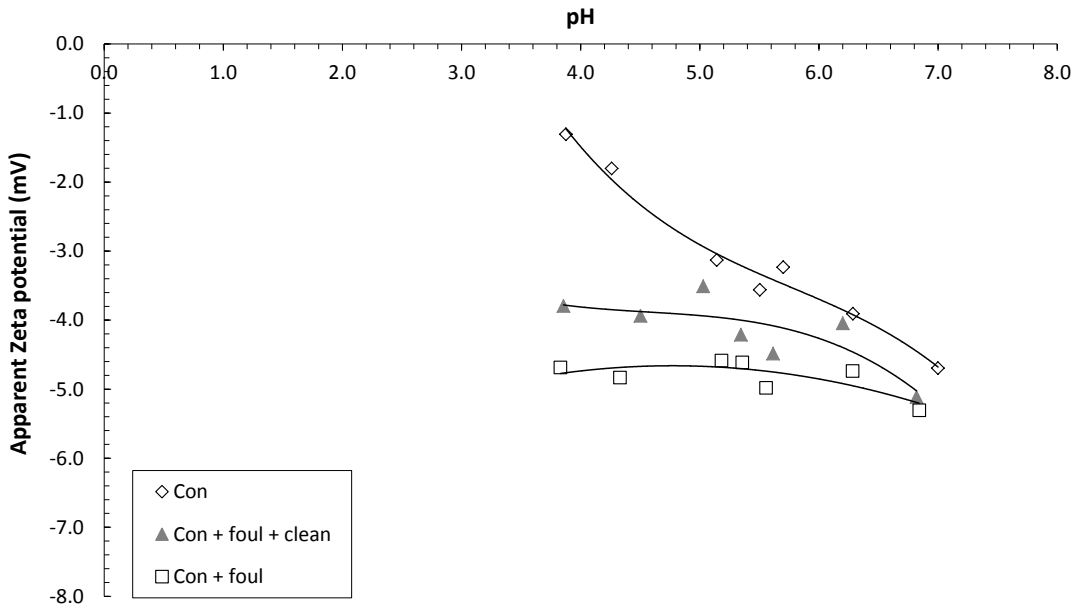

Figure 4.28: Apparent zeta-potentials on the pore walls of Protocol 1 treated FP membranes at different pH values, used for the UF filtration of SSL.

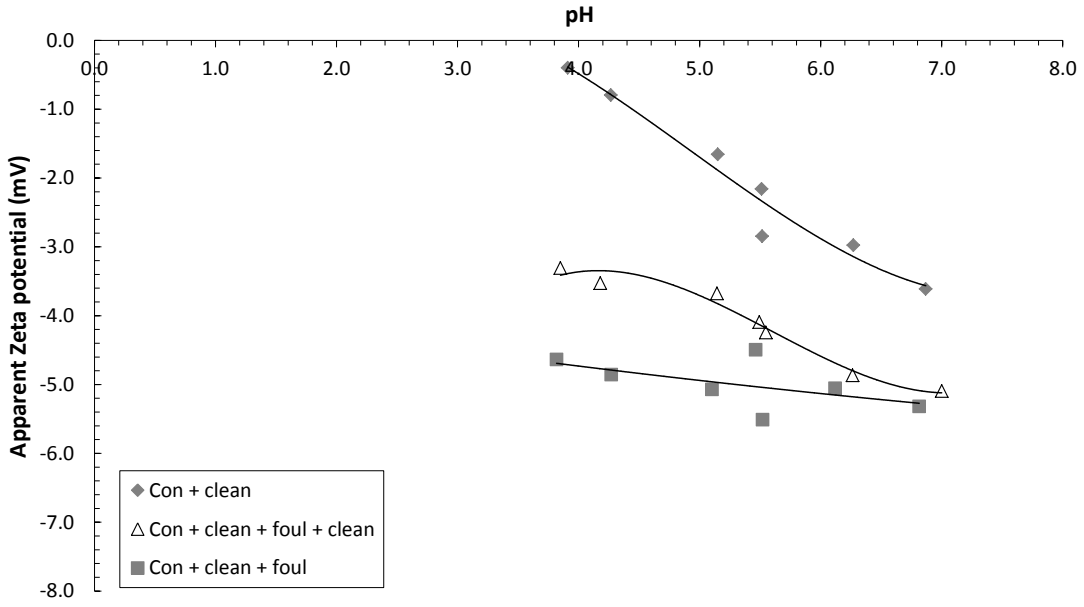

Figure 4.29: Apparent zeta-potentials on the pore walls of Protocol 2 treated FP membranes at different pH values, used for the UF filtration of SSL.

4.6.7. ATR-FTIR

The analysis of the FTIR spectra was performed using Perkin Elmer 2000 software Spectrum (ver. 5.0.1) to enhance its appearance and extract more information from the data. A sequence of manipulation was put in practice on both sets of data to increase the integrity of the results. This involves removing the blank spectra (the CO_2 and moisture peaks), introducing a baseline correction, smoothing the noise level of the spectra and normalizing the data to reset the Y axis (absorbance) from 0 to 1.

4.6.7.1. FTIR Spectra for Conditioned Membranes

The conditioned virgin spectrums for the Protocol 1 and Protocol 2 Ps*f* membranes are shown in Figure 4.30. The conditioning of the membrane was required to remove the preservative agent glycerine that can affect the performance of the membrane. Holser (2008) states that glycerine should have a broad absorption band associated with the hydroxyl groups of glycerol at 3250 cm^{-1} with the carbon–oxygen absorptions characteristic of primary and secondary alcohols occurring at 1030 and 1100 cm^{-1}. Figure 4.30 indicates that the two Protocols used on both membranes removed the majority of the glycerine.

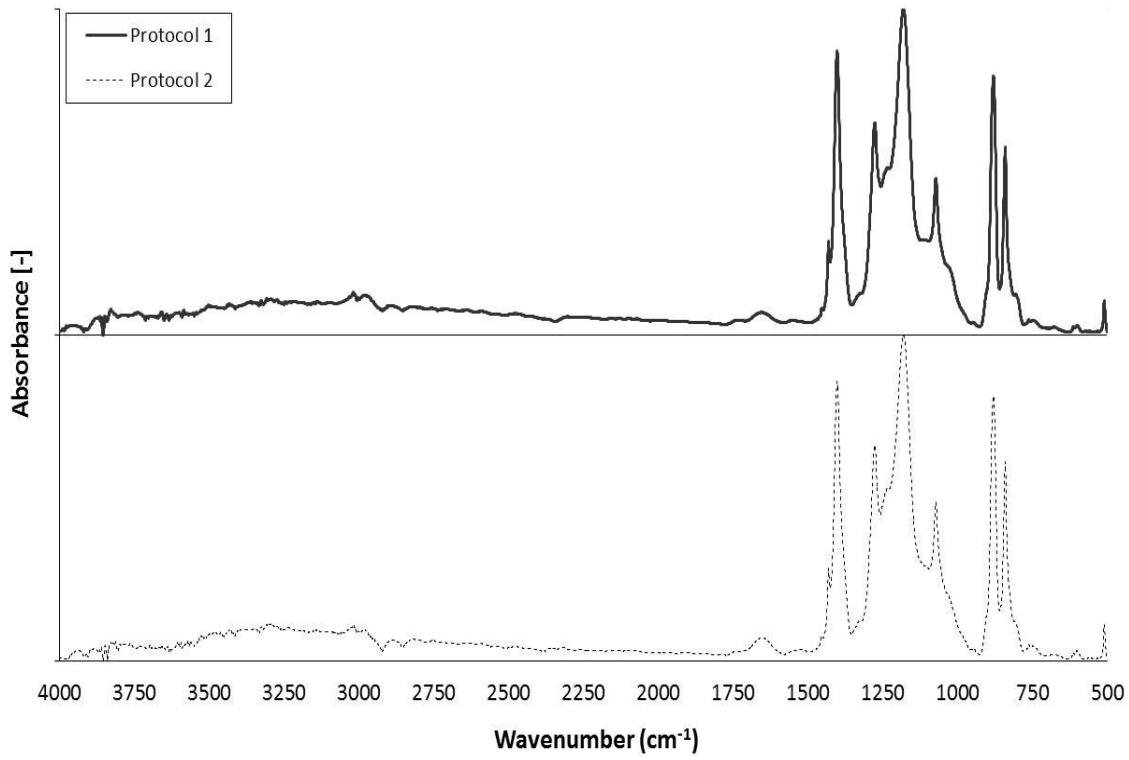

Figure 4.30: Infrared spectra comparison of virgin Protocol 1 FP 20 kDa membrane (Top), and Protocol 2 treated FP kDa membranes (Bottom) (all spectra shown with water subtracted).

4.6.7.2. FTIR Spectra for SSL Fouled and Cleaned Membranes

The SSL feedstock used for the separation process in this study was a complex mixture and determining the specific fouling species was difficult. A study on the chemical composition of the lignosulphonates in SSL used in this study has been performed by Marques *et al*. (2009a). The chemical composition of SSL and the chemical analysis of the lignosulphonates are shown in Chapter 3.2.1 (Table 3.1). This information was used to help identify the fouling species on the FP membrane.

The possible structure units (PSU) found by the Perkin-Elmer search program (Search Plus) for the conditioned, fouled and cleaned FP membranes are displayed in Table 4.3. The PSU found can be part of various chemical structures and is not related to just one substance. The intensity of infrared absorption bands can be used to quantify the amount of material present on the membrane. However, in this study the FTIR spectrum could only be used qualitatively to compare the surface conditions. The peaks have been compared to reference data and an attempt to identify evidence of fouling and the performance of cleaning has been performed.

The FTIR spectra of Protocol 1 and Protocol 2 treated membranes are shown in Figures 4.31 and 4.32. The overlapping of peaks in the spectra makes it difficult to accurately determine the functional groups of polymer, the fouling material and the cleaning agents. Some bands within the spectra show changes whilst some do not change their peak height/area significantly. This results from the build-up of fouling. This fouling layer can block out light and some of the functional groups of the membrane polymer reacting by increasing or decreasing peak height/area, because they are more sensitive than others, making it difficult to classify the specific substances.

The scans for water and virgin membranes have been subtracted from the graph in Figure 4.33, so that the scans indicate only those of the foulants or cleaning agents deposited on the membrane surface, or within the porous structure. These spectra are a useful comparison to identify the fouling species and effects of cleaning. The FTIR spectrum of lignosulphonates has been studied by Marques *et al*. (2009a) and the data wavelength areas and peaks which are characteristic of lignosulphonates were identified. Comparing this data with all the fouling spectra in this section, evidence of lignosulphonates fouling is shown in the following regions; (i) a common aromatic ring vibration bands at 1579 and 1486 cm^{-1}, (ii) an asymmetric C-H deformation at 1432 cm^{-1}, (iii) and specific bands at 1181, 1006, 831 and 719 cm^{-1} which confirm the presence of significant amounts of sulphonic groups. The 1323/1298 cm^{-1} doublet band is asymmetric SO_2 stretching and the band at 1181 cm^{-1} is symmetric SO_2 stretching. Several of these peaks can be seen in both the Protocol 1 treated membrane and the Protocol 2 treated membrane. Figure 4.33 shows that NaOH cleaning after water conditioning (P2) does affect the membrane and alter the profile of the species attaching. Significantly, the spectrum recorded after P2 conditioning and subsequent fouling is extremely similar to the spectrum seen after water conditioning (P1) fouling and subsequent NaOH cleaning. This could be due to the NaOH species attached, before the fouling altered the nature of the surface. Both FP membrane surfaces after fouling and cleaning demonstrated a slight modification to the surface. The P1 fouled membrane attracts different species to the other three treatments. This indicates that the NaOH pre-treated membranes when subsequently fouled can display a similar attachment profile to a water conditioned surface subsequently fouled and then cleaned using NaOH.

Table 4.3: Possible structures found by the Perkin-Elmer search program for fouled and cleaned FP membranes

Class number	Possible structural units	Possible bands (cm^{-1})
201	Alkyl group - general	1486, 1240, 1152, 1105, 1072
259	Aromatic compound	1578, 1486, 1323, 1240, 719
402	Hydroxy group	1240, 1152, 1105, 1072
511	Aliphatic alcohol	1486, 1010
2710	Aryl-ether	1578, 1486, 1323, 1152, 1105
2724	Phenoxy - general	1578, 1486, 1323, 1152, 1105, 1072, 879, 834, 719
2906	Aromatic primary amine	1578, 1486
4002	Aromatic sulphone	1578, 1486, 1323, 1152, 1105, 1072, 879, 834, 778, 719, 557
4911	Carbonyl compound	1675, 1672

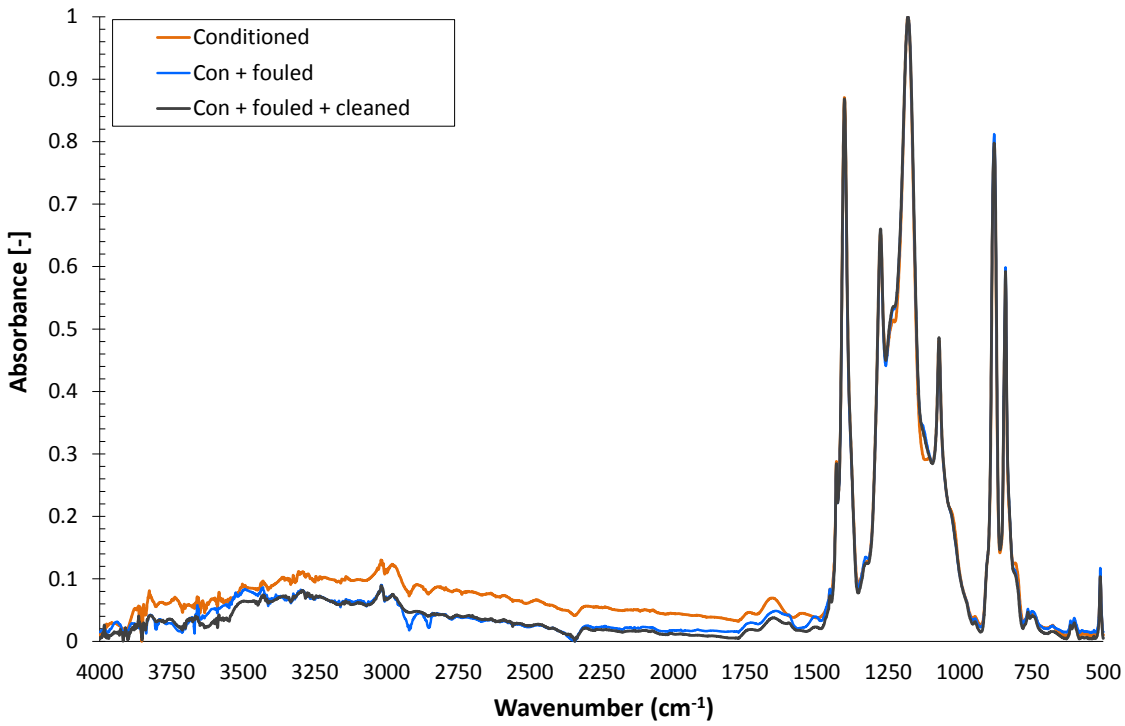

Figure 4.31: Infrared spectra comparison of FP 20 kDa membranes under different fouling conditions. Each membrane has been conditioned with water only (Protocol 1) (all spectra shown with water subtracted).

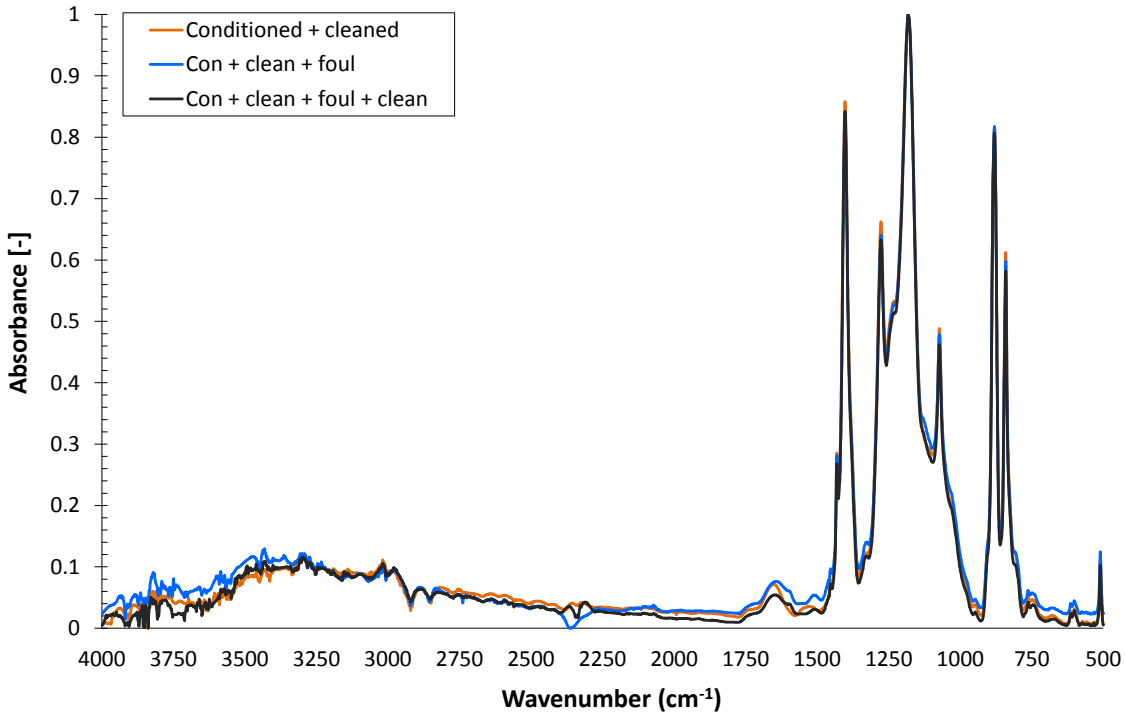

Figure 4.32: Infrared spectra comparison of FP 20 kDa membranes under different fouling conditions. Each membrane has been conditioned with water and 0.50 wt. % NaOH (Protocol 2) (all spectra shown with water subtracted).

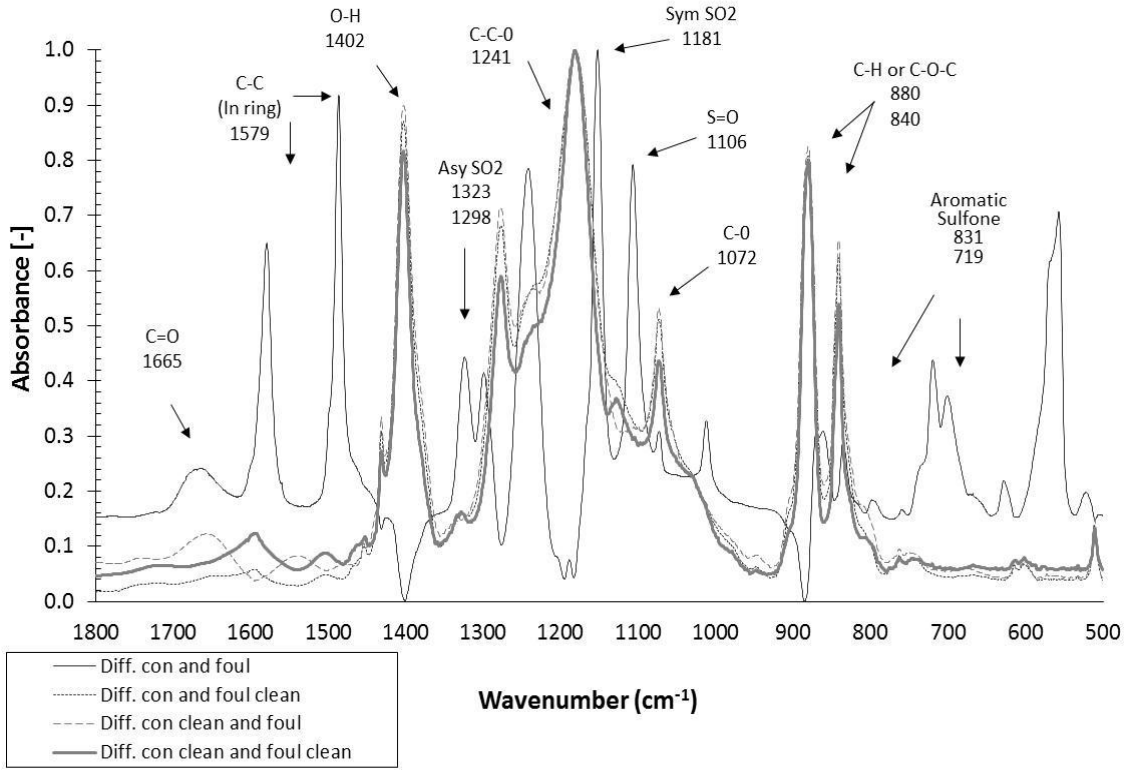

Figure 4.33: Infrared spectra comparison of 20 kDa FP membranes subjected to different treatments for the filtration of SSL (all spectra shown with water and virgin membrane absorbance traces subtracted).

The different spectra shown in Figure 4.33 have some of the same peak locations, though with different intensities (peak heights). Indicating that different amounts of species are attracted to the membranes under different conditioning Protocols. Three samples of each membrane were tested and the peak heights of selected significant peaks averaged and the standard deviation calculated. The peak heights for common functional groups are shown in Table 4.4. The heights of the peaks are directly related to the degree of fouling/removal and therefore a change of peak height will give information about the cleaning mechanism. The main differences seen in the peak heights are the differences between the functional groups present on the fouled membrane spectrum and those present on the membranes subjected to the other three treatments. This is due to the interaction of the NaOH cleaning agent with the membrane and fouling species. The bands which show changes in peak height appear to be mainly in the low wave number region (> 1800 cm^{-1}). The peaks in the higher wave numbers could be due to noise. Lignosulphonates do not appear to be the only foulants on the membrane as there are additional peaks present.

Table 4.4: Averaged peak-heights of FP SSL fouled and cleaned membranes

Membrane Fouling and Cleaning State	Wavenumber (cm^{-1})						
	831 Arom. Sulfone	**840 C-H**	**880 C-O-C**	**1072 C-O**	**1106 S=O**	**1181 Sym. SO_2**	**1187 C-C-O**
P1 Foul	0.25	0.21	0.04	0.31	0.79	0.05	0.07
P2 Foul	0.32	0.65	0.82	0.53	0.31	1.00	0.98
P1 Foul + Clean	0.30	0.62	0.81	0.51	0.32	1.00	0.97
P2 Foul + Clean	0.22	0.53	0.80	0.43	0.30	1.00	0.96
Membrane Fouling and Cleaning State	**Wavenumber (cm^{-1})**						
	1241 C-C-O	**1276 Asy. SO_2**	**1323 Asy. SO_2**	**1402 O-H**	**1486 C=C**	**1579 C=O**	**1665 C=C**
P1 Foul	0.78	0.10	0.44	0.00	0.92	0.65	0.24
P2 Foul	0.56	0.71	0.15	0.90	0.07	0.05	0.12
P1 Foul + Clean	0.56	0.68	0.16	0.87	0.04	0.04	0.04
P2 Foul + Clean	0.48	0.59	0.15	0.81	0.07	0.09	0.07

4.6.8. SEM Images for SSL Fouled Membranes

The FP 20 kDa membranes used in this study contained pores that were not clearly visible using the SEM technique. It was therefore not a valuable tool for the ultrafilters. Figure 4.34 displays an image of a conditioned membrane and a fouled membrane. The conditioned membrane image is not particularly clear and the pore structure cannot be identified. Deposits can be seen in the fouled membrane image and cover a large area of the membrane. The elements identified using X-ray Diffraction on the SSL fouled FP membranes were found to be oxygen, fluoride, calcium, and sulphur.

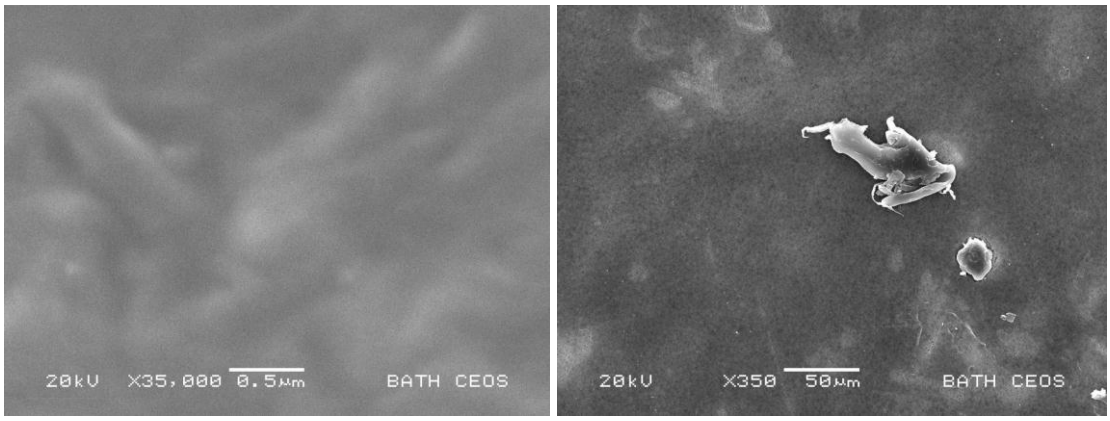

Figure 4.34: SEM showing conditioned 20 kDa FP membrane (left) and fouled 20 kDa FP membrane (right).

4.6.9. AFM

Bowen and Doneva (2000) and Vrijenhoek *et al*. (2001) state that surface roughness is one of the most significant properties for influencing fouling (adhesion) and is more important than physical and chemical operating conditions. The roughness, waviness and the architecture of the active top layers of the polymeric membranes have been investigated using AFM. R_A (the mean roughness) was calculated as an average value of that determined from each scan line for 5 x 5 micron AFM images. The R_A values for Protocol 1 and Protocol 2 membranes can be seen in Table 4.5. The two pre-treatment Protocols employed lead to similar roughness values for (i) conditioned membranes, (ii) fouled membranes, (iii) fouled then cleaned membranes. P1 (water) and P2 (water & NaOH) conditioned FP membranes displayed almost identical roughness (R_A) values of 18.8 and 19.0 nm respectively. After fouling, all membranes displayed increased R_A values (P1: 25.6 and P2: 25.9 nm), indicating that relatively rough surface deposits were present. This rougher surface also resulted in an increase of in-pore deposits; which is

confirmed by the increase in negative charge shown in the zeta potential data. Once cleaning had occurred, the surface roughness values reduced (P1: 22.9 and P2: 22.4 nm), but did not return to the initial roughness values, indicating that the surfaces had not been returned to a pristine condition. This supports the data obtained from the contact angle measurements.

Table 4.5: R_A surface roughness values as measured by AFM

Sample	R_A (nm)		
	Conditioned	Fouled	After Clean
FP (P1)	18.8 ± 1	25.6 ± 1	22.9 ± 1
FP (P2)	19.0 ± 1	25.9 ± 1	22.4 ± 1

4.6.10. Contact Angle

The hydrophobicity of the membrane samples are shown in Table 4.6. No statistical difference could be detected between the effect of pre-treatment Protocols 1 and 2 by measuring contact angles. The Protocol 1 and 2 membranes tested were both considered to be moderately hydrophilic as the contact angles measured were less than 90º. After conditioning, the Protocol 1 treated membrane decreased from 64º to 62º, while the Protocol 2 treated membrane increased from 64º to 66º. Any glycerine remaining on the membrane makes the surface more hydrophilic. The FP membranes became more hydrophilic after fouling when conditioned with Protocol 1 and 2, this would suggest that more water would pass through the membrane which is reflected in the flux data. After fouling and cleaning cycles, the membrane surface had a contact angle between that of a virgin and a fouled surface, implying that the membrane had not returned to its original state.

Table 4.6: Contact angles of water drops made with membrane surfaces

Membrane	Contact Angle (º)			
	Unconditioned	Conditioned	Fouled	After Cleaning
FP (P1)	64 ± 2	62 ± 2	45 ± 3	60 ± 2
FP (P2)	64 ± 2	66 ± 3	50 ± 2	58 ± 3

4.7. Pre-Treatment of 20 kDa FP Membranes – Multiple Cycles

It is important that fouling and cleaning processes are investigated synergistically, considering the whole process over multiple operational cycles. Wallberg *et al.* (2001) recommend that the performance of the system should be judged on how the membrane responds after fouling and cleaning, i.e. how quickly the membrane re-fouls. The previous work (section 4.6) has been extended by comparing the effect of the two pre-treatment methods (Protocol 1 and Protocol 2) over multiple operational cycles.

4.7.1. Flux Data – Multiple Cycles

The flux data has been normalised, with the initial PWF taken as 1.0, and the other data scaled accordingly for each Protocol. The initial flux for Protocol 1 treated membrane was 451 L m^{-2} hr^{-1} and that for the Protocol 2 membrane was 405 L m^{-2} hr^{-1}. For ease of data interpretation, Figure 4.35 shows the average steady state flux values for all stages in a four cycle filtration process. As discussed in section 4.6 previous workers have shown that the flux decline during SSL filtration is due to a range of fouling phenomena such as concentration polarisation, irreversible fouling, pore blocking and gel layer formation (Weis *et al*., 2003, 2005; Bhattacharya *et al*., 2005). In Figure 4.35, the steady state PWF values after fouling in cycle 1 showed a substantial decline from the clean membrane PWF value (*ca*. 80 %). After cycle 1, there was a slightly greater flux decline as the cycles progressed. This indicated that the nature of the membrane material had little additional influence upon subsequent foulant layer development. The permanent build-up of fouling material became dominant over the FP surface. The values of a single fouled membrane did not differ much from 4x fouled membrane. With increasing cycle numbers the product flux recovery after NaOH cleaning for both Protocols decreased linearly. This decline illustrates the poor removal of the fouling material on the membranes, which is consistent with the increase in irreversible fouling resistance (section 4.6.3). This decline in flux recovery was also seen by Weis (2004) when cleaning with NaOH; where it was hypothesised that the decline was due to the presence of sodium ions, which neutralised the charges on the lignosulphonates. This making the membrane surface more hydrophobic and subsequently more attractive for additional hydrophobic foulants. Weis *et al*. (2003) found that after seven cycles a quasi-steady state was reached. Figure 4.36 shows that for this system a quasi-steady state was reached after eight cycles, where no further decline in product flux and flux

recovery was seen. The fouling fluxes for cycle 5 onwards were similar; this was probably due to the accumulation and detachment of the fouling cake layer reaching equilibrium (Bian *et al*., 2000).

Protocol 1 results in a slightly superior fouling flux performance over the first cycle than Protocol 2 (3.6 % enhanced flux). Protocol 1 continued to outperform Protocol 2 during the first cleaning cycle. However, after fouling and cleaning the PWF positions were reversed, and Protocol 2 provided a flux recovery of 95 % (± 1), compared to 87 % (± 1) seen for Protocol 1. During cycle numbers two to four, the fouling fluxes for both protocols showed no statistically significant differences. Comparison of the PWF values after fouling and cleaning with the original PWF of a clean membrane provides the best indication of the state of the membrane. In cycle 2, the application of Protocol 2 provided a flux recovery of 51 % compared to only 44 % obtained for Protocol 1 treated membranes. The PWF performance at the end of cycle 3 was similar for both Protocols, and no significantly relevant differences was seen (approx. 41 % recovery). The positions were then reversed after four fouling and cleaning cycles where Protocol 1 had an enhanced flux recovery of 30 % compared to 25 % seen by Protocol 2. The product fluxes after cycle 4 had similar results. These results showed that Protocol 2 had an improved performance over Protocol 1 in the first three cycles, though as the cycle number increased the extent of these improvements decreased. This trend continued, and after 8 cycles, Protocol 1 treated membranes gave a statistically superior filtration flux performance to Protocol 2 treated membranes. These results indicated the importance of examining membrane performance over multiple operational cycles.

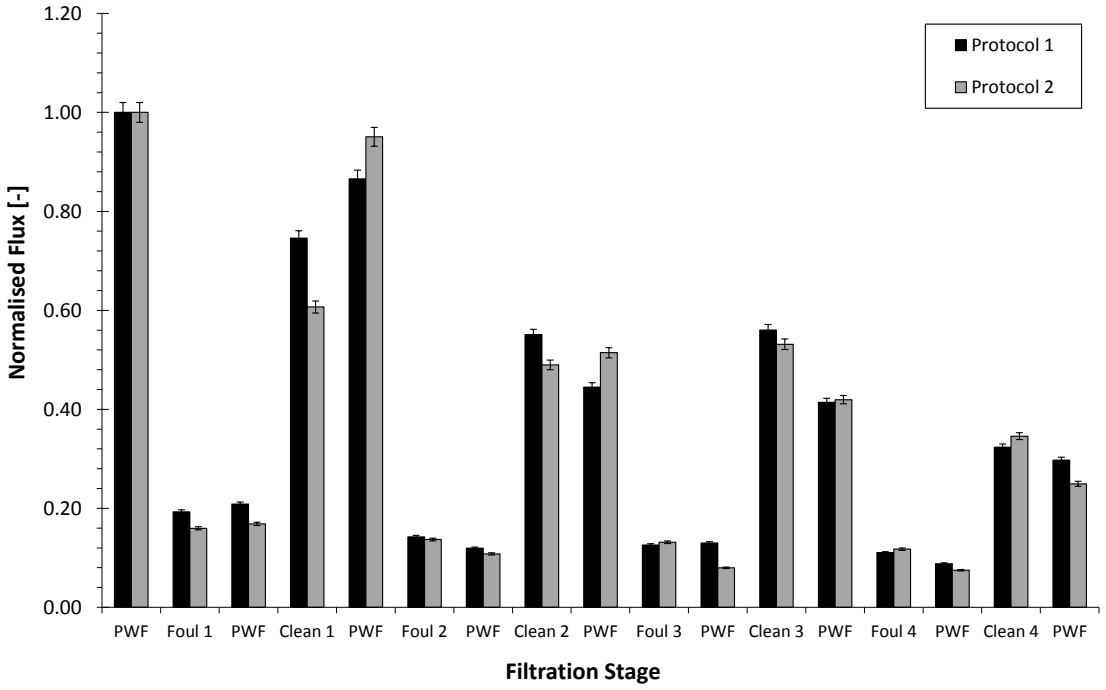

Figure 4.35: UF of SSL with 20 kDa FP membranes: Graph to show normalised steady state PWF, fouling flux and cleaning flux for four filtration cycles. Average initial flux; P1: 451 L m^{-2} hr^{-1}, P2: 405 L m^{-2} hr^{-1}.

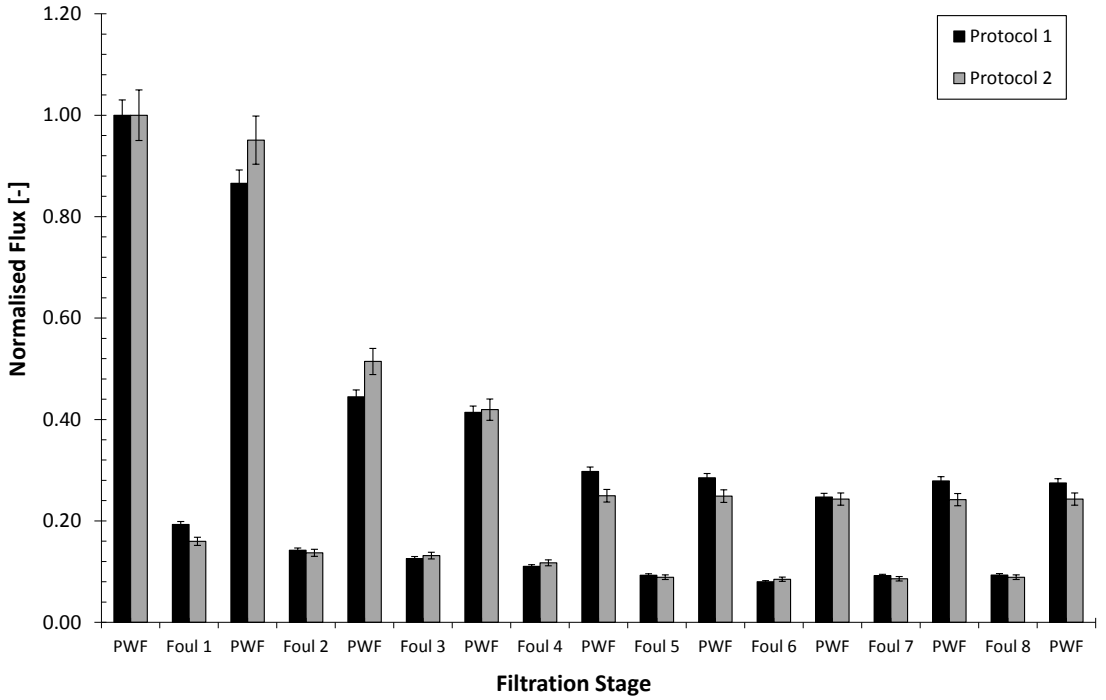

Figure 4.36: UF of SSL with 20 kDa FP membranes: Graph to show normalised steady state PWF before fouling and fouling flux for eight filtration cycles.

4.7.2. Resistances – Multiple Cycles

Figure 4.37 shows the magnitude of the resistances, under steady state conditions for SSL fouling for both pre-treatment Protocols. The membrane resistance before fouling for the Protocol 1 treated membrane was 8.88 x 10^{11} m^{-1} and 9.53 x 10^{11} m^{-1} for Protocol 2 treated membrane. For the first cycle, the application of Protocol 2 lead to a total resistance of 1.92 x 10^{13} m^{-1}, whilst Protocol 1 lead to a total resistance of 1.25 x 10^{13} m^{-1}. The resistance breakdown shows that the R_{cp} was principally responsible for the majority of the fouling resistance when applying both Protocols. The total resistance increased from cycle 1 to 2, where there was an increase in R_I and resistance due to R_{cp}. The amount of R_{cp} for cycle 2 to cycle 4 had similar values for all cycles. However, R_{cp} accounted for 48 % (P1) and 42 % (P2) of the total resistance for cycle 1 and 42 % (P1) and 40 % (P2) of the total resistance for cycle 4. The amount of R_{cp} increased from cycle 4 onwards, where after 8 cycles the values of R_{cp} was 3.4 x 10^{13} m^{-1} (P1) and 3.6 x 10^{13} m^{-1} (P2). The value of R_I increased as the cycle progressed for both pre-treatment Protocols (P1: 46 %, P2: 59 % increase after 8 cycles). R_R accounted for 19 % (P1) and 14 % (P2) of the total resistance for cycle one and 12 % (P1) and 13 % (P2) of the total resistance for cycle 8. This decrease was due to the increase in fouling material which couldn't be removed by rinsing. The membranes treated with Protocol 2 lead to an increase in the total resistance over Protocol 1 for cycle 1 of the filtration process. There was no statistical difference in the total fouling resistances recorded for membranes treated with the two Protocols for cycle 2 to 8.

The irreversible fouling resistance value is that which is recorded when the membrane is rinsed with RO water only; it does not take into account the use of a cleaning agent. The membrane resistance values after fouling and cleaning cycle 1 were 9.23 x 10^{11} and 9.76 x 10^{11} m^{-1} for P1 and P2 treated membranes respectively, illustrating that the cleaning regime removed most of the in-pore fouling resistance (Figure 4.38). As the cycles progressed, the resistance after cleaning increased dramatically for both Protocols until cycle 4. This was due the higher proportion of irreversible fouling present that is not removed after cleaning as the cycle number increased. The Protocol 2 treated membrane displayed a higher resistance after cleaning (P2: 4.1 x 10^{12} m^{-1}) than the Protocol 1 membrane (P1: 3.2 x 10^{12} m^{-1}) after 4 fouling and cleaning cycles. From cycle 4 to 8 the membrane resistance only marginally increased, with the final

membrane resistance after eight fouling and cleaning cycles being 3.7 x 10^{12} m^{-1} (P1) and 4.33 x 10^{12} m^{-1} (P2). This suggests that as the cycle number increased, the membranes were not being cleaned sufficiently by the existing cleaning regime.

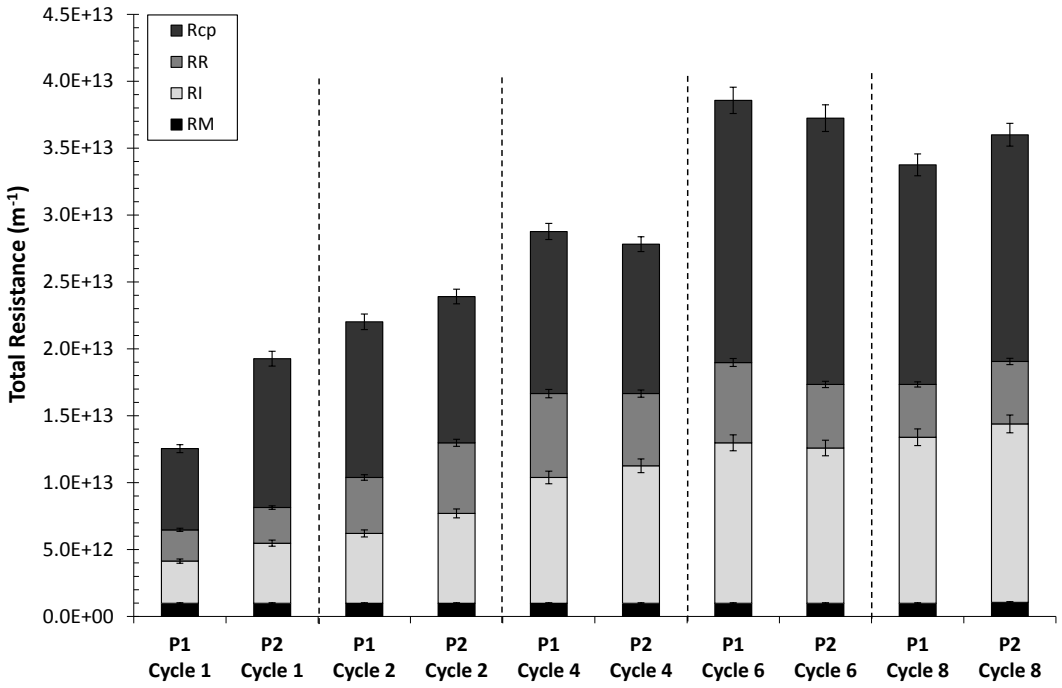

Figure 4.37: Graph to show the breakdown of fouling resistance at steady state (after 90 min) when both pre-treatment Protocol are used for the filtration of SSL with a 20 kDa FP membrane during selected filtration cycles.

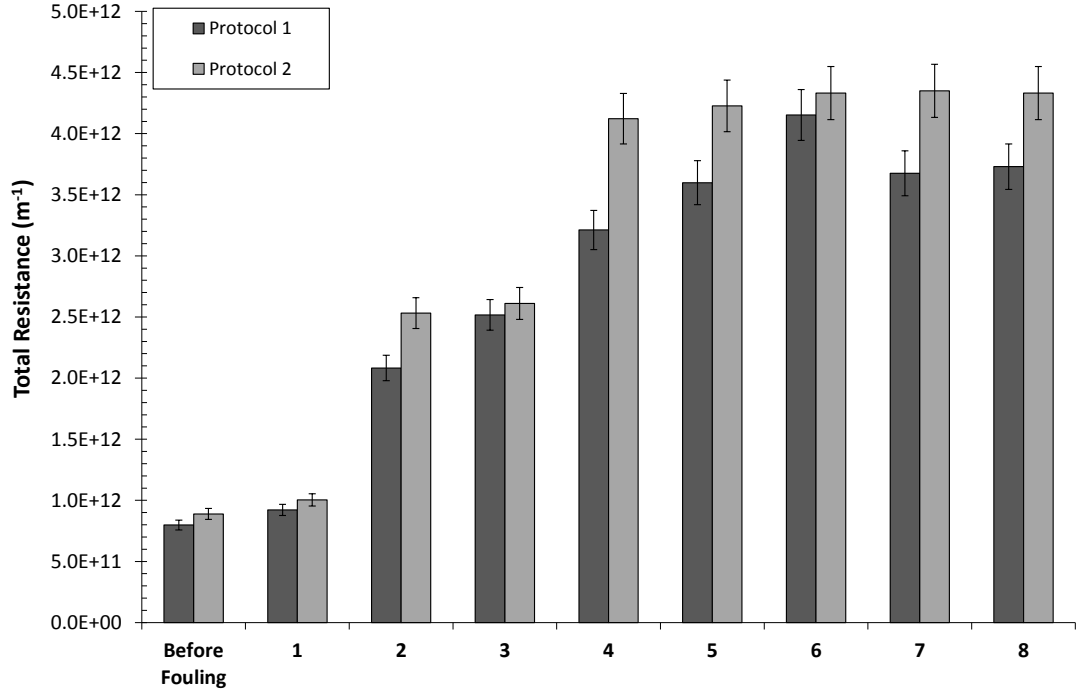

Figure 4.38: Graph to show pure water membrane resistances after fouling and cleaning for each fouling cycle for Protocol 1 and Protocol 2 treated membranes.

4.7.3. Solids Rejection – Multiple Cycles

In Figure 4.39 the FP membrane apparent rejection coefficient can be seen following fouling with SSL over eight filtration cycles. As the cycles increased there was a slight increase in solid rejection. Protocol 1 increased from 0.30 to 0.38 (± 0.2 %), and Protocol 2 increased from 0.31 to 0.39 (± 0.2 %) over eight cycles. The increases in solid rejection was presumably due to the build-up of fouling material on the surface causing the membrane pores to get narrower. Dal-Cin *et al*. (1996) found that pore plugging is the most significant fouling mechanism when working with ultrafiltration membranes and wood pulp. However, the differences in the solids rejection values recorded were not statistically significant, and the data set as a whole did not indicate that there is any change in the solids transmission as a result of the application of the NaOH preconditioning treatment.

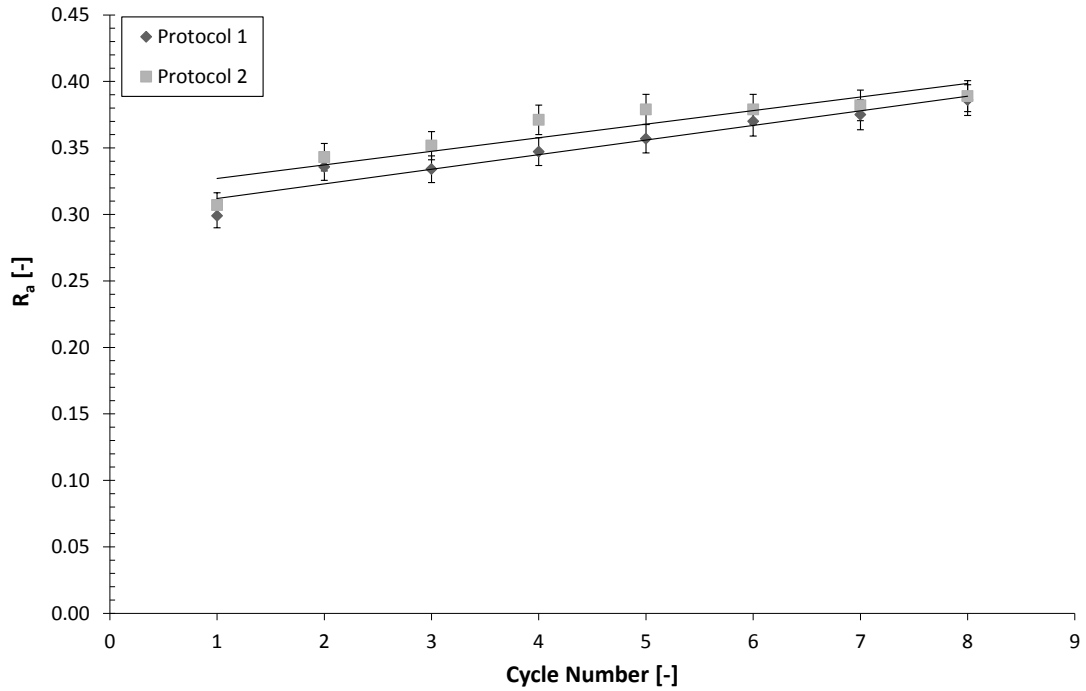

Figure 4.39: Graph to show the apparent rejection coefficient over multiple cycles through a 20 kDa FP membrane when fouled with SSL (60 ºC, 1.89 ms^{-1} CFV).

4.7.4. Zeta Potential – Multiple Cycles

Zeta potential measurements were used to provide an indication of particle-particle and particle-surface interactions. Such interactions have been shown to be of importance to membrane performance (Huisman *et al*., 1998). In Figures 4.40 to 4.42, the variation of apparent zeta potential on the pore walls has been determined for all the FP 20 kDa

membranes at different parts of the four cycles. Over the pH range examined (3.7 – 7.0), the conditioned FP membrane (Protocol 1) displayed a highly negative charge (-1.30 to -4.70 mV), with the charge becoming more negative as the pH increases. The FP membrane that was treated with water and NaOH (Protocol 2) showed similar trends to the membrane treated with only water (Protocol 1) but had a less negative charge (-0.40 to -3.61 mV). The increased values could suggest the attachment of Na^+ ions to the negative functional groups, modifying the surface. Figure 4.40 shows that once the membrane has become fouled it becomes more negatively charged regardless of the pre-treatment method. This suggests that there are negatively charged foulants adhering to the pore wall surfaces. Nyström and Zhu (1997) also found that there was no difference in the ZP of the membranes that had been fouled with or without pre-cleaning. Once the membrane is cleaned the zeta potential values recorded are between those of the conditioned membrane and the fouled membrane. This has been discussed in detail in section 4.6.6.

As the filtration cycle number increased, the fouled surfaces became more negative for both Protocols (Figures 4.41 and 4.42). For Protocol 1 treated membranes, the 1x fouled membrane and the 2x fouled membranes displayed similar ZP values, of *ca.* -5.0 mV (Figures 4.40 and 4.41). Protocol 2 treated membranes displayed more marked differences, with the 1x fouled membrane having a ZP of approximately -5.0 mV, whereas the 2x fouled membrane had a ZP of approximately -6.0 mV (Fig 6 (b)). The 4x fouled membrane for Protocol 1 treatment displayed a ZP of *ca.* -6.5 mV, whilst the equivalent value for Protocol 2 treated membranes was *ca.* -7.5 mV. This indicates that the application of Protocol 2 lead to a greater adsorption of negatively charged ions. Protocol 2 treated membranes had a greater negative charge on all fouled membranes than Protocol 1 treated membranes, suggesting that the Protocol 2 membranes had experienced a greater degree of in-pore fouling. This is supported by the flux data. However, surface fouling was also present in addition to in-pore fouling, as revealed by AFM measurements (see section 4.7.6).

Neither Protocol 1 nor Protocol 2 treated membranes were restored to the virgin charge condition. This is consistent with the percentage flux recovery observed. The Protocol 2 four times fouled & cleaned membrane was restored to a similar ZP value to that of the

2x fouled cleaned membrane. This suggests that either the foulants were more easily removed with increased fouling cycle numbers or that there were additional cations attracted to the membrane surface. The ZP values for the 4x fouled and cleaned membrane treated with Protocol 2 showed more negative ZP values than those recorded for Protocol 1 treated membranes (Figure 4.41 and 4.42). Zhu and Nyström (1998), Huisman *et al*. (2000) and Lawrence *et al*. (2006) also found that the zeta potentials of membranes which were cleaned before use had changed, suggesting that the cleaning agents had modified the membrane charge.

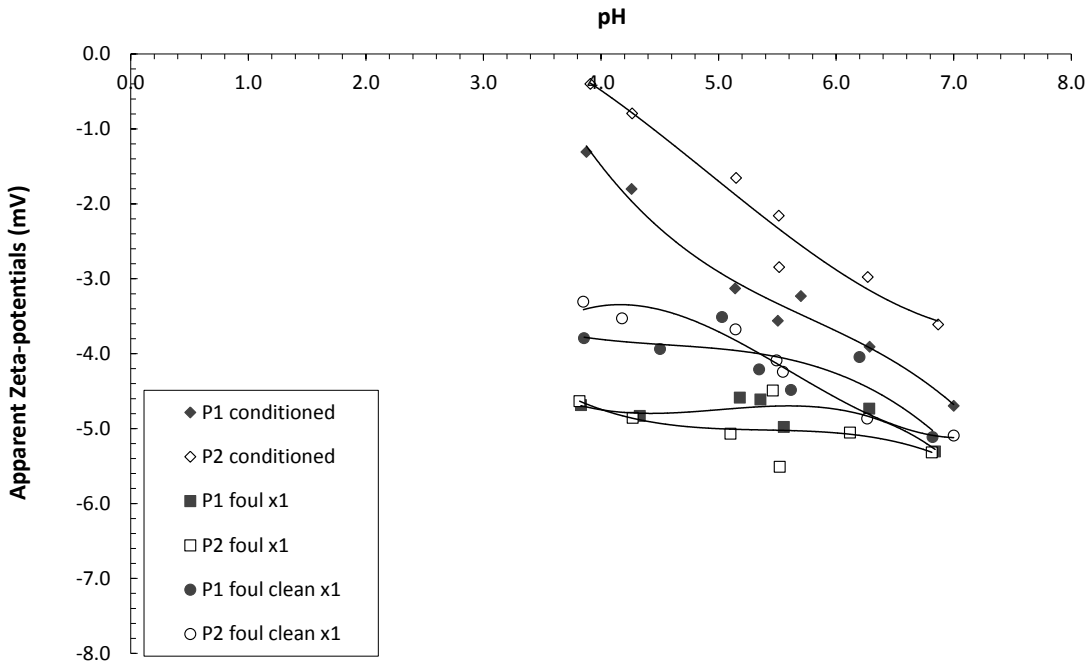

Figure 4.40: Apparent zeta-potentials on the pore walls of Protocol 1 and Protocol 2 treated FP membranes at different pH values, used for the cycle 1 of the UF filtration of SSL.

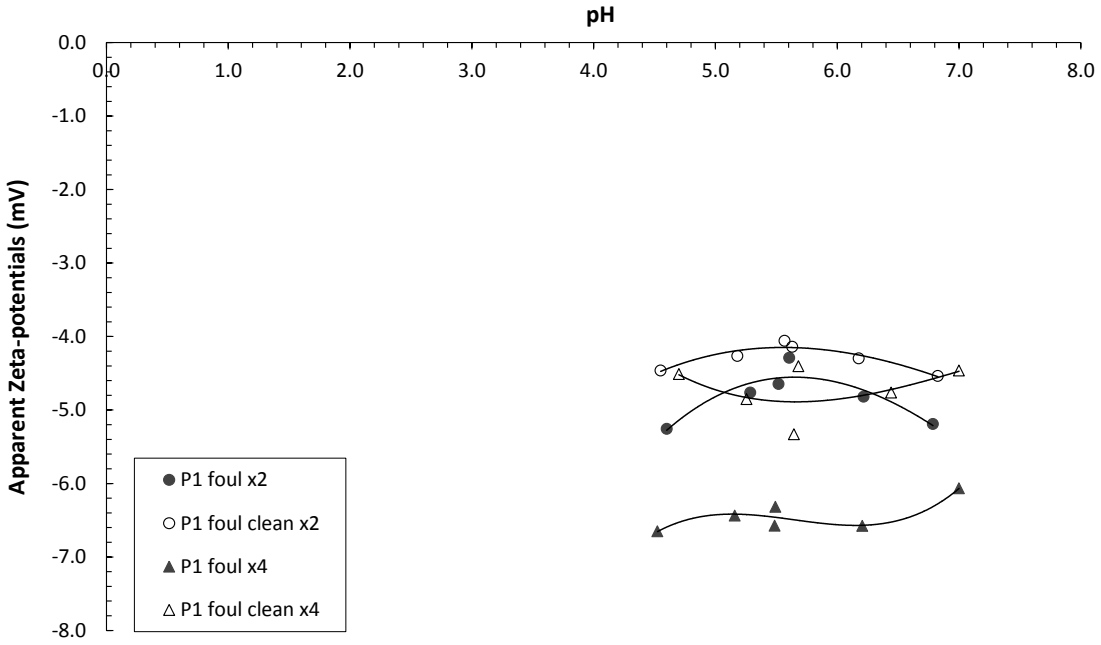

Figure 4.41: Apparent zeta-potentials on the pore walls of Protocol 1 treated FP membranes at different pH values, used for cycle 2 and cycle 4 of the UF filtration of SSL.

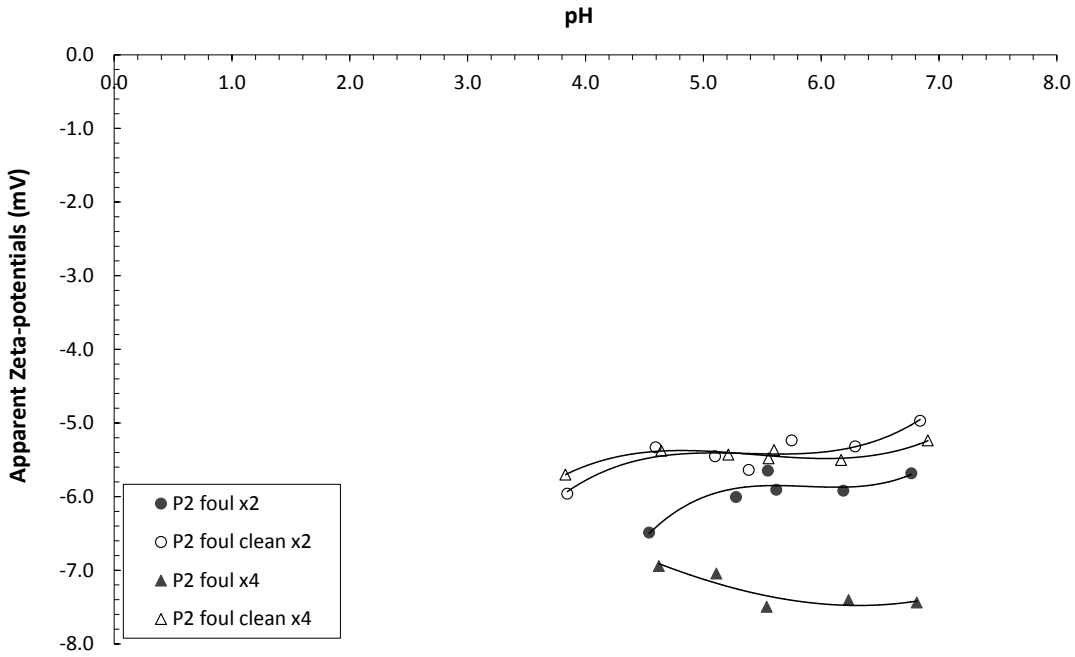

Figure 4.42: Apparent zeta-potentials on the pore walls of Protocol 2 treated FP membranes at different pH values, used for cycle 2 and cycle 4 of the UF filtration of SSL.

4.7.5. ATR-FTIR – Multiple Cycles

FTIR is a technique able to detect relatively small changes in the degree of fouling present on a surface. The functional groups detected by the Perkin-Elmer search program (Search Plus) following functional groups at different stages in the filtration

cycles are displayed in Table 4.3. The identification of chemical structure is possible, but care has to be taken as reference spectra and peaks are obtained from pure material. However, an attempt to interpret the material has been performed, especially trying to identify the foulants e.g. the lignosulphonates. As discussed previously the FTIR spectrum for lignosulphonates has been studied by Marques *et al*. (2009a). Comparing this data with all the fouling spectra, lignosulphonate fouling is evident with a common aromatic ring vibration bands at 1578 and 1486 cm^{-1} and bands of sulphonic groups at 1181, 1010, 834 and 719 cm^{-1}.

The variations caused by the two pre-treatment Protocols can be observed in Figures 4.43 (a, b, & c) to 4.44 (a & b). The scans for water and virgin membranes have been subtracted from the graphs, so that the scans represent those of the foulants or cleaning agents deposited on the membrane surface, or within the porous structure. The figures demonstrate that NaOH cleaning after water conditioning (P2) altered the species attachment profile. The possible attachment of NaOH species before fouling may have altered the nature of the surface. For cycle 1 the Protocol 2 spectrum after fouling was comparable to the Protocol 1 treated membrane which has been fouled and subsequently cleaned with NaOH. Further surface modification was evident for FP membrane surfaces following fouling and cleaning, with the Protocol 1 fouled membrane attracting different species to the other three treatments. Once the Protocol 1 membranes have been cleaned the species on the membrane changed after fouling a second time. The species profile was then the same as that observed for the Protocol 2 treated membranes. The membranes that have been fouled twice have the same species as the membranes that have been fouled and cleaned, though with different peak intensities. However, once the Protocol 1 and Protocol 2 membranes have been subjected to four fouling cycles, different species have attached to the membrane surface. These species are present due to (i) the removal of certain fouling species from the membrane surface after cleaning, or (ii) the cleaning agent masking the foulant species, or (iii) further fouling cycles resulting in different species attaching to the membrane surface. It seems most likely that the increased amount of fouling results in different SSL components attaching to the surface. The noticeable differences in the spectra for the 4x fouled membranes are larger peaks at approximately 1672 (C=O), 1608 (C=C, C-H), 1312 (C-H, C-SO_2-C) and 778 (S-O-CH_2) cm^{-1}.

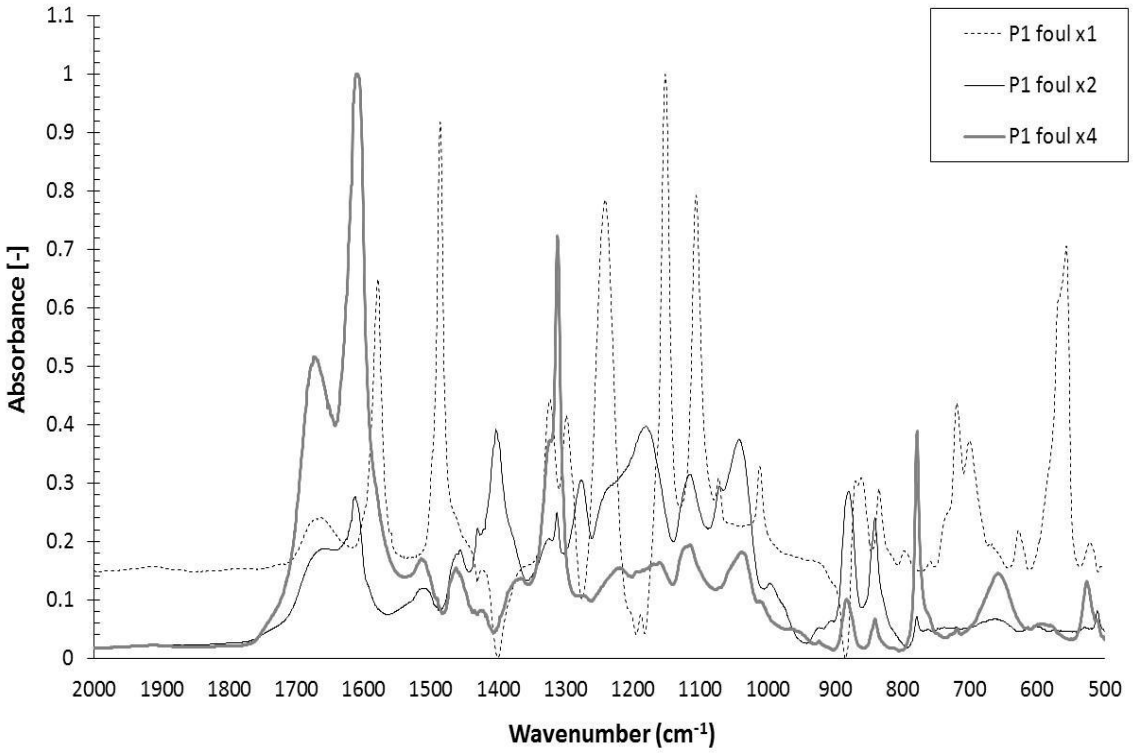

Figure 4.43 (a): Comparison of fouling infrared spectra of 20 kDa FP membranes subjected to different treatments for the filtration of SSL (all spectra shown with water and virgin membrane subtracted).

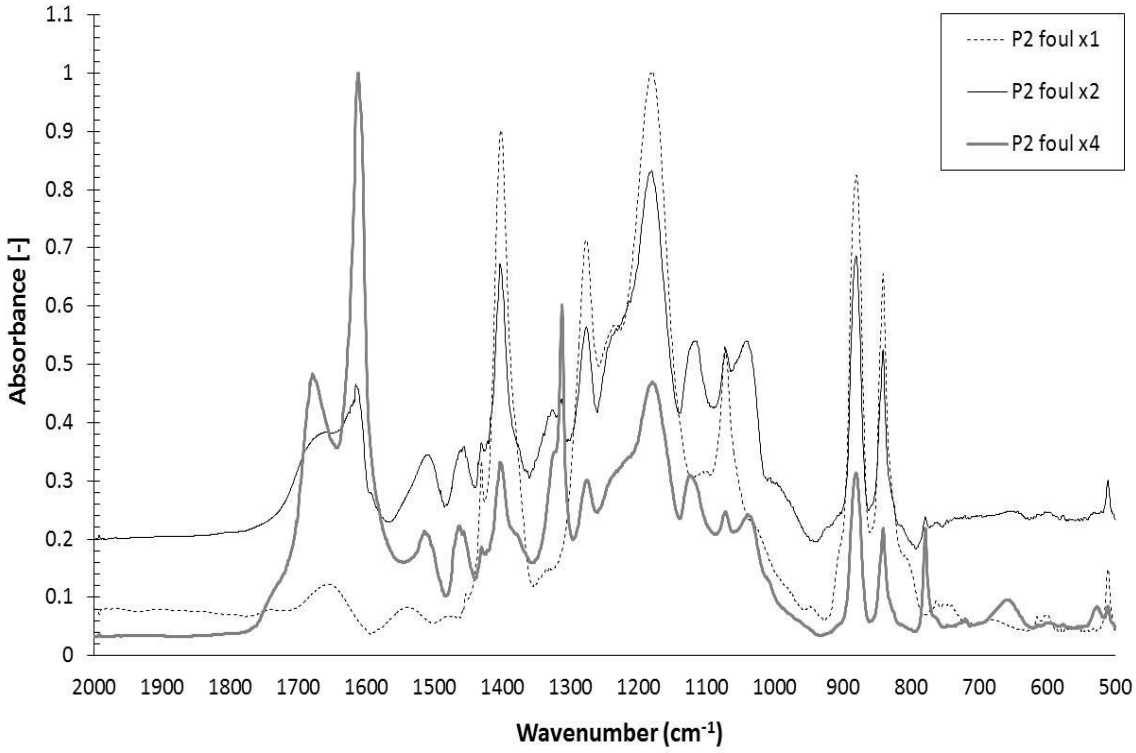

Figure 4.43 (b): Comparison of fouling infrared spectra of 20 kDa FP membranes subjected to different treatments for the filtration of SSL (all spectra shown with water and virgin membrane subtracted).

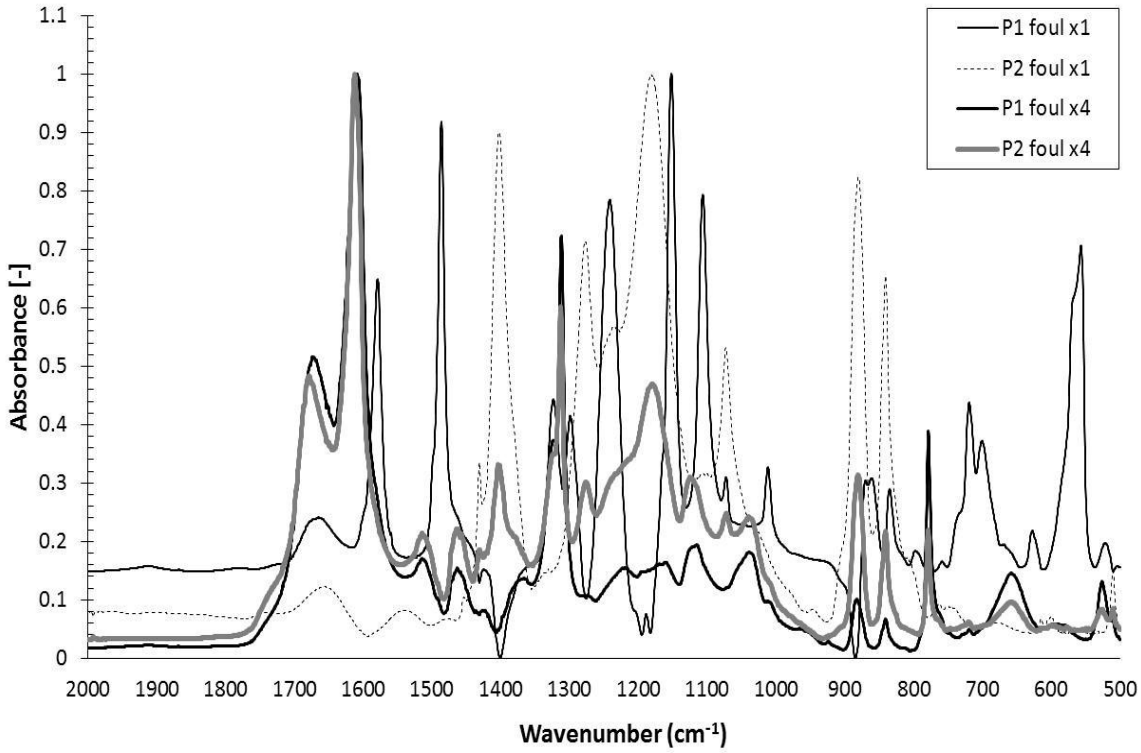

Figure 4.43 (c): Comparison of fouling infrared spectra of 20 kDa FP membranes subjected to different treatments for the filtration of SSL (all spectra shown with water and virgin membrane subtracted).

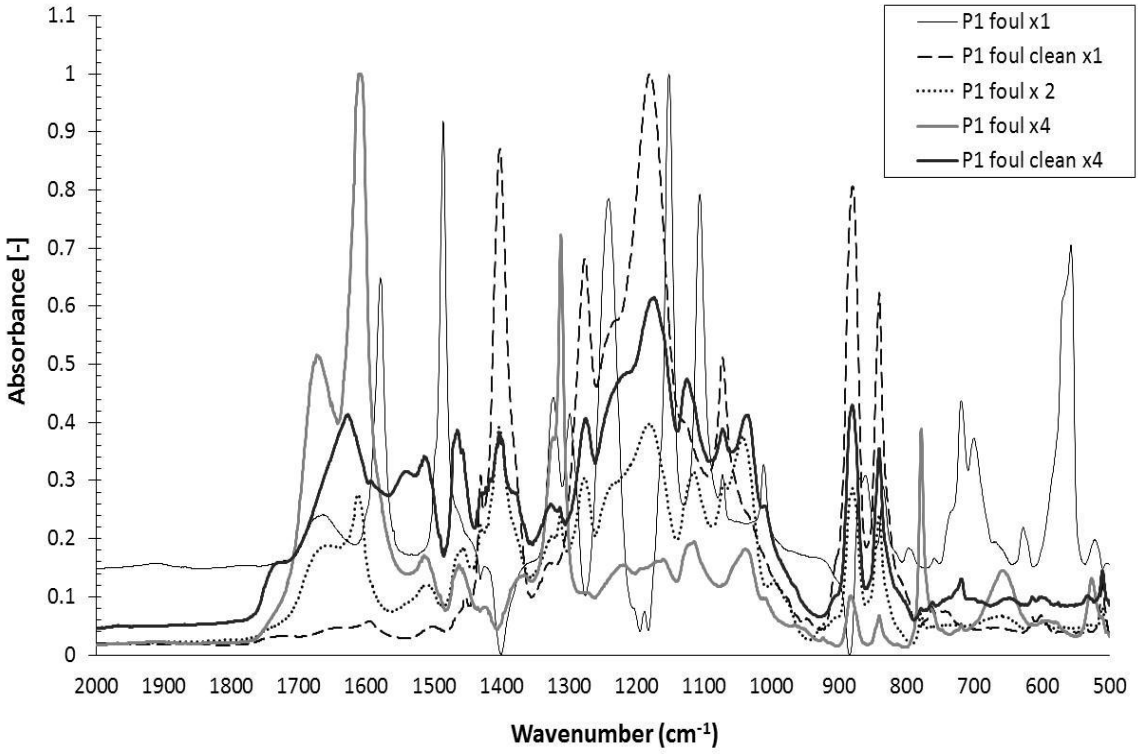

Figure 4.44 (a): Comparison of fouling and cleaning infrared spectra of 20 kDa FP membranes subjected to different treatments for the filtration of SSL (all spectra shown with water and virgin membrane subtracted).

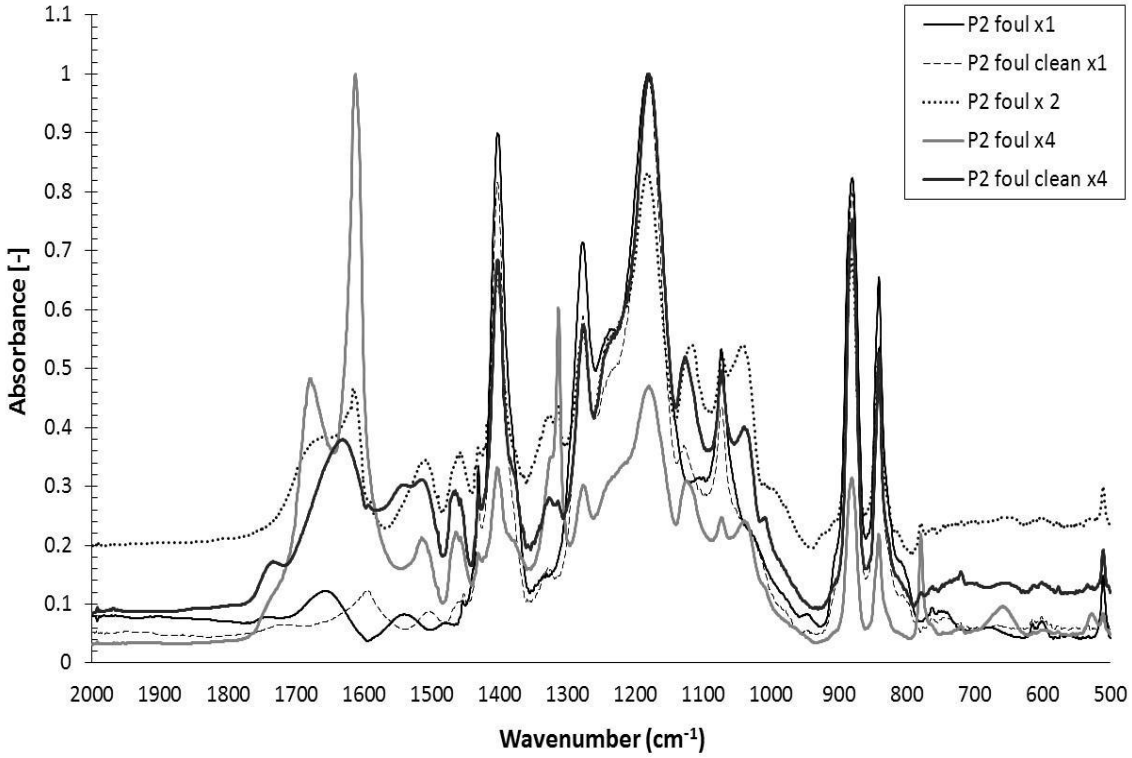

Figure 4.44 (b): Comparison of fouling and cleaning infrared spectra of 20 kDa FP membranes subjected to different treatments for the filtration of SSL (all spectra shown with water and virgin membrane subtracted).

4.7.6. AFM – Multiple Cycles

Surface roughness values were determined by AFM measurements. Values obtained for both pre-treatments were similar for conditioned, fouled and fouled then cleaned membranes over one, two and four operational cycles (Table 4.7). Following fouling, membranes displayed increased R_A values, indicating that relatively rough surface deposits were present. The roughness increased markedly from average values of 25.7 nm (after one cycle) to 28.9 nm (after two cycles) to 36.9 nm (after four cycles). Cleaning resulted in a reduction in the roughness of the deposits remaining on the surface for all cycles examined. However, the roughness values recorded confirmed that the surfaces had not been fully cleaned. This conclusion is supported by the flux, charge and contact angle data. The Protocol 2 membranes after the four complete cycles displayed lower R_A values than those seen for the Protocol 1 membranes, although differences were not statistically significant.

Table 4.7: R_A surface roughness values as measured by AFM

Cycle	Con P1	Con P2	Foul P1	Foul P2	Clean P1	Clean P2
1	18.8 ± 1	19.0 ± 1	25.6 ± 1	25.9 ± 1	22.9 ± 1	22.4 ± 1
2	18.8 ± 1	19.0 ± 1	29.4 ± 1	28.4 ± 1	27.8 ± 1	28.1 ± 1
4	18.8 ± 1	19.0 ± 1	37.3 ± 1	36.5 ± 1	30.9 ± 1	30.7 ± 1

4.7.7. Contact Angle – Multiple Cycles

The contact angles of water drops on the membrane surface are shown in Table 4.8. The FP 20 kDa membrane tested was considered to be moderately hydrophilic as the contact angle measured was less than 90º (Mulder, 2000). No statistical difference could be detected between the effect of pre-treatment Protocols 1 and 2 by measuring contact angles for the first cycle. Following each fouling and cleaning cycle, the membrane surface had a contact angle between that of a virgin and a fouled surface, implying that the membrane had not returned to its original state. As the fouling cycles increased the membranes became more hydrophilic. Protocol 2 treated membranes after filtration cycles 2 and 4 became significantly more hydrophilic than the Protocol 1 treated membranes. An increase in the attachment of hydrophilic species on Protocol 2 treated membranes was not supported by the flux data, where the PWF values were lower than those seen for Protocol 1 treated membranes. However, a possible explanation is that the Protocol 2 treated membranes developed more in-pore fouling than the Protocol 1 treated membranes as the filtration cycles increased, meaning that under the conditions investigated size exclusion effects are more important than hydrophilic interactions in determining flux values.

Table 4.8: Contact angles of water drops on membrane surfaces

Cycle	Contact Angle (º)							
	Virgin P1	Virgin P2	Con P1	Con P2	Foul P1	Foul P2	Clean P1	Clean P2
1	64 ± 2	64 ±2	62 ± 2	66 ± 3	45 ± 3	50 ± 2	60 ± 2	58 ± 3
2	64 ± 2	64 ±2	62 ± 2	66 ± 3	41 ± 2	29 ± 2	56 ± 2	30 ± 3
4	64 ± 2	64 ±2	62 ± 2	66 ± 3	30 ± 3	21 ± 5	44 ± 4	26 ± 5

4.8. Summary

SSL was studied in the cross flow rig with two different materials; Polysulphone (Ps*f*) and Fluoropolymer (FP) membranes. This section has investigated two different issues; (i) the fouling and cleaning optimisation of SSL filtration, and (ii) the effect of pre-treatment cleaning on the filtration of SSL.

The first part of this chapter was important so that any further experiments performed with SSL were maximised in performance. The fouling conditions were optimised by varying CFV, TMP and temperature. The results show that the rate of increase of flux with TMP became less apparent as pressure increased gradually to a high value for both membranes Ps*f* and FP. A limiting flux was seen at 3.0 bar. The increase in TMP caused an increase in the polarised layer thickness which acted as a secondary membrane. This increasing fouling layer which formed was found to be increasingly more difficult to remove. Increasing the fouling temperature of the SSL on the Ps*f* and FP membranes showed increased initial permeate fluxes. As the fouling cycles reached steady state the final fouling fluxes showed similar values for the 60 ºC and 70 ºC feed temperatures. The changes in viscosity of SSL did not affect the fouling process at the higher temperatures. The optimal fouling temperature for filtering SSL was found to be 60 ºC. The lower filtration temperature though can reduce the irreversible fouling resistance and increase both rinsable and concentration polarisation resistances. The optimised fouling conditions were found to be: a TMP of 3.0 bar, a CFV of 1.89 ms^{-1} and a temperature of 60 ºC for 90 min. The standard rinsing and cleaning conditions were also optimised. The FP membrane overall had a superior performance over the Ps*f* membrane.

The objective of the second part of the chapter was to determine whether the application of a simple NaOH pre-treatment could affect both the type of foulant species attaching to the membrane surface, and improve the separation performance. The use of a FP membrane to separate SSL did result in the attachment of different fouling species depending upon the pre-treatment Protocol used, as demonstrated by FTIR results. Zeta potential measurements, FTIR and electron microscopy demonstrated that both in-pore and surface fouling was present. The data collected indicated that the pre-treatment Protocols did have some effect upon the subsequent separation and cleaning

performance. The deposits formed on the membranes subjected to conditioning with NaOH displayed some of the same characteristics as those deposits formed on membranes conditioned only with water, then subsequently cleaned using NaOH following fouling. The pre-treatment of polymeric membranes with dilute NaOH solutions thus appears to have a positive effect upon subsequent membrane filtration performance after fouling and cleaning for one cycle. Once the Protocol 1 and Protocol 2 membranes had been subjected to four fouling cycles, different species had attached to the membrane surface. The results presented show that Protocol 2 treated membranes had an improved pure water flux performance over Protocol 1 treated membranes for the first three cycles, although as the cycle number increased these improvements became less significant. After four fouling and cleaning cycles had been completed, NaOH preconditioning offered no significant improvement upon pre-treatment with water alone. These findings are significant, as they offer support to the recommendations made by some polymeric membrane manufacturers that conditioning Protocols should include a NaOH step. However, in the system examined, the effect of NaOH pre-treatment resulted in an improvement in the subsequent performance only over the first two or three complete filtration cycles.

Chapter 5

The Influence of Fouling and Cleaning Conditions upon Performance of Microfiltration for Processing Molasses

5.1. Introduction

This chapter details the experimental results concerning the filtration of molasses. The membrane samples have been compared and described both quantitatively and qualitatively, in terms of flux performance and surface characteristics of the membrane. Molasses was studied in the cross flow rig with three different pore size Polysulphone (Ps*f*) membranes (0.5 μm, 0.9 μm, and 1.5 μm). The majority of the experiments were performed with the 1.5 μm Ps*f* membrane. This chapter is split into two sections: (i) the fouling and cleaning optimisation of molasses filtration, and (ii) the effect of pre-treatment cleaning on the filtration of molasses. The first section discusses the molasses filtration in terms of flux performance, resistances and rejection. The second section explains the filtration process in further detail using various analytic techniques.

5.2. Conditioning

Conditioning was required to remove glycerine from the membrane surfaces before further experiments could be performed; this was performed using the protocol developed in Weis *et al*. (2005), with reverse osmosis (RO) water at 60 ºC, 1.0 bar transmembrane pressure (TMP), and 1.89 ms^{-1} cross flow velocity (CFV) for 120 min. The RO water was changed frequently for fresh RO water to ensure the removed glycerine didn't re-foul the membrane surface. These conditions were found to be sufficient to remove the glycerine coatings. A flux decline was seen for the 1.5 μm Ps*f* membrane from 1350 L m^{-2} hr^{-1} to an average of 1020 L m^{-2} hr^{-1}. To ensure the reliability of the experimental data multiple measurements were performed. This resulted in an error of ± 7 %; this is acceptable for the study of membrane fouling. Further experiments were performed on the effects of this conditioning step. These results are presented in section 5.6.

5.3. Microfiltration of Molasses - Fouling Conditions Optimisation

Molasses is a thick syrup by-product from the processing of sugar beet into sugar and contains mainly: (i) sugar, (ii) water and (iii) inorganic matter (crystalline and dissolved calcium sulphate, calcium oxalate monohydrate and calcium oxalate dihydrate). The purpose of membrane separation in this study was the clarification of molasses to protect the downstream process, e.g. precipitation, and chromatography. This required the removal of the crystals, calcium sulphate, calcium oxalate, and calcium oxalate monohydrate. Microfiltration offers the possibility of separating the crystalline material (retained in the retentate) from the sugar and divalent ionic species (which are passed through to the permeate stream). Removing the undesired compounds is one of the most severe problems in the sugar industry (Šereš *et al*., 2005). The molasses concentration was measured in terms of ºBrix. The Brix (% of solute solid materials in water) of feed, permeate and retentate were measured using a refractometer.

5.3.1. Fouling Conditions

The fouling conditions have been optimised by varying concentration, temperature and TMP on 1.5 µm Ps*f* membranes. The equations discussed in Chapter 4 (Equations 4.1 to 4.7) have been used throughout this chapter to optimise the fouling conditions in the filtration of molasses.

5.3.1.1. Molasses Concentration

The molasses concentration was varied whilst maintaining a constant TMP of 3.0 bar, CFV of 1.89 ms^{-1} at 60 ºC for 90 min where standard rinsing and cleaning conditions were used. RO pure water fluxes (PWF) were maintained constant before and after fouling and after cleaning (22 ºC, 1.0 bar, and 1.89 ms^{-1}). The effect of molasses concentration variation (15, 25, 35, 45, & 55 ºBrix) is presented in Figure 5.1. It shows the first, last and average flux value in the fouling section of the cycle. The last fouling point indicates when the flux has reached steady state. The molasses was required to be used at as low dilution rate as possible, it couldn't be used in delivered form as its viscosity was too high for pumping around the circuit and for effective separation. The low dilution rate was required as it cuts down further downstream processing. The lowest dilution rate possible for filtration in this study was 55 ºBrix. The 55 ºBrix molasses produced flux values of ~26 (± 3) L m^{-2} hr^{-1}, which was too low for a viable

process. Higher concentrations provide higher osmotic pressure and larger driving forces for deposit formation. The 45 ºBrix produced an average steady state flux value of ~62 (± 3) L m^{-2} hr^{-1}. This is a reasonable fouling flux performance. Figure 5.2 shows the fouling flux data as a function of TMP at different molasses concentrations. The TMPs where the limiting flux occurred for the lower concentrations of 15 ºBrix and 25 ºBrix was 3.0 bar to 3.5 bar. This TMP decreased to between 2.5 bar to 3.0 bar at the higher concentrations of 35 ºBrix and 45 ºBrix. The effects of the fouling problems are discussed in more detail in section 5.6.

Figure 5.3 displays the breakdown of the different resistive layers present at steady state as a function of molasses concentration. The viscosity of molasses due to concentration changes has been incorporated into the fouling resistance calculation. The resistance breakdown shows that the total resistance (R_T) increased with increasing concentration. The resistances due to R_{cp} and R_I were responsible for the increase. This coincides with a decrease in rinsable resistance (R_R). The increase in concentration from 45 ºBrix to 55 ºBrix increased the R_T significantly (1.19 x 10^{13} m^{-1} to 1.94 x 10^{13} m^{-1}), this was contributed by a large increase in R_{cp} (from 5.54 x 10^{12} m^{-1} to 9.47 x 10^{12} m^{-1}) and R_I (from 4.74 x 10^{12} m^{-1} to 8.57 x 10^{12} m^{-1}). Figure 5.4 shows the membrane resistance after fouling and cleaning (0.25 wt. % sodium hydroxide (NaOH), 1.0 bar, 1.89 ms^{-1} and 50 ºC) compared to the membrane resistance before fouling. The lower concentration resulted in a higher degree of cleanability. This was due to the decrease in irreversible fouling and concentration polarisation at higher dilutions. This can be explained by Figure 5.5; which displays the apparent solids rejection data as a function of molasses concentration for the 1.5 µm Ps*f* membranes. The apparent rejection increased with increasing concentration and TMP, resulting in more solids on the retentate side. This could have been contributed to the tightening of the effective pore size through the fouling layer as the concentration increased (Eagles and Wakeman, 2002). This increase in solids caused more fouling, in terms of pore blocking and surface fouling, which was not entirely removed after the cleaning process was completed.

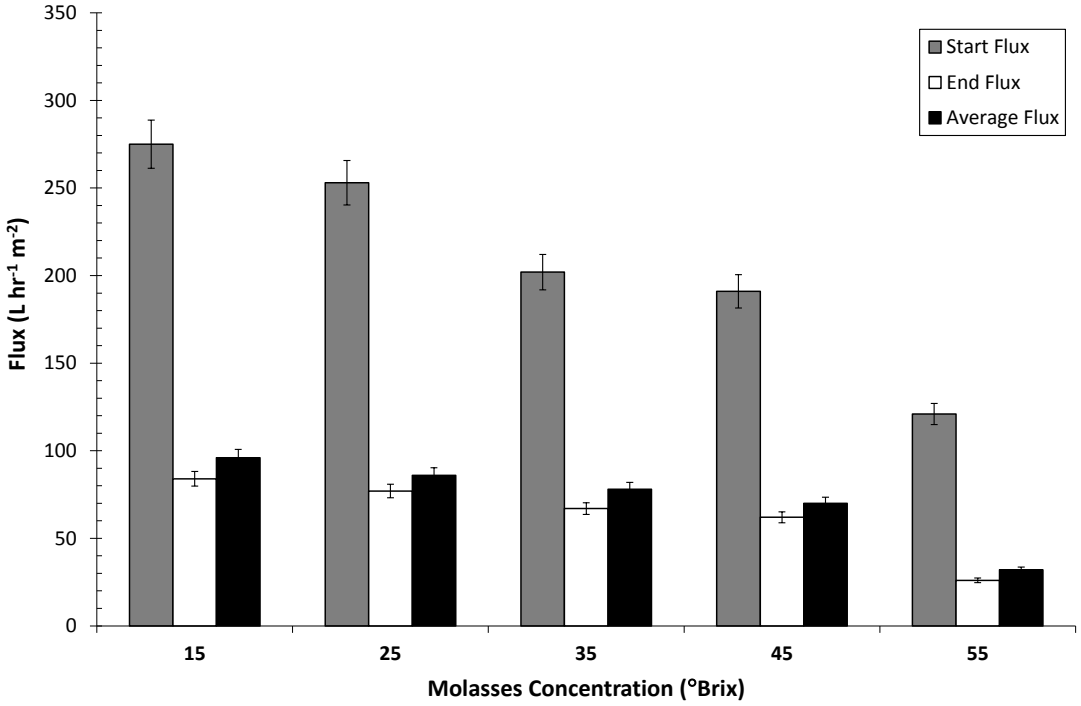

Figure 5.1: Graph to show fouling flux data as a function of fouling concentration on 1.5 µm Ps*f* membranes when fouled with molasses (60 ºC, 3.0 bar TMP, 1.89 ms^{-1} CFV) for 90 min.

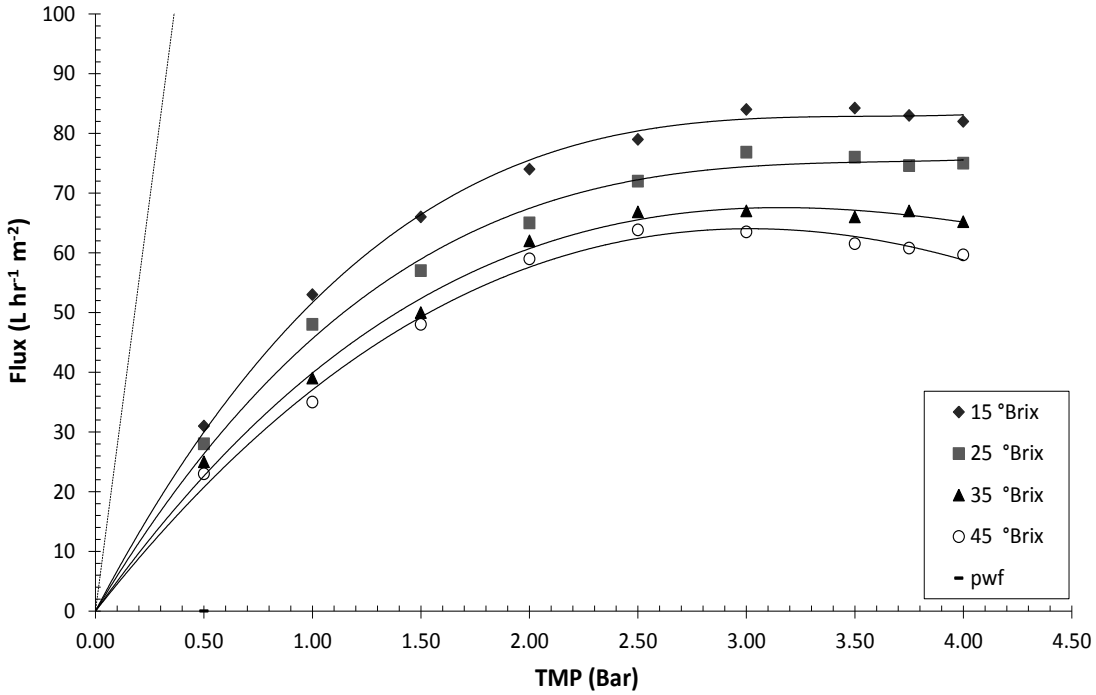

Figure 5.2: Graph to show fouling flux data as a function of TMP on 1.5 µm Ps*f* membranes when fouled with molasses (60 ºC, 1.89 ms^{-1} CFV) at different molasses concentrations for 90 min.

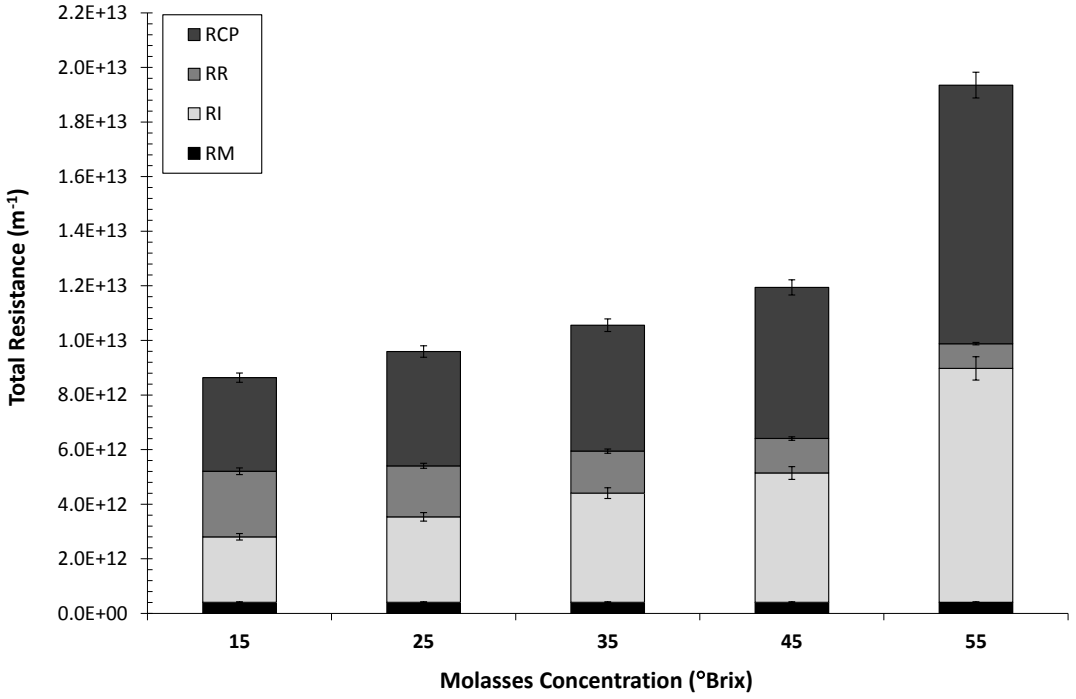

Figure 5.3: Graph to show fouling resistance data as a function of fouling concentration on 1.5 µm Ps*f* membranes when fouled with molasses (60 ºC, 3.0 bar TMP, 1.89 ms^{-1} CFV) for 90 min.

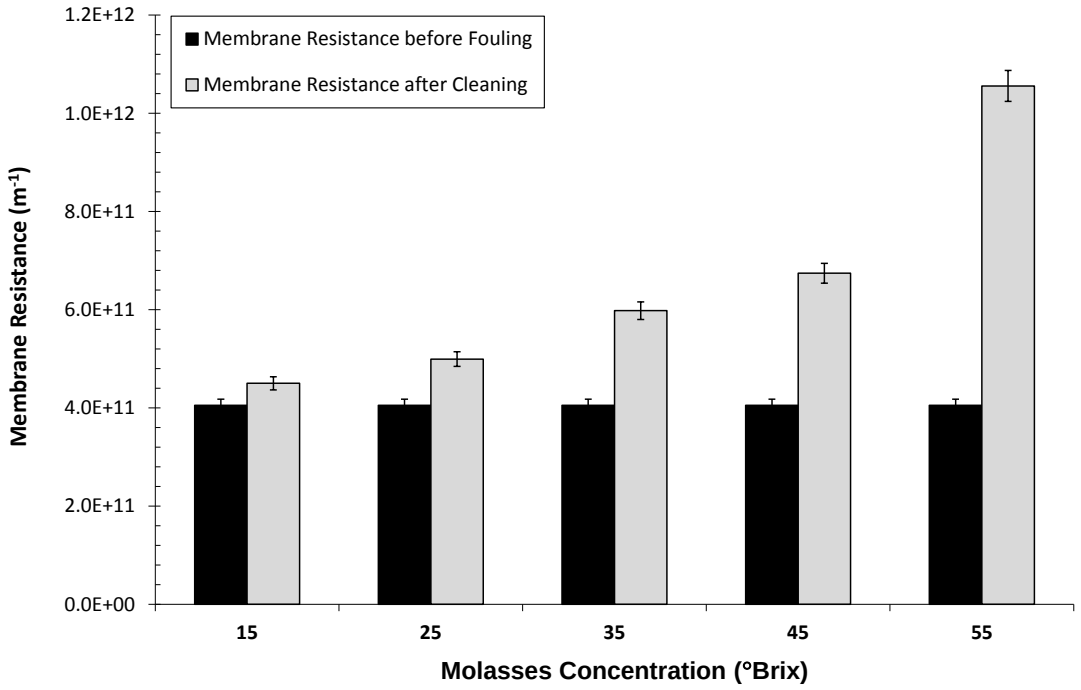

Figure 5.4: Graph to show pure water membrane resistances before fouling and after cleaning vs. fouling concentration variation on 1.5 µm Ps*f* membranes when fouled with molasses (60 ºC, 3.0 bar TMP, 1.89 ms^{-1} CFV) for 90 min. All cleaning conditions maintained at 0.25 wt. % NaOH, 1.0 bar, 1.89 ms^{-1} and 50 ºC.

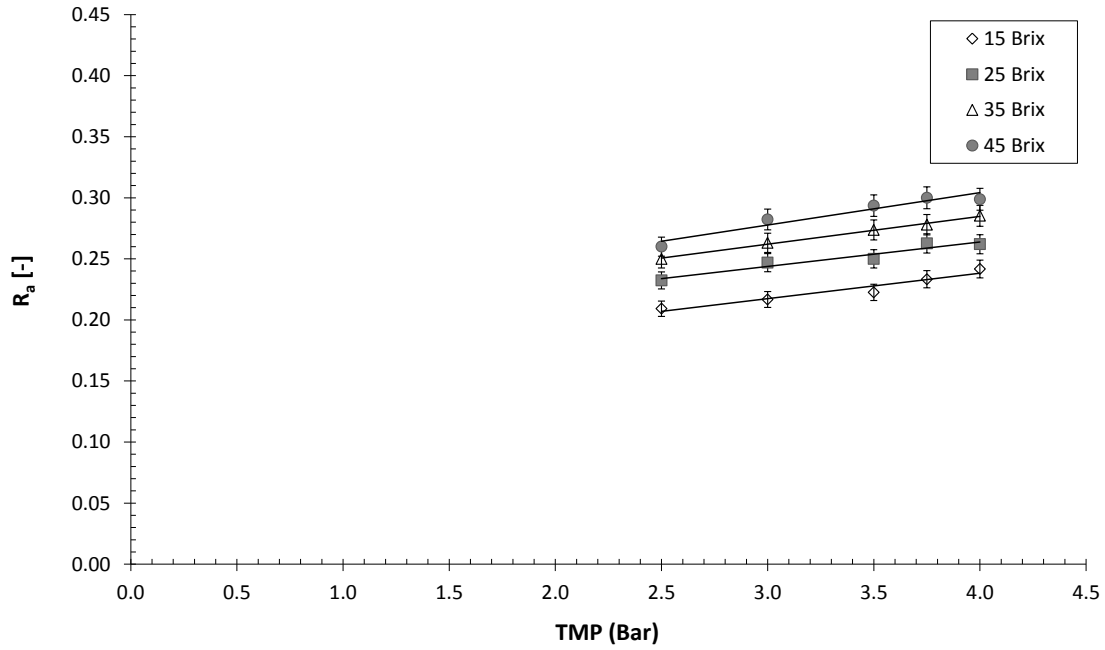

Figure 5.5: Graph to show apparent rejection coefficient as a function of concentration and TMP variation through 1.5 µm Ps*f* membranes when fouled with molasses (60 ºC, 1.89 ms^{-1} CFV) for 90 min.

5.3.1.2. Temperature

The fouling temperature was varied whilst maintaining a constant 45 ºBrix, TMP of 3.0 bar, and CFV of 1.89 ms^{-1} for 90 min where standard rinsing and cleaning conditions were used. RO pure water fluxes were maintained constant (22 ºC, 1.0 bar, and 1.89 ms^{-1}) before and after fouling and after cleaning. Molasses can be studied up to temperatures as high as 70 ºC when diluted, without any changes to the molasses properties (Nordzucker, 2008). A recommended condition of 50 ºC was investigated due to the precipitation step after the separation occurring at this temperature. Room temperature (22 ºC), 40 ºC, 60 ºC and 70 ºC were also studied for comparison. Figure 5.6 displays the fouling flux data for the 1.5 µm Ps*f* membrane. It shows the first, last and average flux value in the fouling section of the cycle. The last fouling point indicates when the flux has reached steady state. As the temperature of the feed is increased so does the initial, last and average flux. This shows that the viscosity of the feed is very important in the filtration of molasses. The molasses should be used at as high a temperature as possible. The optimal temperature for the filtration of molasses was 60 ºC; as there was no benefit of increasing the temperature to 70 ºC. In terms of fouling flux, the effect of decreasing viscosity at increasing temperature (70 ºC) stabilised. Other interactions must therefore have been occurring.

Figure 5.7 shows a breakdown of the different resistive layers present at steady state versus fouling temperature. As the change in viscosity due to temperature changes has already been incorporated into the fouling resistance calculation, the differences are associated with other factors. The total resistance (R_T) decreased significantly from 2.40 x 10^{13} m^{-1} to 1.11 x 10^{13} m^{-1} as the molasses temperature increased from 22 ºC to 70 ºC. The increases in R_R and R_{cp} resistances for the 22 ºC fouled membranes were responsible for the increases in the total resistance over the higher temperatures. The R_I increased considerably from 2.67 x 10^{12} m^{-1} for the 22 ºC fouled membrane to 4.70 x 10^{12} m^{-1} for the 60 ºC fouled membrane. This increase in R_I was responsible for the increase of resistance after fouling and cleaning as the molasses temperature was raised (Figure 5.8). The membrane resistance after fouling and cleaning compared to the membrane resistance before fouling show that the cleaning regime (0.25 wt. % NaOH, 1.0 bar, 1.89 ms^{-1} and 50 ºC) did not remove the majority of the fouling resistance. The deposit strength was probably slightly higher when fouling occurred at the higher temperatures as the membrane resistances are greater at increased temperatures. Also more in-pore fouling could have resulted due to the higher fluxes through the membrane. The cleaning regime has been further optimised in section 5.4. Figure 5.9 shows the apparent solids rejection data versus fouling temperature for the Ps*f* membrane. Increasing the temperature from 22 – 60 ºC decreased the rejection from 0.40 to 0.28. The rejection coefficient is further decreased to 0.25 at 70 ºC. This decrease could be due to increased flux going through the membrane forcing more solids through to the retentate side.

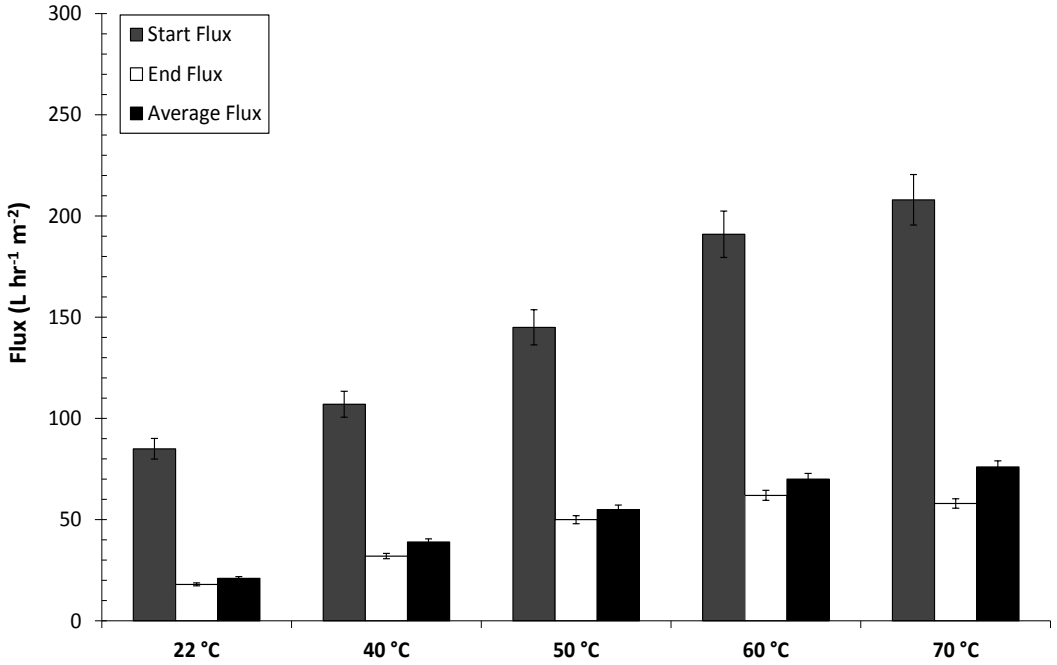

Figure 5.6: Graph to show fouling flux data as a function of fouling temperature on the 1.5 µm Ps*f* membranes when fouled with molasses (3.0 bar TMP, 1.89 ms^{-1} CFV, 45 ºBrix) for 90 min.

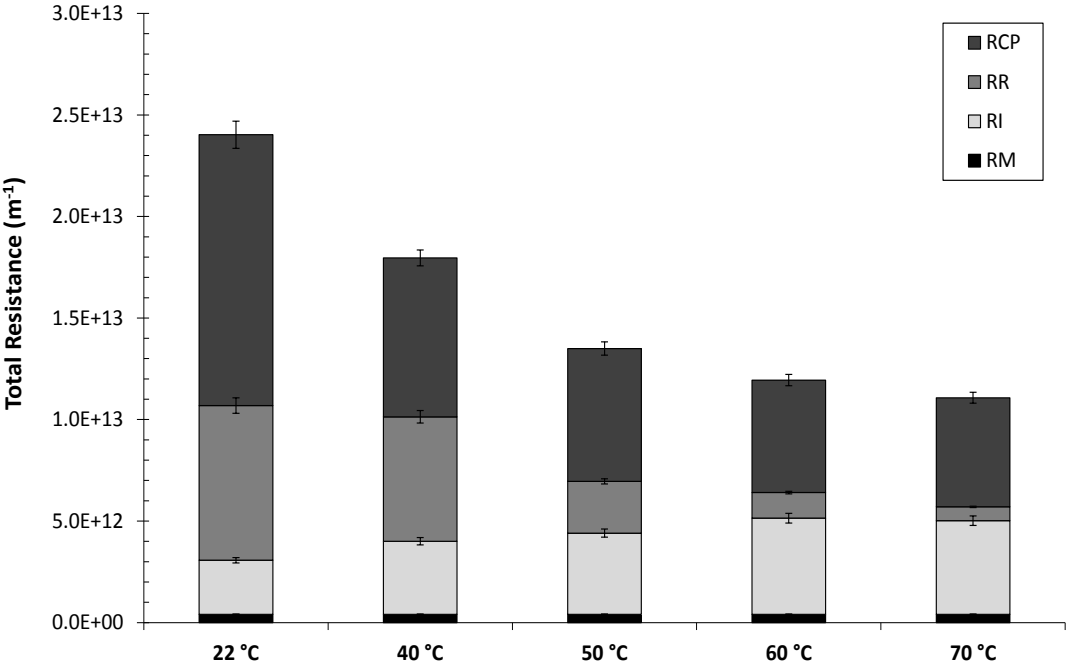

Figure 5.7: Graph to show fouling resistance data as a function of fouling temperature on 1.5 µm Ps*f* membranes when fouled with molasses (3.0 bar TMP, 1.89 ms^{-1} CFV, 45 ºBrix) for 90 min.

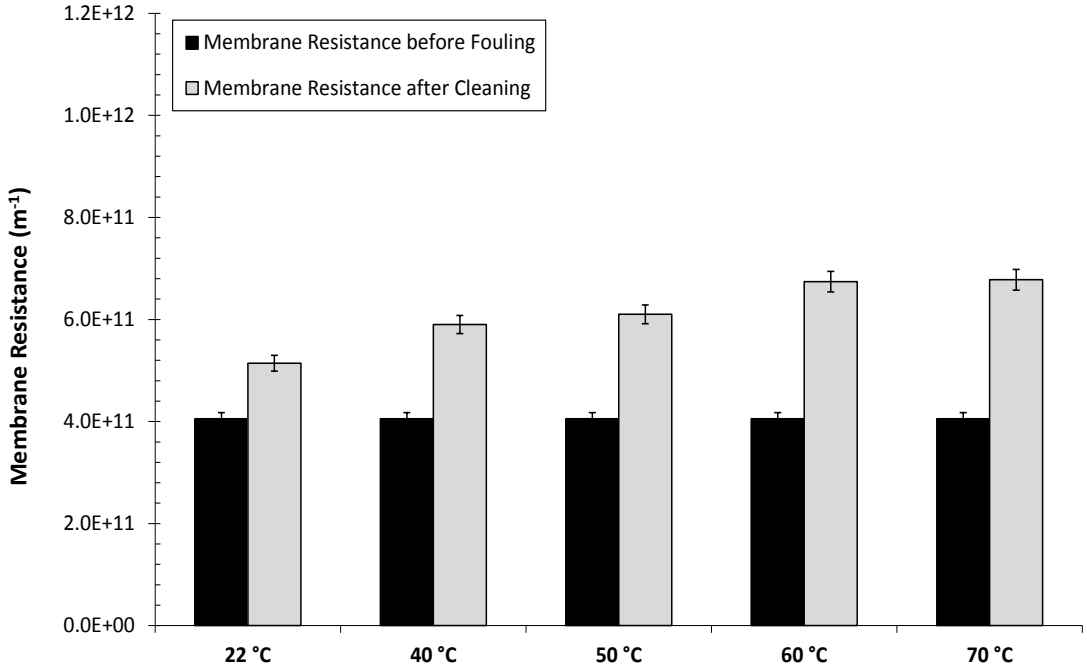

Figure 5.8: Graph to show pure water membrane resistances before fouling and after cleaning vs. fouling temperature variation on 1.5 µm Ps*f* membranes when fouled with molasses (3.0 bar TMP, 1.89 ms^{-1} CFV, 45 ºBrix) for 90 min. All cleaning conditions maintained at 0.25 wt. %, 1.0 bar, 1.89 ms^{-1} and 50 ºC.

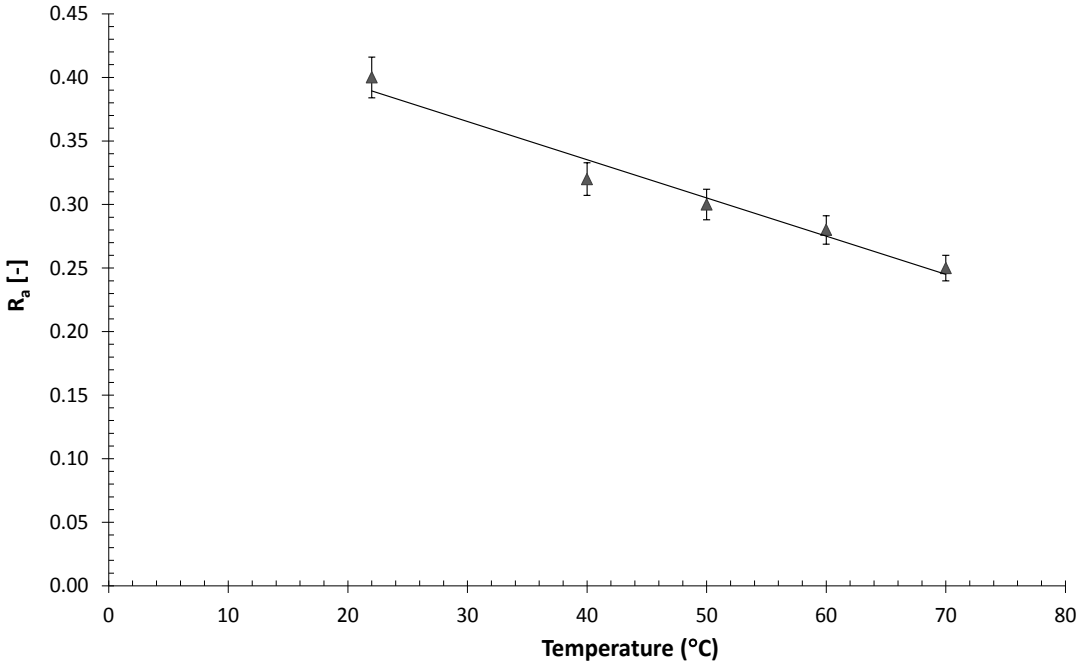

Figure 5.9: Graph to show the apparent rejection coefficient as a function of fouling temperature variation through 1.5 µm Ps*f* membranes when fouled with molasses (3.0 bar TMP, 1.89 ms^{-1} CFV, 45 ºBrix) for 90 min.

5.3.1.3. Transmembrane Pressure

The fouling TMP was varied from 1.0 to 4.0 bar whilst maintaining a constant 45 ºBrix, CFV of 1.89 ms^{-1} and a temperature of 60 ºC for 90 min where standard rinsing and cleaning conditions were used. RO pure water fluxes (22 ºC, 1.0 bar, and 1.89 ms^{-1}) were maintained constant before and after fouling and after cleaning. Figure 5.10 shows the first, last and average flux values in the fouling section of the cycle. The data shows that increasing the TMP increases the fouling flux until ~3.0 bar TMP where the limiting flux effect occurs. The limiting flux at 1.89 ms^{-1} with steady state flux was 62 L m^{-2} hr^{-1}. The limiting flux in relation to varying CFVs has been further investigated in the mass transfer section 5.3.2.

Figure 5.11 shows a breakdown of the different resistive layers present at steady state versus TMP. The resistance breakdown shows that the resistance due to concentration polarisation (R_{cp}) was responsible for the increased resistance (R_T) with increasing TMP. R_{cp} was accountable for 35 % of the total resistance at 1.0 bar and 49 % of the total resistance at 4.0 bar. This increase in concentration polarisation was due to the increased pressure causing greater back diffusion and a greater degree of foulants at the membrane surface. The R_I increased from 3.79 x 10^{12} m^{-1} for 1.0 bar TMP to 5.00 x 10^{12} m^{-1} at 4.0 bar TMP for the Ps*f* fouled membranes. R_R decreased from 2.21 x 10^{12} m^{-1} for 1.0 bar TMP to 1.26 x 10^{12} m^{-1} at 3.0 bar TMP. This irreversible resistance is when rinsed with RO water only; the increased TMP also affected the cleanability of the membrane. Figure 5.12 shows that the membrane resistance after fouling and cleaning increases as the fouling TMP increases. When fouling at higher TMPs an increased fouling layer is formed which is increasingly difficult to remove. This could be due to the overall higher fluxes resulting in higher drag forces on particles towards the membrane surface at higher concentrations. This fouling layer would also be less porous hindering the separation performance. This causes further pore blockages and surface fouling. This indicates that at the lower pressures there is a higher degree of cleanability.

Figure 5.14 displays the apparent solids rejection data versus fouling TMP for the Ps*f* membrane. Increasing the TMP from 1.0 bar to 2.0 bar increased the rejection coefficient from 0.21 to 0.26. The rejection coefficient was further increased to 0.29 at

3.0 bar. This was due to the increased polarised layer and fouling layer at the membrane surface which resulted in decreased pore sizes allowing altered size exclusion (Blainpain *et al*., 1993; Kallioinen *et al*., 2007). This has been discussed further in section 5.3.2.

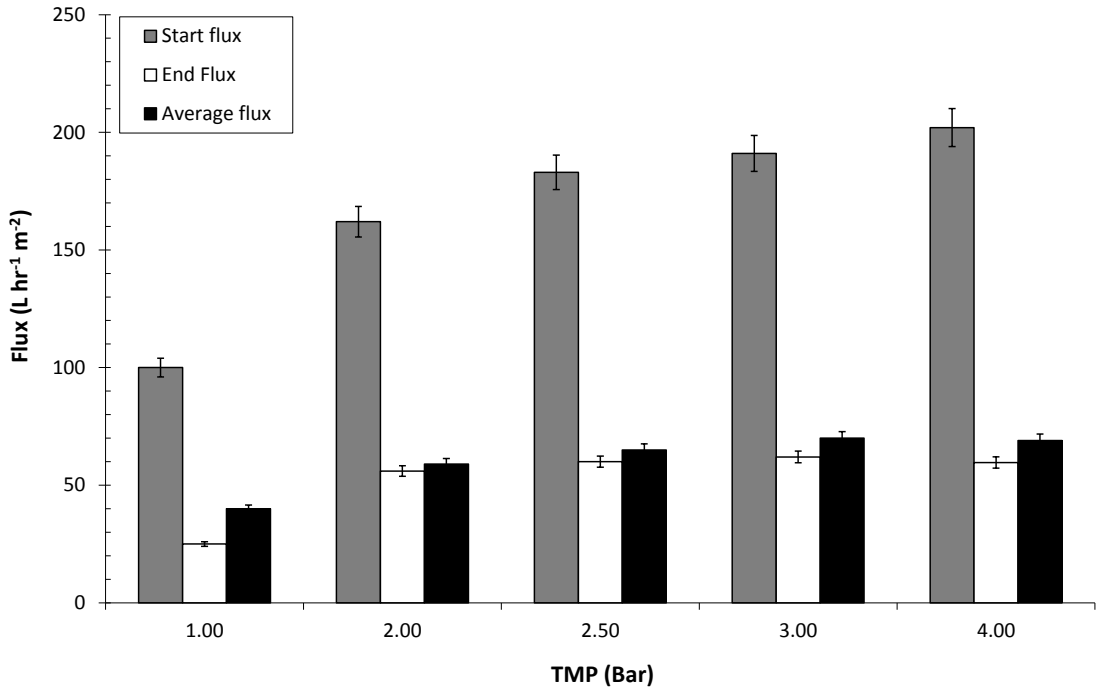

Figure 5.10: Graph to show variation of fouling flux data as a function of fouling TMP on 1.5 µm Ps*f* membranes when fouled with molasses (60 ºC, 1.89 ms^{-1} CFV, 45 ºBrix) for 90min.

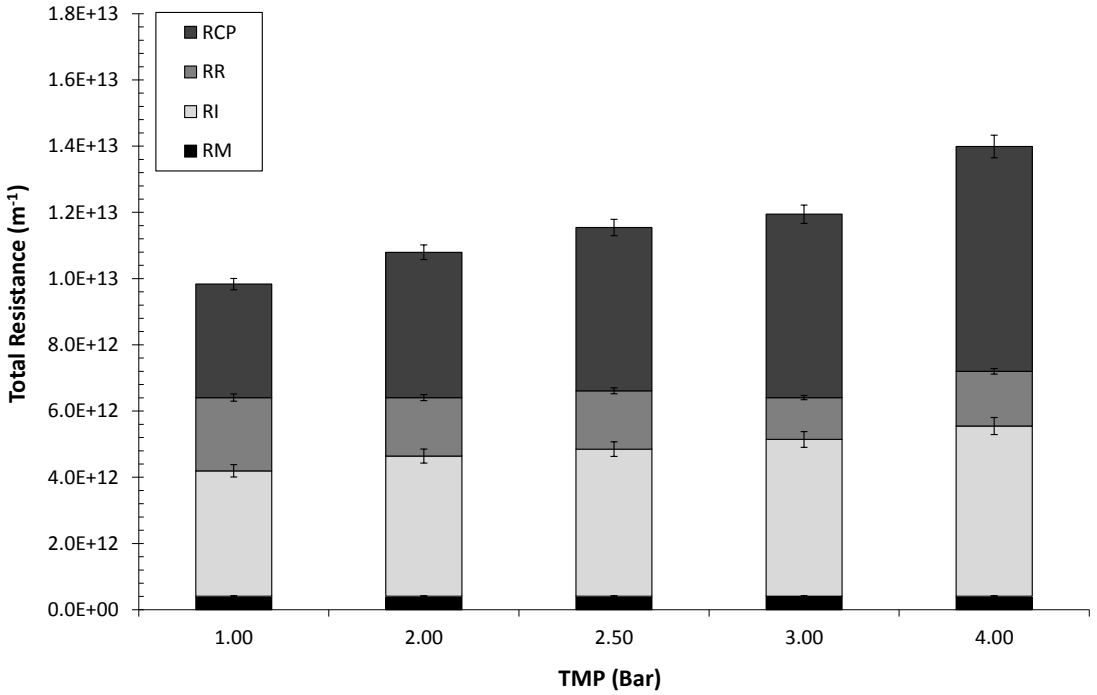

Figure 5.11: Graph to show fouling resistance data as a function of TMP on 1.5 µm Ps*f* membranes when fouled with molasses (60 ºC, 1.89 ms^{-1} CFV, 45 ºBrix) for 90 min.

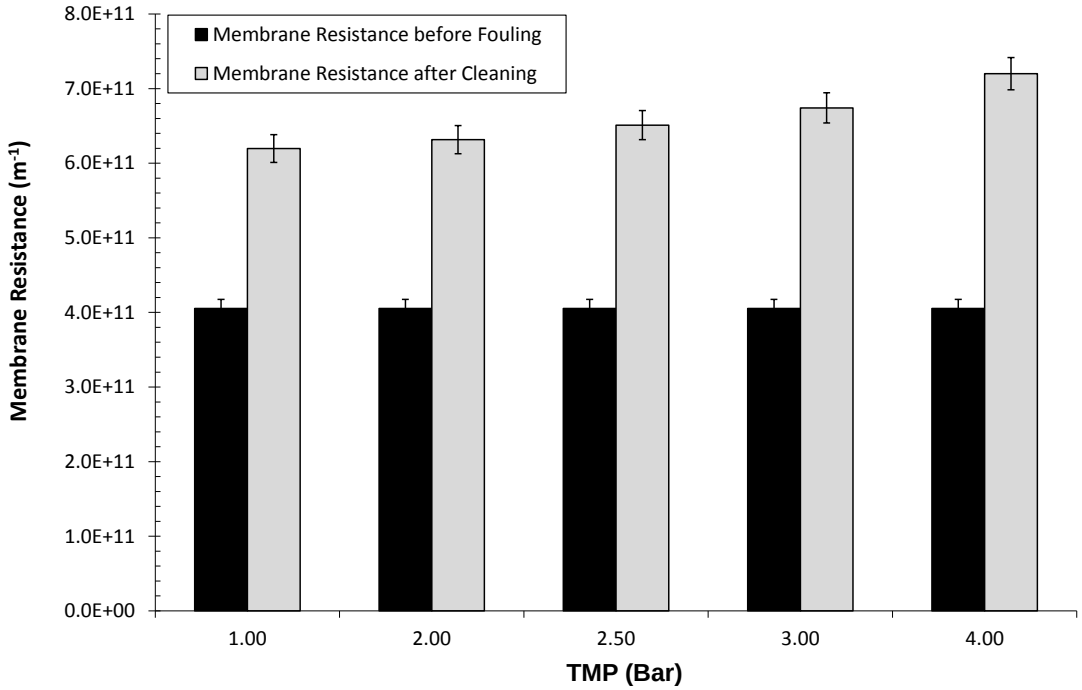

Figure 5.12: Graph to show pure water membrane resistances before fouling and after cleaning vs. TMP variation on 1.5 µm Ps*f* membranes when fouled with molasses (60 ºC, 1.89 ms^{-1} CFV, 45 ºBrix) for 90 min. All cleaning conditions maintained at 0.25 wt. % NaOH, 1.0 bar, 1.89 ms^{-1} and 50 ºC.

5.3.2. Mass Transfer Information

Figure 5.13 displays the fouling flux data as a function of TMP (0.5 to 4.0 bar) and CFV (0.29 to 2.86 ms^{-1}) for the 1.5 µm Ps*f* membranes. The data shows that the limiting TMP for all CFVs was between 2.5 and 3.0 bar. After this pressure the fouling fluxes began to decline slightly. It was therefore not advantageous to work at pressure higher than 3.0 bar. The build-up of solute particles near the membrane was reduced by the higher CFVs. Figure 5.14 displays the apparent solids rejection data as a function of fouling TMP and CFV for the 1.5 µm Ps*f* membrane. The apparent rejection coefficient slightly increased linearly with increasing TMP, whereas it decreased with increasing CFV. The effects of varying TMP and CFV on membrane fouling have been further investigated in Chapter 6.3.3 with the aid of the Fluid Dynamic Gauging.

The limiting region of 2.5 bar to 4.0 bar has been used in Equation 4.6 to plot Figure 5.15. The plots of $\ln[(1-R_a)/R_a]$ against flux for CFVs of 0.57, 1.14, 1.89 and 2.29 ms^{-1} (Re = 1000 – 4000) were used for the estimation of mass transfer coefficients. As shown in Figure 5.15, all the experimental data are well fitted by straight lines with a

slope which varied with CFV. Extrapolation of the y-axis of the lines connecting the flux rejection data can be seen. The lines converged towards a similar y-axis intercept of -0.37, which corresponds to a true (actual) rejection coefficient of approximately 0.59 (59 % solids rejected). This actual rejection converts to an estimated membrane surface concentration (C_m). The concentration on the surface, C_m for the CFV of 1.89 ms^{-1} (Re = 3300) and 3.0 bar was 32 % greater than the concentration in the bulk stream, C_b. This implies that there is a high degree of concentration polarisation occurring, as validated in this work (Figure 5.11). The gradients of the lines in Figure 5.15 have been used calculate the mass transfer coefficients and are displayed in Figure 5.16. The gradient of the turbulent line is only slightly promoted compared to the laminar data. The membrane filtered at 1.89 ms^{-1} (Re = 3300) had a mass transfer number of 1.37 x 10^{-5} ms^{-1}.

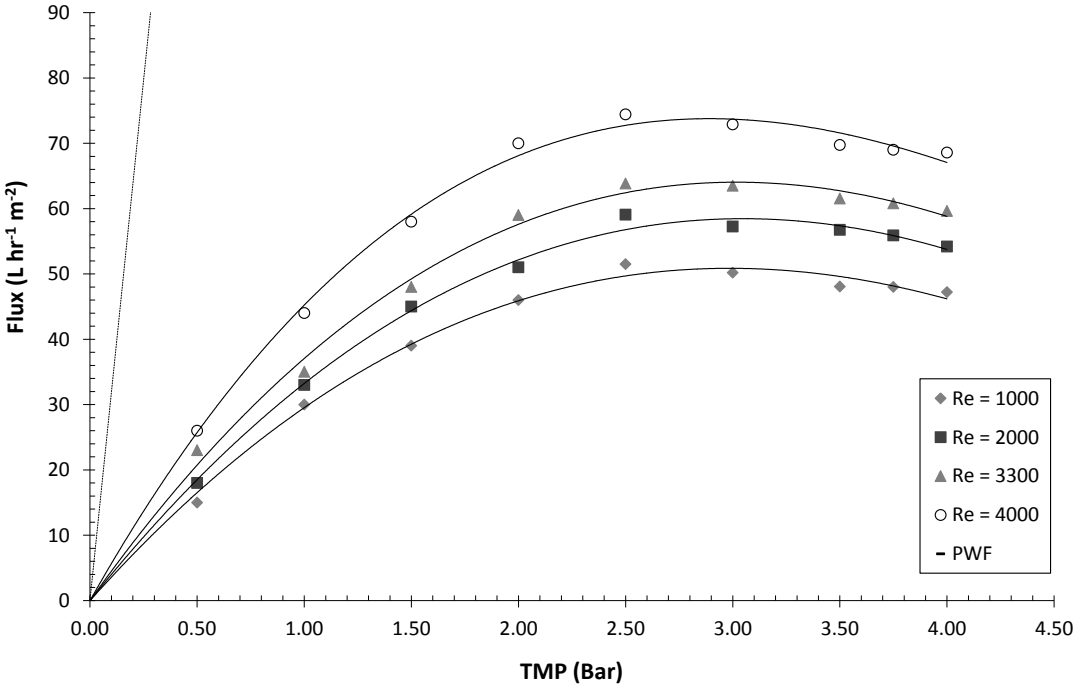

Figure 5.13: Graph to show fouling flux data as a function of TMP on 1.5 µm Ps*f* membranes when fouled with molasses (60 ºC, 45 ºBrix) at different Reynolds numbers (CFV) for 90 min.

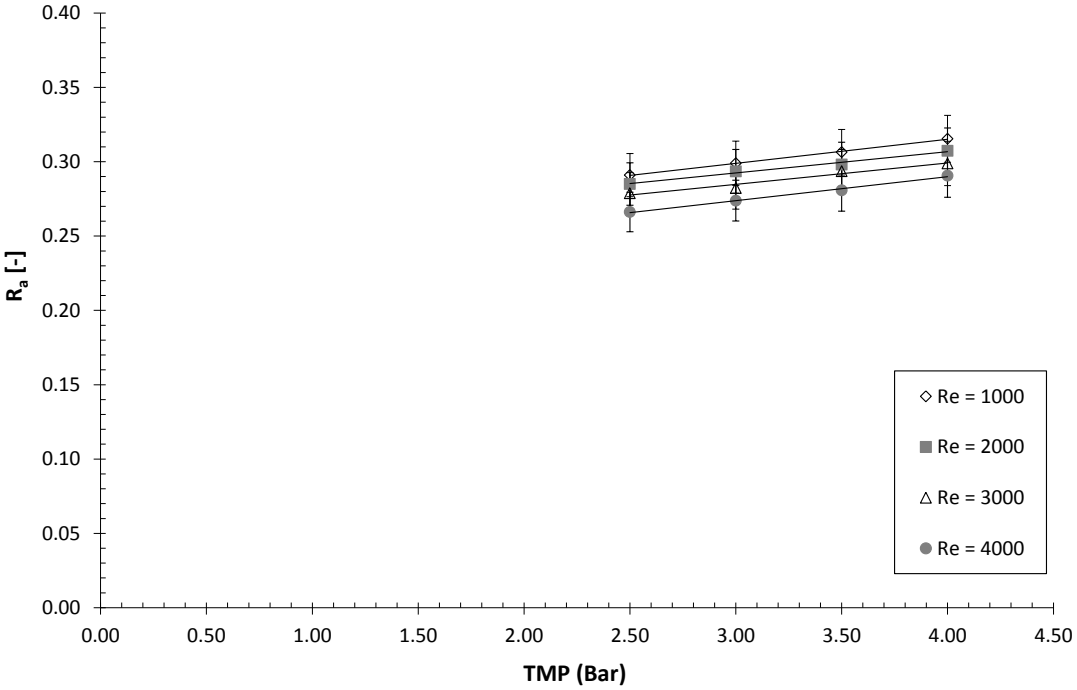

Figure 5.14: Graph to show the apparent rejection coefficient as a function of applied TMP on 1.5 µm Ps*f* membranes when fouled with molasses (60 ºC, 45 ºBrix) at different Reynolds numbers (CFV) for 90 min.

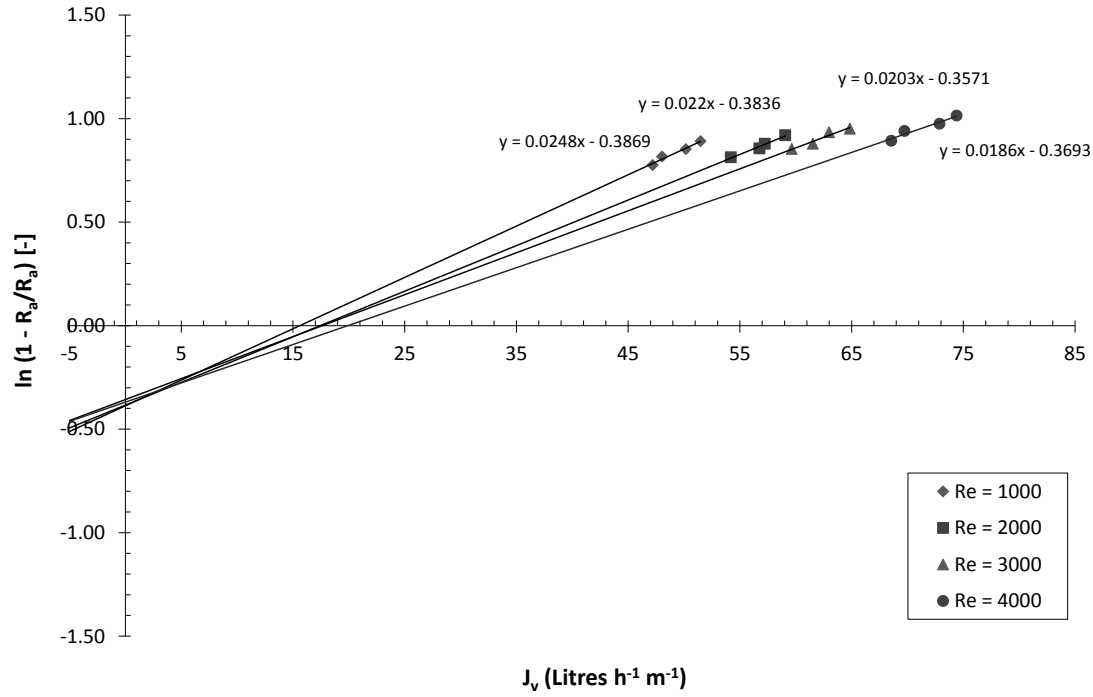

Figure 5.15: Linearised plot of the concentration polarisation equation for various CFVs with trend lines extrapolated to meet the y-axis. Constant concentration (45 ºBrix) and temperature (60 ºC). Varied Re: 1000, 2000, 3000, 4000 and TMP: 2.5, 3.0, 3.5, 4.0 bar.

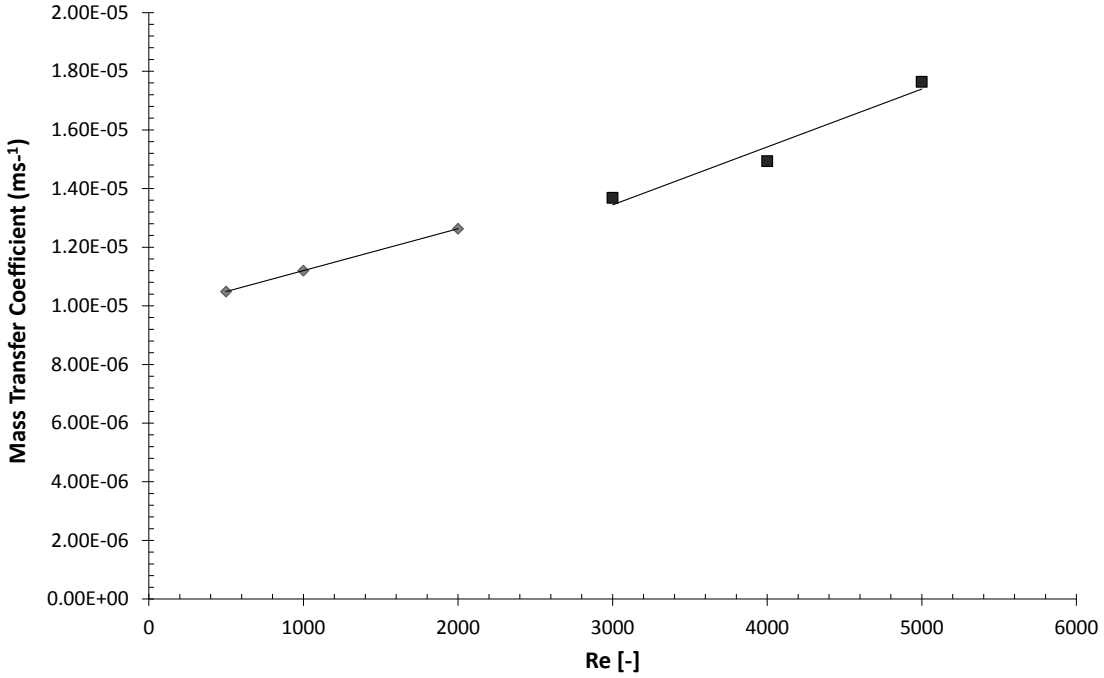

Figure 5.16: Mass transfer coefficient variation for laminar and turbulent flow regimes during molasses filtration.

5.3.3. Membrane Pore Size

The 0.5 µm, 0.9 µm and 1.5 µm Ps*f* membranes were fouled by filtering a 45 ºBrix molasses solution, at 3.0 bar TMP, CFV of 1.89 ms^{-1} at a temperature of 60 ºC for 90 min where standard rinsing and cleaning conditions were used. The steady state flux values for the three membranes can be seen in Figure 5.17, comparing the different molasses concentrations. The 0.5 µm membranes produced a fouling flux of 35 (± 2) L m^{-2} hr^{-1}. The 0.9 µm produced a similar fouling flux of 39 ((± 2) L m^{-2} hr^{-1}. Nordzucker (2008) reported that the crystals in the molasses are *ca.* 1 – 6 µm wide and 5 – 20 µm long. These crystal sizes caused the filtration of the molasses to be unpractical with the two smaller pore size membranes. The 1.5 µm Ps*f* membranes were the preferred membranes for this study with fouling fluxes of an average of 63 (± 3) L m^{-2} hr^{-1} and acceptable solids removal.

Figure 5.18 shows a breakdown of the different resistive layers present at steady state versus molasses concentration. The total resistance increased as the membrane pore sizes decreased, responsible for this was the extra resistances, that of concentration polarisation and irreversible fouling (R_{cp} and R_I). The R_{cp} decreased dramatically from 2.00 x 10^{13} m^{-1} for the 0.5 µm Ps*f* 45 ºBrix fouled membrane to 5.53 x 10^{12} m^{-1} for the

1.5 µm 45 ºBrix fouled Ps*f* membrane. The R_I decreased somewhat from 7.20 x 10^{12} m^{-1} for the 0.5 µm Ps*f* 45 ºBrix fouled membrane to 4.74 x 10^{12} m^{-1} for the 1.5 µm 45 ºBrix fouled Ps*f* membrane. The amount of rinsable fouling also decreased slightly from 2.27 x 10^{12} m^{-1} for the 0.5 µm Ps*f* 45 ºBrix fouled membrane to 1.26 x 10^{12} m^{-1} for the 1.5 µm 45 ºBrix fouled Ps*f* membrane. However, the R_R accounted for 11 % of the total resistance for the 1.5 µm membrane compared to 8 % for the 0.5 µm membrane. Figure 5.19 shows that for all membranes tested the membrane resistance after fouling and cleaning increased as molasses concentration increased. The 0.5 µm membrane had the most resistance after cleaning, which is expected as more in-pore fouling occurs in the smaller pore membranes. This shows that the cleaning regime performed (0.25 wt. % NaOH, 1.0 bar, 1.89 ms^{-1} and 50 ºC) on the 0.5 µm and 0.9 µm membranes are not removing enough of the fouling material. Figure 5.20 shows the apparent solids rejection data as a function of fouling concentration for the 0.5 µm, 0.9 µm, and 1.5 µm Ps*f* membranes. The apparent rejection increased with increasing concentration and decreasing pore size. Increasing the pore size from 0.5 to 1.5 µm decreased the rejection from 0.26 to 0.22 (15 ºBrix) and 0.40 to 0.28 (45 ºBrix) respectively. This was probably due to the smaller pores causing more in-pore and surface fouling causing fewer solids to be able to pass through the membrane.

The fouling flux and R_a data was then used to gather further mass transfer information (Figure 5.21). The mass transfer information for the three membranes was gathered using Equations 4.1 to 4.7; using the concentration variation method. Here, the concentration of molasses was varied at constant CFV, temperature and TMP (1.98 ms^{-1} 60 ºC, and 3.0 bar). Extrapolation of the y-axis of the lines connecting the flux rejection data can be seen. The following y-axis intercepts (-1.23 (0.5 µm), -0.34 (0.9 µm), -0.17 (1.5 µm)) correspond to true (actual) rejection coefficients of approximately 0.77 (0.5 µm), 0.58 (0.9 µm) and 0.53 (1.5 µm). The gradients of the lines in Figure 5.21 have been used to calculate the mass transfer coefficients. The 0.5 µm membrane produced a mass transfer coefficient of 5.81 x 10^{-6} ms^{-1}. As the membrane pore size increased to 0.9 µm the mass transfer increased to 1.12 x 10^{-5} ms^{-1}. This was further increased to 1.63 x 10^{-5} ms^{-1} for the 1.5 µm membrane. The 1.5 µm membrane was the preferred choice in this study in terms of separation performance.

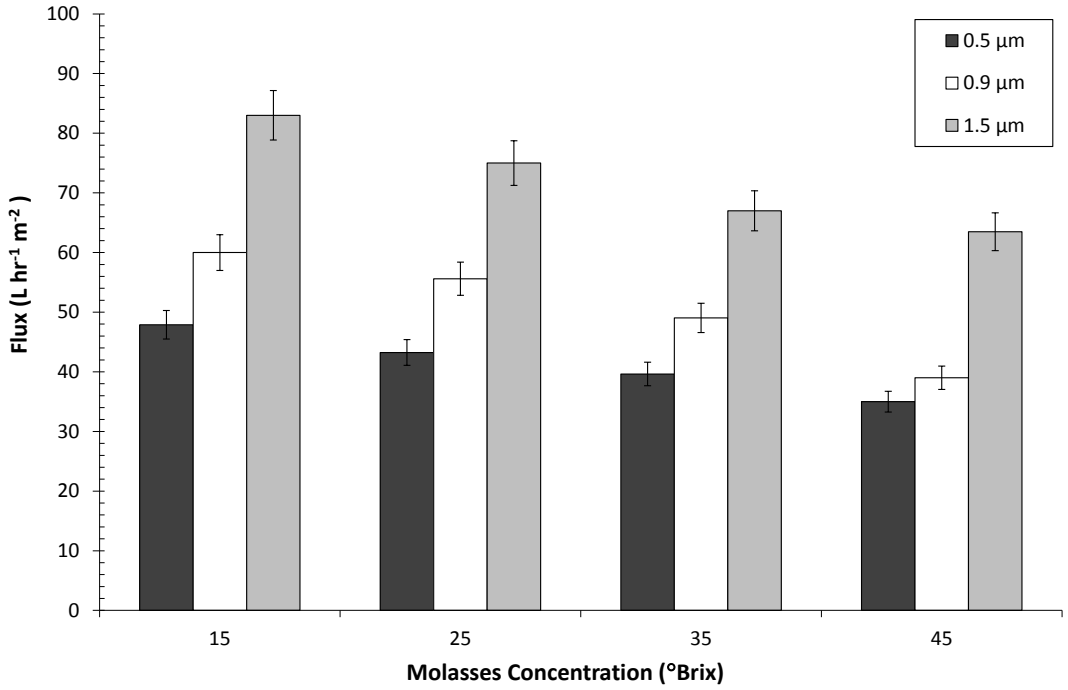

Figure 5.17: Graph to show fouling flux data as a function of fouling concentration on 0.5 µm, 0.9 µm and 1.5 µm Ps*f* membranes when fouled with molasses (60 ºC, 3.0 bar TMP, 1.89 ms^{-1} CFV) for 90 min.

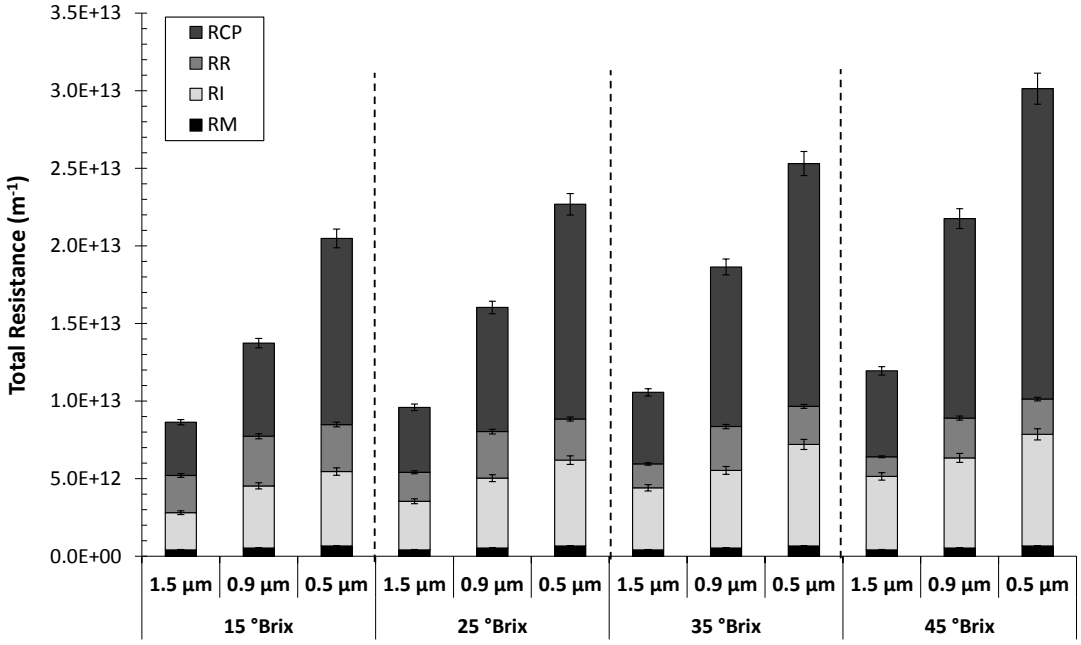

Figure 5.18: Graph to show fouling resistance data as a function of fouling concentration on 0.5 µm, 0.9 µm, and 1.5 µm Ps*f* membranes when fouled with molasses (60 ºC, 3.0 bar TMP, 1.89 ms^{-1} CFV) for 90 min.

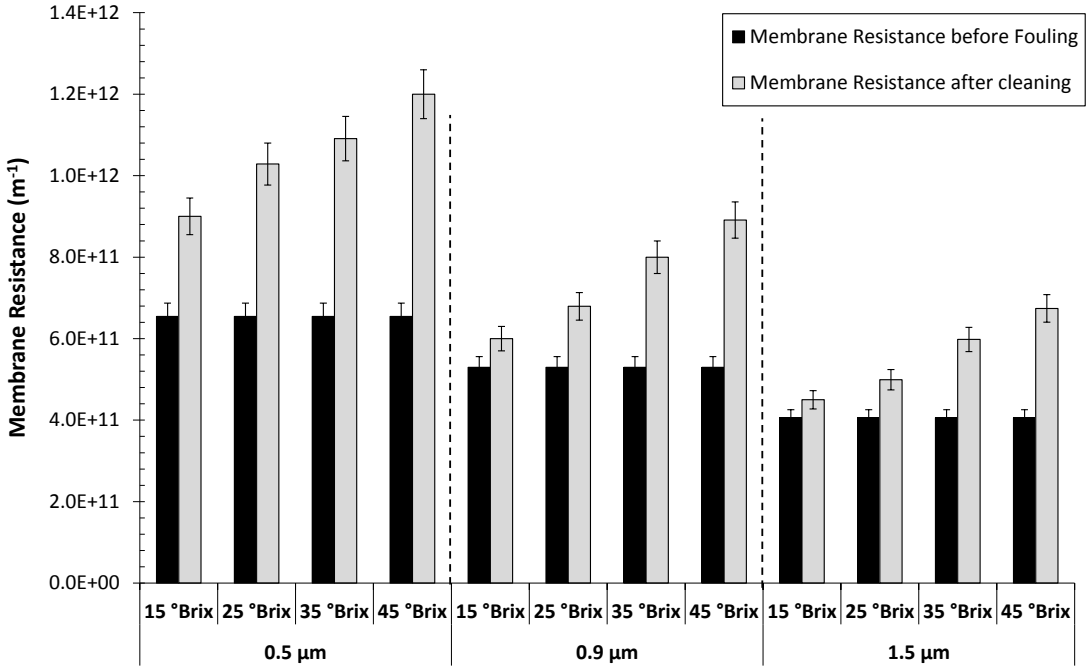

Figure 5.19: Graph to show pure water membrane resistances after cleaning vs. fouling concentration variation on 0.5 µm, 0.9 µm, and 1.5 µm Ps*f* membranes when fouled with molasses (60 ºC, 3.0 bar TMP, 1.89 ms^{-1} CFV) for 90 min.

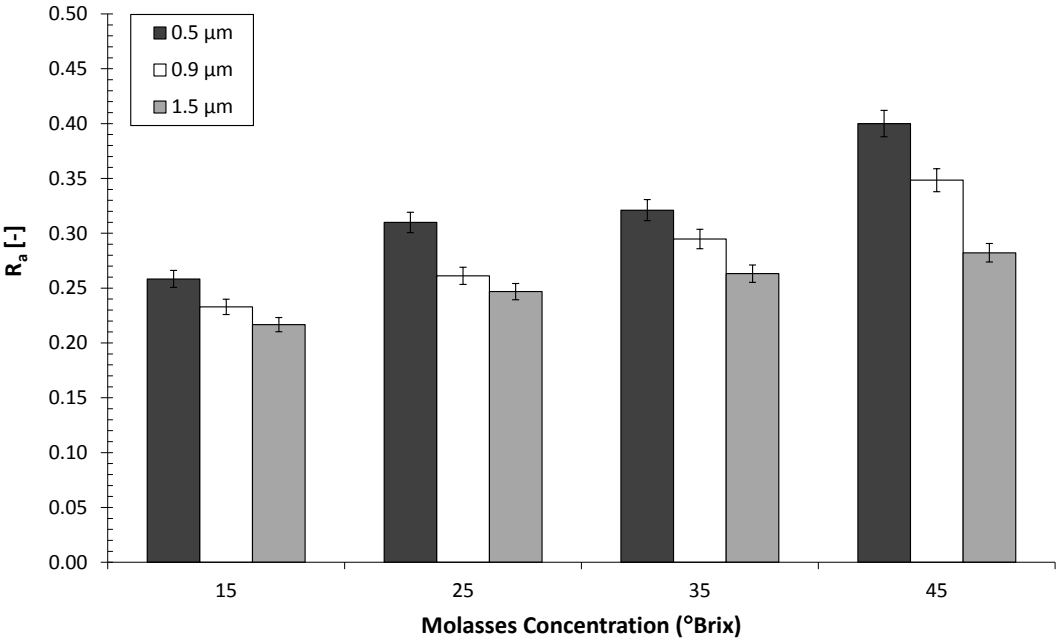

Figure 5.20: Graph to show the apparent rejection coefficient on 0.5 µm, 0.9 µm and 1.5 µm Ps*f* membranes when fouled with molasses (60 ºC) at different molasses concentrations for 90 min.

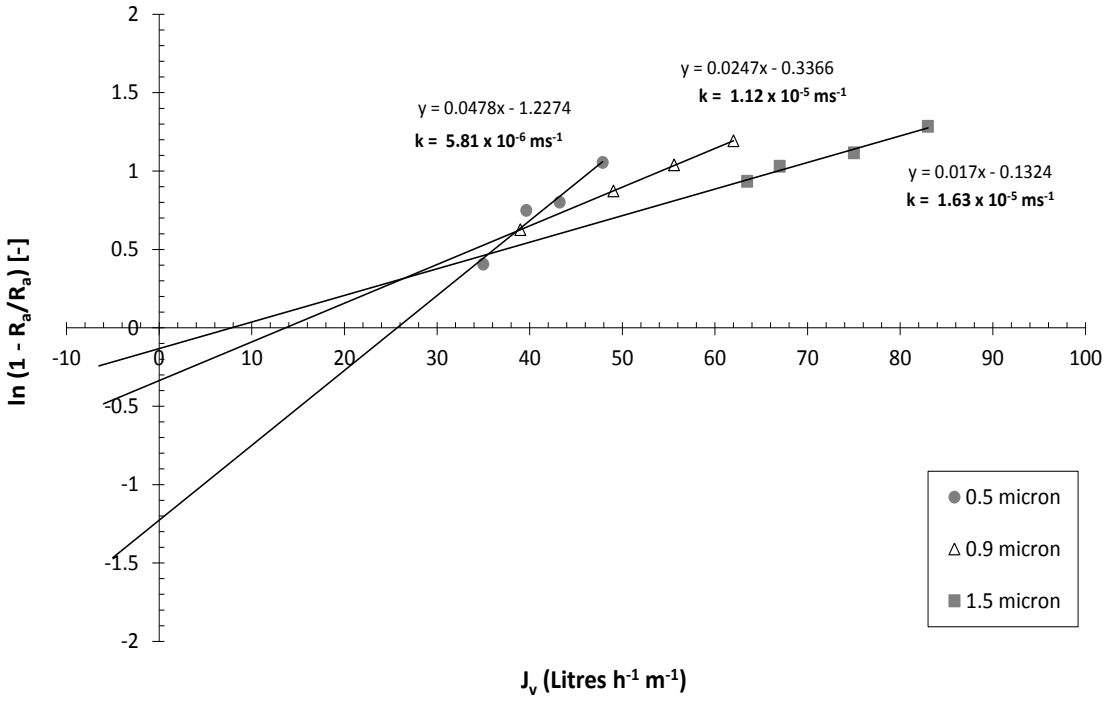

Figure 5.21: Linearised plot of the concentration polarisation equation for various membrane pore sizes with trend lines extrapolated to meet the y-axis. Constant: 60 ºC, 3.0 bar TMP, 1.89 ms^{-1} CFV. Varied concentration: 15, 25, 35, 45 ºBrix.

5.4. Microfiltration of Molasses - Cleaning Conditions Optimisation

The 1.5 µm Ps*f* membranes were fouled by filtering a 45 ºBrix molasses solution under the same operating conditions (60 ºC, 3.0 bar, 1.89 ms^{-1}). For all cleaning experiments the molasses feed was filtered until it reached the same normalised steady state flux (Error ± 6 %). The steady state flux was approximately 7 % of the initial flux value. The rinsing stage before cleaning was performed at 22 ºC, 1.0 bar TMP, and 1.89 ms^{-1} CFV for 15 min; this removed the majority of the loosely bound particulates. As molasses is a complex solution it was required to be cleaned with an acid and alkali solution (citric acid and NaOH).

5.4.1. Effect of Cleaning Operating Conditions

The cleaning conditions were optimised by varying concentration, TMP and temperature. The cleaning efficiency was evaluated by the ratio of the pure water flux after cleaning (J_c) to the pure water flux measured before fouling (J_w) for each cleaning stage. The percentage flux recovery ($\%J_r$) was calculated using Equation 4.7. The cleaning process was investigated in two stages. The first stage was to optimise the cleaning in terms of operating conditions and chemical sequences. The second stage

was to use Fluid Dynamic Gauging (FDG) to track the thickness of the cake layer during fouling and its removal rate during cleaning, as an aid to understanding removal mechanisms (results in Chapter 6.3.5).

5.4.1.1. Cleaning Agent Concentration

The acid (citric acid) and alkali (NaOH) concentration was varied whilst maintaining a constant TMP of 1.0 bar, CFV of 1.89 ms^{-1}, and temperature of 50 ºC for 30 min. Three concentrations were chosen; 0.10 wt. %, 0.25 wt. % and 0.50 wt. %. Figure 5.22 compares the flux data for citric acid and NaOH concentration variation on Ps*f* membranes. It shows the first, last and average flux values in the cleaning section of the cycle. The concentration polarisation layer was removed first followed by swelling of the fouling deposits. According to Nigam *et al*. (2008) this swelling of the fouling deposits due to the cleaning solution diffusing into the deposit matrix and controls the cleaning process. The swelling causes disruptions of the chemical linkages leading to the movement of the deposit particles away from the membrane into the bulk stream. Swelling of the membrane can also occur at the higher concentrations resulting in compression of any remaining cake layer (decreased cake porosity) on the membrane surface (Madaeni *et al*., 2009). The rinsing after cleaning increased the permeate fluxes by the removal of soluble material or desorption of foulants (Bartlett *et al*., 1995; Popović *et al*., 2009). This is reflected in the PWF after fouling and cleaning in Figure 5.23. Figure 5.23 also shows the effect of citric acid and NaOH concentration on the product (fouling) flux after the first cycle of fouling and cleaning. It compares the PWF after cycle 1 to the fouling, cleaning and PWF after cycle 2. The variation of cleaning concentration did have an effect on the fouling fluxes in the 2nd cycle. The increased concentration of 0.50 wt. % for both citric acid and NaOH decreased the fouling fluxes by 28 % (acid) and 40 % (alkali) respectively from the 0.25 wt. % cleaned membranes. The highest PWFs after 2 cycles was 0.10 wt. % for the citric acid cleaned Ps*f* membrane (455 L m^{-2} hr^{-1}), whereas the middle concentration of 0.25 wt. % was superior for the NaOH cleaned Ps*f* membrane (468 L m^{-2} hr^{-1}).

Figure 5.24 shows the effect of citric acid and NaOH concentration on the PWF recovery after fouling and cleaning for two cycles. Cleaning with water only was shown to be insufficient for a realistic PWF recovery. Water achieved a PWF recovery of only

14 %. The lowest concentration of citric acid tested (0.10 wt. %) recovered the greatest PWF recovery of 52 % after cycle 1, although this value was not statistically different from the other recovery values recorded for 0.25 and 0.50 wt. %. After cycle 2 the differences were more noticeable, with 0.10 wt. % recovering 51 % of PWF. The optimal concentration of NaOH was inconclusive after cycle 2; the PWF recoveries were all similar for the concentrations tested. It would therefore be more practical to use the lower concentrations of 0.10 wt. % or 0.25 wt. %. The increasing concentration of the acid and alkali solutions could have caused the lower flux recovery by; (i) the enhancement in the swelling of the fouling deposits which block the pores and seal the membrane surface and/or (ii) the lower concentrations ability to keep the pores relatively unplugged whereas a chemical induced gelation could have happened when the higher cleaning solution was introduced (Bartlett *et al*., 1995; Nigam *et al*., 2008).

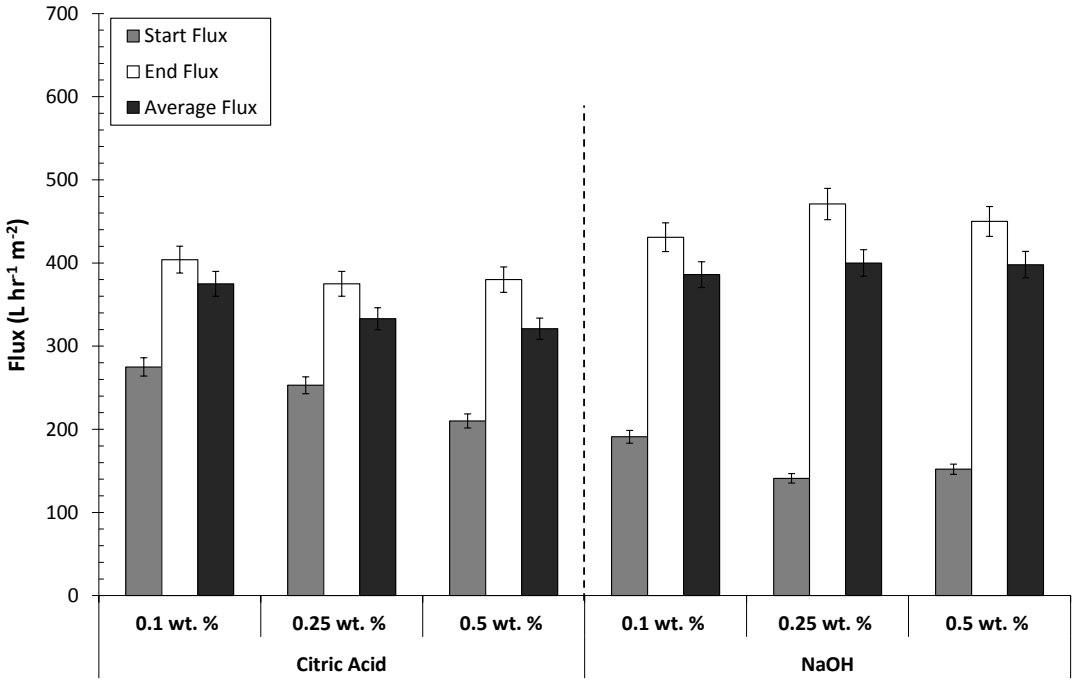

Figure 5.22: Graph to show citric acid and NaOH cleaning fluxes as a function of cleaning concentration variation on 1.5 µm Ps*f* membranes when fouled with molasses (3.0 bar, 60 ºC, 1.89 ms^{-1}) for 90 min. All cleaning conditions maintained at 1.0 bar TMP, 1.89 ms^{-1} and 50 ºC.

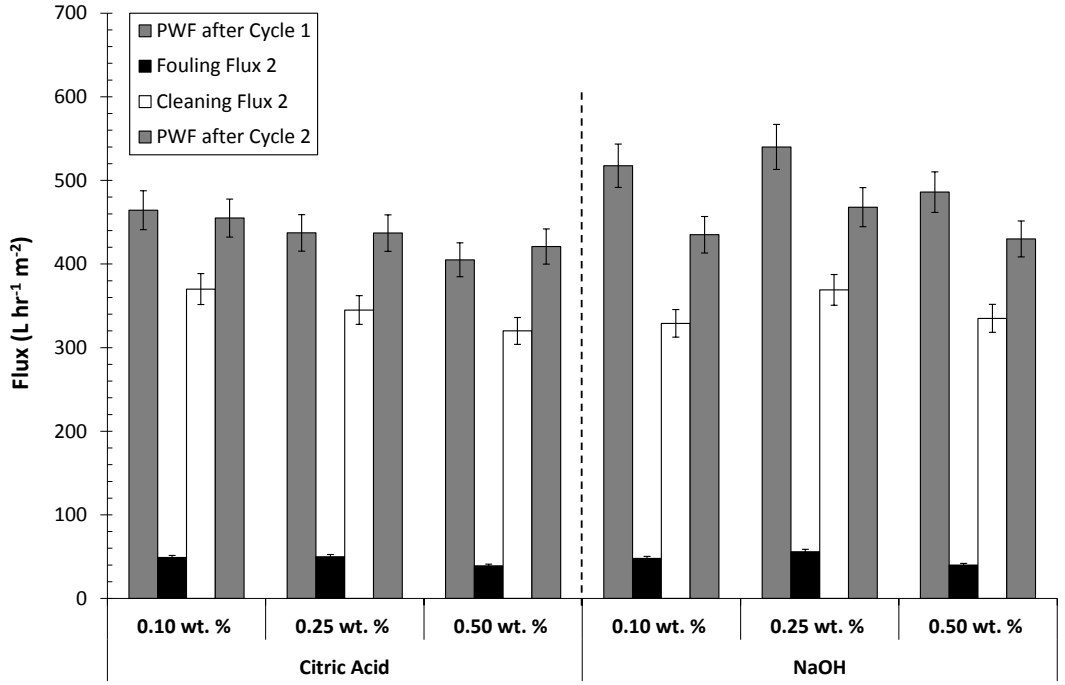

Figure 5.23: Graph to show the PWFs, fouling fluxes and cleaning fluxes for twice fouled membranes vs. cleaning concentration variation on 1.5 µm Ps*f* membranes when fouled with molasses (3.0 bar TMP, 60 ºC, 1.89 ms^{-1}) for 90 min. All cleaning conditions maintained at 1.0 bar TMP, 1.89 ms^{-1} and 50 ºC.

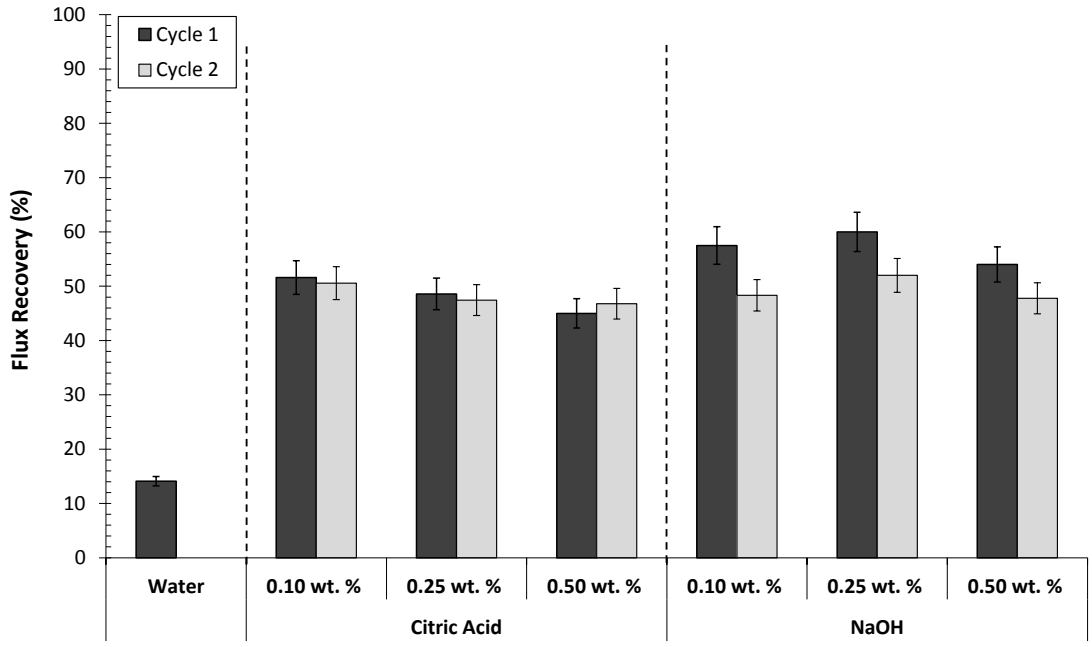

Figure 5.24: Graph to show PWF recovery as a function of cleaning concentration variation on 1.5 µm Ps*f* membranes when fouled with molasses (3.0 bar TMP, 60 ºC, 1.89 ms^{-1} CFV, 45 °Brix) for 90 min. All cleaning conditions maintained at 1 bar TMP, 1.89 ms^{-1} and 50 ºC.

5.4.1.2. Transmembrane Pressure

The TMP was varied while maintaining a constant citric acid and NaOH concentration of 0.25 wt. %, CFV of 1.89 ms^{-1}, and temperature of 50 ºC for 30 min. The TMP pressures tested were 0.5, 1.0 and 2.0 bar. Figure 5.25 compares the flux data for cleaning TMP variation on Ps*f* membranes. It shows the first, last and average flux values in the cleaning section of the cycle. The marginally better cleaning flux for citric acid was 0.5 bar, whereas cleaning with NaOH at 1.0 bar was vastly superior. Figure 5.26 shows the effect of TMP on the product (fouling) flux after the first cycle of fouling and cleaning. It compares the PWF after cycle 1 to the fouling, cleaning and PWF after cycle 2. The fouling fluxes after cleaning were lower when cleaning with either chemical at 2.0 bar. The highest PWFs after 2 cycles was 1.0 bar for the citric acid cleaned membrane (427 L m^{-2} hr^{-1}), and 1.0 bar for the NaOH cleaned membrane (468 L m^{-2} hr^{-1}).

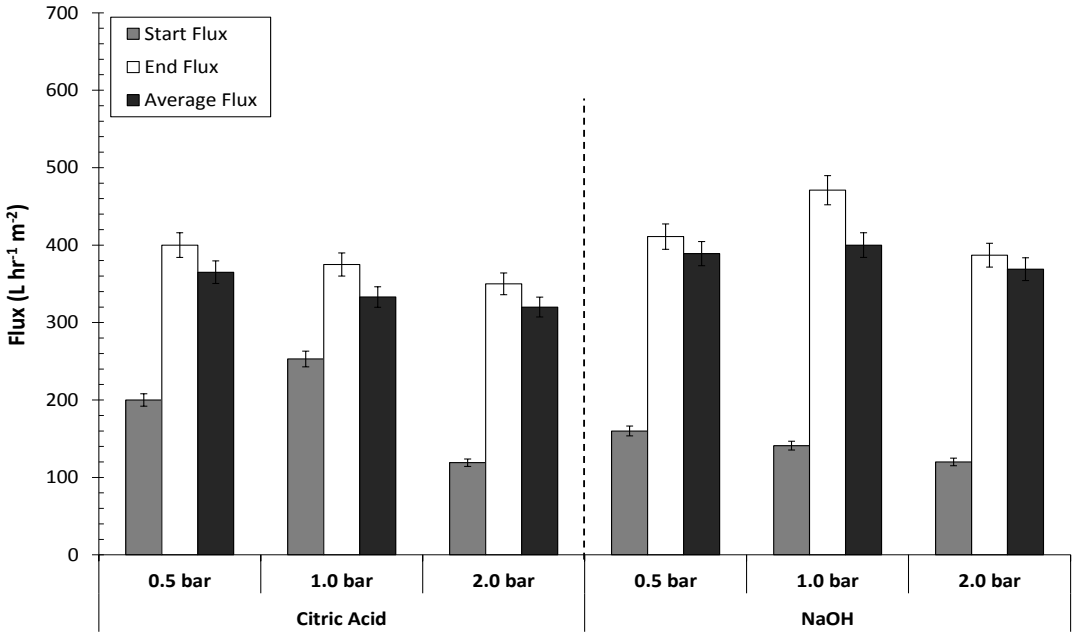

Figure 5.25: Graph to show citric acid and NaOH cleaning flux as a function of cleaning TMP variation on 1.5 µm Ps*f* membranes when fouled with molasses (3.0 bar, 60 ºC, 1.89 ms^{-1}) for 90 min. All cleaning conditions maintained at 0.25 wt. %, 1.89 ms^{-1} and 50 ºC.

Figure 5.27 shows the effect of TMP variation on the PWF recovery after fouling and cleaning for two cycles. The optimal TMP after one cycle for PWF recovery after NaOH cleaning was 1.0 bar with a flux recovery of 60 % compared to 54 % (0.5 bar) and 50 % (2.0 bar). The trend was identical for citric acid cleaning with an increased flux recovery of 49 % (1.0 bar) compared to 48 % (0.5 bar) and 44 % (2.0 bar).When

operating at too low a pressure, not enough force is generated for effective separation whereas too high a pressure can cause compaction of the membrane (Jönsson and Trägårdh, 1990), this is the most likely reason why 1.0 bar is the optimal pressure for this process.

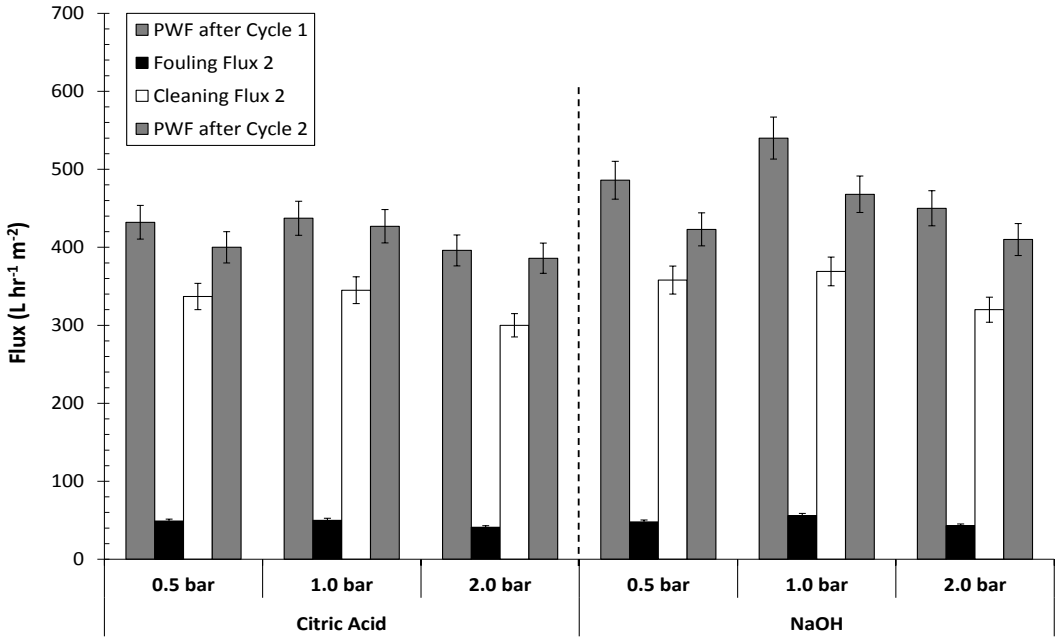

Figure 5.26: Graph to show the PWFs, fouling fluxes and cleaning fluxes for twice fouled membranes vs. cleaning TMP variation on 1.5 µm Ps*f* membranes when fouled with molasses (3.0 bar TMP, 60 ºC, 1.89 ms^{-1}) for 90 min. All cleaning conditions maintained at 0.25 wt. %, 1.89 ms^{-1} and 50 ºC.

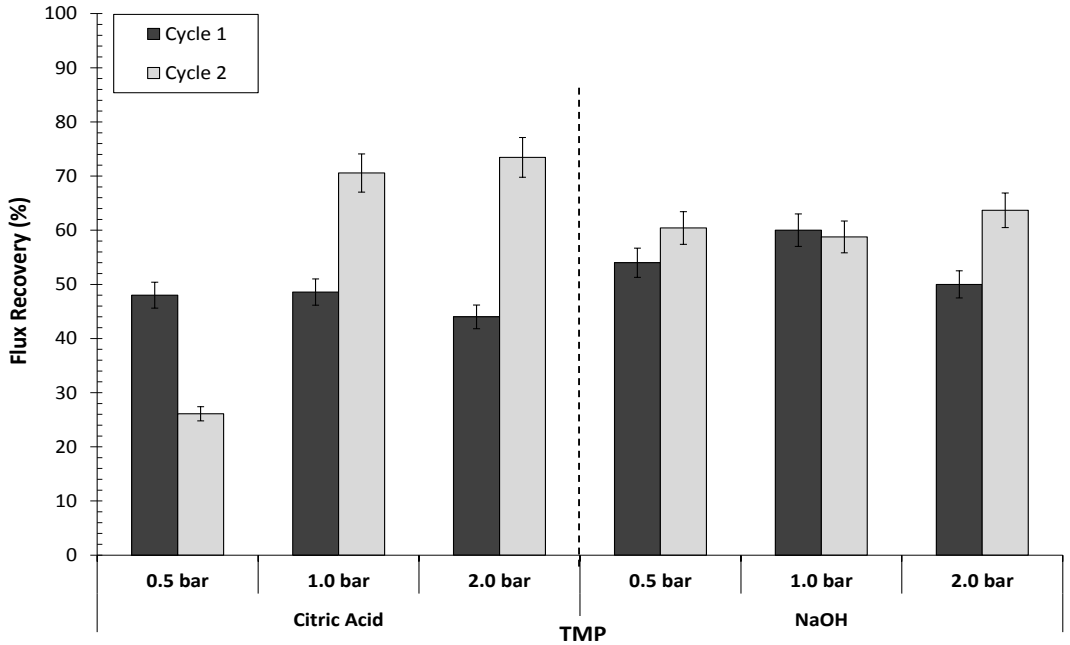

Figure 5.27: Graph to show PWF recovery as a function of cleaning TMP variation on 1.5 µm Ps*f* membranes when fouled with molasses (3.0 bar TMP, 60 ºC, 1.89 ms^{-1} CFV, 45 ºBrix) for 90 min. All cleaning conditions maintained at 0.25 wt. %, 1.89 ms^{-1} and 50 ºC.

5.4.1.3. Temperature

The temperature was varied while maintaining a constant citric acid and NaOH concentration of 0.25 wt. %, CFV of 1.89 ms^{-1}, with a TMP of 1.0 bar for 30 min. Figure 5.28 compares the flux data for cleaning temperature variation on Ps*f* membranes. It shows the first, last and average flux values in the cleaning section of the cycle. Three cleaning temperatures were chosen, 22 ºC, 50 ºC and 60 ºC. Previous work at Bath University (Weis *et al*., 2003; Evans and Bird, 2006) found that 50 ºC is the ideal temperature for cleaning membranes fouled with a wide range of food and bioproducts. The lower and higher temperatures were thus selected to facilitate a meaningful comparison. The cleaning fluxes increased with increasing temperature fairly dramatically from 22 ºC to 50 ºC. This was probably due to decreased viscosity, improved diffusion, increased solubility of both the cleaning agent and foulants and increased reaction rates of the cleaning agent when the temperature was raised. Madaeni *et al*. (2009) found that both the rate of chemical agent with the deposited foulant and the diffusive transport of the foulants from the fouling layer to the bulk solution were proportional to temperature. That at higher temperatures the swelling of the gel layer might have contributed to weaken its structural stability. Shorrock and Bird (1998) hypothesised that it was more likely thermal energy, rather than kinetic energy responsible for the increased deposit removal at the higher temperature.

Figure 5.29 shows the effect of temperature on the product (fouling) flux after the first cycle of fouling and cleaning. It compares the PWF after cycle 1 to the fouling, cleaning and PWF after cycle 2. The fouling fluxes after cleaning at 22 ºC with both the acid and alkali were greatly reduced. The 22 ºC acid cleaned membrane fouling flux reduced by 63 % from the 1st cycle (alkali: 59 % reduction). The 50 ºC and 60 ºC fouling fluxes only decreased slightly. At 22 ºC the flux recovery after cycle 1 for the Ps*f* membrane was only 28 % (acid) and 31 % (alkali) respectively (Figure 5.30). The results obtained for temperatures 50 ºC and 60 ºC were similar; it is therefore preferable to use the lower temperature of 50 ºC for all further cleaning experiments with molasses.

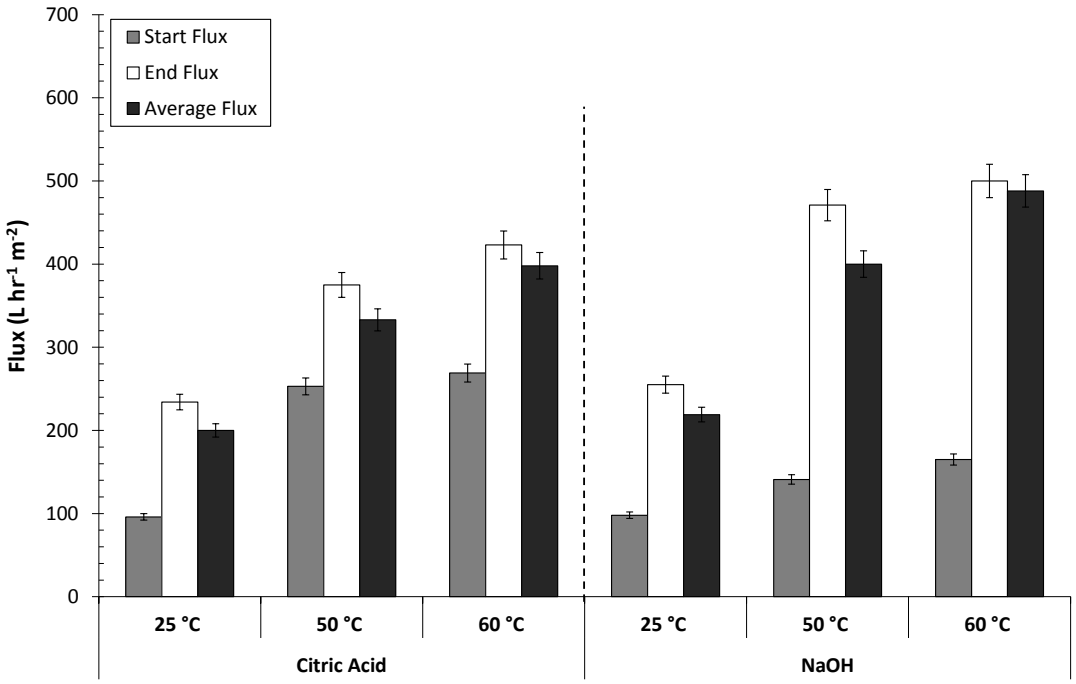

Figure 5.28: Graph to show citric acid and NaOH cleaning flux as a function of cleaning temperature variation on 1.5 µm Ps*f* membranes when fouled with molasses (60 ºC, 3.0 bar, 1.89 ms^{-1}) for 90 min. All cleaning conditions maintained at 0.25 wt. %, 1.89 ms^{-1} and 1.0 bar TMP.

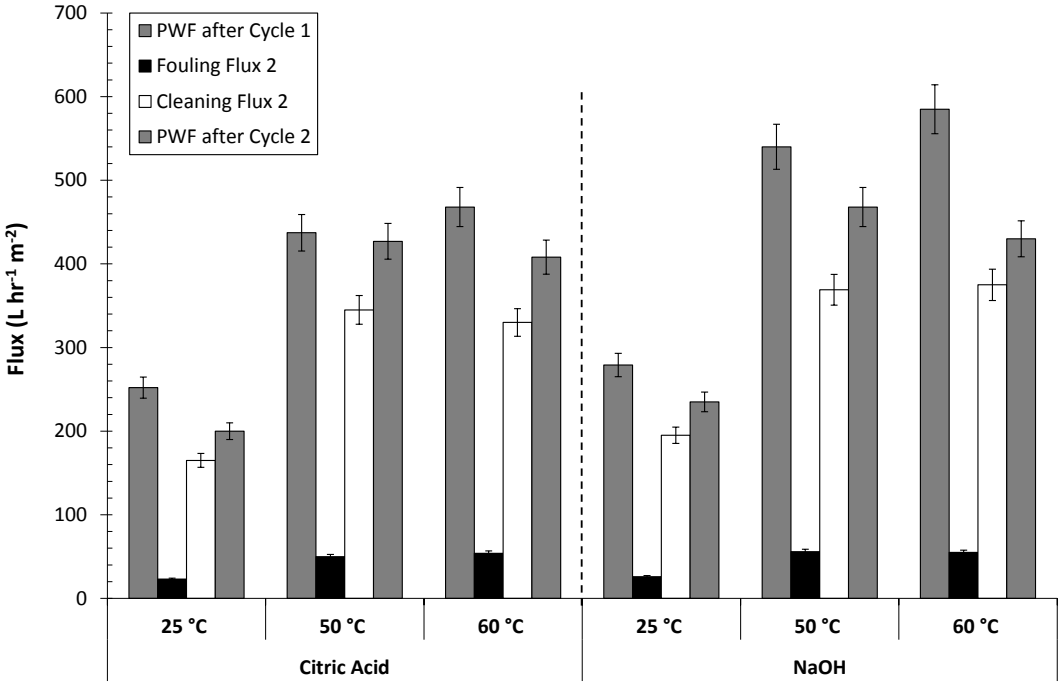

Figure 5.29: Graph to show the PWFs, fouling fluxes and cleaning fluxes for twice fouled membranes vs. cleaning temperature variation on 1.5 µm Ps*f* membranes when fouled with molasses (3.0 bar TMP, 60 ºC, 1.89 ms^{-1}) for 90 min. All cleaning conditions maintained at 0.25 wt. %, 1.89 ms^{-1} and 1.0 bar TMP.

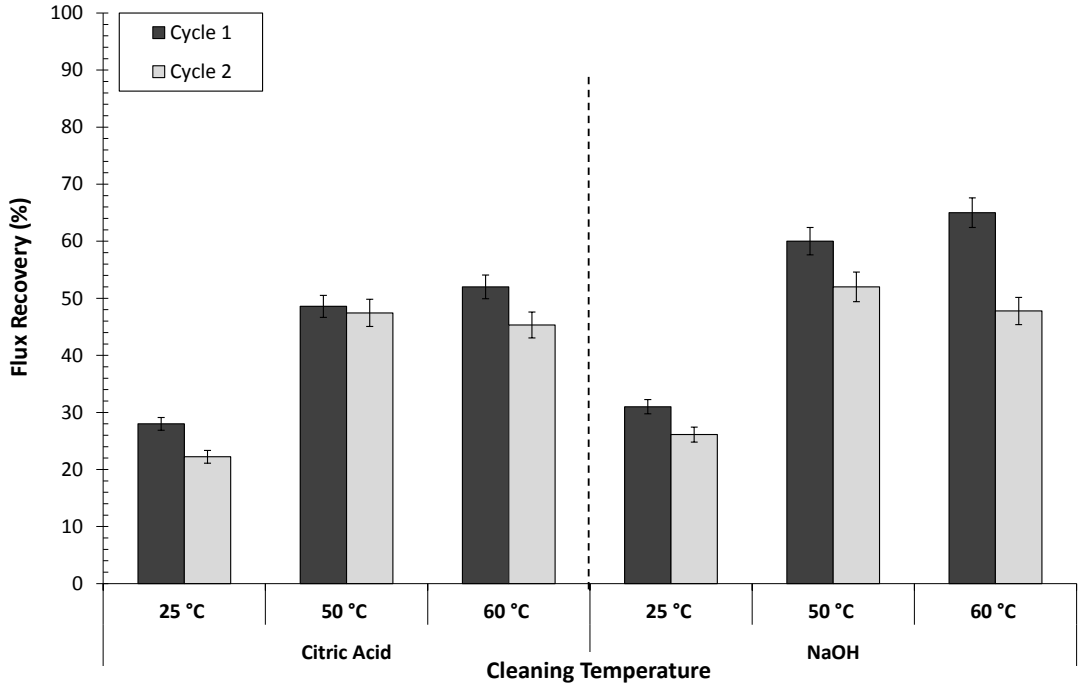

Table 5.30: Graph to show PWF flux recovery as a function of cleaning temperature variation on 1.5 µm Ps*f* membranes when fouled with molasses (60 ºC, 3.0 bar TMP, 1.89 ms^{-1}, 45 °Brix) for 90 min. Constant acid and alkali concentration of 0.25 wt. %, 1.89 ms^{-1}, 1.0 bar for 30 min.

5.4.2. Efficiency of Acid/Alkali Cleaning Sequences

The molasses fouled membranes required cleaning by both acid and alkali. The sequence of which is performed is important to the overall flux recovery. The sequence of applying the various cleaning agents has been investigated and discussed for different feeds by previous authors (Liu *et al*., 2000; Chen *et al.,* 2003). Most cleaning regimes consist of an alkali step followed by an acid step (D'Souza and Mawson, 2005). However, in some cases an acid solution has been recommended as the first step, particularly where mineral fouling may be more important (Trägårdh, 1989; Daufin *et al*., 1991). It is also common to follow an alkali then acid step with a second alkaline clean to make it a three stage cleaning process. Trägårdh (1989) found that this second alkali clean improved the flux recovery further. In the current study, twelve treatment protocols were evaluated, comprising of (i) alkali then acid, (ii) acid then alkali and (iii) alkali / acid / alkali steps. Concentrations of 0.10 wt. % and 0.25 wt. % were tested for both NaOH and citric acid cleaning agents. Table 5.1 shows the twelve different cleaning sequences that were tested and the relevant flux recoveries at each cleaning stage.

Figure 5.31 to 5.33 displays the cleaning flux recovery during cleaning for each cleaning stage. A similar trend is seen for all cleaning stages except when cleaning with a lower concentration of citric acid after a higher concentration of cleaning solution. An initial increase and subsequent reduction in flux during chemical cleaning was seen for both acid and alkali treatments. This supports previous membrane cleaning findings for the removal of food based foulants based on the simultaneous removal of the cake and the swelling of in-pore bound deposition (Bird and Bartlett, 2002). Figure 5.34 shows the final PWF recovery at the end of the cleaning cycle. The noticeable differences are the first band of treatments (T1 to T4) which are cleaned with NaOH followed by citric acid and results in the highest amount of PWF recovery (77 % to 89 %). Interestingly the two treatments (T1 and T3) with the lower concentration of acid (0.1 wt. %) yielded the highest flux recovery. The addition of a subsequent alkali cleaning step, in T9 to T12, resulted in a reduction in the flux obtained and is therefore not preferred.

Table 5.1: Details the cleaning sequences and the relevant flux recoveries

Treatment Number	NaOH (wt. %)	Recovery (%)	Citric Acid (wt. %)	Recovery (%)	NaOH (wt. %)	Recovery (%)	End Recovery (%)	PWF Recovery (%)
T1	0.10	59	0.10	85			85	86
T2	0.25	58	0.25	77			77	77
T3	0.25	60	0.10	83			83	89
T4	0.10	56	0.25	83			83	80
T5			0.10	51	0.10	73	73	69
T6			0.25	50	0.25	79	79	76
T7			0.25	48	0.10	70	70	68
T8			0.10	52	0.25	76	76	69
T9	0.10	59	0.10	85	0.10	65	65	67
T10	0.25	60	0.10	83	0.25	57	57	60
T11	0.10	56	0.25	83	0.10	67	67	67
T12	0.25	58	0.25	77	0.25	62	62	66

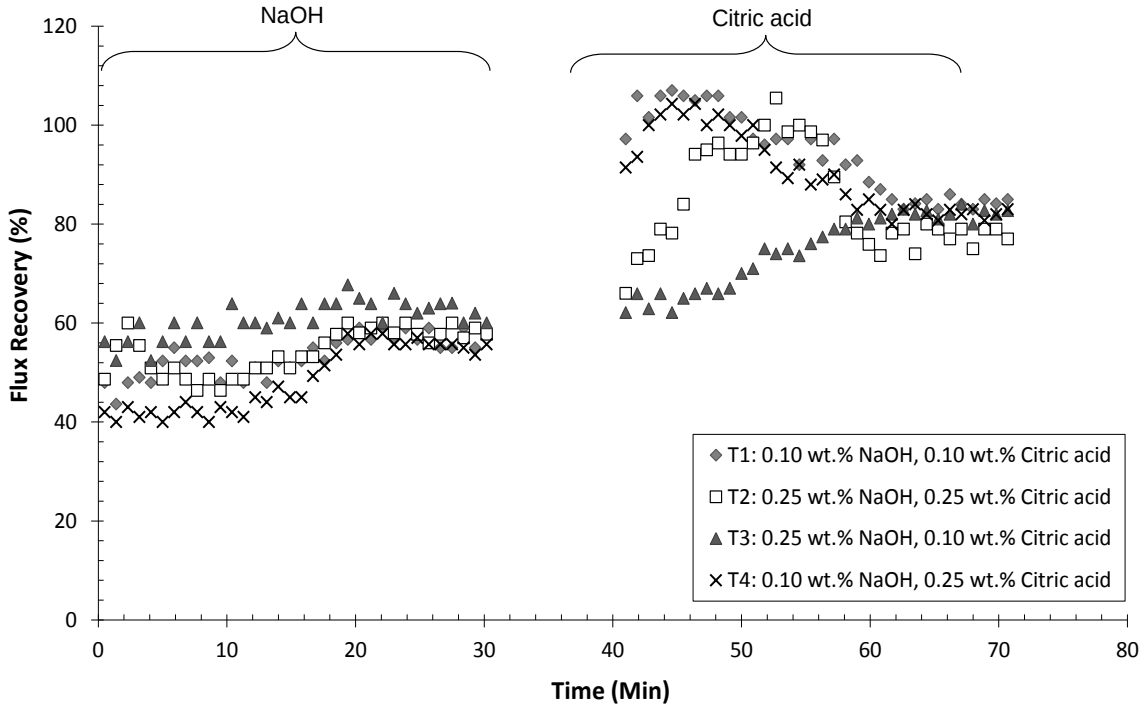

Figure 5.31: Graph to show the effect of acid and alkali cleaning sequences on the cleaning flux recovery after fouling with molasses (60 ºC, 3.0 bar TMP, 1.89 ms^{-1}, 45 ºBrix) for 90 min. Constant acid and alkali conditions of 50 ºC, 1.89 ms^{-1}, 1.0 bar for 30 min.

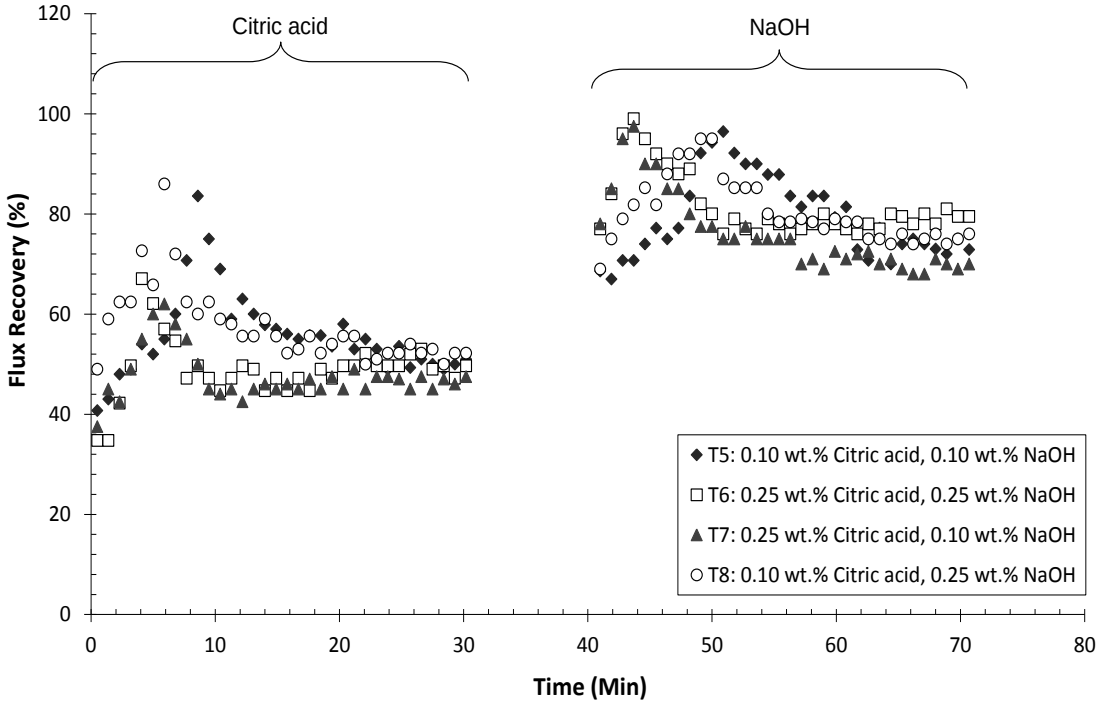

Figure 5.32: Graph to show the effect of acid and alkali cleaning sequences on the cleaning flux recovery after fouling with molasses (60 ºC, 3.0 bar TMP, 1.89 ms^{-1}, 45 ºBrix) for 90 min. Constant acid and alkali conditions of 50 ºC, 1.89 ms^{-1}, 1.0 bar for 30 min.

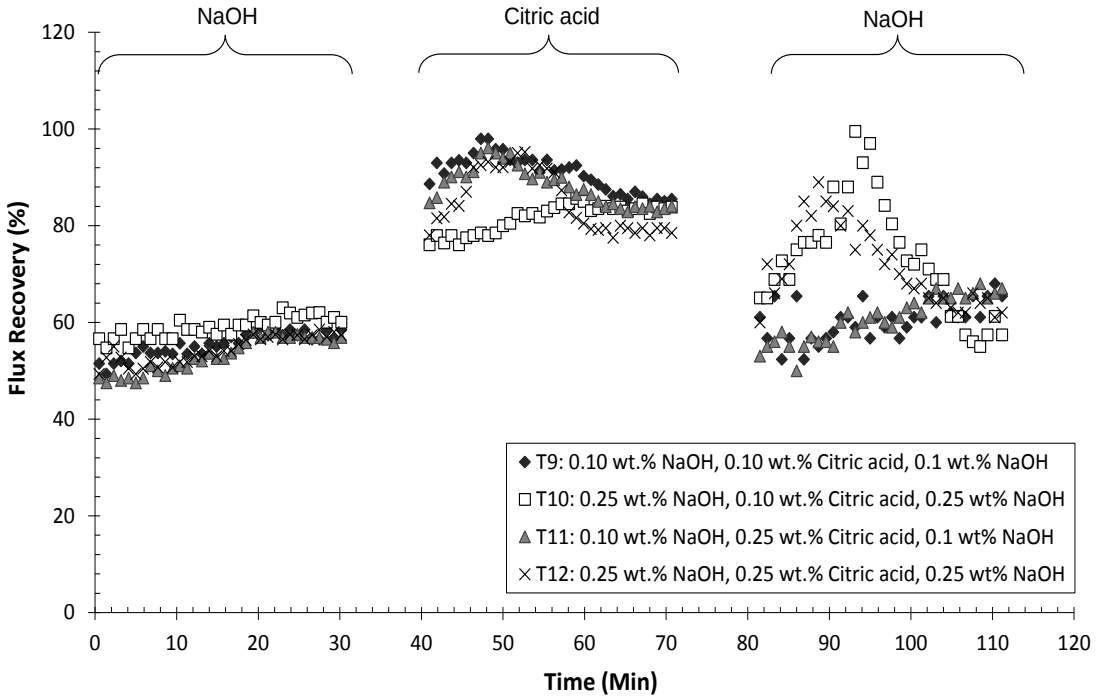

Figure 5.33: Graph to show the effect of acid and alkali cleaning sequences on the cleaning flux recovery after fouling with molasses (60 ºC, 3.0 bar TMP, 1.89 ms^{-1}, 45 ºBrix) for 90 min. Constant acid and alkali conditions of 50 ºC, 1.89 ms^{-1}, 1.0 bar for 30 min.

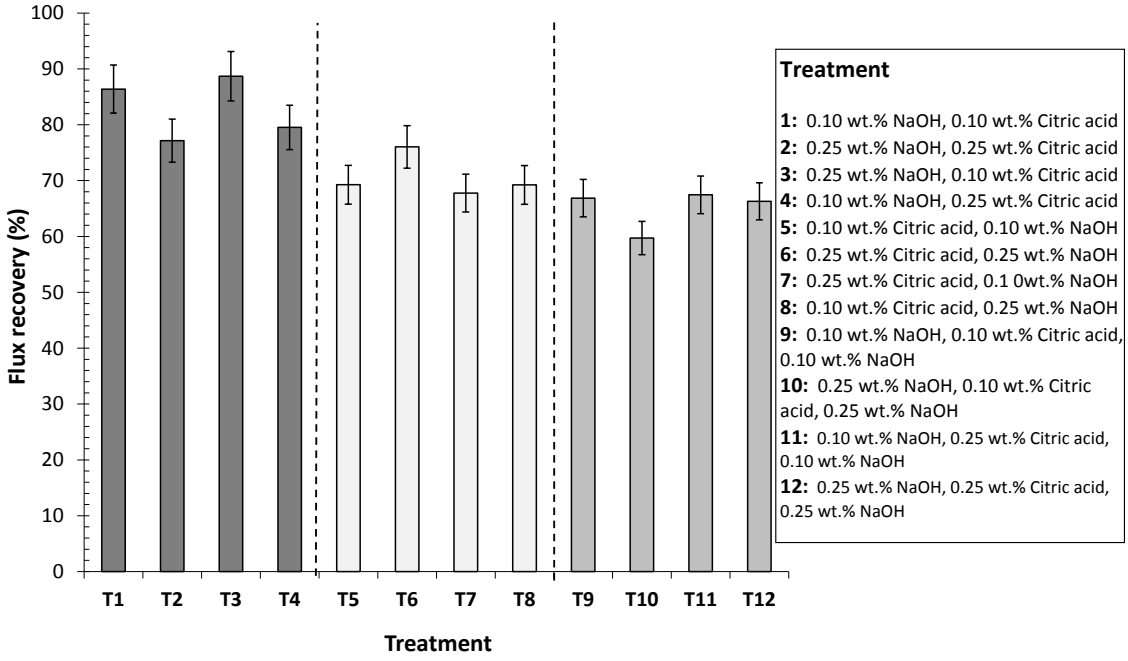

Figure 5.34: Graph to show the effect of acid and alkali cleaning sequences on the PWF flux recovery after fouling and cleaning when fouled with molasses (60 ºC, 3.0 bar TMP, 1.89 ms^{-1}, 45 ºBrix) for 90 min. Constant acid and alkali conditions of 50 ºC, 1.89 ms^{-1}, 1.0 bar for 30 min.

5.5. Optimal Molasses Fouling and Cleaning Filtration Conditions

The fouling conditions have been optimised by varying concentration, CFV, TMP and temperature. The optimised conditions were a TMP of 3.0 bar, a CFV of 1.89 ms^{-1} and a temperature of 60 ºC for 90 min. The reason a CFV of 1.89 ms^{-1} was chosen was because operating at any higher CFV can cause instability of the fouling and cleaning rig. The standard rinsing and cleaning conditions were also optimised. A summary of all the conditions can be found in Table 5.2. These conditions were used for all other experiments concerning the filtration of molasses.

Table 5.2: Summary of the filtration cycle conditions

Stage	Fluid	Protocol
Conditioning	Reverse osmosis water	60 ºC, 120 min, 1.0 bar, 1.89 ms^{-1}
PWF measurements	Reverse osmosis water	22 ºC, 10 min, 1.0 bar, 1.89 ms^{-1}
Fouling	Molasses	60 ºC, 90 min, 3.0 bar, 1.89 ms^{-1}
PWF after fouling	Reverse osmosis water	22 ºC, 10 min, 1.0 bar, 1.89 ms^{-1}
Rinsing	Reverse osmosis water	22 ºC, 15 min, 1.0 bar, 1.89 ms^{-1}
PWF after rinsing	Reverse osmosis water	22 ºC, 10 min, 1.0 bar, 1.89 ms^{-1}
Cleaning stage 1	NaOH (0.25 wt. %)	50 ºC, 30 min, 1.0 bar, 1.89 ms^{-1}
Cleaning stage 2	Citric Acid (0.10 wt. %)	50 ºC, 30 min, 1.0 bar, 1.89 ms^{-1}
PWF after cleaning	Reverse osmosis water	22 ºC, 10 min, 1.0 bar, 1.89 ms^{-1}

5.6. Pre-Treatment of 1.5 μm Ps*f* Membranes

The objective of this part of the study was to determine whether the application of a NaOH pre-treatment could affect both the type of foulant species attaching to the membrane surface, and result in an improved separation performance. This can be extended beyond simple conditioning (which is needed to remove a preservative layer of glycerine which new polymeric membranes are typically coated with during manufacture) to form an anti-fouling pre-treatment strategy. Further details on previous studies can be found in section 4.6. The effect of two pre-treatment methods for the filtration of a molasses solution (45 ºBrix) using a Ps*f* membrane (1.5 μm pore size) has been investigated. The pre-treatment methods used in this study involved: (i) conditioning with water at 60 ºC only, and (ii) conditioning with water at 60 ºC, followed by cleaning with 0.50 wt. % NaOH. Membrane surface characteristics such as

hydrophobicity, charge, and roughness affect the membrane separation characteristics. Fouled membrane surfaces were subsequently characterised using (i) Streaming potential measurements, (ii) Fourier Transform Infra-Red (FTIR) spectral peak height analysis, (iii) Scanning electron microscopy (SEM), (iv) Atomic force microscopy (AFM) and (v) Contact angle measurements.

5.6.1. Conditioning Flux Data for Molasses with 1.5 μm Ps*f* Membranes

Conditioning was required to remove glycerine from the membrane surfaces; it was performed using the protocol developed in Weis *et al*. (2005), with RO water at 60 ºC, 1.0 bar TMP, and 1.89 ms^{-1} CFV for 120 min. The average conditioning flux data as a function of time for the Protocol 1 (P1) and Protocol 2 (P2) treated membranes are shown in Figure 5.35. The Ps*f* membranes exhibited slightly different flux trends but with a general slight decline. There are variations in the flux performance of both the two sets of membranes; therefore the normalised flux was used to compare the other samples.

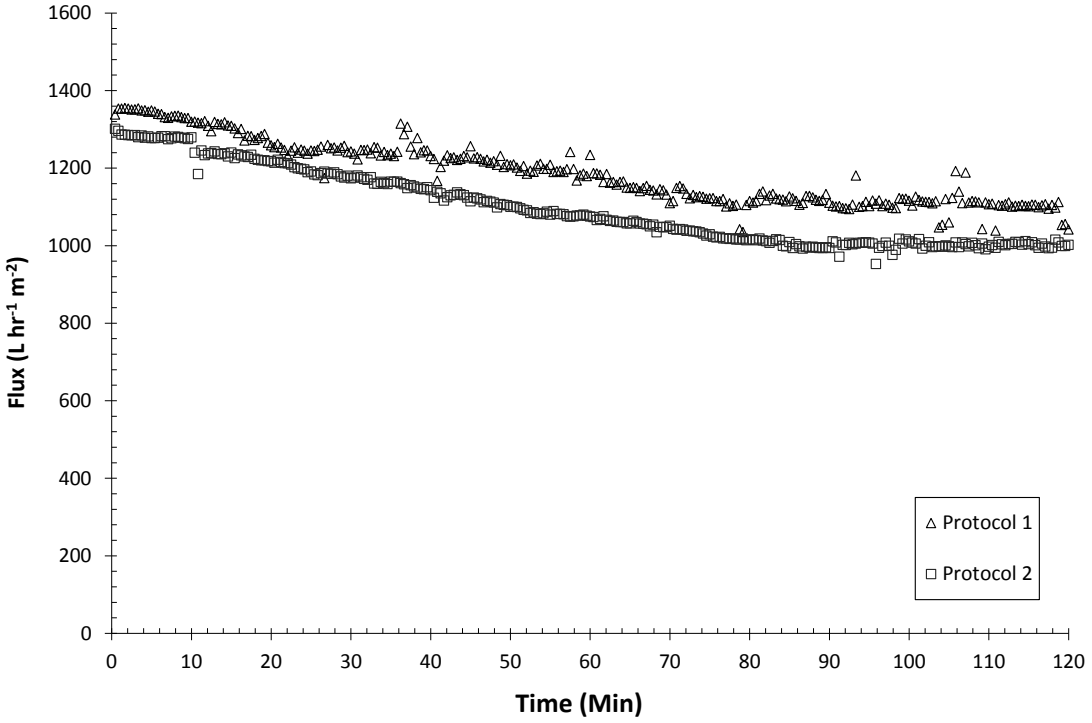

Figure 5.35: Graph to show the average effect of conditioning on flux for Protocol 1 and Protocol 2 treated 1.5 μm Ps*f* membranes. Graph shows the conditioning with 60 ºC water for 120 min. The cleaning with NaOH on Protocol 2 membranes was performed after this stage.

5.6.2. Flux Data for Molasses with 1.5 μm Ps*f* Membrane

The optimised fouling conditions have been used in this section. The fouling TMP was maintained at a constant TMP of 3.0 bar, CFV of 1.89 ms^{-1} and a temperature of 60 ºC for 90 min where standard rinsing and cleaning conditions were used. RO pure water fluxes (22 ºC, 1.0 bar, and 1.89 ms^{-1}) were maintained constant before and after fouling and after cleaning. The cleaning cycle following molasses filtration was carried out using 0.10 wt. % NaOH followed by 0.10 wt. % citric acid, each for 15 minutes (50 ºC, 1.0 bar, and 1.89 ms^{-1} CFV).

The flux data has been normalised; with the initial PWF taken as 1.0, and the other data scaled accordingly for each Protocol. The initial flux for the Protocol 1 treated membrane was 1123 L m^{-2} hr^{-1} and that for the Protocol 2 membrane was 934 L m^{-2} hr^{-1}. These values refer to the PWF recorded after the corresponding conditioning Protocol. These values were taken rather than those for the virgin membrane; otherwise a false comparison of the cleaning of the membrane overtime is made. The two pre-treatment conditioning methods displayed similar flux trends, which are shown in Figures 5.36. A typically sharp decline in fouling flux is shown which developed into a much lower steady state flux, being *ca.* 10 % of the value of the PWF recorded for the conditioned membranes. This sharp decline could be due to pore blockage as the molasses feed contained calcium crystals ranging from 1 μm to 20 μm (Nordzucker, 2008). These crystals and other high molecular mass components would have been retained in the molasses and contribute to the membrane fouling. Additionally, surface fouling is also evident in this filtration, as shown in the FTIR and SEM data. The application of Protocol 2 results in a slightly superior fouling flux performance compared to Protocol 1 (1.8 % enhanced flux). However, this is not statistically significant. As Protocol 1 produced an error of ± 3 % and Protocol 2 had an error of ± 4 %. Protocol 2 also gives a superior cleaning flux (36 % ± 1) compared to Protocol 1 (29 % ± 1) after 30 minutes of cleaning. However, the fluxes after fouling and cleaning for both sets of conditions are inadequately recovered, and appear likely to remain so for any reasonable time period using this cleaning protocol. If each part was extended the flux would have improved. Improved cleaning protocols have been developed (section 5.4).

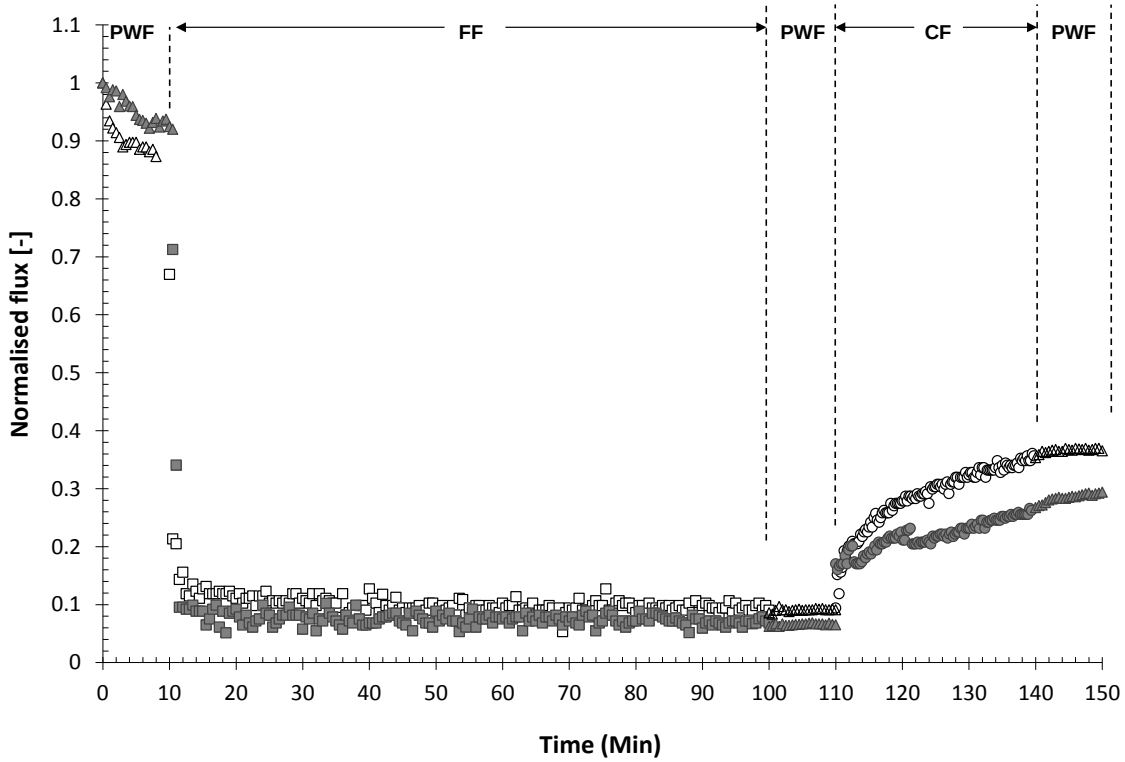

Figure 5.36: MF of molasses using 1.5 µm Ps*f* membranes: Graph to show normalised PWF, fouling flux and cleaning flux vs. Time. Symbols: ▲ – PWF, ■ – fouling (FF), ● – cleaning (CF); solid symbols – P1, open symbols – P2. Average initial flux; P1: 1123 L m^{-2} hr^{-1}, P2: 934 L m^{-2} hr^{-1}. Average final flux; P1: 326 L m^{-2} hr^{-1}, P2: 336 L m^{-2} hr^{1}.

5.6.3. Resistances

The resistance in series model was used to evaluate the different fouling resistances as detailed in Chapter 4 (section 4.3). Figure 5.37 displays the magnitude of the resistances, under steady state for molasses fouled membranes. The membrane resistance before fouling for the Protocol 1 membrane was 3.21 x 10^{11} m^{-1} and 3.86 x 10^{11} m^{-1} for Protocol 2. The initial PWF fluxes for Protocol 1 and Protocol 2 membranes are 1123 L m^{-2} hr^{-1} and 934 L m^{-2} hr^{-1} respectively. Figure 5.37 shows that the application of Protocol 2 (NaOH) leads to a statistically significant reduction in the total resistance (1.03 x 10^{13} m^{-1}) when compared to Protocol 1 membranes (9.17 x 10^{12} m^{-1}). The resistance breakdown shows that for both pre-treatment Protocols there was a high proportion of irreversible fouling (46 % and 45 % of total resistance for P1 and P2 respectively) that was not removed after cleaning. This explains the membrane resistance after fouling and cleaning, where the values were 1.09 x 10^{12} m^{-1} for Protocol 1 and 1.06 x 10^{12} m^{-1} for Protocol 2 (Figure 5.38). This was reflected in the poor flux recovery seen in Figure 5.36.

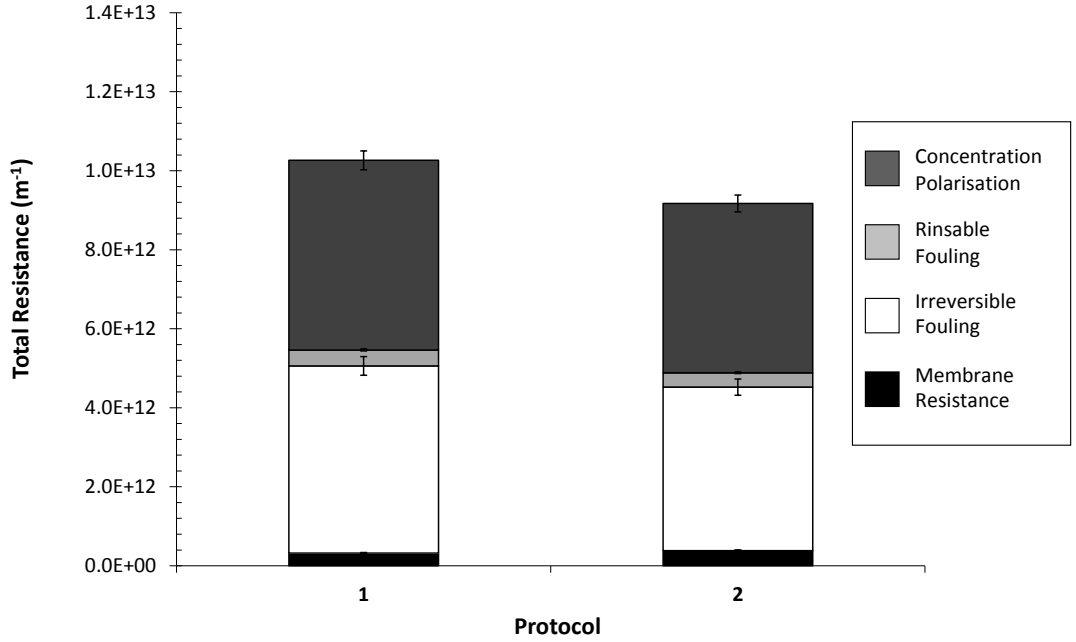

Figure 5.37: Graph to show breakdown of fouling resistance at steady state (after 90 min) when pre-treatment Protocol is varied for 1.5 μm Ps*f* membranes during the filtration of molasses feeds.

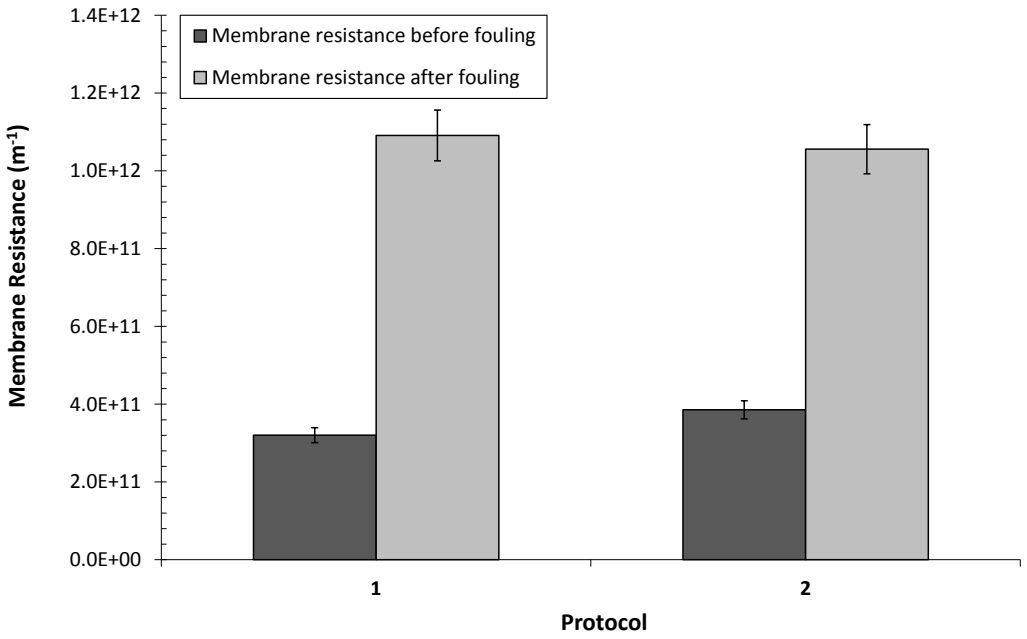

Figure 5.38: Graph to show pure water membrane resistances after fouling and cleaning vs. pure water membrane resistance before fouling when the pre-treatment Protocol is varied for 1.5 μm Ps*f* membranes during the filtration of molasses.

5.6.4. Streaming Potential through Pores

The variation of apparent zeta potential (ZP) on the pore walls has been determined from streaming potential measurements for the Ps*f* 1.5 μm membrane. Over the pH

range examined (3.7 – 7.0) all the membranes displayed a negative charge, with the charge becoming increasingly negative as the pH value increased.

5.6.4.1. Zeta-potential Measurements for Conditioned Membranes

Figure 5.39 shows the apparent zeta potential on the pore walls of the two pre-treatment methods. The Protocol 1 conditioned Ps*f* membrane displayed a slightly negative charge (-1.20 to -2.15 mV). The Ps*f* membrane that was treated with Protocol 2 showed similar trends to the membrane treated with water only (Protocol 1) with a similar charge (-1.52 to -2.00 mV). The surfaces become only slightly more negatively charged with increasing pH, indicating that charge modification with increasing pH is limited. The pH at which the transition from positive to negative charges occurs is called the iso-electric point, i.e. the surface carries no net electrical charge. The two membranes that were tested displayed no iso-electric point within the pH range examined. Kim *et al*. (1996) found that the iso-electric point of Ps*f* ranged from 3.1 to 5.3. The experimental set up could not be run above pH 7.0 as the increased alkaline conditions erode the silver coating of the electrodes and below pH 3.7 the accumulation of the H+ ions become so large that they disturb the function of the electrodes. Therefore the iso-electric point for this membrane, if it exists is outside the experimental limits.

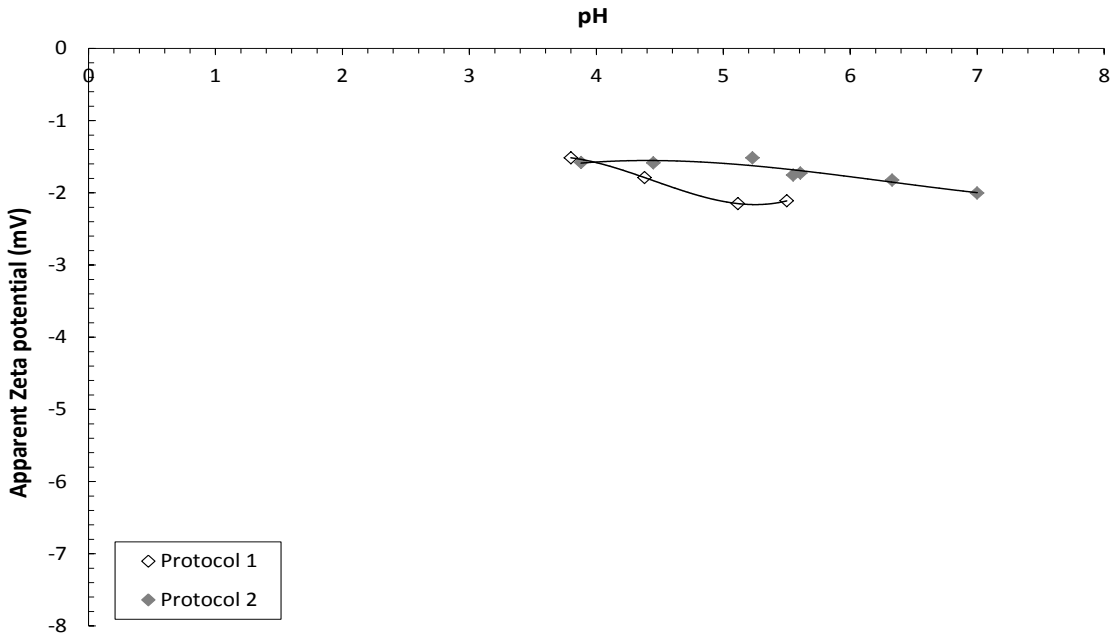

Figure 5.39: Apparent zeta-potential on the pore walls of conditioned 1.5 µm Ps*f* membranes at different pH values. Temperature, 25 ºC; pH adjustments were made with 0.001 M KCl.

5.6.4.2. ZP Measurements for Molasses Fouled and Cleaned Membranes

The variations of the apparent zeta potentials on the pore walls determined from streaming potential with the Ps*f* 1.5 μm membrane are given in Figures 5.40 to 5.41. Over the pH range examined (3.7 – 7.0) all of the fouled Ps*f* membranes tested displayed a negative charge, where the surface becomes more negatively charged with increasing pH values. This is in agreement with works of Kim *et al*. (1992) and Kim *et al*. (1996) for Ps*f* membranes. The membranes became only slightly more negatively charged for Protocol 1 treated membranes, and markedly more negatively charged for Protocol 2. Figure 5.41 shows that the pre-treatment of NaOH cleaning (P2) may make the membrane slightly more prone to fouling, suggesting that there are more negatively charged foulants adhering to the pore wall surfaces. The two pretreatment Protocols had a similar effect upon the ZP values recorded for membranes 'fouled then cleaned'. As these membranes have been treated with both NaOH and subsequently citric acid, the surface charge has become less negative, suggesting that the foulants have been removed from the membrane pore wall surfaces. This was not supported by the flux data, where poor flux recovery was shown. FTIR has been performed to determine the nature and extent of the fouling present.

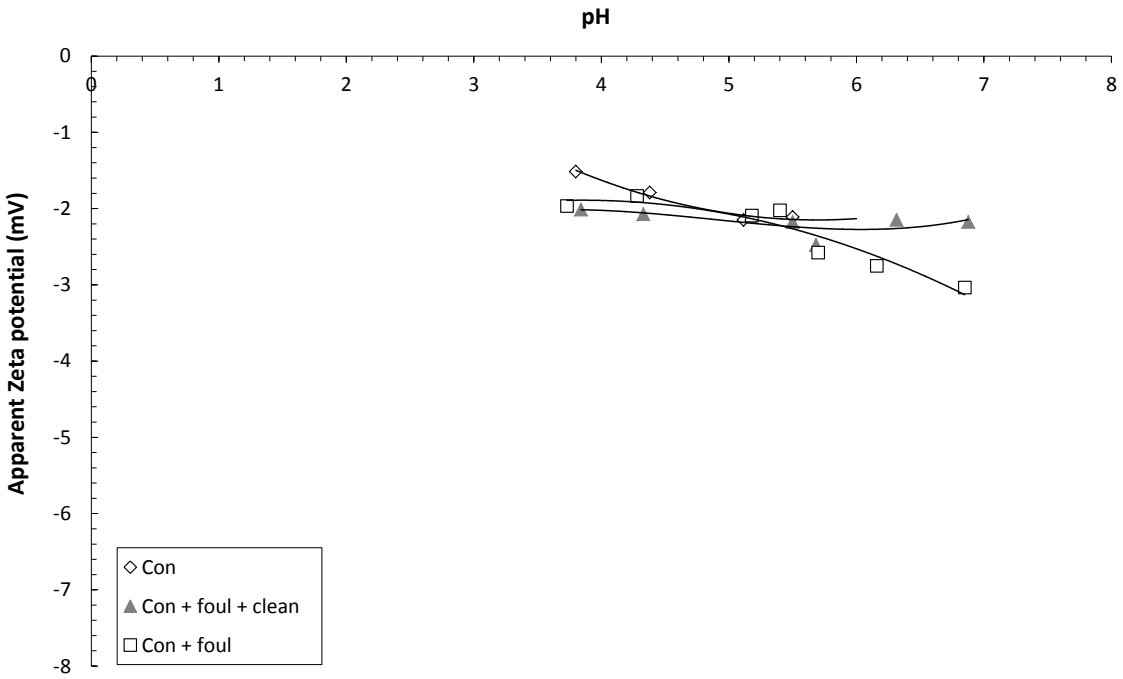

Figure 5.40: Apparent zeta-potentials on the pore walls of Protocol 1 treated Ps*f* membranes at different pH values, for the MF filtration of molasses.

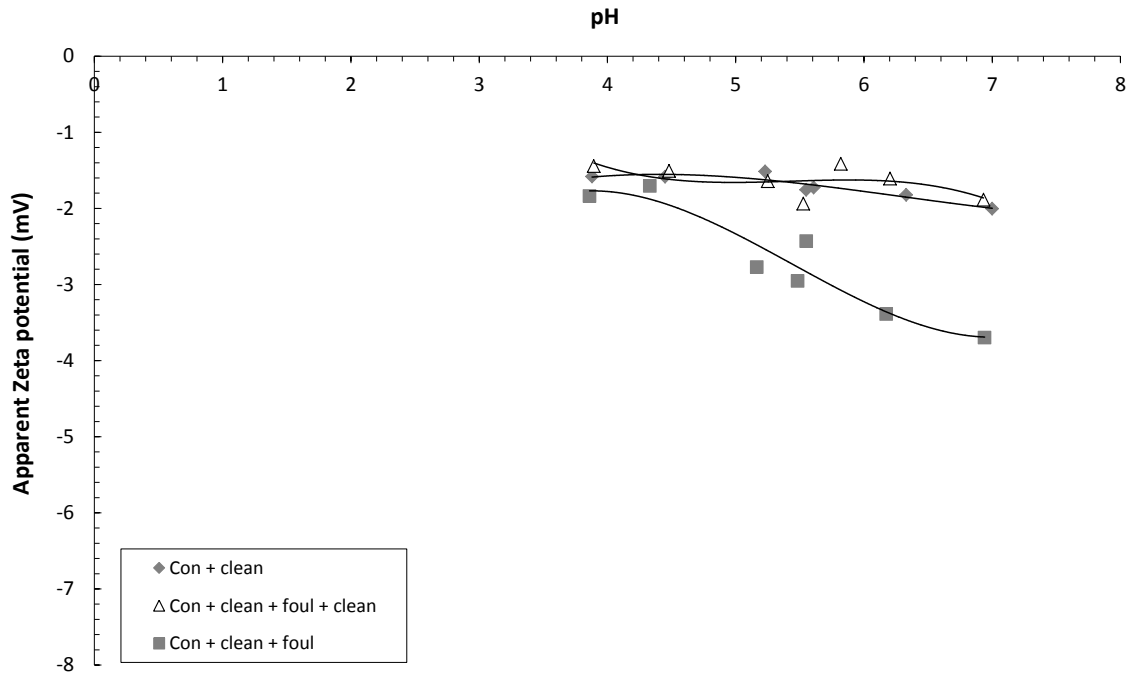

Figure 5.41: Apparent zeta-potentials on the pore walls of Protocol 2 treated Ps*f* membranes at different pH values, for the MF filtration of molasses.

5.6.5. ATR-FTIR

The analysis of the FTIR spectra was performed using PE 2000 software Spectrum (ver. 5.0.1) to enhance its appearance and aid data interpretation. A sequence of manipulation was put in practice on both sets of data to increase the integrity of the results. This involved removing the blank spectra (the CO_2 and moisture peaks), introducing a baseline correction, smoothing the noise level of the spectra, and normalizing the data to reset the Y axis (absorbance) from 0 to 1.

5.6.5.1. FTIR Spectra for Conditioned Membranes

The conditioned virgin spectrums for the Protocol 1 and Protocol 2 Ps*f* membranes are shown in Figures 5.42. The conditioning of the membrane was required to remove the preservative agent glycerine that can affect the performance of the membrane. Holser (2008) states that glycerine should have a broad absorption band associated with the hydroxyl groups of glycerol at 3250 cm^{-1} with the carbon–oxygen absorptions characteristic of primary and secondary alcohols occurring at 1030 cm^{-1} and 1100 cm^{-1}. Figure 5.42 shows that the two Protocols used on both membranes remove the majority of the glycerine.

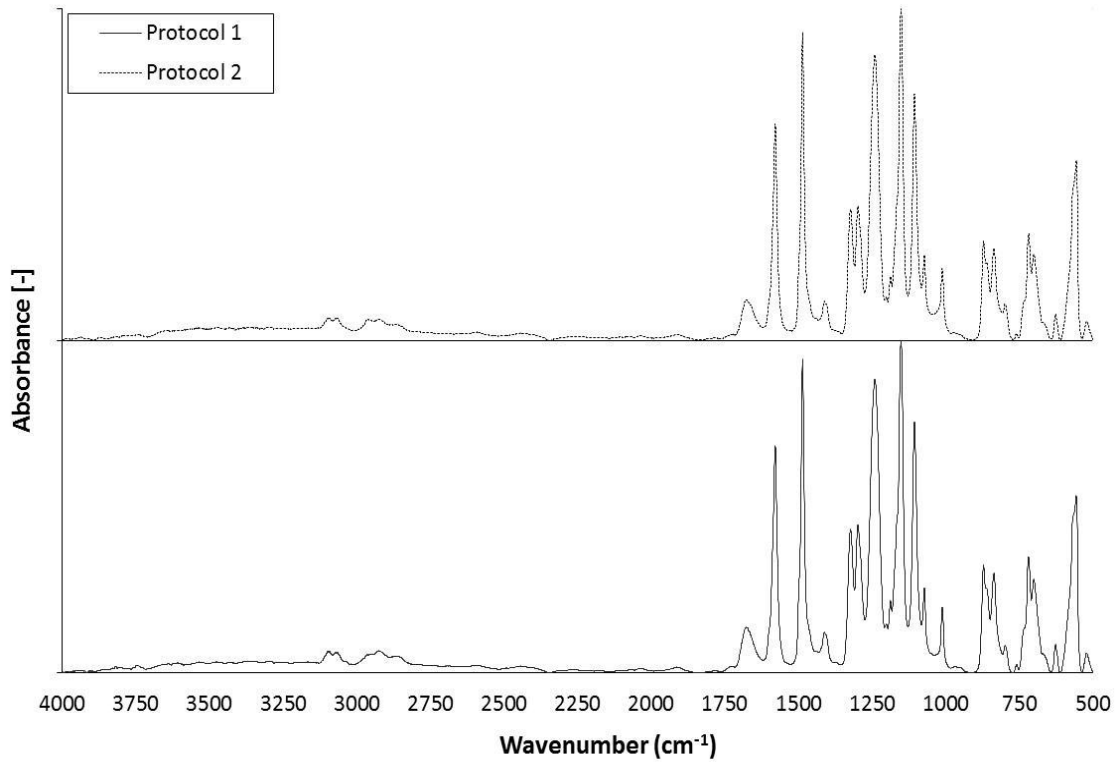

Figure 5.42: Infrared spectra comparison of virgin conditioned only (P1) Ps*f* 1.5 µm membrane (Bottom), and conditioned and cleaned (P2) treated Ps*f* membrane (Top) (all spectra shown with water subtracted).

5.6.5.2. FTIR Spectra for Molasses Fouled and Cleaned Membranes

Molasses is a complex mixture and determining the specific fouling species is difficult. A study on the properties of molasses used in this study was performed by Nordzucker (2008). The chemical composition is shown in Chapter 3.2.2 (Table 3.2). This information was used to help identify the fouling species on the Ps*f*.

The possible structure units (PSU) found by the Perkin-Elmer search program (Search Plus) for the conditioned, fouled and cleaned Ps*f* membranes are shown in Table 5.3. The search program identified a large number of possible structures, which could be the membrane polymer, foulants or cleaning agent. Many of the PSU found can be part of various chemical structures and none of the PSU is uniquely related to specific substances. The identification of chemical structure is possible, but care has to be taken as reference spectra and peaks are obtained from pure material. However, an attempt to interpret the material has been performed, especially in trying to identify the foulants.

Table 5.3: Possible structures found by the Perkin-Elmer search program for the fouled and cleaned Ps*f* membrane

Class number	Possible structural units	Possible bands (cm^{-1})
201	Alkyl group - general	1486, 1241, 1152, 1106, 1090
259	Aromatic compound	1578, 1486, 1324, 1241, 719
402	Hydroxy group	1241, 1151, 1106, 1090
511	Aliphatic alcohol	1486, 1010
2710	Aryl-ether	1578, 1486, 1324, 1151, 1106
2724	Phenoxy - general	1578, 1486, 1324, 1151, 1106, 1090, 872, 836, 719
2906	Aromatic primary amine	1578, 1486
4002	Aromatic sulphone	1578, 1486, 1324, 1151, 1106, 1090, 872, 836, 799, 719
4911	Carbonyl compound	1675, 1672

The peaks in Figures 5.43 and 5.44 for the Ps*f* membrane show similar results to; Fontyn *et al*. (1991), Zhu and Nyström (1998) and Puro *et al*. (2006). The peaks around 1579 cm^{-1} and 1486 cm^{-1} are that of aromatic bands, which is due to the C=C stretching vibration of the aromatic ring. The 1320/1290 cm^{-1} doublet band is asymmetric SO_2 stretching and the band at 1150 cm^{-1} is symmetric SO_2 stretching. As these peaks are normal for Ps*f* membranes they can be taken away from the fouled and cleaned membrane. The bands which show the majority of changes in peak height appear to be mainly in the low wave number region (> 1800 cm^{-1}). The peaks in the higher wave numbers could be due to noise. Though there is a defined peak at 2963 cm^{-1}, which is a CH_3 asymmetric stretch. The peaks in region 3200 and 3500 cm^{-1} are signs of a hydroxyl group, such as an alcohol. This could be the results of the large number of sugar molecules in the molasses. These peaks are a sign of fouling.

A scan for water and virgin membranes have been subtracted from the graph in Figures 5.45, so that the scans indicate only those of the foulants or cleaning agents deposited on the membrane surface, or within the porous structure. This is a useful comparison to identify the fouling species and effects of the pre-treatment Protocols. As molasses is prominently a mixture of sugars, it was practical to compare the fouling spectra with

those of a typical sugar (Ring, 2009). The large fouling peaks and changes in intensity in Figure 5.45 indicate the start of fouling, since these wavelength areas and peaks are characteristic for sugars. The peaks at 1490 cm^{-1} (C-$(CH_3)_2$ stretching vibrations), 1324 cm^{-1} (SO_2 asymmetric stretching vibrations), 1093 cm^{-1}, 1020 cm^{-1}, 871 cm^{-1} (C-C stretching vibrations) and 799 cm^{-1} (C-H rocking vibrations) are common wave numbers for different sugars, i.e. Dextrose, D-glucose (Shimadzu, 2009). The peaks at 1020 cm^{-1}, 1093 cm^{-1}, 1152 cm^{-1} (SO_2 symmetric stretching vibrations) and 1241 cm^{-1} (O stretching vibrations) are also commonly found for sucrose or D-fructose (Ring, 2009). The identification of these peaks show there is definite fouling on the Ps*f* membrane through the sugar in the molasses. A study at Nordzucker (2008) showed that the molasses feed contained crystals of calcium sulphate, calcium oxalate dihydrate, and calcium oxalate monohydrate. These crystals are approximately 1-6 μm wide and 5 – 20 μm long, which could also contribute to the fouling, seen in the FTIR spectra and flux data. The fouling peaks at wave numbers 1324 cm^{-1}, 1106 cm^{-1} and 556 cm^{-1} could indicate the presence of calcium oxalate dihydrate and monohydrate (McAlister *et al*., 2000; Rogé *et al*., 2007). The peaks at 1665 cm^{-1}, 700 cm^{-1} and 521 cm^{-1} could further indicate the presence of calcium sulphate (Yue *et al*., 2006).

Figure 5.45 shows that cleaning after conditioning (P2) does affect the membrane and the species subsequently attached compared to conditioning with water alone (P1), this being a similar conclusion to that made for the SSL filtration system discussed previously. The magnitudes of the absorbance recorded are very different for all of the treatments examined. Nevertheless, the spectrum recorded after applying P2 and subsequently fouling membranes is broadly similar to the spectrum seen after P1 conditioned samples, fouled and then cleaned. This again indicates that the NaOH pre-treated membranes can display a similar attachment profile following fouling to those seen for a water conditioned surface subsequently fouled and then cleaned using NaOH as a subsequent treatment.

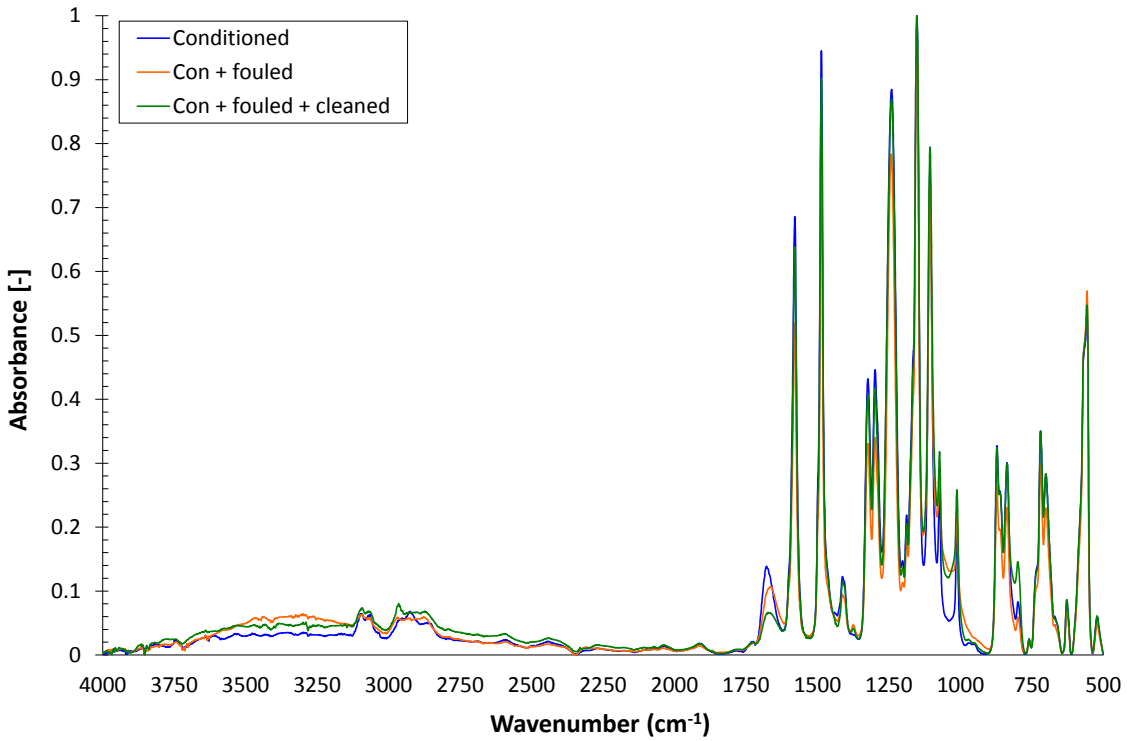

Figure 5.43: Infrared spectra comparison of 1.5 μm Ps*f* membranes under different fouling conditions. Each membrane has been conditioned with water only (all spectra shown with water subtracted).

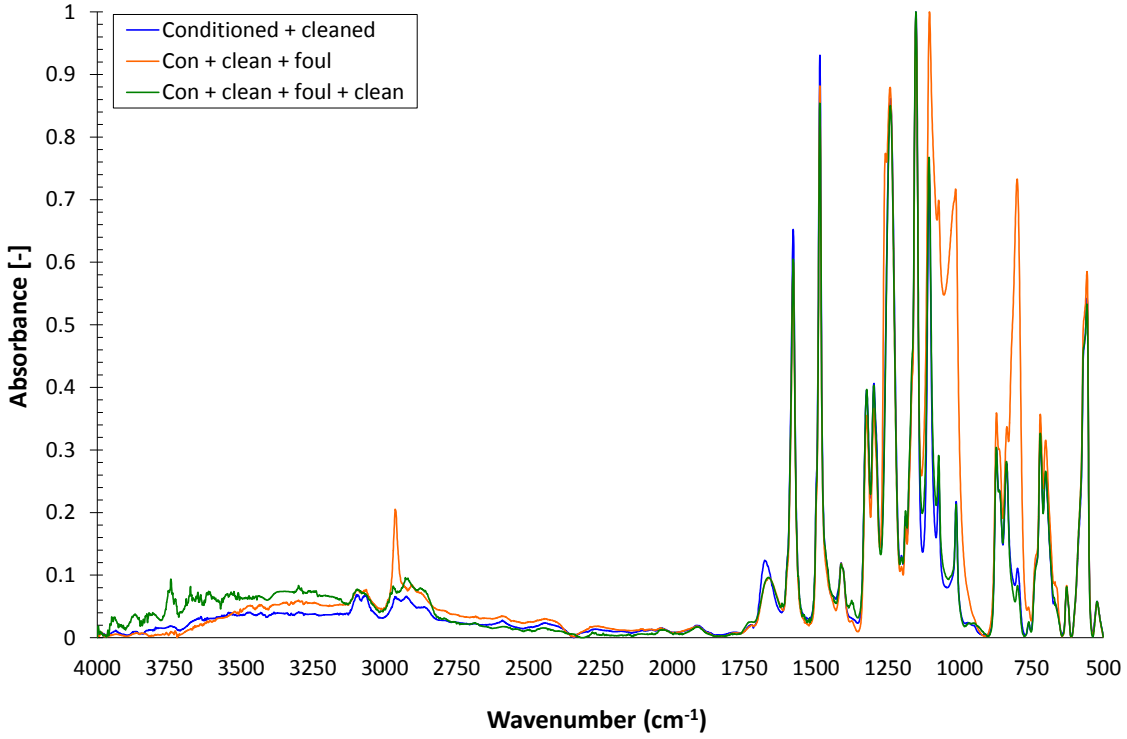

Figure 5.44: Infrared spectra comparison of 1.5 μm Ps*f* membranes under different fouling conditions. Each membrane has been conditioned with water and NaOH (all spectra shown with water subtracted).

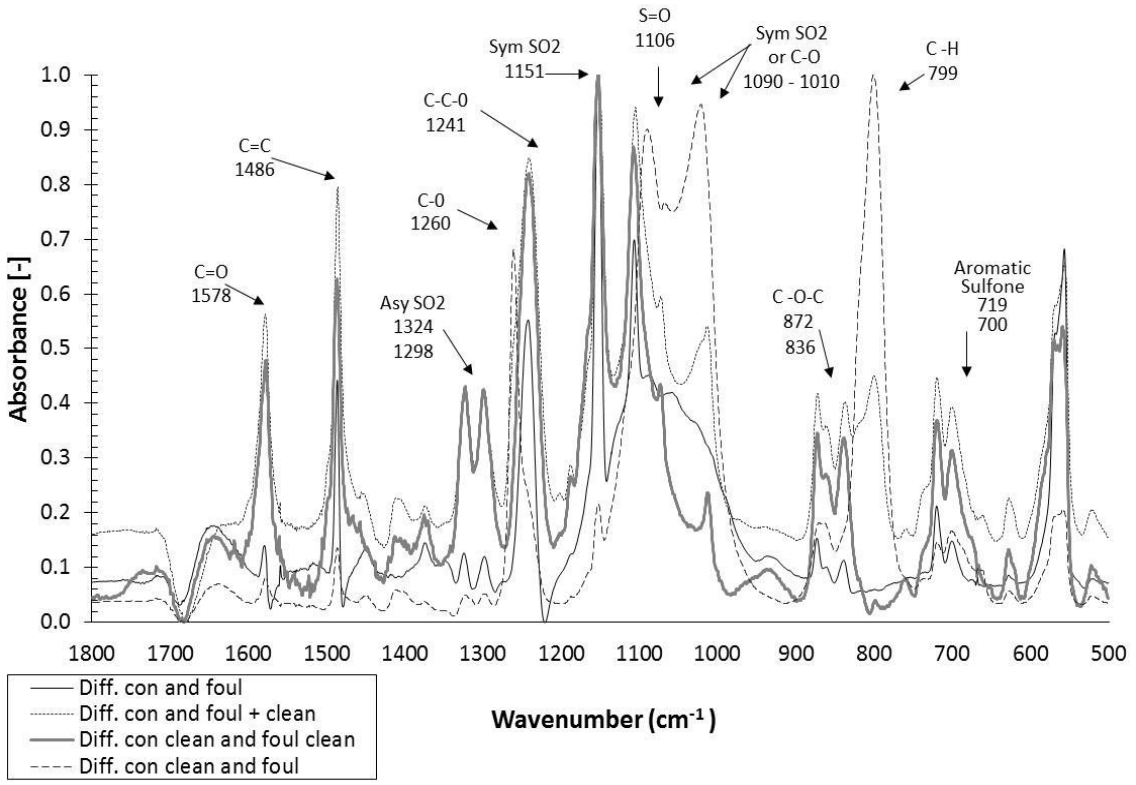

Figure 5.45: Infrared spectra comparison of 1.5 μm Ps*f* membranes subjected to different treatments for the filtration of molasses (all spectra shown with water and virgin membrane absorbance traces subtracted).

The different spectra shown in Figures 5.43 to 5.45 have a lot of the same peak locations, though with different intensities. Three samples of each membrane were tested and the peak heights of selected significant peaks were averaged and the standard deviation calculated. The peak heights for common functional groups are shown in Table 5.4. The heights of the peaks are directly related to the degree of fouling/removal and therefore a change of peak height will give information about the cleaning mechanism. The membranes that were cleaned before fouling displayed different larger peak heights than the other three membranes. The changes in peak heights between fouled and cleaned membranes are very different, indicating that there have been changes to the surface after cleaning. It seems that different amounts of fouling occur on the Ps*f* membrane when subjected to the different pre-treatment Protocols.

Table 5.4: Averaged peak-heights of Ps*f* molasses fouled and cleaned membranes

Membrane Fouling and Cleaning State	Wavenumber (cm^{-1})						
	719 Arom. Sulfone	**799 C-H**	**872 C-O-C**	**1021 C-O**	**1072 Sym. SO_2**	**1090 Sym. SO_2**	**1106 S=O**
P1 Foul	0.21	0.06	0.15	0.35	0.41	0.45	0.69
P2 Foul	0.15	1.00	0.18	0.95	0.75	0.90	0.55
P1 Foul + Clean	0.45	0.45	0.42	0.51	0.59	0.68	0.94
P2 Foul + Clean	0.37	0.04	0.34	0.17	0.43	0.49	0.85
Membrane Fouling and Cleaning State	**Wavenumber (cm^{-1})**						
	1151 Sym. SO_2	**1241 C-C-O**	**1260 C-O**	**1298 Asy. SO_2**	**1486 C=C**	**1578 C=O**	**2963 O-H**
P1 Foul	0.94	0.54	0.14	0.12	0.43	0.13	0.12
P2 Foul	0.21	0.22	0.67	0.05	0.14	0.08	0.26
P1 Foul + Clean	0.99	0.85	0.53	0.42	0.80	0.56	0.27
P2 Foul + Clean	0.96	0.82	0.32	0.42	0.61	0.48	0.16

5.6.6. SEM

The morphology of fouled deposits on membrane surfaces for a range of different conditions has been inspected using SEM. Figure 5.46 shows the image of the conditioned 1.5 μm Ps*f* membrane. This image displays a wide distribution of both pore locations and pore sizes. The surface seems to have a few deposits on the surface already. This could be due to the removal of the protective layer glycerine from the surface.

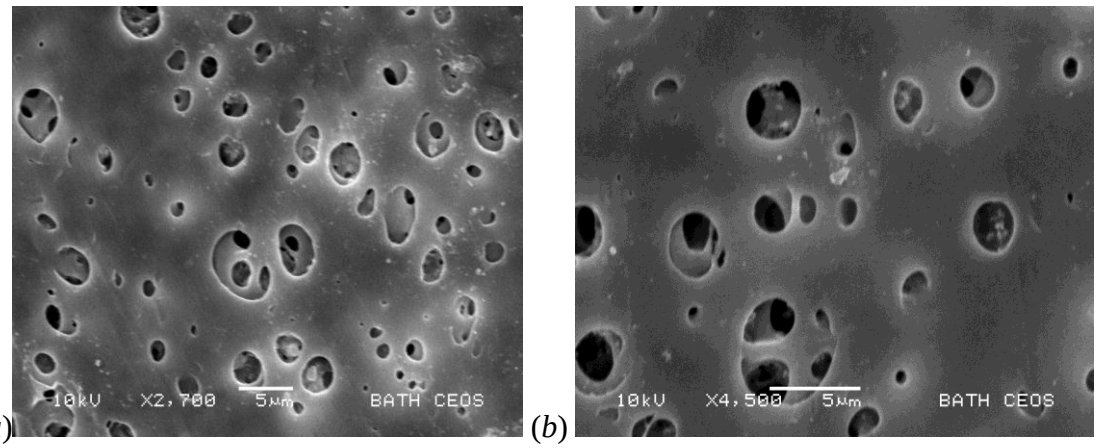

(*a*) (*b*)

Figure 5.46: SEM showing (*a*) Protocol 1 and (*b*) Protocol 2 conditioned 1.5 μm Ps*f* membranes.

Figures 5.47 (a) and (b) show the images of the fouled 1.5 μm Ps*f* membranes. The morphology of the deposits showed considerable variation. Some surface aggregation is seen. The porous cake layer is typical of deposits seen previously in our laboratory (Shorrock and Bird 1998; Wu and Bird, 2007). The images do show some pore blockage, but mainly surface fouling is seen, which is in agreement with the flux data, zeta potential and FTIR results. A greater extent of fouling can be seen in the membranes that have been cleaned before being fouled (Protocol 2 treated membrane). This is supported by the zeta potential results for the molasses fouled membranes, where the Protocol 2 treated membranes attract the adhesion of additional negatively charged foulant species.

Figures 5.48 (a) and (b) shows the effects of cleaning after fouling on the Ps*f* 1.5 μm membranes. The inspection of the cleaned membrane surfaces by SEM indicate that the cleaning protocol established are not effective in removing the cake layer of deposition and pore blockage from the membrane surfaces. X-ray diffractometry was used for identifying the elements present. The large deposits seen in the SEM pictures on the fouled membranes have been identified as containing calcium, sulphur and oxygen; these are probably crystals of calcium sulphate, calcium oxalate dihydrate, and calcium oxalate monohydrate. These crystals have previously been approximated to be 1 - 6 μm wide and 5 – 20 μm long (Nordzucker, 2008); the images recorded the presence of crystals within these size ranges.

(*a*) 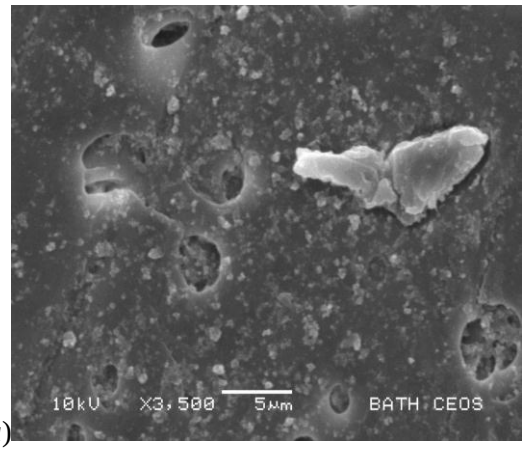

(*b*) 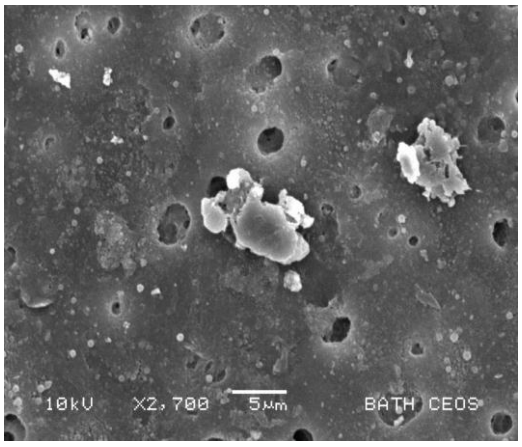

Figure 5.47: SEM showing deposit fouling on a (*a*) Protocol 1 and (*b*) Protocol 2 fouled 1.5μm Ps*f* membrane.

(*a*) 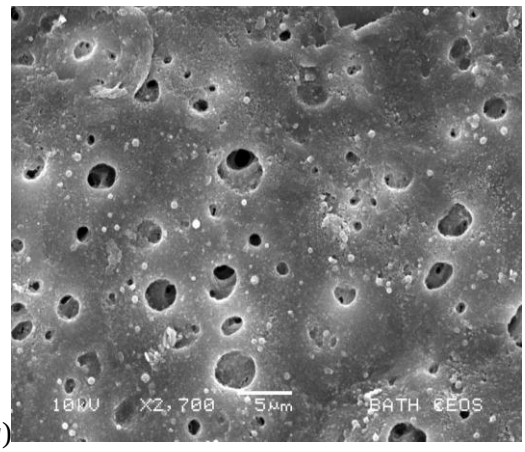

(*b*) 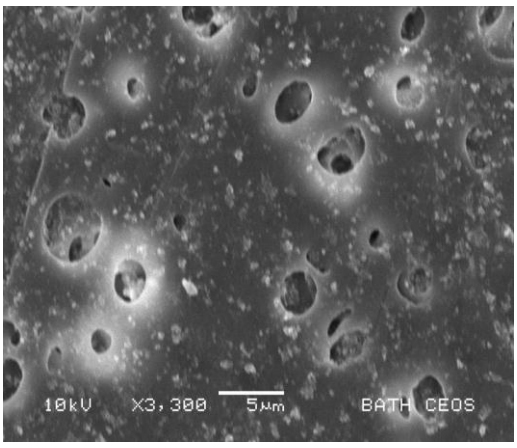

Figure 5.48: SEM showing deposit removal on a (*a*) Protocol 1 and (*b*) Protocol 2 cleaned 1.5µm Ps*f* membrane.

5.6.7. AFM

The AFM images provided an indication of the surface morphology. The roughness, waviness and the architecture of the active top layers of the polymeric membranes is illustrated in these figures. R_A (the mean roughness) was calculated as an average value of that determined from each scan line for 5 x 5 micron AFM images. The R_A values for both pre-treatments can be seen in Table 5.5. The two pre-treatment Protocols employed lead to similar roughness values for (i) conditioned membranes, (ii) fouled membranes, (iii) fouled then cleaned membranes. Ps*f* membranes tested displayed R_A values of 13.8 (P1) and 14.1 (P2) nm. The R_A value for the virgin 1.5 µm Ps*f* membrane was similar to that recorded previously in our laboratory (Weis *et al*., 2005). After fouling both Protocol 1 and Protocol 2 membranes have a higher R_A value, indicating that relatively rough surface deposits were present. This rougher surface is associated with an increase of in-pore deposits; this is confirmed by the increase in negative charge shown in the zeta potential work. Once cleaning had occurred, the surface roughness values reduced, but did not return to the initial roughness values, indicating that the surfaces had not been returned to a pristine condition. This is supported by both the SEM images and the contact angle data.

Table 5.5: R_A surface roughness values as measured by AFM

Sample	R_A (nm)		
	Conditioned	Fouled	After Clean
Ps*f* (P1)	13.8 ± 1	32.6 ± 1	20.9 ± 1
Ps*f* (P2)	14.1 ± 1	31.9 ± 1	20.5 ± 1

5.6.8. Contact angle

The hydrophobicity of the membrane samples are shown in Table 5.6. The membranes tested were all considered to be moderately hydrophilic, as the contact angles measured were less than 90º. Any glycerine remaining on the membrane makes the surface more hydrophilic. After fouling and cleaning cycles, the membrane surface had a contact angle between that of a virgin and a fouled surface, implying that the membrane has not returned to its original state. No statistical difference could be detected between the effect of pre-treatment Protocols 1 and 2 by measuring contact angles.

Table 5.6: Contact angles of water drops on membrane surfaces

Sample	Contact Angle (º)			
	Unconditioned	Conditioned	Fouled	After Clean
Ps*f* (P1)	57 ± 3	66.5 ± 3	50 ± 2	60 ± 2
Ps*f* (P2)	57 ± 3	67 ± 2	48 ± 3	62 ± 2

5.7. Summary

Molasses was studied in the cross flow rig with three different pore size Polysulphone (Ps*f*) membranes (0.5 μm, 0.9 μm, and 1.5 μm). The majority of the experiments were performed with the 1.5 μm Ps*f* membrane. This chapter was split into two sections: (i) the fouling and cleaning optimisation of molasses filtration, and (ii) the effect of pre-treatment cleaning on the filtration of molasses.

The fouling conditions were optimised by varying concentration, CFV, TMP and temperature. The molasses was required to be used at as low a dilution rate as possible, it cannot be used in its delivered form as its viscosity was too high for pumping around the circuit and for effective separation. The highest possible dilution rate for filtration in this study produced flux values which were too low for a viable process and the lower the concentration resulted in a higher degree of cleanability. The 45 ºBrix produced a compromise and a reasonable fouling flux performance. The molasses should be used at as high a temperature as possible, as the viscosity of the feed is particularly influential in the filtration process. The optimal temperature for the filtration of molasses was 60 ºC; as there was no benefit of increasing the temperature to 70 ºC. The results showed that increasing the TMP increases the fouling flux until between ~2.5 and

3.0 bar where the limiting flux effect occurs. After this pressure, the fouling fluxes began to decline slightly. It was therefore not advantageous to work at higher pressures than 3.0 bar. The optimised fouling conditions were a TMP of 3.0 bar, a CFV of 1.89 ms^{-1} and a temperature of 60 ºC for 90 min.

Effective membrane cleaning protocols following molasses filtration to remove both cake and in-pore bound deposition require both alkali and acid cleaning steps. By optimising a two stage cleaning process, optimal temperature and concentrations were identified for the microfiltration of a 45 ºBrix molasses solution. The best cleaning regime from the range tested achieved a pure water flux recovery of 89 % using a NaOH concentration of 0.25 wt. % followed by a stage using 0.10 wt. % citric acid. The process conditions were the same for each stage (50 ºC, 30 min, 1.0 bar, and 1.89 ms^{-1}).

The objective of the second part of the chapter was to determine whether the application of a simple NaOH pre-treatment could affect both the type of foulant species attaching to the membrane surface, and improve the separation performance. The pre-treatment Protocol used resulted in the adhesion of different species when molasses was treated using Ps*f* membranes. Protocols 1 and 2 resulted in the attachment of different species to the membrane, as shown by the resulting FTIR spectra. However, the functional groups in the cleaning agents partially masked the molasses foulant responses in the FTIR spectra, making data difficult to interpret. The peak height data suggests that different amounts of fouling had occurred on Ps*f* membranes subjected to the different pre-treatment Protocols. The fouling species in the molasses deposition displayed a slight negative charge, becoming slightly more negative with increasing pH. The zeta potential data indicated that the cleaning pre-treatment Protocol 2 at 50 ºC water followed by NaOH) made the membranes more prone to in-pore fouling than those subjected to pre-treatment Protocol 1 (50 ºC water only), but flux data indicated that the subsequent cleaning removed this in-pore fouling more easily than the fouling which occurred on membranes subjected to pre-treatment Protocol 1. The results obtained when filtering molasses also suggest that surface fouling plays a key role in the process.

Chapter 6

The Application of Fluid Dynamic Gauging in the Investigation of Synthetic Membrane Surface Phenomena

6.1. Introduction

This chapter details the experimental results concerning Fluid Dynamic Gauging (FDG) of polymeric membranes. This chapter is divided into three sections; (i) dead-end dynamic gauging, (ii) cross flow filtration dynamic gauging and (iii) deposit analysis. Dead-end filtration was used to validate the application of FDG for the measurements of fouling on polymeric membranes. The results were compared with works of Chew *et al.* (2007). This was then advanced to FDG studies in the cross flow filtration mode. Deposit analysis was performed in terms of porosity and resistance.

6.2. Dead-end Filtration Dynamic Gauging

FDG has been used to track simultaneously the thickness of cake and permeate *in situ* and in real time. The experiments have been performed with sugar beet molasses; using 0.5 μm, 0.9 μm, and 1.5 μm pore size Ps*f* membranes. Stainless steel microweaves of sizes 5 μm and 10 μm were also tested for validation of the FDG technique.

6.2.1. Calibration

The calibration experiments were performed using the protocol developed by Chew *et al.* (2007). Three different pore sizes of membranes in the dead-end filtration cell were tested, the results can be seen in Figure 6.1 with 0.5 μm, 0.9 μm, and 1.5 μm membranes in the permeate condition as described in section 3.5.4. The profile shows the two distinct regions as seen in previous work by Chew *et al.* (2004a) and Chew *et al.* (2007); the *asymptotic zone* where the gauging flow is independent of the distance from the foulants surface and the *incremental zone* where the flow rate is sensitive to distance, this is used to detect the location of the surface when $h/d_t \leq 0.25$. The flux results (not shown) suggested that for $h/d_t \leq 0.25$, the fluid flowing comes from the

reservoir under the membrane as well as the gauging flow. This is shown from the slightly lower flux values in the incremental region as the gauge approaches the surface. This effect was only slight in the asymptotic zone suggesting that when the nozzle was far from the membrane, typically $h/d_t > 0.25$, the permeate flux was unaffected. This profile is extremely similar to those reported previously for solid impermeable surfaces (Tuladhar *et al.*, 2000) and impermeable surfaces (Chew *et al.*, 2007). This technique can therefore be applied to the fouling layers on porous/permeable surfaces and can be used in this study.

Microweaves were studied as a tool to assist the design of the cross flow FDG rig. Figure 6.2 shows the calibration profile for two different microweaves with pore sizes 5 µm and 10 µm. The microweaves again show a similar profile to the polymeric membrane results and the experiments by Chew *et al.* (2007). This implies that the calculations presented by Tuladhar *et al.* (2000) for the analysis of thickness measurements can be assumed to be valid. The smaller pore sizes of 5 µm show a higher mass flow rate than 10 µm. This could be due to the tighter pores allowing less flow through the membrane.

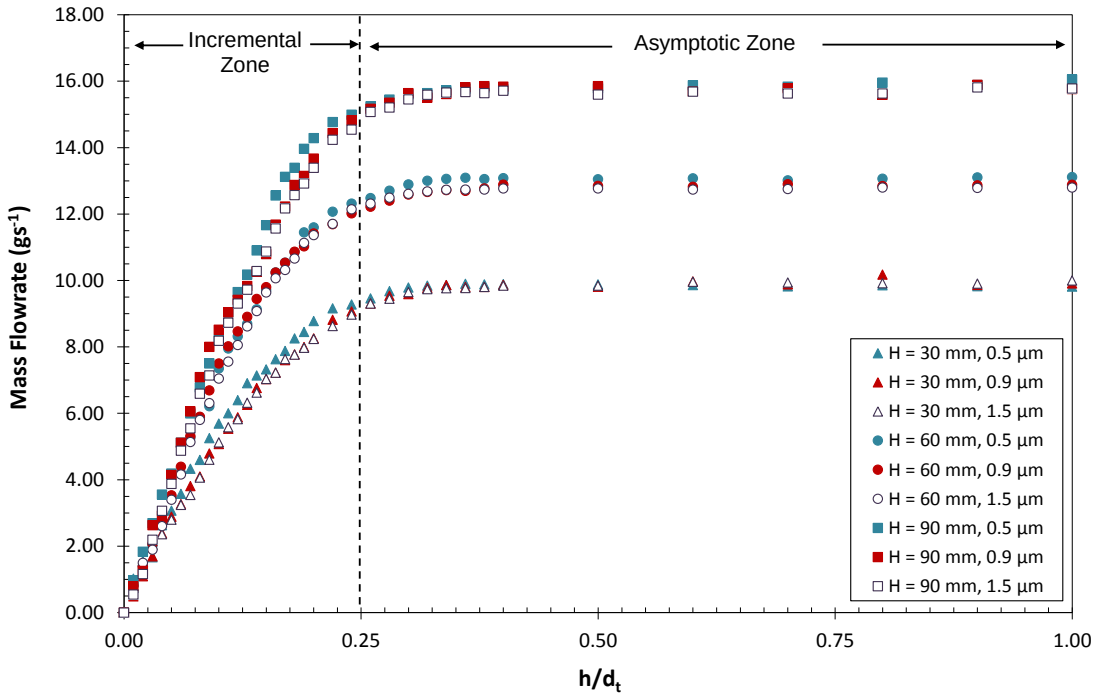

Figure 6.1: Flow rate-clearance profile of FDG (d_t = 5 mm) for calibration of 0.5 µm, 0.9 µm, and 1.5 µm pore size Ps*f* membranes.

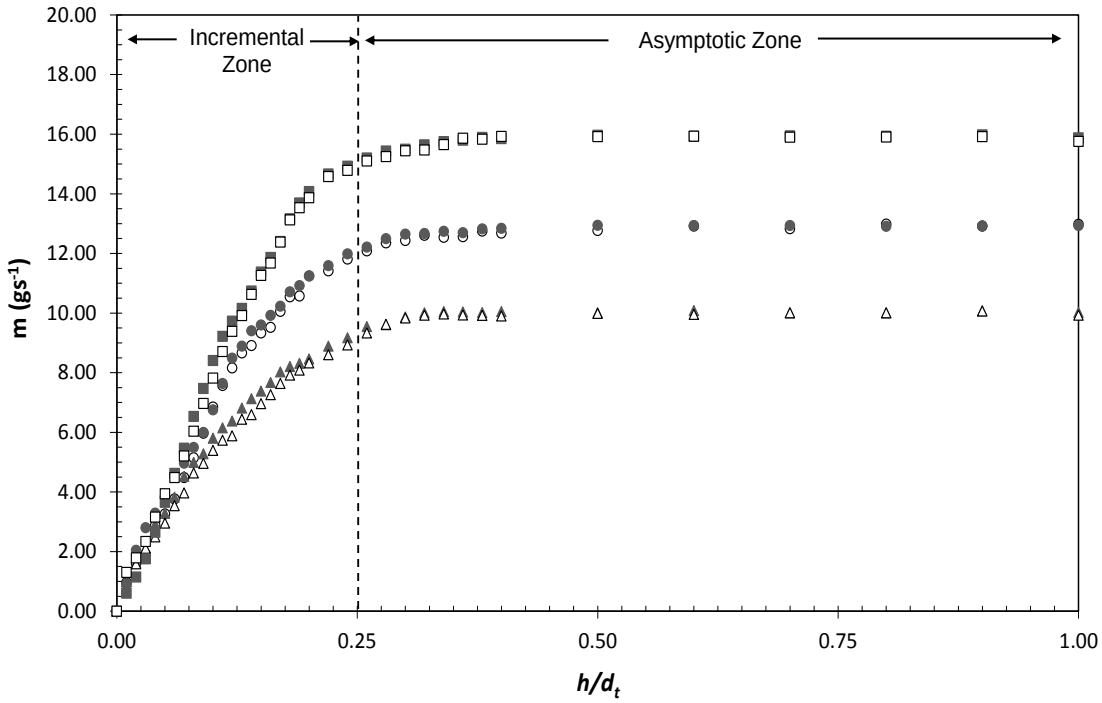

Figure 6.2: Flow rate-clearance profile of FDG (d_t = 5 mm) for calibration of 5 μm and 10 μm microweaves. Filled symbols: 5 μm; open symbols: 10 μm. Squares: H = 90 mm, circles: H = 60 mm, triangles: H = 30 mm.

6.2.1.1. Discharge coefficient (C_d) Analysis

The discharge coefficient, C_d, is used to characterise the flow around the nozzle; it accounts for energy losses due to flow near the nozzle entrance (i.e. gap between the nozzle and the gauged surface and divergent section of nozzle inlet) and is defined as the ratio of the actual to ideal mass flow rate through the nozzle, *viz*, defined by Equation 6.1 and 6.2.

$$C_d = \frac{m_{actual}}{m_{ideal}} = \frac{m}{\frac{\pi d_t^2}{4}\sqrt{2\rho \Delta P_{13}}} \qquad 6.1$$

where:

$$\Delta P_{13} = \Delta P_{14} - \Delta P_{34} = \rho g H - \frac{128 \mu m l_{eff}}{\pi d^4 \rho} \qquad 6.2$$

where ρ is the density of the liquid, μ is the viscosity of the liquid, m is the mass flowrate through the gauge, l_{eff} is the effective length of tube between points 3 and 4 on Figure 2.16, and d is the diameter of the gauging tube. The subscripts on pressure drop

relate to different locations as shown in Figure 2.16. The value of l_{eff} was determined by independent experiments (Appendix C4). The effective length experiment was essential to determine the length of the *hypothetical* straight tube that would support the same resistance to flow as does the *real* tube at the same flow rate. The effective length was found to be 1.79 m from a real tube length of 0.95 m. For a small clearance, the flow pattern through the nozzle is complex and affected by the proximity of the gauging surface (Chew *et al*., 2004b). In Figure 6.3 and 6.4 by plotting graphs of C_d vs. h/d_t, it was found that C_d has a strong function of h/d_t, *i.e.* when $h/d_t < 0.25$.

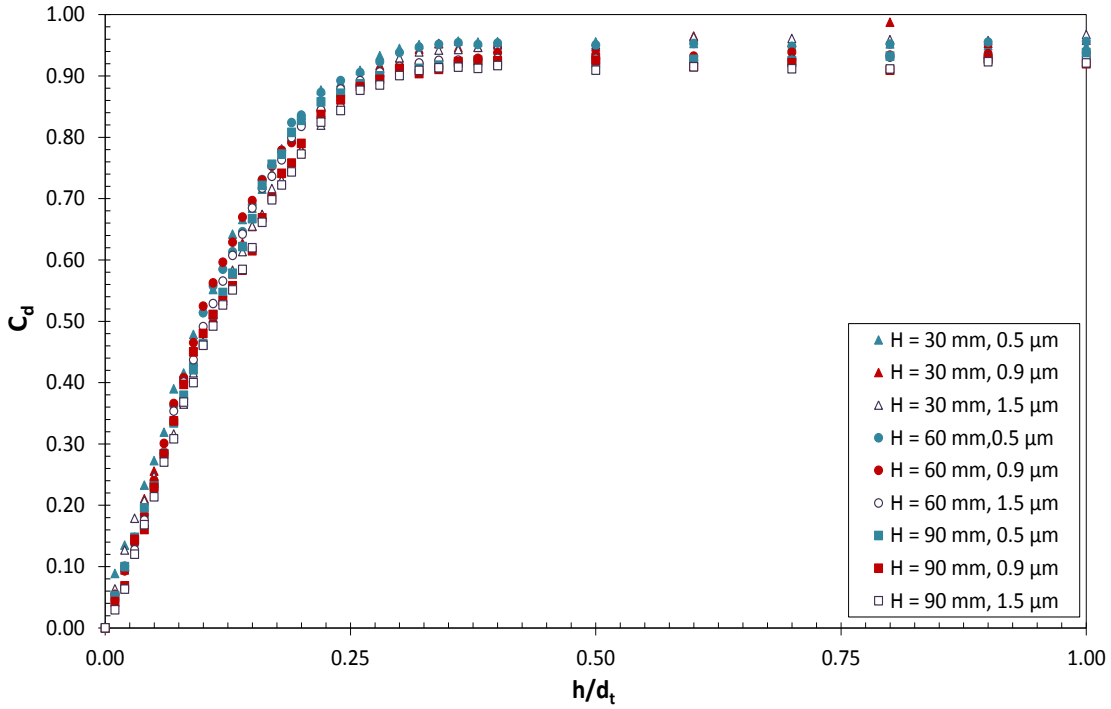

Figure 6.3: C_d vs. h/d_t profiles for calibration of 0.5 µm, 0.9 µm, and 1.5 µm pore size Ps*f* membranes (d_t = 5 mm).

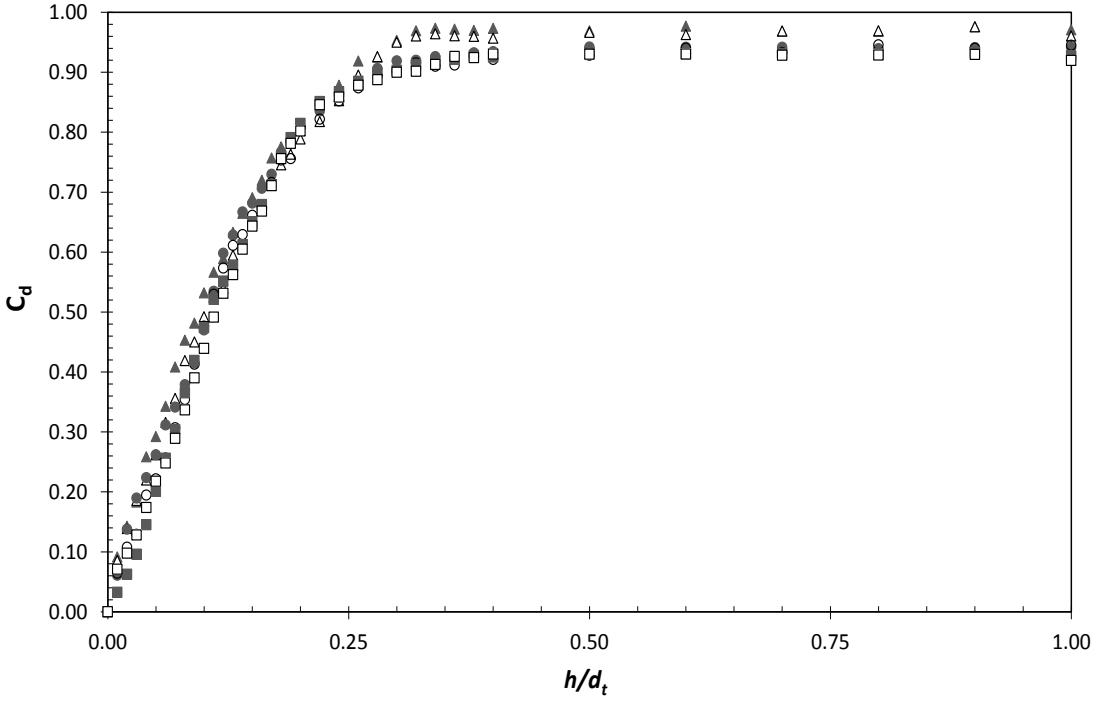

Figure 6.4: C_d vs. h/d_t profiles for calibration of 5 μm and 10 μm microweaves (d_t = 5 mm). Filled symbols: 5 μm; Open symbols: 10 μm. Squares: H = 90 mm, circles: H = 60 mm, triangles: H = 30 mm.

6.2.2. Fouling Thickness Experiments

The permeate flux (averaged over the whole membrane area) and deposition process (filter cake build-up) was measured via the cake thickness measurements, δ, for molasses solution. Figure 6.5 shows the molasses filtration with the polymeric Ps*f* membranes. The 0.5 μm pore size membrane produced too small flux values to be used for reliable results. In Figure 6.5, a rapid decline initially in the first 300 seconds can be seen. This could be due to pore blockage (Chew *et al.*, 2007; Chen *et al.*, 2004a). After this time, a cake layer occurs on the top layer of membrane after blockage resulting in long-term decline. As the pore size increases the rate of cake thickness growth decreases, this could be due to more fouling material needed for pore blockage to occur. Flux decline occurs at a greater rate in the smaller pore samples. The 0.9 μm and 1.5 μm membranes after 500 seconds reach similar steady state flux values. Figure 6.5 also shows that the rate of flux decline is higher than the rate of cake layer growth for all samples; this can be seen by comparing the gradients of the flux and thickness lines. The sign of fouling growth can be seen visibly with experimental observations.

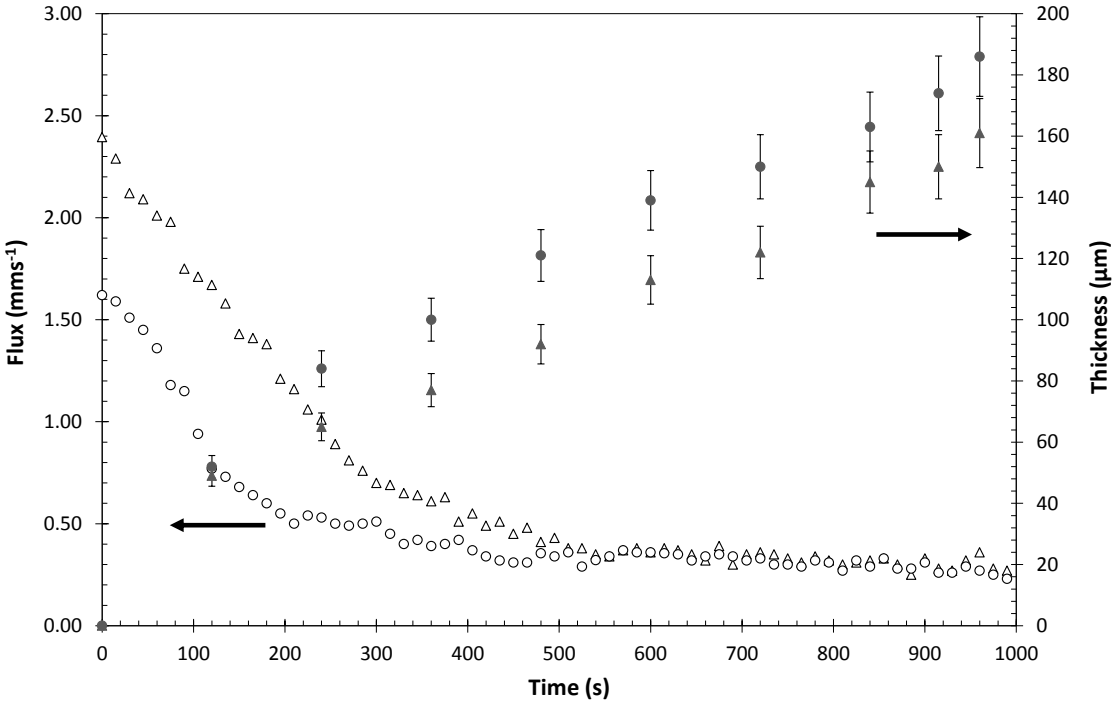

Figure 6.5: Permeate flux and cake thickness as a function of time (25 ºBrix molasses). Filled symbols: cake layer thickness (right axis); open symbols (left axis). Circles: 0.9 µm, triangles: 1.5 µm Ps*f* membrane.

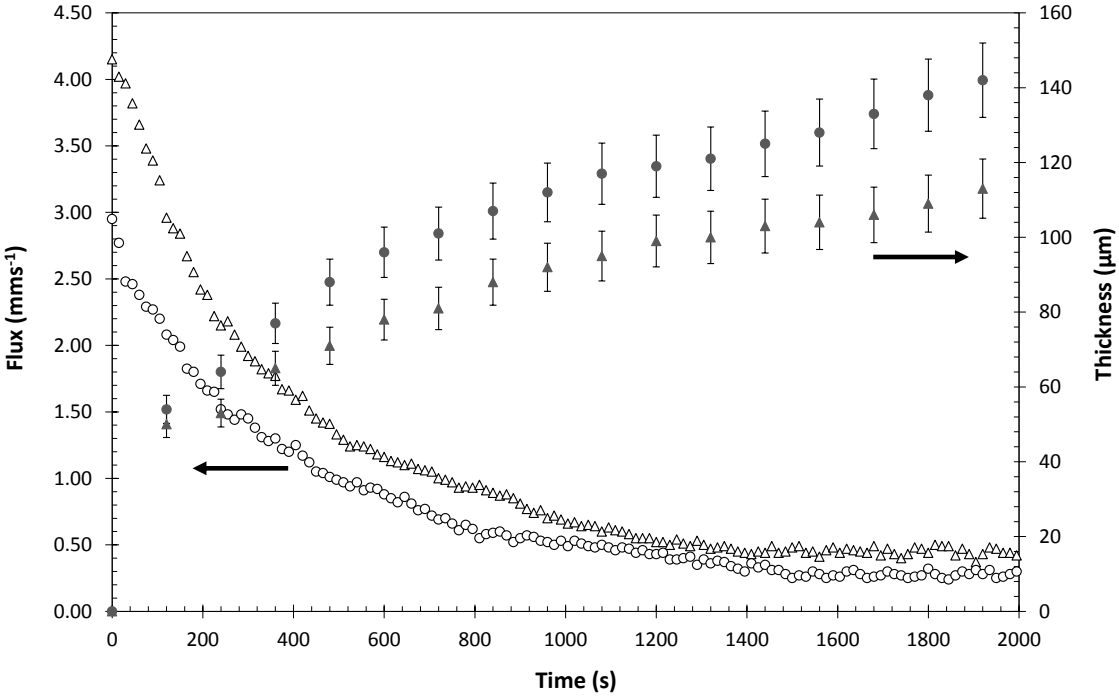

Figure 6.6: Permeate flux and cake thickness as a function of time (25 ºBrix molasses). Filled symbols: cake layer thickness (right axis); open symbols (left axis). Circles: 5 µm, triangles: 10 µm microweaves.

Figure 6.6 shows the filtration of molasses with 5 μm and 10 μm stainless steel microweaves. It shows very similar results to the polymeric membranes, except for the decreased fouling layer thickness. The error in these experiments is relatively high ± 10 %; this could be due to the small driving force in the dead-end filtration set-up resulting in extremely small fluxes through the membrane. To improve the accuracy of these results a thicker fouling layer would be required for the size of the nozzle, this could be achieved by increasing the value of H (driving force).

6.3. Cross-flow Fluid Dynamic Gauging

In these experiments, the thickness of cake and the permeate flux during the filtration of molasses were tracked simultaneously. The aim of this work was to demonstrate the applicability of pressure mode fluid dynamic gauging to the study of cake fouling in cross-flow microfiltration, and perform subsequent in-situ measurements of the deposit thickness.

6.3.1. Calibration

Calibration experiments were performed to test the operability of the FDG in this mode and enable the calculation of deposit thickness. Initial calibration experiments included the use of the gauge in a similar set up to those described by Tuladhar *et al*. (2003) and Lister *et al.* (2011), whereby the mass flow rate was measured at various distances from the membrane surface (Figure 6.7). The mass flow rate vs. h/d_t profile of transmembrane pressure (TMP) variation confirms that FDG is suitable for use on membranes in this cross flow filtration rig, as it produces similar results to those reported previously. The plot shows the two distinct regions; the *asymptotic zone*, where the gauging flow is independent of the distance from the surface, and the *incremental zone*, where the flow rate is sensitive to distance and is used to locate the surface. The transition occurs around $h/d_t \sim 0.25$.

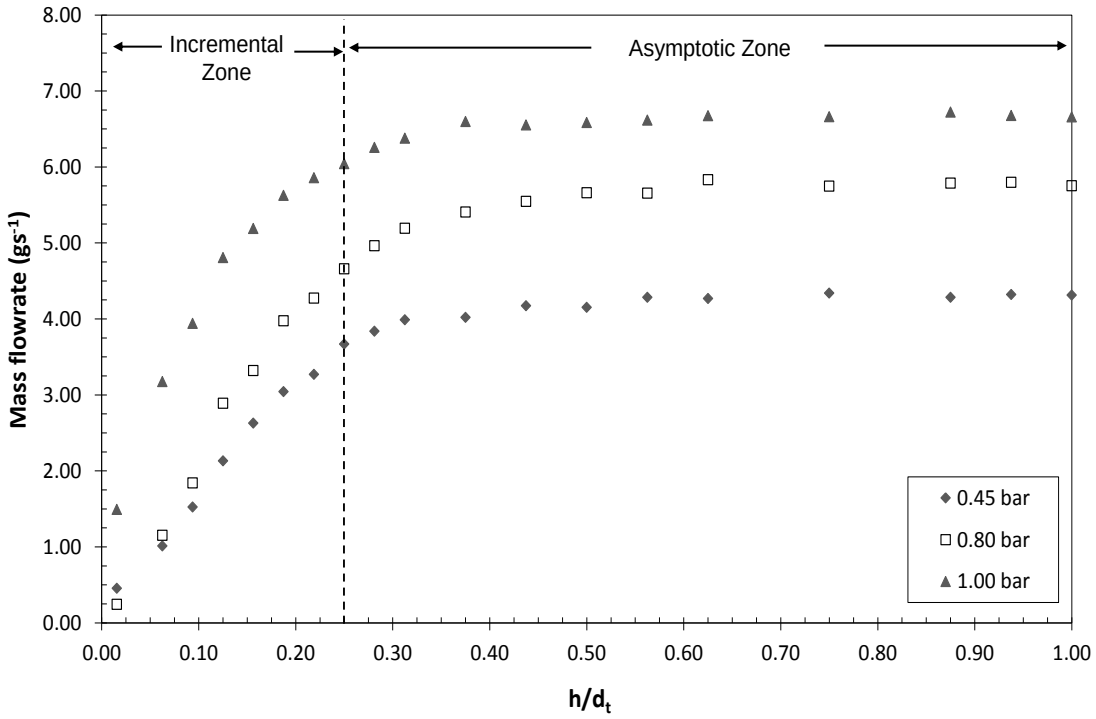

Figure 6.7: Flow rate-clearance profiles for FDG (d_t = 1 mm) calibration in fixed gauging pressure mode at different duct TMP. Conditions: 22 ºC, Re_{duct} = 9815.

In the majority of this work, a different mode of operation was employed, where, *m*, is set and the measurement of pressure drop across the nozzle is used to locate the position of the surface. The pressure drop across the nozzle, ΔP_{14}, is sensitive to the clearance, so that *h* may be obtained from knowledge of this pressure difference and the mass flow rate. This operating mode is termed *fixed gauging flow* (Pressure-mode FDG). This has the advantage of controlling the amount of liquid withdrawn from the bulk system and maintaining the flow rate constant, further benefits have been discussed in Chapter 2.7.3.3. For clarity, ΔP_N is used for the pressure drop across the nozzle (equivalent to ΔP_{14}). Figures 6.8 (a) to 6.10 (a) show gauging profiles where the flow rate through the gauge was fixed, and the differential pressure measured. An example gauging profile for the effect of cross flow velocity (CFV), TMP and temperature are shown. The corresponding calibration charts for the fouling conditions tested were performed before the different filtration experiments were undertaken. The Reynolds number through the gauge (calculated using d_t as the characteristic length scale), Re_g, was set at ~ 415 for all calibration experiments, with a gauge: duct flow fraction of 1 – 3 % (for Re_{duct} = 14815 – 4000). This value was chosen to avoid a significant reduction in the feed side flow downstream of the gauge. These profiles again exhibit the asymptotic and incremental

zones observed in Figure 6.7. As the nozzle approaches the membrane surface, the pressure drop across the nozzle, ΔP_N increases. These figures indicate that FDG can be used for this application, as the pressure remains sensitive to the approach to the surface at low h/d_t. It also suggests that the use of the FDG had no significant effect upon the permeate flux, as the values recorded were similar at all distances from the surface.

The discharge coefficient, C_d, was used to quantify the performance of the nozzle (Equation 6.3).

$$C_d = \frac{m_{actual}}{m_{ideal}} = \frac{m}{\frac{\pi d_t^2}{4}\sqrt{2\rho\Delta P_{13}}} \quad \text{where:} \quad \Delta P_{13} = \Delta P_{14} - \Delta P_{34} = \Delta P_{14,measured} - \frac{32\mu u l_{eff}}{d^2} \qquad 6.3$$

The subscripts on pressure drop relate to different locations as shown in Figure 2.16. For a small clearance, the flow pattern through the nozzle is complex and affected by the proximity of the gauging surface (Chew *et al*., 2004b), so it was not useful to try to separate 2 and 3. The effective length, l_{eff}, was determined from separate experiments; where l_{eff} was found to be 0.34 m, *cf*. a linear tube length of 0.20 m. A nozzle with d_t = 1 mm has been shown to give an accuracy of ± 10 μm (Chew *et al.*, 2007; Lister *et al*., 2011). Gordon *et al*. (2010a) showed that the accuracies of the FDG technique can be improved to ± 5 μm, for a fully automated FDG system. Figures 6.8 (b) to 6.10 (b) shows the data from Figures 6.8 (a) to 6.10 (a) re-plotted in dimensionless terms as C_d versus h/d_t. C_d is a strong function of h/d_t, when $h/d_t < 0.25$, as expected, and the gauging behaviour is sensitive to the approach to the surface. The curves follow the same general trend, indicating that the gauging behaviour is not strongly modified by the presence of the channel walls (Tuladhar *et al.*, 2003). The relationship between C_d and h/d_t is independent of measurement mode. This can be used to infer the clearance, h, enabling the calculation of deposit thickness. The viscosity of the fluid is taken into account. The thickness of a deposit on the membrane is measured through a series of stages: (i) measurements of flow rate, m, and ΔP_{14} are used to calculate C_d, (ii) h/d_t is estimated through linear interpolation of the C_d vs. h/d_t plot, (iii) this value is then multiplied by d_t to give h, from which the deposit thickness (δ) is calculated by $h_o - h$. The flow rate-clearance profiles exhibit an almost linear relationship when $h/d_t < 0.25$

and FDG thickness measurements are made with the nozzle located at $0.10 < h/d_t < 0.20$ (Lister *et al*., 2011).

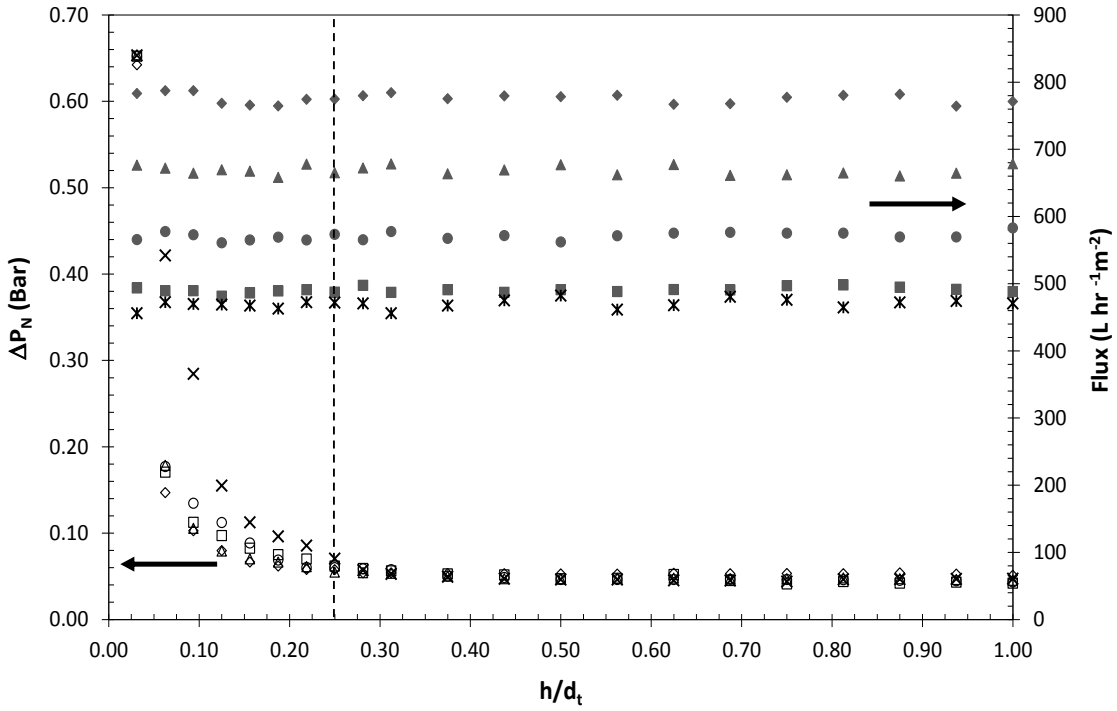

Figure 6.8a: Gauging profiles in duct flow at different duct temperatures, symbols: ✱ 22 ºC, ■ 35 ºC, ● 40 ºC, ▲ 50 ºC, ♦ 60 ºC; (1.00 bar TMP, Re_{duct} = 9815). Open symbols: ΔP_N, solid symbols: permeate flux (d_t = 1 mm).

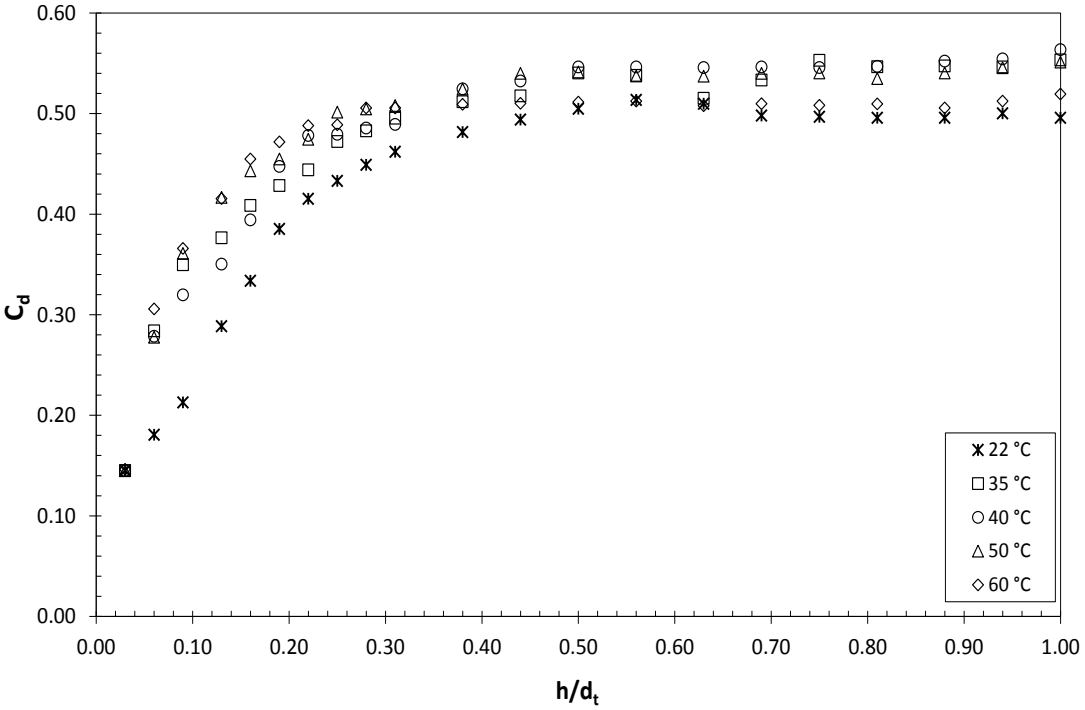

Figure 6.8b: Data re-plotted as C_d vs. h/d_t (d_t = 1mm). Conditions: 1.00 bar TMP, Re_{duct} = 9815.

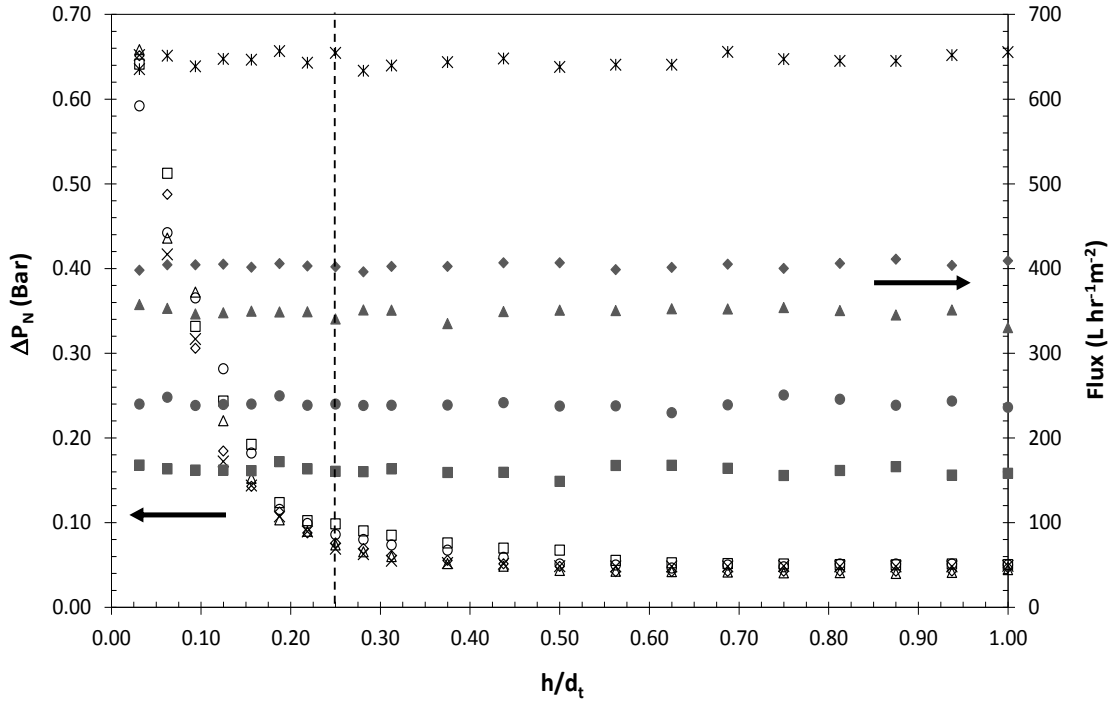

Figure 6.9a: Gauging profiles in duct flow at different TMP, symbols: ■ 0.35 bar, ● 0.55 bar, ▲ 0.80 bar, ♦ 1.00 bar, ∗ 2.00 bar; (22 ºC, Re_{duct} = 9815). Open symbols: ΔP_N, solid symbols: permeate flux (d_t = 1 mm).

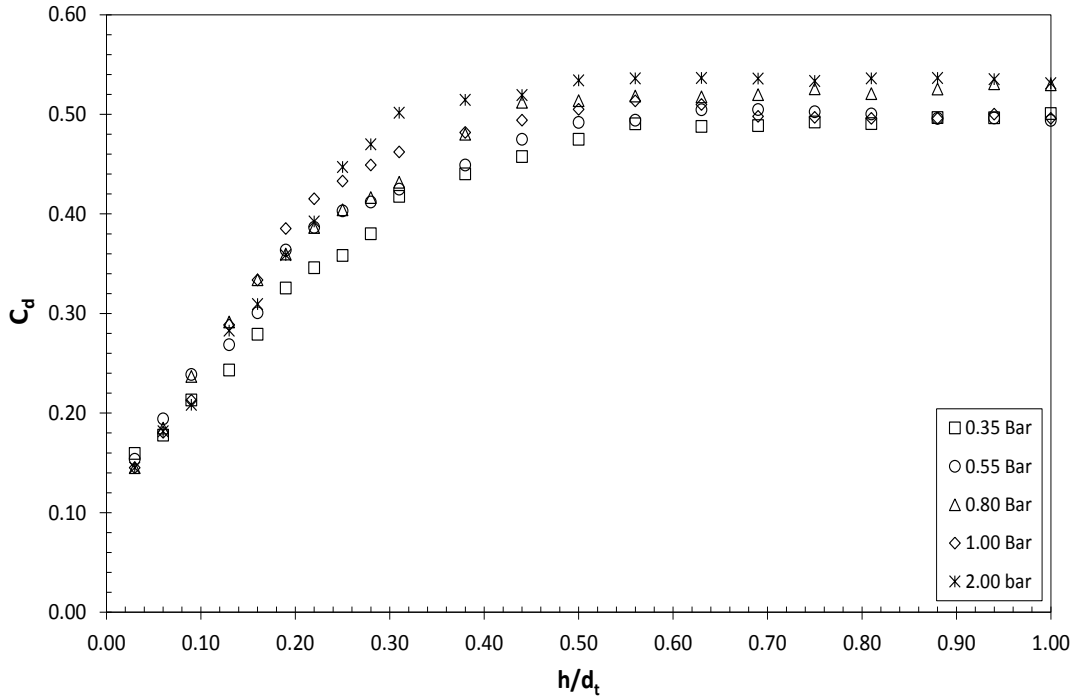

Figure 6.9b: Data re-plotted as C_d vs. h/d_t (d_t = 1 mm). Conditions: 22 ºC, Re_{duct} = 9815.

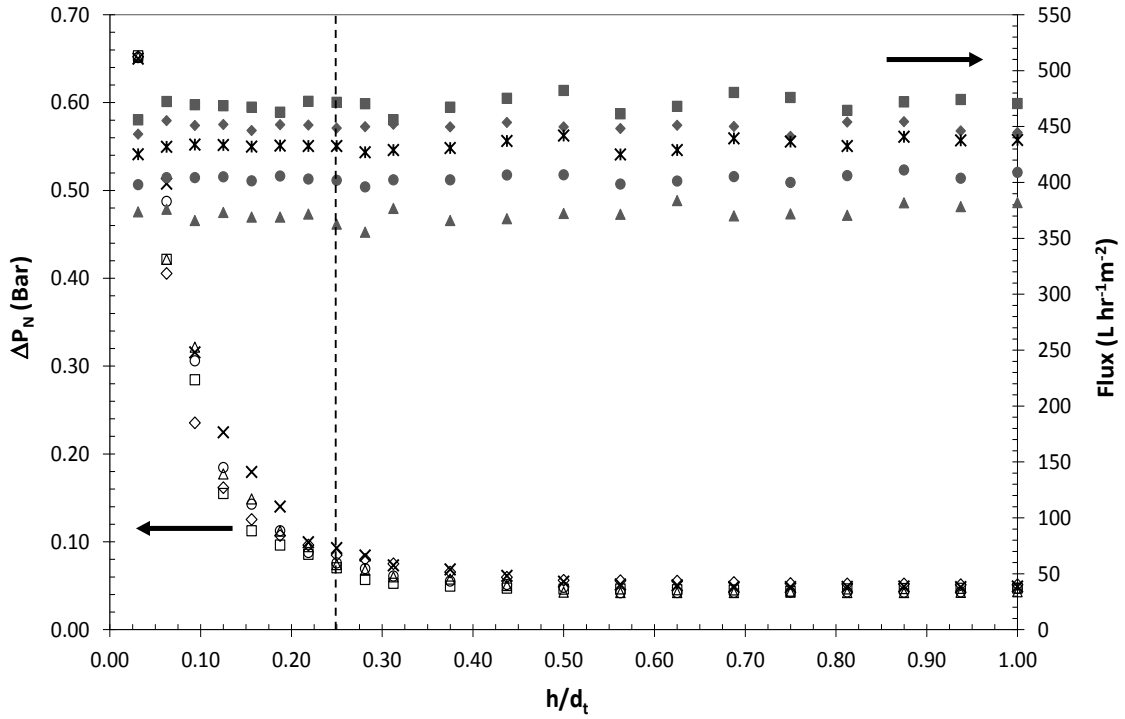

Figure 6.10a: Gauging profiles in duct flow at different duct cross flow velocities. Symbols (Re_{duct} values): ▲ 4000, ● 9815, ✱ 12593, ♦ 13887, ■ 14815; (22 ºC, 1.00 bar TMP). Open symbols: $\Delta P_{N,}$ solid symbols: permeate flux (d_t = 1 mm).

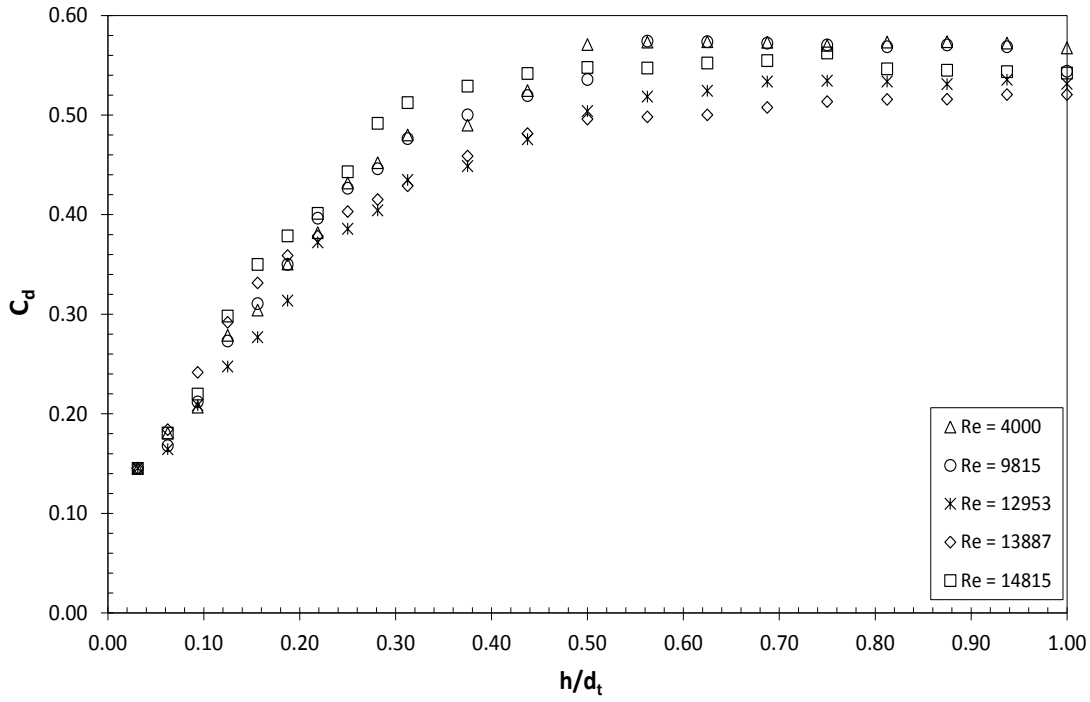

Figure 6.10b: Data re-plotted as C_d vs. h/d_t (d_t = 1 mm). Conditions: 22 ºC, 1.00 bar TMP.

6.3.2. Validation of Technique

The FDG has been validated by carrying out several experiments under the same operating conditions (22 ºC, 0.25 bar TMP, Re_{duct} = 2500, 45 ºBrix molasses). Figure 6.11 shows that there is a slight variation of the three curves but the margin of error is ± 5 µm. This error margin has been deemed acceptable for the reliability of the FDG in this cross flow membrane filtration module.

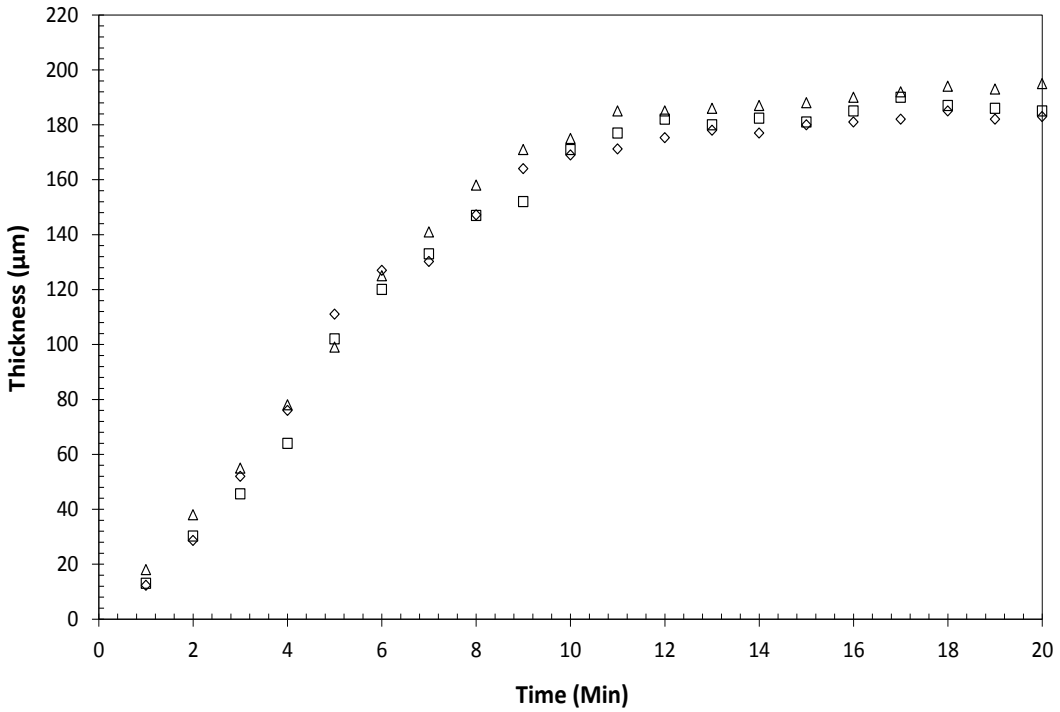

Figure 6.11: Effect of repeat experiments on deposit build up operating under the same conditions. Conditions: 22 ºC, 0.25 bar, Re_{duct} = 2500, 45 ºBrix molasses.

6.3.3. Effect of Operating Conditions

In these experiments, the thickness of cake and the permeate flux during the filtration of molasses were tracked simultaneously. The gauging flow rate, *m*, was maintained at 1.30 gs^{-1} for all differential pressure measurements. To validate the measurement technique, different values of TMP, CFV (Re_{duct}), and concentration were tested to determine the effect on cake thickness measurements. A margin of error of ± 5 µm applies to the thickness measurements.

Analysis of the molasses deposits was performed. The significant internal properties of a fouling layer include porosity and resistance. The porosity of the fouling layer is one of the most fundamental quantities for estimating fouling resistance (Tung *et al*., 2010).

As the FDG allows us to measure the deposit thickness further information can be gathered. The porosity of the deposit can be calculated using the Carman-Kozeny Equation (Equation 6.4) where the approximate size of the particles in the molasses and the permeability of the deposit are used.

$$k = \frac{1}{36 h_k} \frac{d_g^2 \varepsilon^3}{(1-\varepsilon)^2} \qquad 6.4$$

where k is the permeability, h_k is the Kozeny constant (taken as 5 in this case (Hamachi and Mietton-Peuchot,1999; Okamoto *et al.*, 2001)) and d_g the Sauter diameter (calculated as d_g = 10 μm). The development of the deposit porosity as a function of thickness for different TMP, CFV, and concentration are shown in Figures 6.13, 6.16 and 6.19.

The resistance offered by the deposit and the membrane can be calculated with the knowledge of the flux through the molasses deposit and the thickness of the deposit. Assuming the particles are only retained at the surface of the membrane, *i.e.* no pore blockage, and with the knowledge of the membrane resistance of the clean membrane, the resistance of the deposit at any thickness can be calculated. The development of the deposit resistance as a function of thickness for different TMP, CFV, and concentration are shown in Figures 6.14, 6.17 and 6.20.

6.3.3.1. Effect of CFV (Re_{duct})

Figure 6.12 (a) shows the change in deposit thickness and permeate flux as a function of time for different values of CFV. Temperature, TMP and concentration were kept constant (22 ºC, 1.00 bar TMP, 45 ºBrix molasses). In each case, the flux declined rapidly during the initial period, and then decreased more gradually thereafter, to a lower, steady value. This initial behaviour is probably due to the large amount of particulate deposition at the membrane surface, causing pore blockage (Chew *et al.*, 2007; Chen *et al.*, 2004a). During this initial period, the cross flow velocity has little effect on the kinetics of deposit build-up, and only a few particles are swept away as the permeate flux is perpendicular to the tangential flow and controls the deposition process (Hamachi and Mietton-Peuchot, 2001). Increasing CFV makes it possible to reduce

deposit build-up, as the increased flow sweeps the accumulated particles from the membrane surface. Figure 6.12 (b) (data from Figure 6.12 (a) replotted) shows the cake layer thickness and permeate flux as a function of cumulative permeate flow. The thickness of cake layer grew linearly initially for all CFV values examined, but plateaued off thereafter for the higher velocities tested. For the lowest CFV examined (Re_{duct} = 4000) deposit stabilisation had not occurred for the volume of filtrate tested.

Comparing the flux variation and deposit growth simultaneously there are two different stages occurring. During the initial period for all conditions tested there is a severe flux decline whereas the deposit thickness remains between 0 μm and 20 μm. This means that the initial layer is thin but highly resistant to mass transfer (Mendret *et al*., 2009). This could be due to initial in pore blocking. Though in the second stage, the flux decline is more gradual however the deposit thickness develops further from 20 μm to a minimum of 85 μm. Mendret *et al*., (2009) found that the hydraulic resistance of the deposit is not proportional to its thickness.

Figure 6.13 shows the porosity versus deposit thickness at different operating CFV. Increasing the CFV increases the porosity of the deposit, this results from the effect of mass particle sweeping. The higher CFV swept more of the finer particles from the membrane surface resulting in a layer of larger particles. Increasing the CFV reduces the resistance of the deposit (Figure 6.14), this results from the shearing effect imposed by the bulk flow. The higher CFV swept more of the finer particles from the membrane surface, resulting in a layer of larger particles.

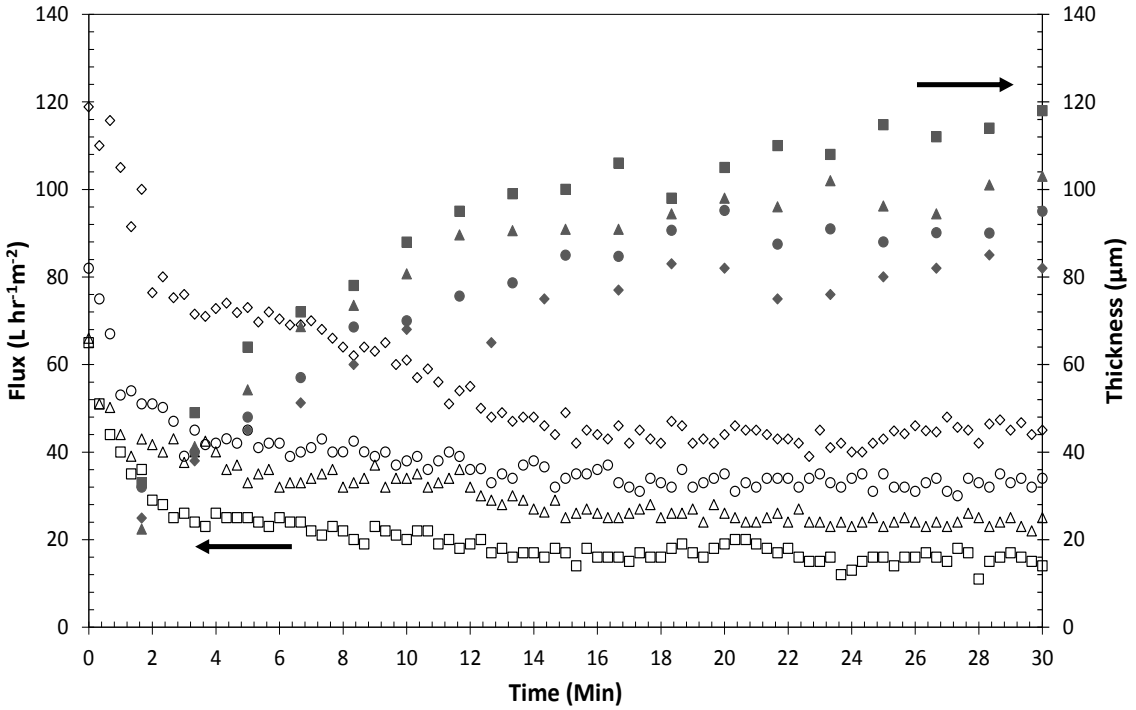

Figure 6.12a: Effect of cross flow velocity on deposit build-up and permeate flux as a function of time. Symbols (Re_{duct}): ■ 4000, ▲ 9815, ● 13887, ♦ 14815; solid symbols: cake thickness, open symbols: permeate flux. Conditions: 22 ºC, 1.00 bar TMP, 45 ºBrix molasses.

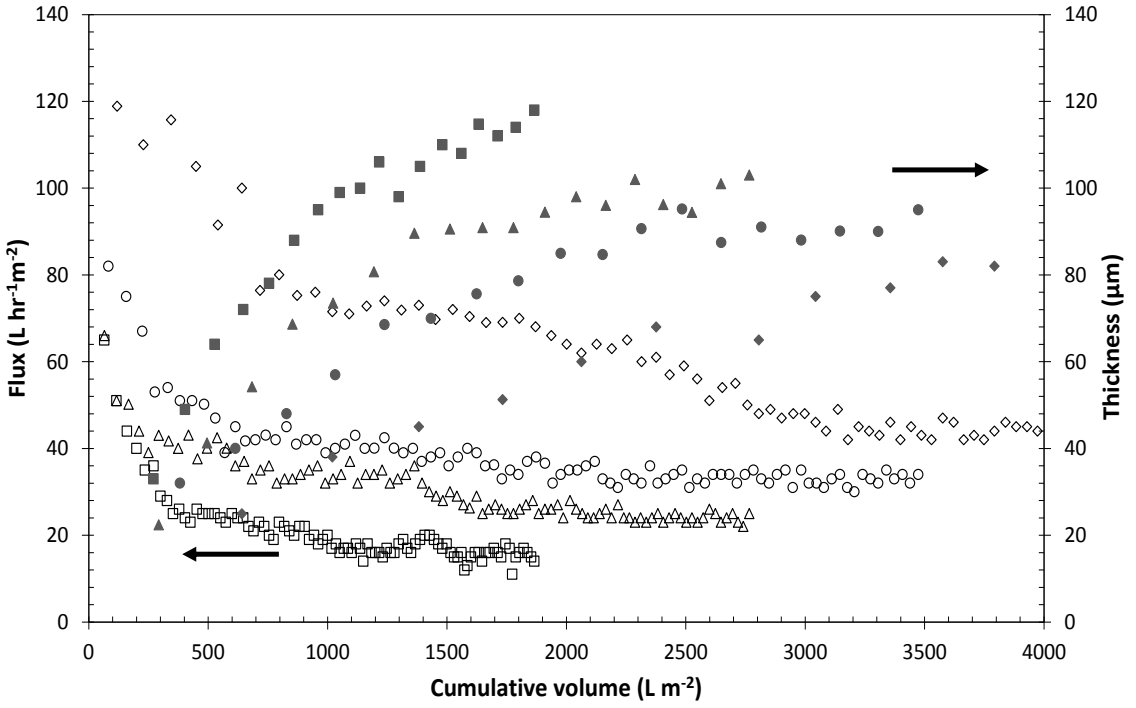

Figure 6.12b: Effect of cross flow velocity on deposit build-up and permeate flux as a function of cumulative permeate flow. Symbols (Re_{duct}): ■ 4000, ▲ 9815, ● 13887, ▼ 14815; solid symbols: cake thickness, open symbols: permeate flux. Conditions: 22 ºC, 1.00 bar TMP, 45 ºBrix molasses.

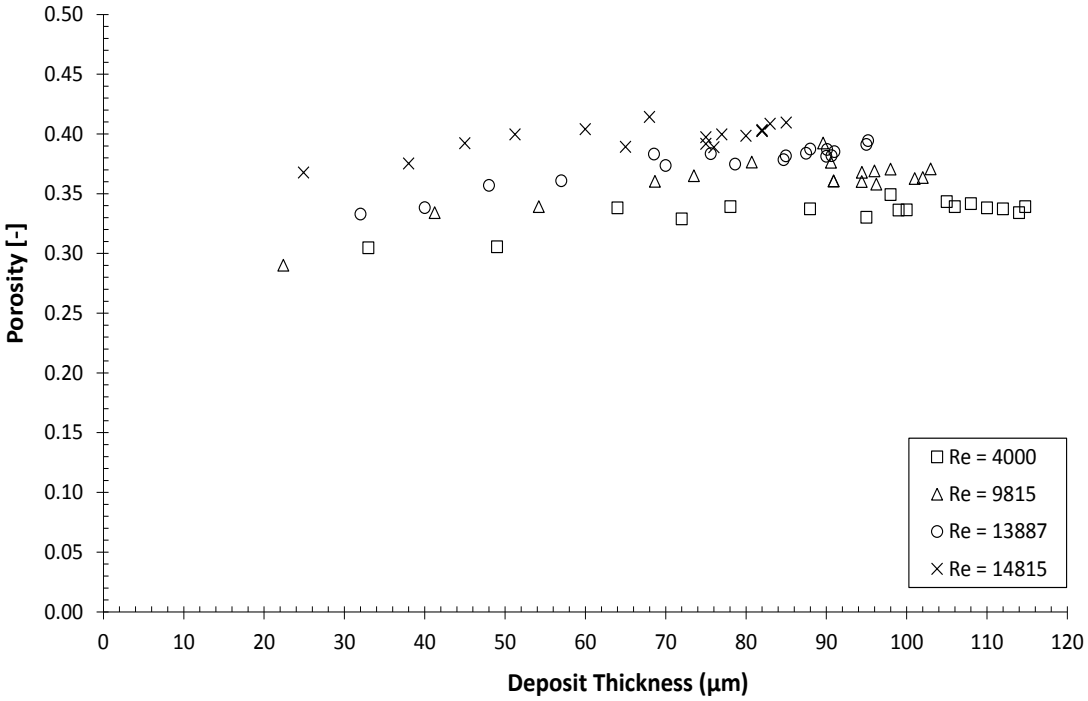

Figure 6.13: Deposit porosity as a function of deposit thickness for varying Re_{duct}. Conditions: 22 ºC, 1.00 bar TMP, 45 ºBrix molasses.

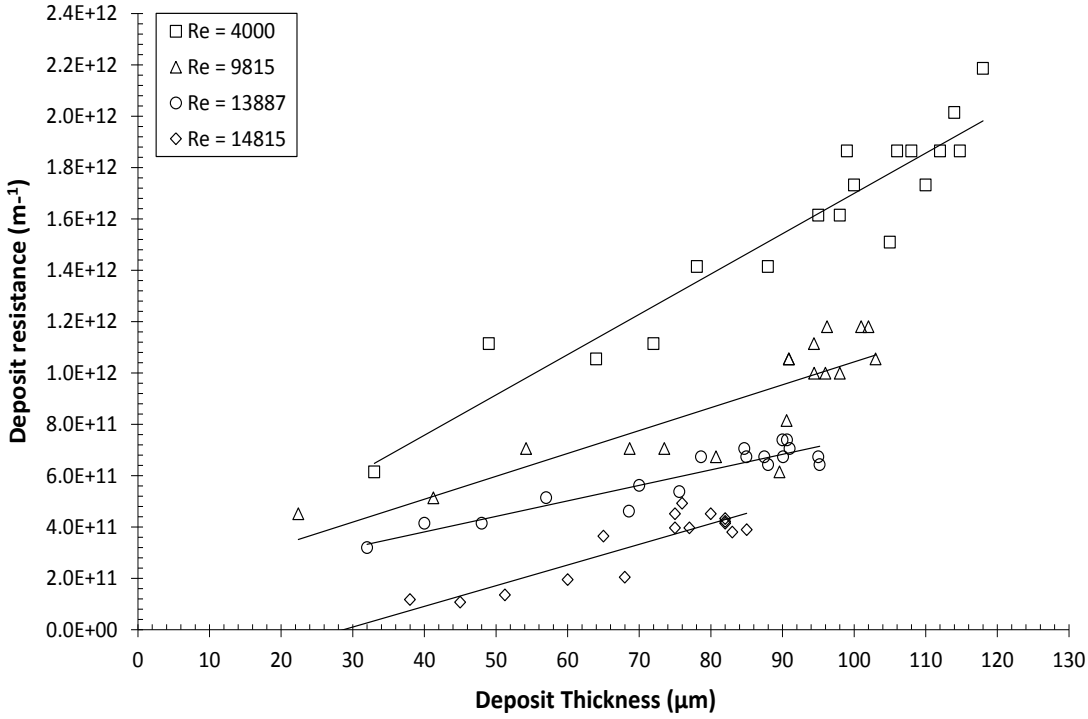

Figure 6.14: Deposit resistance as a function of deposit thickness for varying Re_{duct}. Conditions: 22 ºC, 1.00 bar TMP, 45 ºBrix molasses.

6.3.3.2. Effect of TMP

Figure 6.15 (a) shows the evolution of deposit thickness and permeate flux at a constant temperature, CFV and concentration (22 ºC, Re_{duct} = 9815, 45 ºBrix molasses). The increase in pressure results in an increase in deposit thickness. This deposit growth could be caused by compaction of the membrane, leaving the denser structure with smaller pores and deformation of the pore geometry (Kallioinen *et al.,* 2007), along with compaction of the preliminary fouling layer. The higher fluxes at the increasing pressure will also result in more particles being captured at the membrane surface. Hamachi and Mietton-Peuchot (1999) found that the deposit structure should evolve according to TMP and the effects are more apparent when the filtration time is lengthened. Even though the deposit thickness grows with increased pressure, the changes in flux remain almost the same and tend towards similar steady state values. Figure 6.15 (b) (data from Figure 6.15 (a) replotted) shows cake layer thickness and permeate flux as a function of cumulative permeate flow. The thickness of the cake layers initially showed similar linear growth with increasing cumulative permeate flow for all TMP values tested. However, after 1000 L m^{-2} cake thicknesses became differentiated, with higher pressures resulting in greater thicknesses for a given value of the cumulative permeate flow. Thicknesses also grew less strongly as a function of cumulative permeate flow in the region > 1000 L m^{-2}. This could be the result of a sweeping effect caused by operating in the turbulent flow region.

Figure 6.16 shows the porosity versus deposit thickness at different operating TMP. The deposit porosity decreased with increasing TMP. Tung *et al*., (2010) found that the decreased fouling layer porosity is primarily due to the rearrangement of particles and the compression of the fouling layer, which are caused by frictional drag from fluid and by the compounded foulant mass of deposited particles.

The increase of deposit resistance with TMP, as shown in Figure 6.17, indicates there is some degree of deposit compaction. That the fouling layers are compressible, that is, they become more compact as the pressure forces increases. For a fixed thickness, the deposit resistance does vary linearly with TMP. At a thickness of 55 μm at 0.35 bar the deposit resistance was 10 % as that for 2.00 bar.

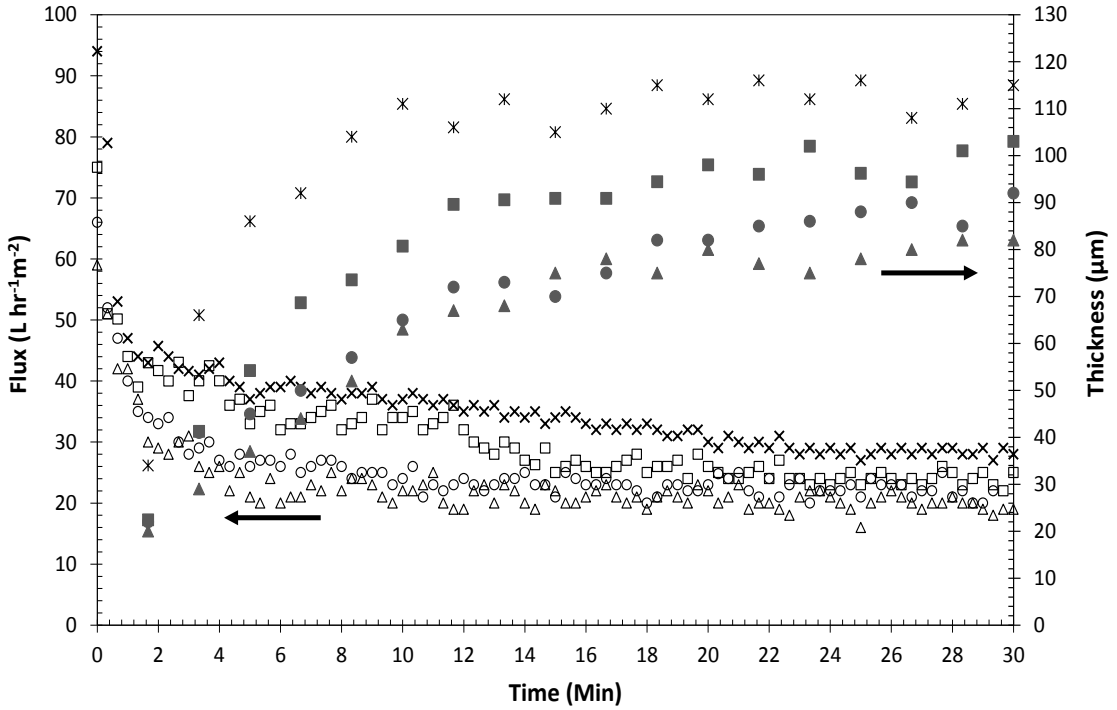

Figure 6.15a: Effect of TMP on deposit build-up and permeate flux as (a) function of time and (b) function of cumulative permeate flow. Symbols (TMP): ⁎ 2.00 bar, ■ 1.00 bar, ● 0.55 bar, ▲ 0.35 bar; solid symbols: cake layer thickness, open symbols: permeate flux. Conditions: 22 ºC, Re_{duct} = 9815, 45 ºBrix molasses.

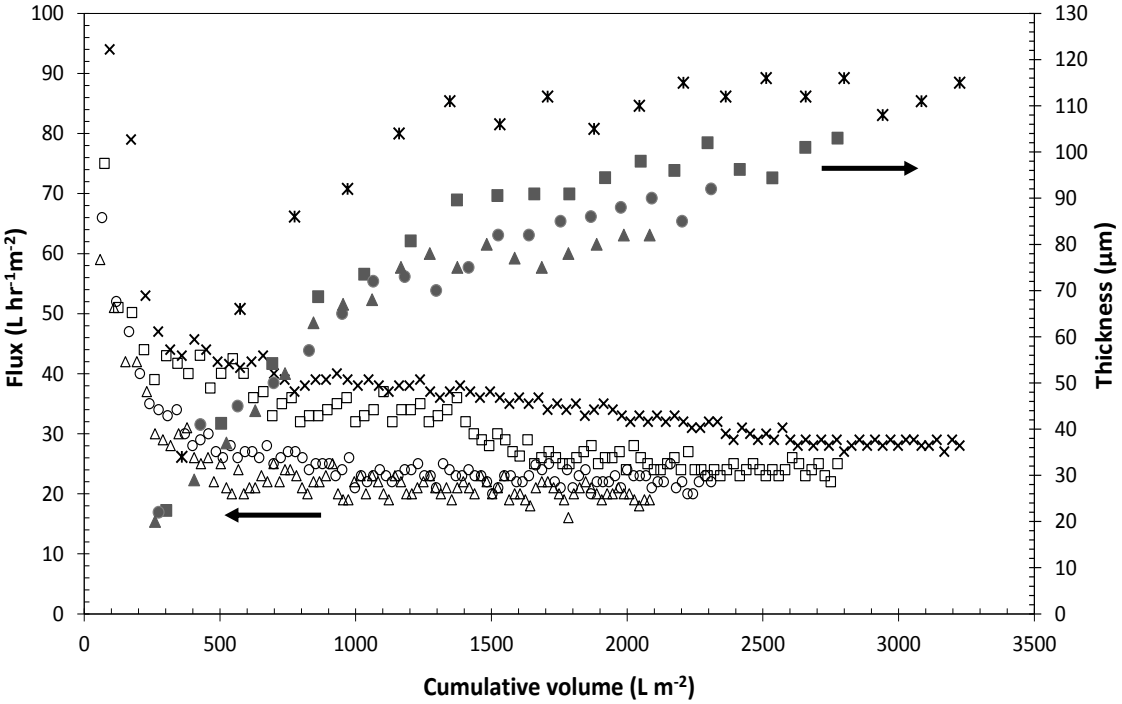

Figure 6.15b: Effect of TMP on deposit build-up and permeate flux as a function of cumulative permeate flow. Symbols (TMP): ⁎ 2.00 bar, ■ 1.00 bar, ● 0.55 bar, ▲ 0.35 bar; solid symbols: cake layer thickness, open symbols: permeate flux. Conditions: 22 ºC, Re_{duct} = 9815, 45 ºBrix molasses.

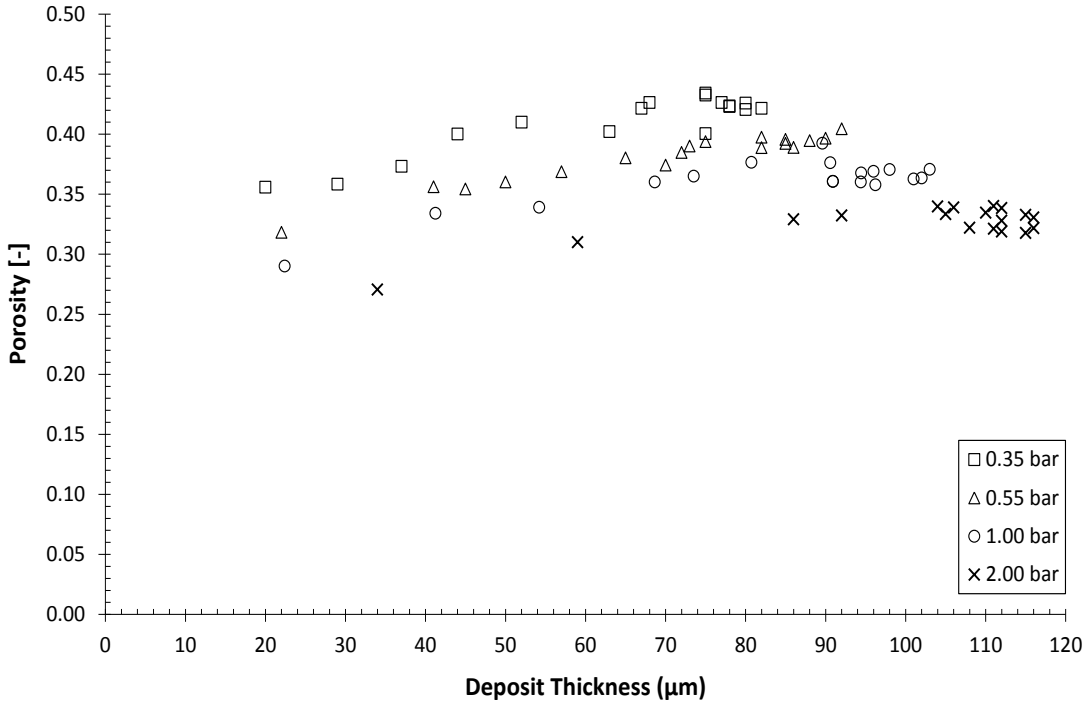

Figure 6.16: Deposit porosity as a function of deposit thickness for varying TMP. Conditions: 22 ºC, Re_{duct} = 9815, 45 ºBrix molasses.

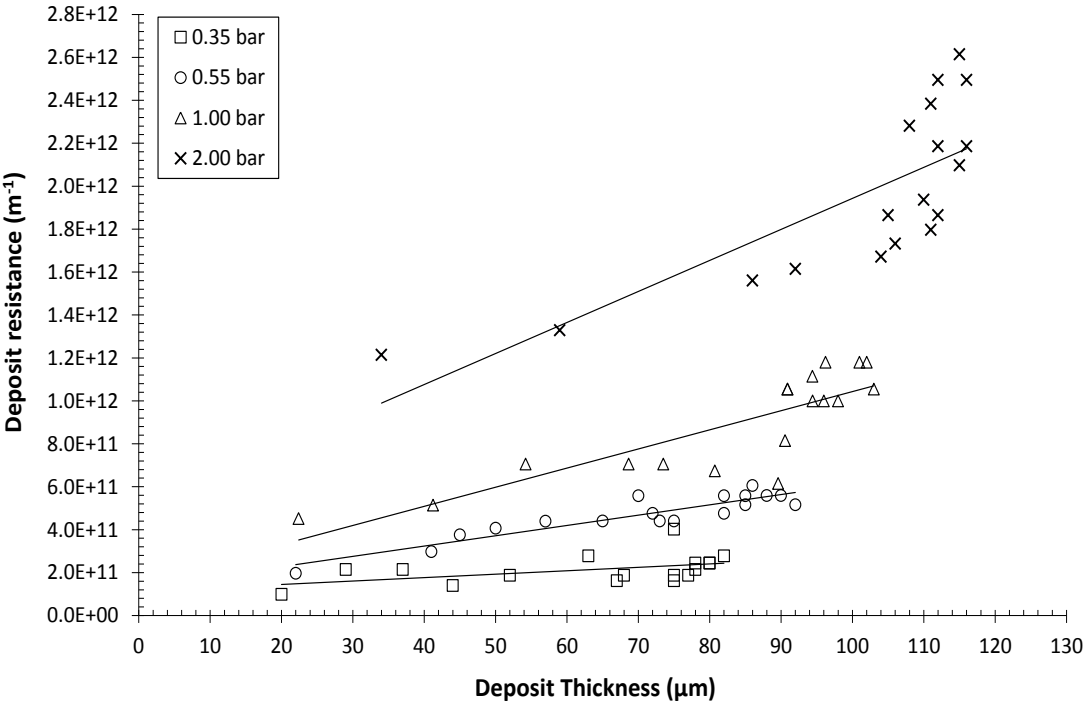

Figure 6.17: Deposit resistance as a function of deposit thickness for varying TMP. Conditions: 22 ºC, Re_{duct} = 9815, 45 ºBrix molasses.

6.3.3.3. Effect of Concentration

Figure 6.18 (a) shows the evolution of deposit thickness and permeate flux at a constant temperature, TMP, and CFV (22 ºC, 1.00 bar TMP, Re_{duct} = 9815). The increase in concentration results in an increase in deposit thickness. The lower concentration of 36 ºBrix reaches a more stable steady state deposit thickness at 15 minutes. The deposit layer continues to grow somewhat for the 45 ºBrix and 52 ºBrix after 30 minutes of molasses filtration. Though whilst filtering at 22 ºC the variation of concentration did not have a substantial effect of the fouling flux. Figure 6.18 (b) (data from Figure 6.18 (a) replotted) shows cake layer thickness and permeate flux as a function of cumulative permeate flow. The trend for all concentrations tested was very similar. Comparing the flux variation and deposit growth simultaneously for each concentration there are two different stages occurring. An initial thinner layer whereby there is a high degree of flux decline (< 5 min) and a thicker second layer with only a gradual flux decline. Mendret *et al*., (2007) and Mendret *et al*., (2009) observed that the first layer of fouling was thin and incompressible whilst the top layer structure was more open and compressible. Whilst Marselina *et al*., (2009) found using the direct observation (DO) technique that the bottom part of the fouling layer became denser than the upper part of the fouling layer due to the fouling deposition throughout the filtration period. These findings relate to the work performed here.

Figure 6.19 shows the porosity versus deposit thickness at different operating concentrations. The porosity of the deposit layer increases slightly with increasing concentration. For all concentrations tested the porosity of the deposit layer also increases slightly with increasing deposit thickness. Previous studies have shown that a porosity gradient through the cake thickness exists and the deposit structure is different at different stages in a fouling run (Hwang *et al.*, 1996; Tarabara *et al*., 2004; Mendret *et al*., 2009). Mendret *et al*., 2009 theorised that the porosity gradient could be associated with particle size distribution, whereby the smallest particles have the greatest effect on filtration performance.

Increasing the concentration decreases the resistance of the deposit slightly (Figure 6.20). The data in Figure 6.20 also displays highly non-linear shape; where there are increases in resistance with only small increases in thickness. This could be explained

by the cake layer reaching a terminal thickness but the gaps in the cake being filled by smaller particles.

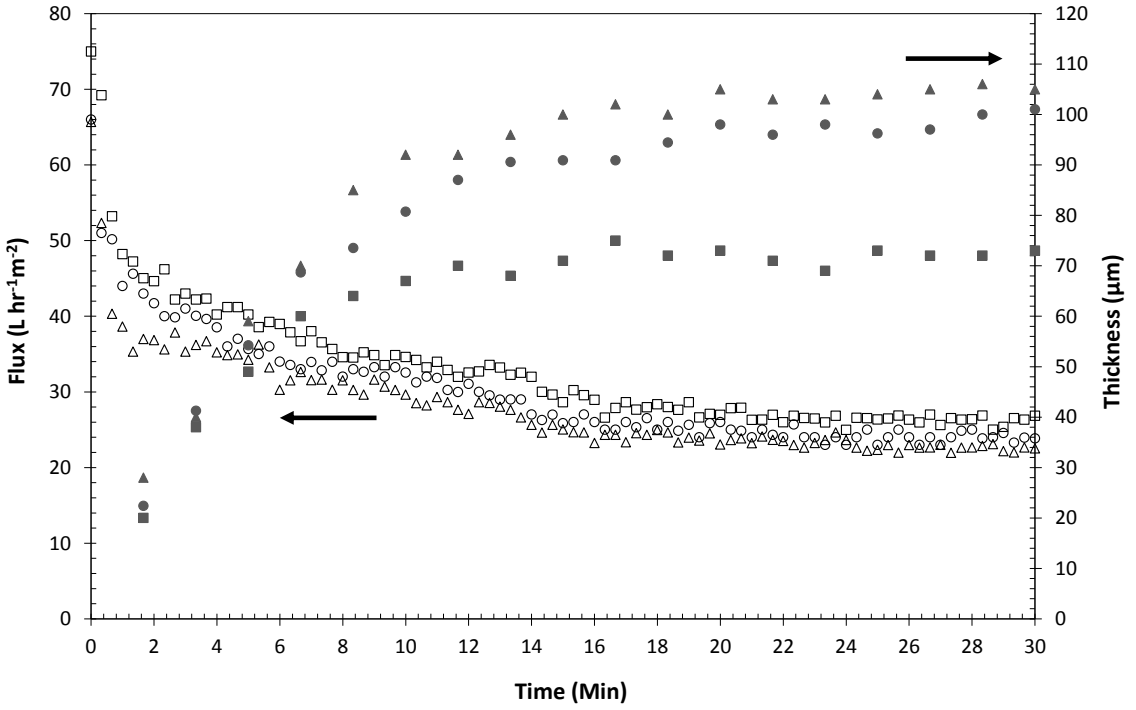

Figure 6.18a: Effect of concentration on deposit build-up and permeate flux as a function of time. Symbols (Brix): ■ 35º, ● 45º, ▲ 52º; solid symbols: cake layer thickness, open symbols: permeate flux. Conditions: 22 ºC, 1.00 bar TMP, Re_{duct} = 9815.

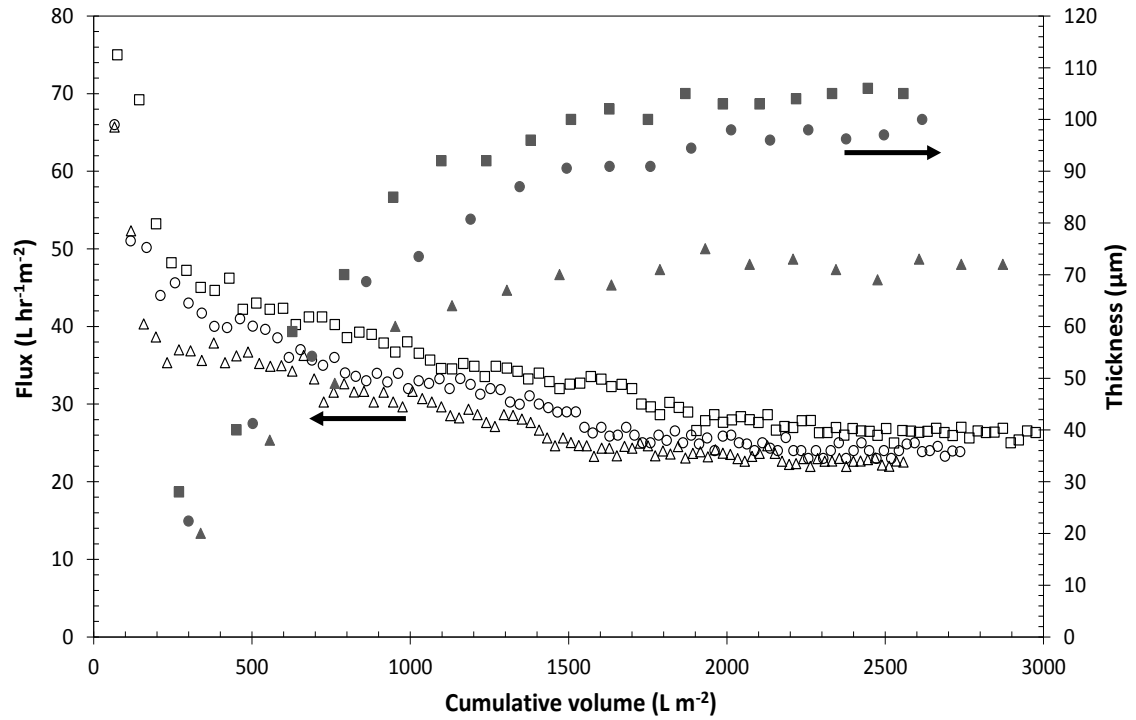

Figure 6.18b: Effect of concentration on deposit build-up and permeate flux as a function of cumulative permeate flow. Symbols (Brix): ■ 35º, ● 45º, ▲ 52º; solid symbols: cake layer thickness, open symbols: permeate flux. Conditions: 22 ºC, 1.00 bar TMP, Re_{duct} = 9815.

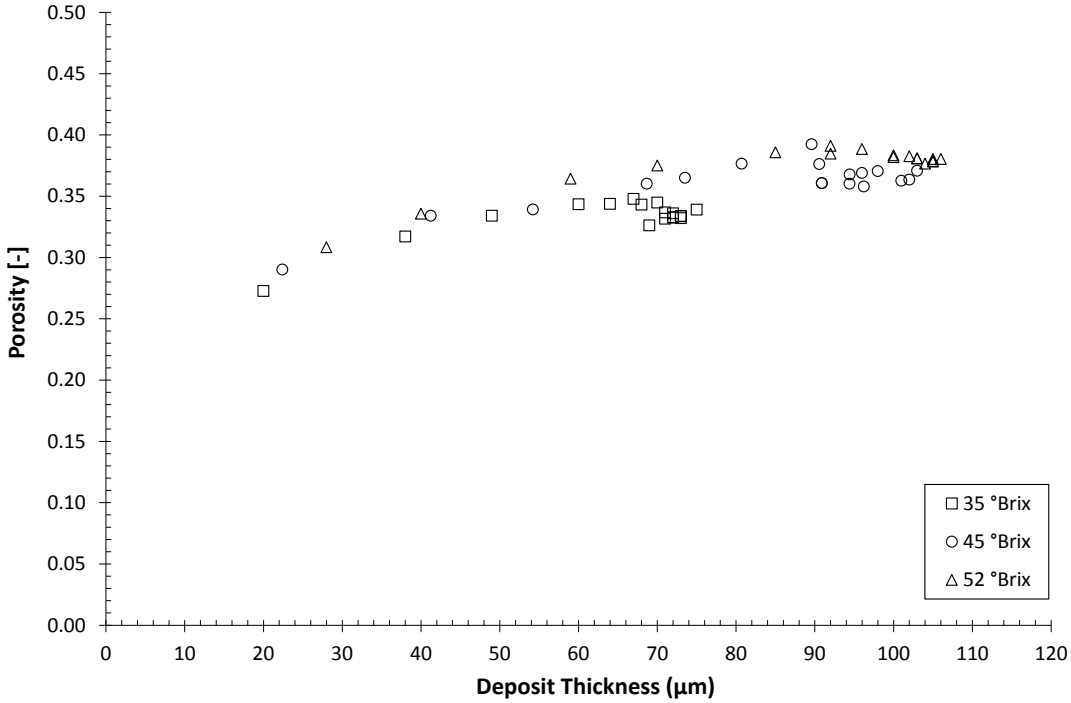

Figure 6.19: Deposit porosity as a function of deposit thickness for varying concentration. Conditions: 22 ºC, 1.00 bar TMP, Re_{duct} = 9815, 45 ºBrix molasses.

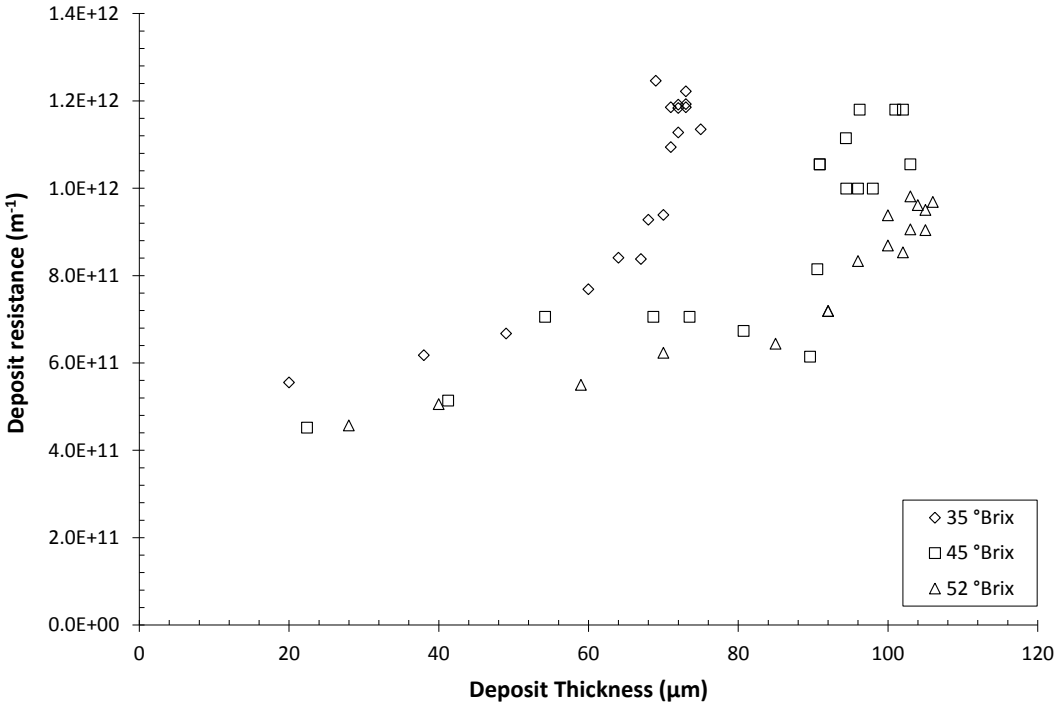

Figure 6.20: Deposit resistance as a function of deposit thickness for varying concentrations. Conditions: 22 ºC, 1.00 bar TMP, Re_{duct} = 9815, 45 ºBrix molasses.

6.3.4. Same Membrane Operating Conditions

Figure 6.21 shows the change in deposit thickness and permeate flux when varying CFV during one filtration run. Temperature, TMP and concentration were kept constant (60 ºC, 1.00 bar TMP, 45 ºBrix molasses). The relevant calibration charts for the conditions tested were performed before filtration experiments were undertaken. The 1.5 µm Ps*f* membrane was filtered at a low CFV (0.55 ms^{-1} (Re_{duct} = 4000)) for 30 minutes until a steady state flux and was achieved. The CFV was then increased to 1.89 ms^{-1} (Re_{duct} = 13887) for a further 30 minutes. The steady state thickness after 30 minutes was ~129 µm, which decreased rapidly to ~103 µm. This decrease in deposit thickness and increase in flux (~23 L m^{-2} hr^{-1} to ~36 L m^{-2} hr^{-1}) shows that the deposit is reversible (Hamachi and Mietton-Peuchot, 2002). The steady state thickness value when increased to a CFV of 1.89 ms^{-1} was a similar value to the experiment when performed with a constant CFV of 1.89 ms^{-1} (~103 µm). The steady state flux values were slightly lower than when performed at constant CFV.

The experiment in Figure 6.21 was performed at 60 ºC whereas the experiment in Figure 6.12a was performed at 22 ºC. The raised temperature increased the deposit thickness by ~15 µm at 1.00 bar TMP, 4000 Re_{duct}, and 45 ºBrix molasses. This increase in thickness could be explained by the swelling of particles at the higher temperature. This swelling of particles offer a lesser resistance thereby causing an increase in filtrate flux (Hamachi and Mietton-Peuchot, 2001).

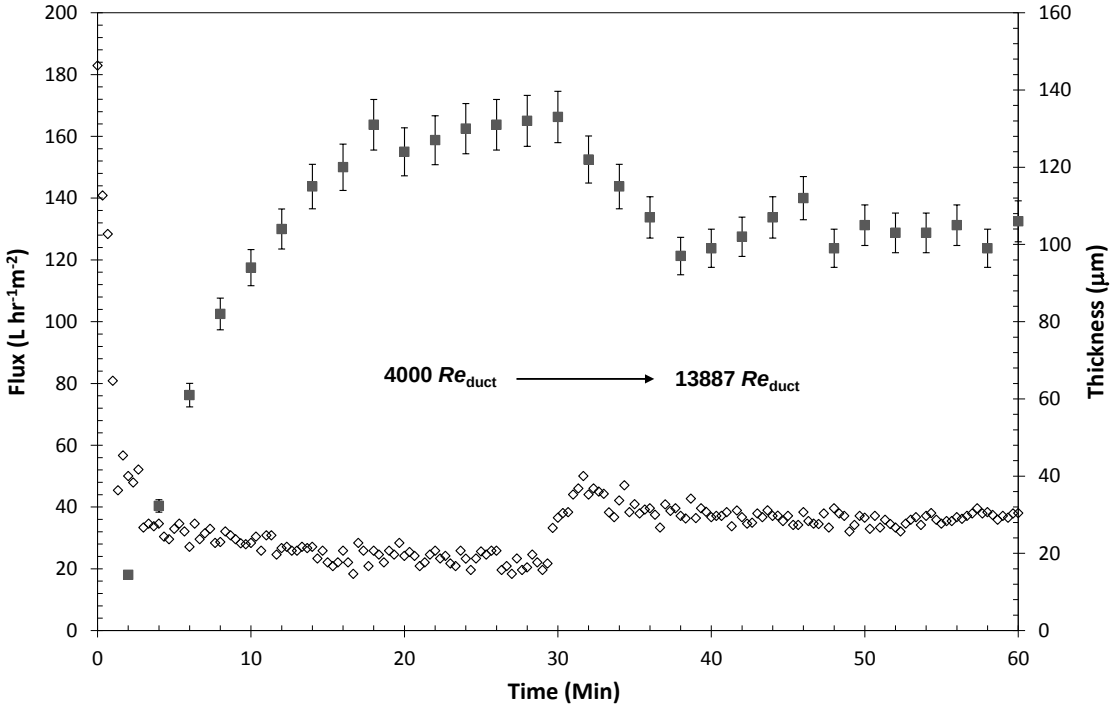

Figure 6.21: Effect of increasing CFV on deposit build-up and permeate flux. Conditions: 60 ºC, 1.00 bar TMP, 45 ºBrix molasses.

Figure 6.22 shows the development in deposit thickness and permeate flux when varying TMP during one filtration run. Temperature, CFV and concentration were kept constant (60 ºC, 1.89 ms^{-1} CFV, 45 ºBrix molasses). The 1.5 µm Ps*f* membrane was filtered at a low TMP (0.50 bar) for 35 minutes until a steady state flux and thickness layer was achieved. The TMP was then increased to 1.00 bar for 20 minutes, then a further 20 minutes at 2.00 bar. The steady state deposit thickness after 35 minutes was ~78 µm, which increased to ~102 µm at 1.00 bar. Followed by a further increase to ~110µm at 2.00 bar. The deposit thickness reached steady state quicker as the TMP increased. This could be explained by the shearing effect of the cross flow having less of an impact at the increased pressure. The fouling layer may be getting further compressed with each pressure step.

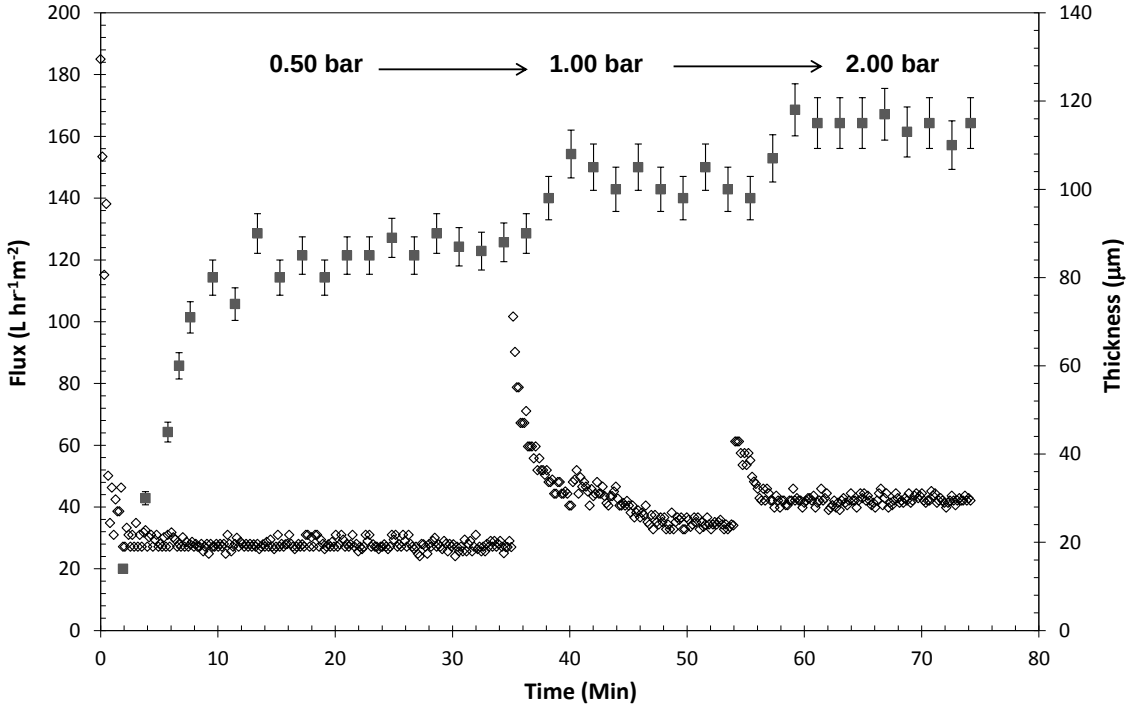

Figure 6.22: Effect of increasing TMP on deposit build-up and permeate flux. Conditions: 60 ºC, 1.89 ms^{-1} CFV, 45 ºBrix molasses.

6.3.5. Cake Layer Removal

FDG was used to investigate the amount of fouling deposit (cake layer) and the subsequent removal occurring during cleaning. The relevant calibration charts for the conditions tested were performed before filtration experiments were undertaken. Molasses was fouled using 1.5 µm Ps*f* membranes at constant conditions (60 ºC, 2.00 bar TMP, 1.89 ms^{-1} CFV, 45 ºBrix molasses). For all cleaning experiments, the flux data were normalised, with the initial pure water flux (PWF) taken as 1.0, and the other data scaled accordingly for each protocol. The average initial PWF for the 1.5 µm Ps*f* membranes was 918 L m^{-2} hr^{-1}. For all cleaning experiments, the molasses feed was filtered until it reached the same normalised steady state flux (error ± 6 %). The steady state flux was approximately 7 % of the initial flux value after 60 minutes. Asymptotic fouling thicknesses of *ca.* 105 µm were developed after 30 minutes of filtration. The rinsing stage before cleaning was performed at 22 ºC, 1.00 bar TMP, and 1.89 ms^{-1} CFV for 10 min.

The molasses fouled membranes were cleaned with either 0.10 wt. % NaOH (alkali) or 0.10 wt. % citric acid (acid) (50 ºC, 1.00 bar TMP, 1.89 ms^{-1} CFV for 30 min). Two possible methods of FDG operation during chemical cleaning were considered: (i)

Method 1 - permeate side open with recycle back to the feed tank, and (ii) Method 2 (also with recycle to the feed tank) - permeate side closed during the first part of the protocol. Method 1 generates flux data, allowing the calculation of membrane resistances during the cleaning period. In Method 2 cleaning took place with the permeate line closed for 15 minutes and then opened for the final 15 minutes. Figures 6.23 and 6.24 show the comparison of alkali and acid cleaning with the permeate line open (PLO) or closed (PLC) on the removal of the cake layer after fouling with 45 ºBrix molasses. Removal of the deposits can be facilitated by two different but synergistic mechanisms; (i) shearing effects created by the flow of cleaning agent and (ii) chemical dissolution of the deposits (Bansal *et al*., 2006).

The cleaning efficiency with the permeate side open was found to be lower than when it was closed. This was also reported by Bartlett (1998) when cleaning proteinaceous deposits from MF membranes. This phenomena is also regularly observed in industry for cleaning tubular ceramics - hence the common practice of ensuring that the first stage of any membrane cleaning process be carried out with the permeate line closed, to rinse off deposits rather than force them into the structure, an outcome which is possible when cleaning with the permeate line open.

For all conditions tested the flux increased within the first few minutes of chemical cleaning. After this rise the cleaning flux decreased slightly for the remaining time. This rise in flux could be due to the removal of the loosely bound fouling material from the cake layer, whereas the decrease in flux thereafter could be associated with the swelling of in-pore fouling. Bartlett *et al*. (1995) and Popović *et al*. (2009) also reported this decreasing trend in flux, stating that it could be associated with the presence of more tightly bound deposits within the pores undergoing morphological changes (particularly swelling) during the cleaning. This process was modelled by Bird & Bartlett (2002), in terms of the unsteady state hydraulic resistance variation of cake and in-pore foulants.

Figures 6.23 and 6.24 also show that during the rinsing stage of the filtration process *ca.* 65 % of the cake layer is removed by the application of water alone. However, the removal of *ca.* 65 % of cake layer only leads to a PWF recovery of *ca.* 10 %, which indicates that the bulk of the resistance to permeate flow, and much of the fouling is

likely to be in-pore, and not removed by water rinsing. The role of rinsing in preparing the membrane for the subsequent chemical cleaning step is critically important, as the removal of as much of the deposited layer as possible during rinsing can maximise the efficiency of the cleaning process in terms of time and cleaning agent reduction (Matzinos and Álvarez, 2002).

A further experiment was performed (Figure 6.25) to evaluate if it was possible to remove the cake layer completely and restore the PWF values by rinsing with water only at 22 ºC. Marselina *et al*., (2009) found that the particles that deposited in the upper part of the fouling layer were weakly attached to the rest of the cake layer during the filtration due to the constant cross flow shear. The rinsing efficiency achieved was less than 15 % in terms of flux recovery and chemical cleaning was still required. Nevertheless, rinsing did remove 72 % (PLO) and 86 % (PLC) of the molasses cake layer after 40 minutes. Rinsing with the permeate line open lead to an asymptotic deposit thickness of *ca*. 25 μm after 40 minutes of rinsing. By comparison, rinsing with the permeate line closed lead to a deposit thickness of 15 μm after 40 minutes of rinsing. This thickness value was still decreasing with time, indicating that further experiments are required to determine whether complete removal of the deposit may be possible by water rinsing alone, if sufficient time is allowed.

Figure 6.26 compares rinsing with water only at 22 ºC and 60 ºC with the PLO for 40 minutes. The rinsing at 60 ºC removed the entire cake layer after 30 minutes. However, this complete removal of cake layer only recovered 27 % of the PWF flux. The membrane rinsed with 22 ºC water had an increased membrane resistance after fouling and rinsing (R_m before = 4.00 x 10^{11} m^{-1}, after = 2.47 x 10^{12} m^{-1}) compared to the 60 ºC rinsed membrane (R_m before = 3.94 x 10^{11} m^{-1}, after = 1.48 x 10^{12} m^{-1}). This confirms there is a high degree of pore blockage not removed when rinsing with water alone.

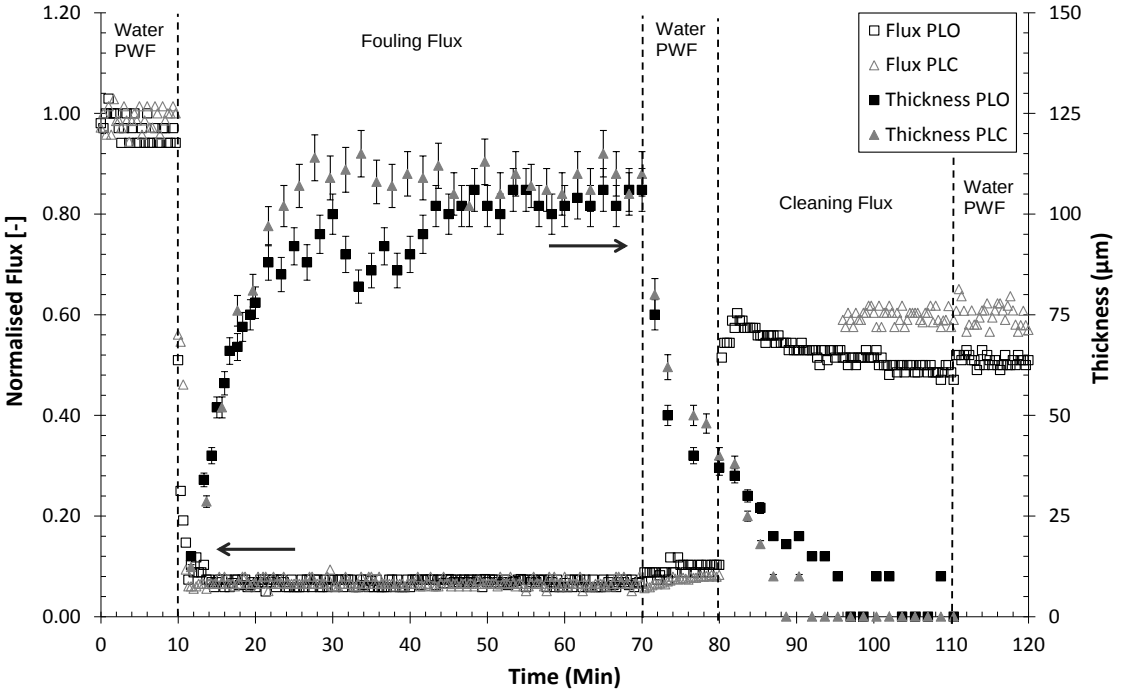

Figure 6.23: Comparison of 0.10 wt. % NaOH cleaning with the permeate line open (PLO) or closed (PLC) during removal of the cake layer following fouling with 45 ºBrix molasses using 1.5 µm Ps*f* membranes. Open symbols: flux, solid symbols: thickness. Average initial flux; PLO: 894 L m^{-2} hr^{-1}, PLC: 925 L m^{-2} hr^{-1}. Fouling temperature: 60 ºC, cleaning agent temperature: 50 ºC.

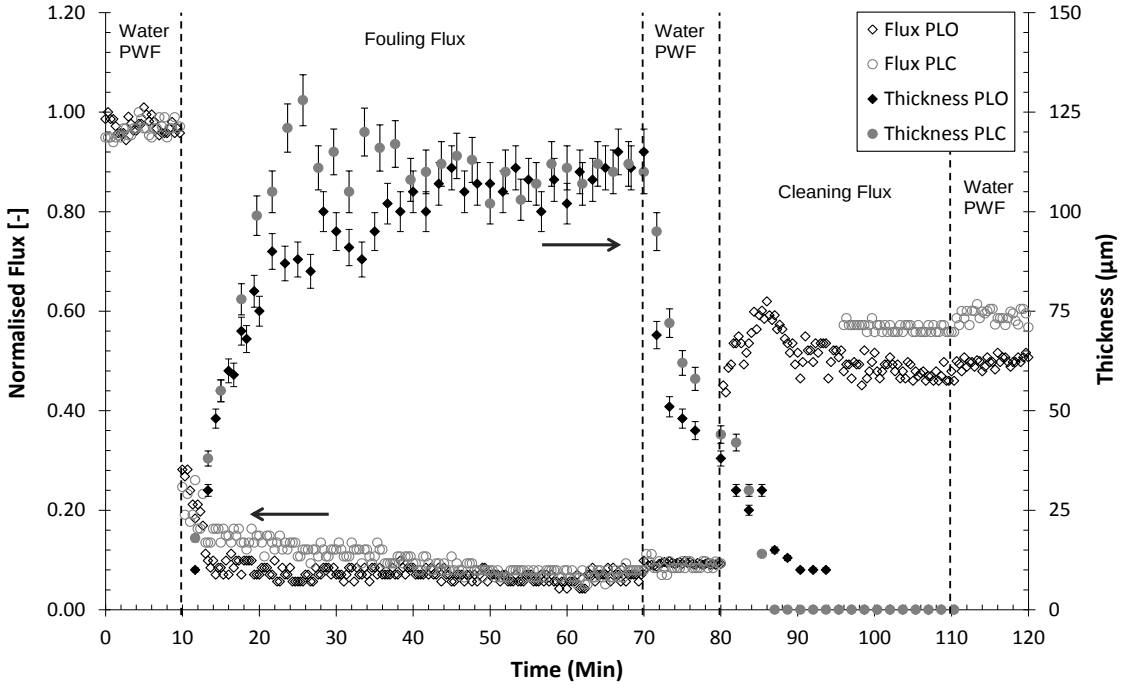

Figure 6.24: Comparison of 0.10 wt.% citric acid cleaning with the permeate line open (PLO) or closed (PLC) during removal of the cake layer following fouling with 45 ºBrix molasses using 1.5 µm Ps*f* membranes. Open symbols: flux, solid symbols: thickness. Average initial flux; PLO: 918 L m^{-2} hr^{-1}, PLC: 927 L m^{-2} hr^{-1}. Fouling temperature: 60 ºC, cleaning agent temperature 50 ºC.

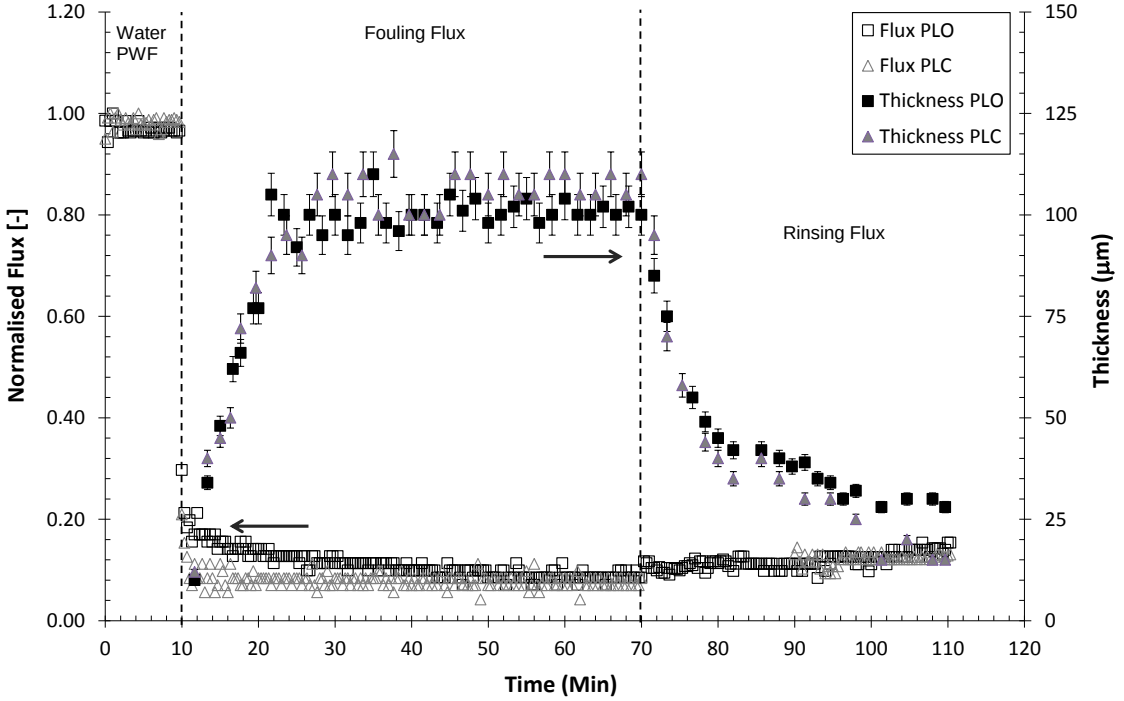

Figure 6.25: Effect of permeate line open or closed during rinsing with water alone on removal of the cake layer formed after fouling with 45 ºBrix molasses using 1.5 µm Ps*f* membranes. Open symbols: flux, solid symbols: thickness. Average initial flux; PLO: 913 L m^{-2} hr^{-1}, PLC: 928 L m^{-2} hr^{-1}. Fouling temperature: 60 ºC, rinsing temperature: 22 ºC.

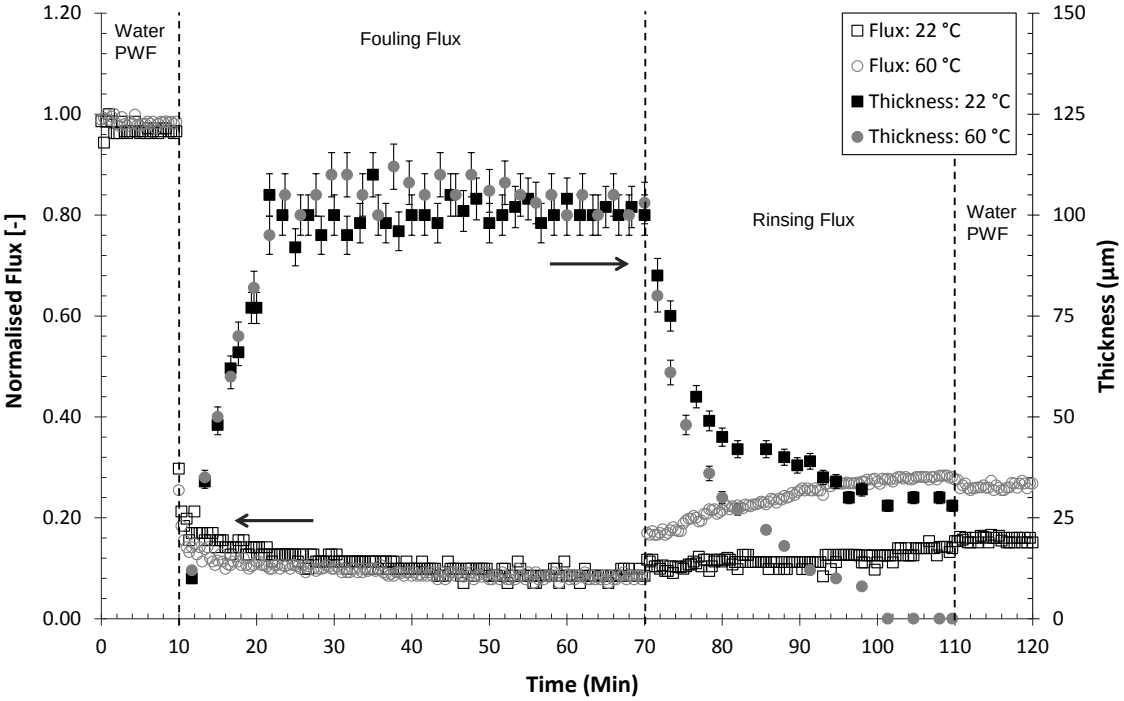

Figure 6.26: Effect of rinsing temperature with water alone on removal of the cake layer formed after fouling with 45 ºBrix molasses using 1.5 µm Ps*f* membranes. Open symbols: flux, solid symbols: thickness. Average initial flux; 22 ºC: 913 L m^{-2} hr^{-1}, 60 ºC: 922 L m^{-2} hr^{-1}. Fouling temperature: 60 ºC.

6.3.6. Fouling Properties after Cleaning

Figure 6.27 shows the development of deposit thickness and permeate flux at constant conditions (60 ºC, 2.00 bar TMP, 1.89 ms^{-1} CFV (Re_{duct} = 13887), 45 ºBrix molasses) over five molasses filtration cycles. The initial PWF for the 1.5 µm Ps*f* membrane for cycle one was 903 L m^{-2} hr^{-1}. The flux data was normalised, with the initial PWF taken as 1.0, and the other data scaled accordingly. The 1.5 µm Ps*f* membrane was cleaned between cycles using the following conditions: 0.10 wt. % NaOH followed by 0.10 wt. % citric acid (50 ºC, 1.00 bar TMP, 1.89 ms^{-1} CFV for 30 min). The rinsing stage before cleaning was performed at 22 ºC, 1.00 bar TMP, and 1.89 ms^{-1} CFV for 10 min.

The fouling filtration fluxes decrease with increasing fouling cycles. This corresponds to the increase in deposit thickness as cycle's progress. The deposit thickness after five cycles was *ca.* 136 µm, which was a 29 % increase over cycle 1 (~106 µm). The deposit thickness increased at a greater rate as the cycles progressed. A deposit thickness of 95 µm was reached at 30 minutes for cycle 1, whereas it only took 16 minutes during cycle 5. Comparing the PWF before fouling for each cycle (fluxes between 0 and 10 min), the flux recovery decreased after cleaning with increasing cycles. After five cycles only 60 % of PWF were recovered. The surface fouling layer is completely removed after each cleaning cycle (results not shown) it is therefore hypothesised that increased in pore fouling remains after each cleaning cycle. The cleaning regime could also affect the pore size and distribution of the membrane.

Figure 6.28 shows the comparison of porosity versus deposit thickness at increasing cycle numbers. The overall deposit porosity decreased with increasing cycle. The porosity values at 105 µm in cycle one was 0.22 whereas it decreased to 0.19. As the cycles increase additional larger particles were deposited. The depositing trend for all cycles seems similar with larger particles being deposited first.

Figure 6.29 shows the deposit thickness and resistance development over five filtration cycles. The deposit resistance increases with increasing cycles and deposit thickness. At 105 µm the deposit resistance at cycle one was 1.20 x 10^{13} m^{-1}, this increased to

1.60 x 10^{13} m^{-1} at cycle five. This can be explained by the reduced cleaning effect with accumulative cycles.

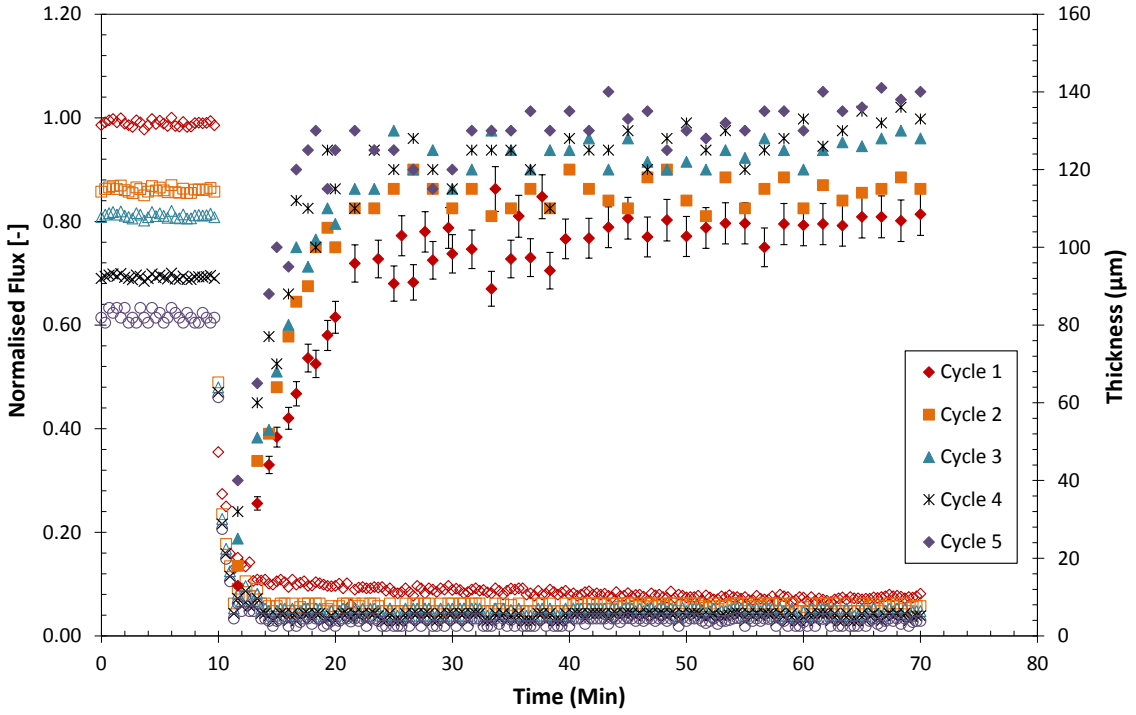

Figure 6.27: Comparison of deposit build-up and permeate flux over five filtration cycles as a function of time. Solid symbols: cake layer thickness, open symbols: permeate flux. Conditions: 60 ºC, 2.00 bar TMP, 1.89 ms^{-1} CFV, 45 ºBrix molasses.

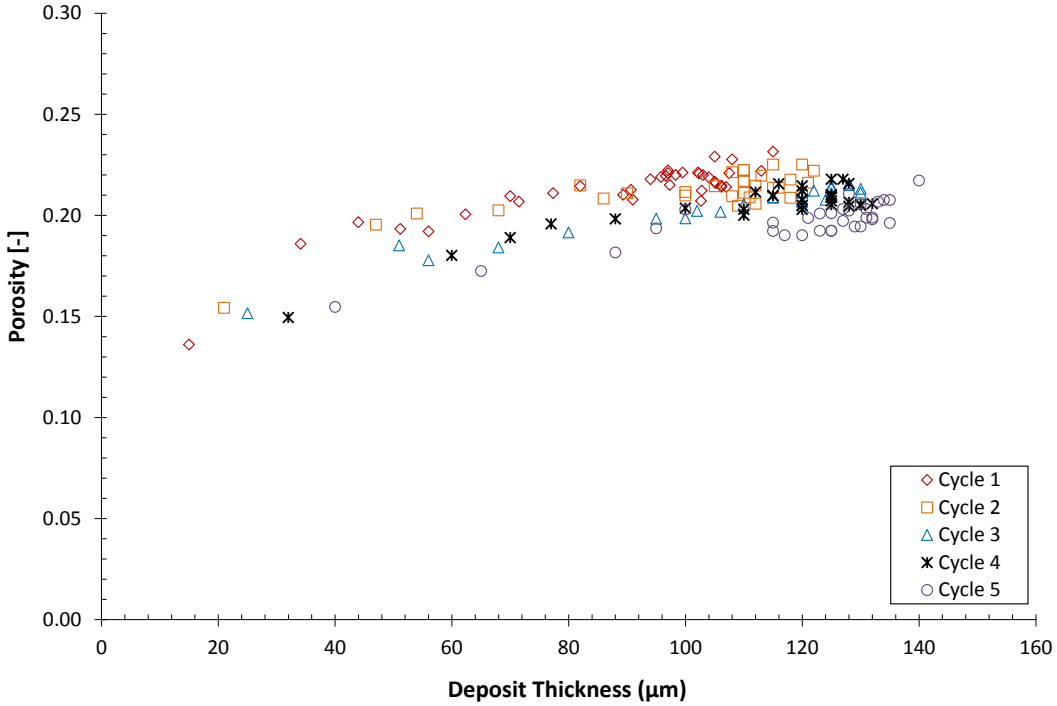

Figure 6.28: Deposit porosity as a function of deposit thickness over five filtration cycles. Conditions: 60 ºC, 2.00 bar TMP, 1.89 ms^{-1} CFV, 45 ºBrix molasses.

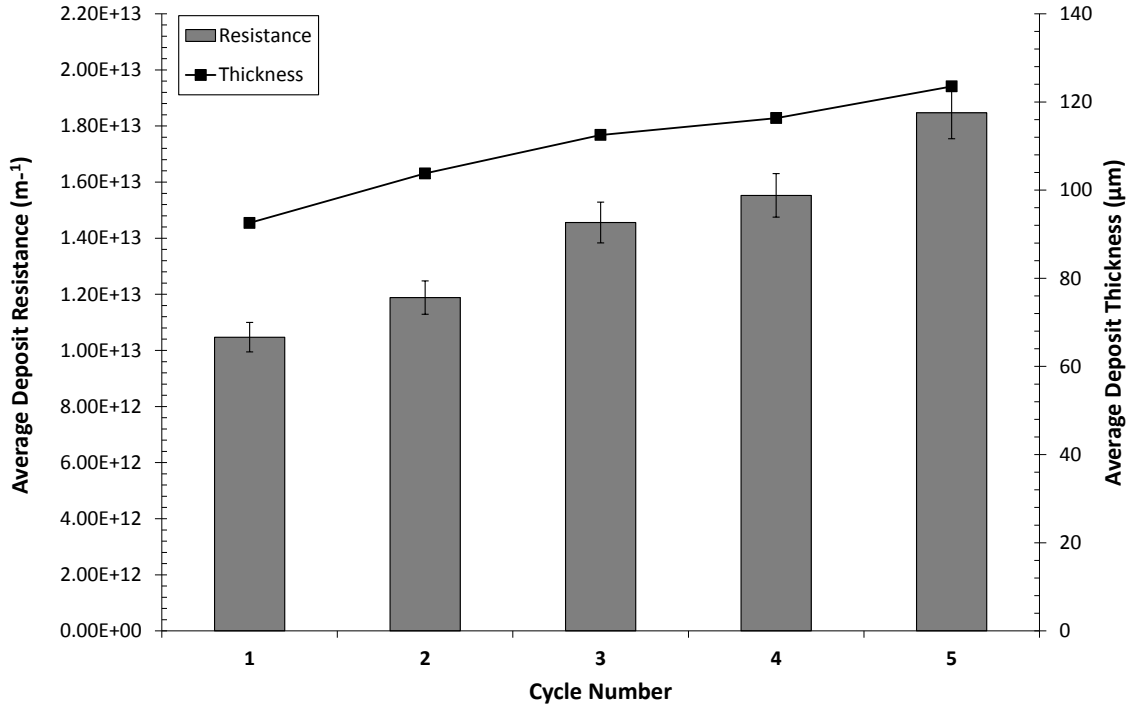

Figure 6.29: Average deposit thickness and resistance development over five filtration cycles. Conditions: 60 ºC, 1.89 ms^{-1} CFV, 2.00 bar TMP, 45 ºBrix molasses.

6.3.7. Membrane pore size

Figure 6.30 shows the evolution of deposit thickness and permeate flux at constant conditions (60 ºC, 2.00 bar, 1.89 ms^{-1} CFV (Re_{duct} = 13887), 45 ºBrix molasses) for 0.5 µm, 0.9 µm, and 1.5 µm pore size Ps*f* membranes. The flux data was normalised, with the initial PWF of the 1.5 µm Ps*f* membrane taken as 1.0, and the other data scaled accordingly. The average initial PWF for the 1.5 µm Ps*f* membrane was 903 L m^{-2} hr^{-1}. The average initial PWF for the 0.9 µm Ps*f* membrane was 678 L m^{-2} hr^{-1} and 557 L m^{-2} hr^{-1} for the 0.5 µm Ps*f* membrane. The rinsing stage before cleaning was performed at 22 ºC, 1.00 bar TMP, and 1.89 ms^{-1} CFV for 10 min. Each membrane was cleaned using the following conditions: 0.10 wt. % NaOH (50 ºC, 1.00 bar TMP, 1.89 ms^{-1} CFV for 30 min).

As expected the deposit thickness increases with decreasing pore size, where the smaller pore membranes increase at a greater rate. The deposits are removed more easily as the membrane pore size increased, though the % flux recovery for all membranes was similar. These results confirm the use of the FDG for membrane systems.

Figure 6.31 shows the comparison of porosity versus deposit thickness for 0.5 µm, 0.9 µm, and 1.5 µm pore size Ps*f* membranes. The porosity of the deposit increased slightly with increasing thickness for all membranes. The porosity increased from 0.19 for the 0.5 µm membrane to 0.22 for the 1.5 µm membrane. This could be due to the reduced pore sizes in 0.5 µm membrane trapping the smaller particles. Figure 6.32 shows the deposit thickness and resistance development for 0.5 µm, 0.9 µm, and 1.5 µm pore size Ps*f* membranes. The deposit resistance increased with the smaller membrane.

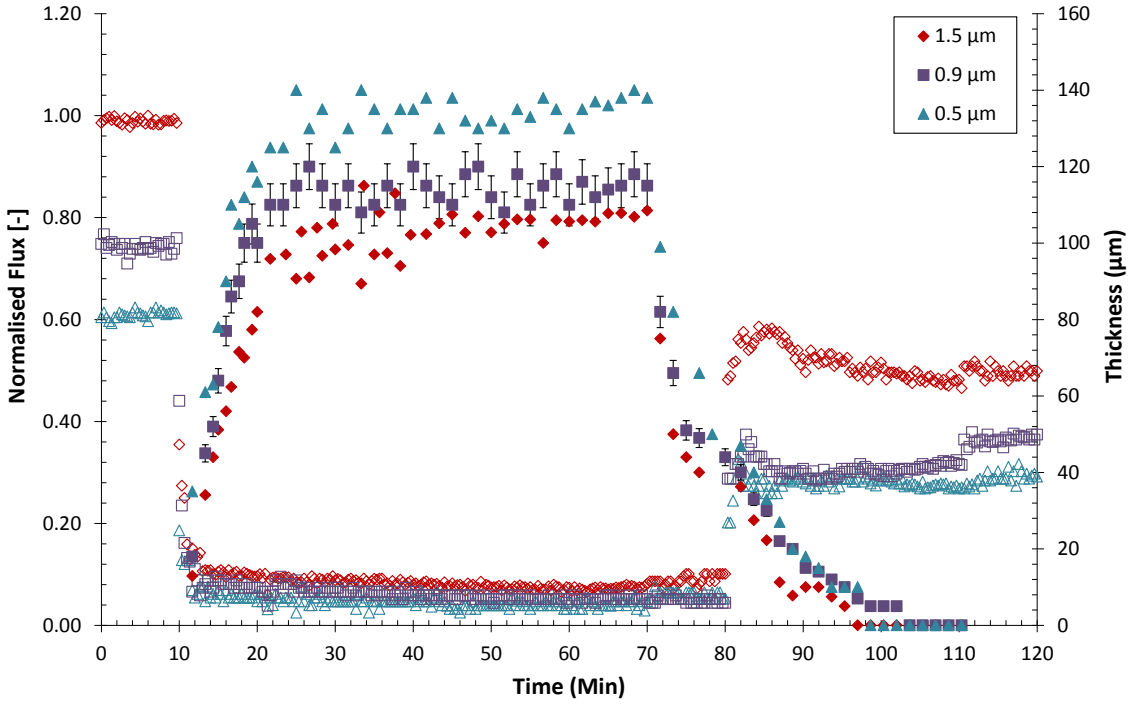

Figure 6.30: Comparison of deposit build-up and permeate flux for 0.5 µm, 0.9 µm, and 1.5 µm pore size Ps*f* membranes. Solid symbols: cake layer thickness, open symbols: permeate flux. Fouling conditions: 60 ºC, 2.00 bar TMP, 1.89 ms^{-1} CFV, 45 ºBrix molasses. Cleaning conditions: 0.10 wt. % NaOH (50 ºC, 1.00 bar TMP, 1.89 ms^{-1} CFV for 30 min).

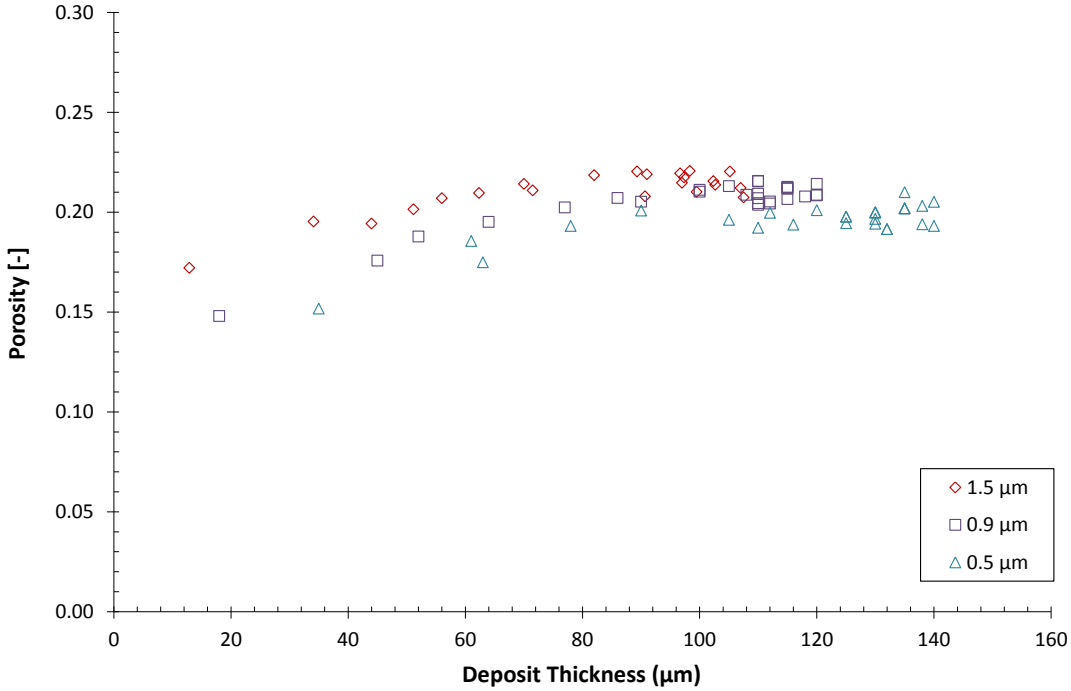

Figure 6.31: Deposit porosity as a function of deposit thickness for 0.5 µm, 0.9 µm, and 1.5 µm pore size Ps*f* membranes. Conditions: 60 ºC, 2.00 bar TMP, 1.89 ms^{-1} CFV, 45 ºBrix molasses.

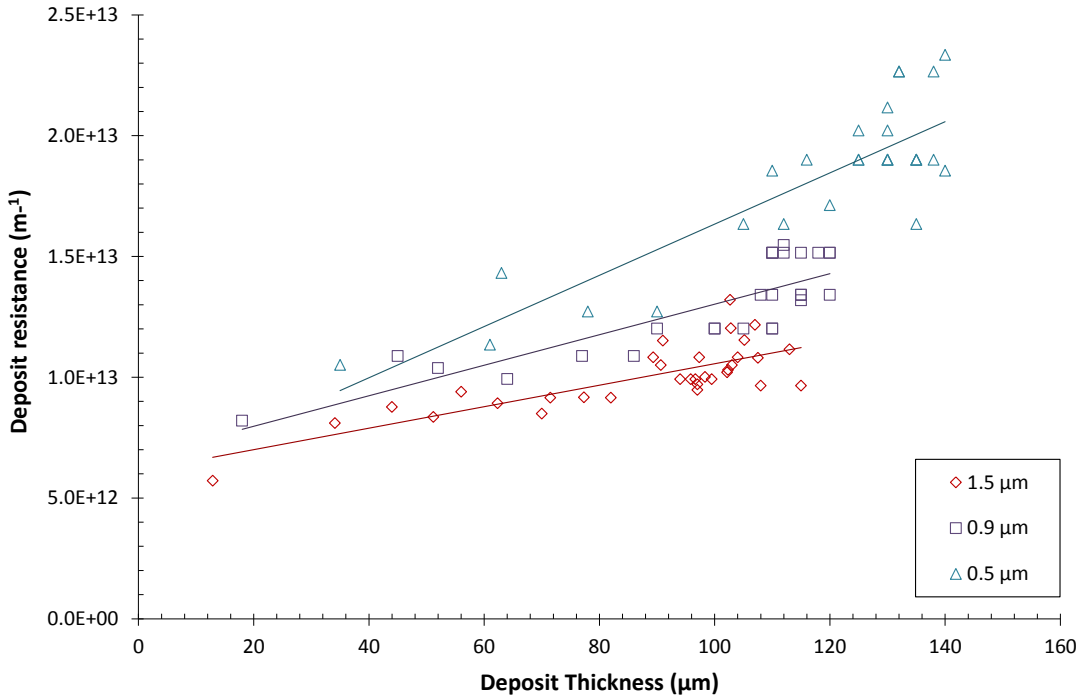

Figure 6.32: Deposit resistance as a function of deposit thickness for 0.5 µm, 0.9 µm, and 1.5 µm pore size Ps*f* membranes. Conditions: 60 ºC, 2.00 bar TMP, 1.89 ms^{-1} CFV, 45 ºBrix molasses.

6.3.8. Scanning Electron Microscopy (SEM) Images

The morphology of fouled deposits on membrane surfaces for a range of different conditions was inspected using SEM; a selection of which are presented in Figure 6.33 to 6.35. Figure 6.33 (a) is a cross-sections through the asymmetric membrane structure. An active layer of *ca.* 50 µm is clearly visible in. Figure 6.33 (b) shows the surface view of the conditioned virgin membrane. The cross-section of the fouled membrane (Figure 6.34 (a) and (b)) shows some pore blockage, but mainly surface fouling, confirming the suitability of FDG for studying the process. X-ray diffraction was used to identify the elements present. The deposits were found to contain calcium, sulphur and oxygen. Whilst the sulphur detected could have come from the Ps*f* membranes, X-ray analysis of molasses filtration deposits obtained in our laboratory using fluoropolymer membranes (i.e. membranes containing no sulphur) also confirmed that sulphur was present in the foulant. The fouling deposits are most likely to be crystals of calcium sulphate, calcium oxalate dihydrate, and calcium oxalate monohydrate. Nordzucker (2008) reported that such crystals are *ca.* 1 – 6 µm wide and 5 – 20 µm long. Figures 6.34 (c) and (d) show fouled membrane surfaces covered with many aggregates in the size range *ca.* 1–6 µm, smaller than those reported by Nordzucker, (2008).

(a) 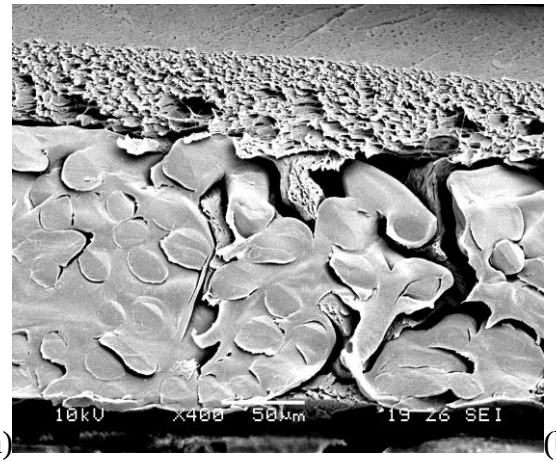

(b) 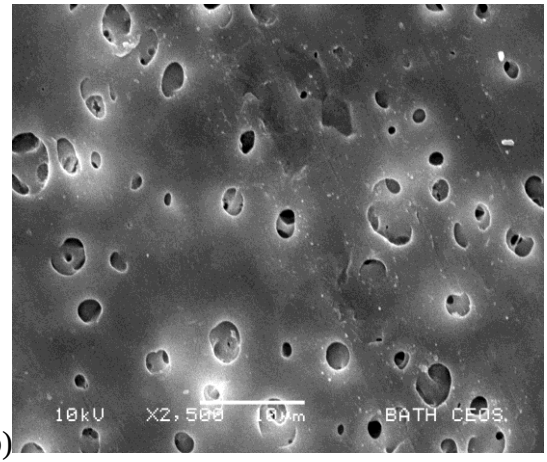

Figure 6.33: Scanning electron micrographs of conditioned 1.5 µm Ps*f* membranes. (a) cross section of a virgin membrane; active layer (feed side) on top, (b) surface view of a conditioned virgin membrane, x2500.

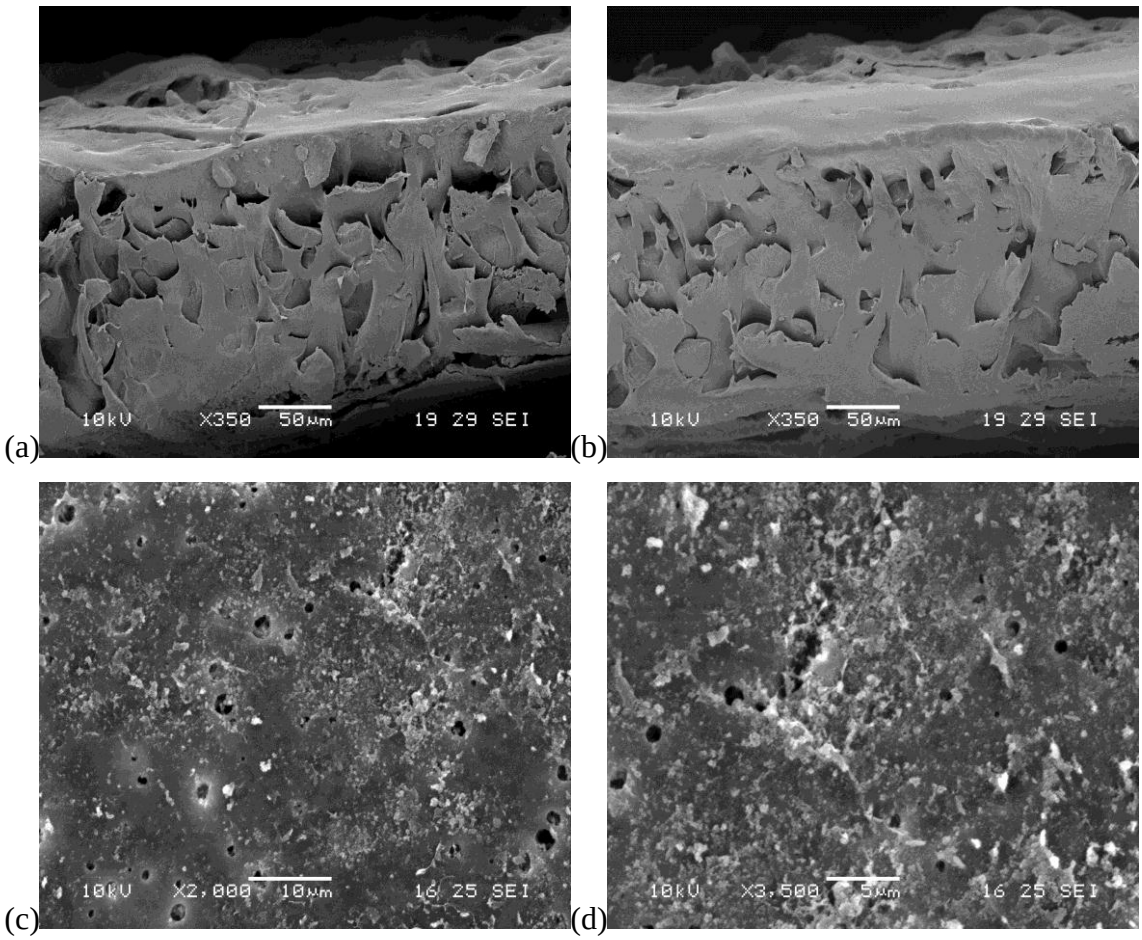

Figure 6.34: Scanning electron micrographs of fouling deposits on 1.5 µm Ps*f* membranes. (a) cross section of a fouled membrane; active layer (feed side) on top, (b) cross section of a fouled membrane; active layer (feed side) on top, (c) surface view of a fouled membrane, x2000, (c) surface view of a fouled membrane, x3500.

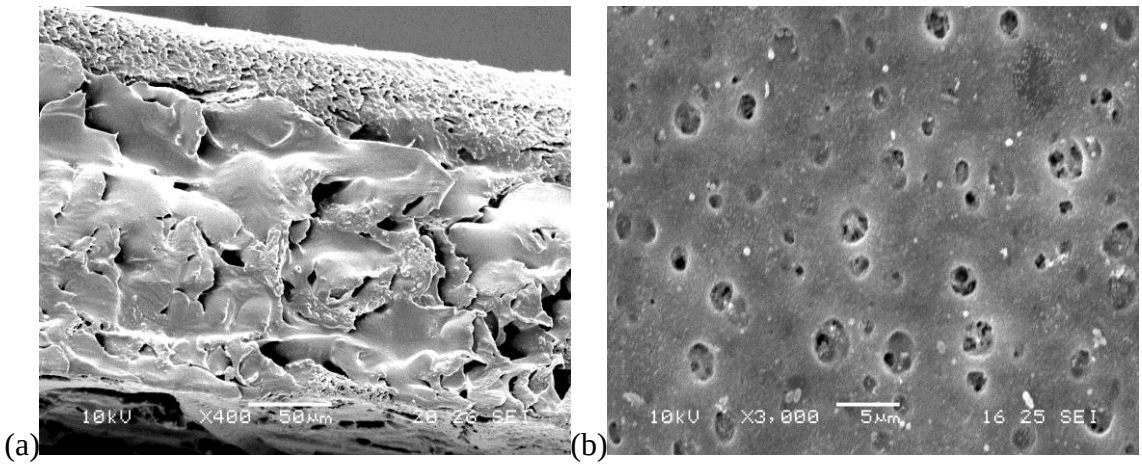

Figure 6.35: Scanning electron micrographs of deposit removal on 1.5 µm Ps*f* membranes. (a) cross section of a fouled and cleaned membrane; active layer (feed side) on top, (b) surface view of a fouled and cleaned membrane, x3000.

6.4. Summary

FDG has been used to simultaneously track the thickness of cake and permeate flux *in situ* and in real time. This chapter discussed the use of FDG in both dead-end mode and cross flow filtration dynamic gauging.

Dead-end filtration was used to validate the application of using FDG for the measurements of fouling on polymeric membranes. The experimental results show that the FDG can be successfully applied to fouling layers on porous surfaces in dead-end filtration. The work here is consistent with previous works of Chew *et al.,* (2007). The results however did show that the feed solutions in a dead-end filtration solution do not give a thick enough fouling layer and a reliably measureable flux. To improve the accuracy of these results a thicker fouling layer would be required for the size of the nozzle, this could be achieved by increasing the value of H (driving force).

Fluid dynamic gauging was successfully used in the cross flow filtration system to simultaneously track the thickness of the fouled cake layer and permeate flux during deposition, rinsing and cleaning cycles. These initial experiments indicate that FDG can be applied to study deposition on permeable surfaces in cross flow microfiltration with some reliability. The work reported here is consistent with previous findings of Chew *et al.* (2007) for dead-end filtration and Lister *et al.* (2011) for cross flow filtration. FDG has been found to be a sensitive tool to variations in operating parameters for filtration. It has been shown that operating conditions have to be carefully chosen to minimize the effect of membrane fouling.

The FDG was used to investigate the effects of different cleaning options for the deposit removal on microfiltration membranes. The results support the common industrial practice of cleaning with the permeate line closed to aid removal of cake deposits. Asymptotic fouling thicknesses of *ca.* 105 μm were developed after 30 minutes of filtration. Accordingly, flux declines were severe at *ca.* 93 %. Cleaning with the permeate line closed (PLC) is preferable to cleaning with the permeate line open (PLO). PLC operation leads to the complete removal of the deposit layer, and the recovery of 60 % of the flux (implying that there are still significant in-pore bound foulants

present). However, PLO operation leads to only a 50 % flux recovery and an asymptotic deposit thickness of 10 μm.

The above results show that FDG is a versatile and powerful technique for characterising the dynamics and mechanical behaviour of fouling layers on membrane surfaces. A particular advantage of the FDG technique is its ability to determine the thickness of fouling layers where other techniques would find difficulty. For example, the layers formed in this study were opaque, and consequently the determination of the development of deposit thickness with time would have been very challenging using conventional optical microscopy techniques. The information provided by FDG should improve our understanding of the interaction between surface chemistry and surface physics during the membrane filtration of complex food based materials. The future uses of FDG will include an evaluation of particle sweeping, as this is a determining factor in deposit control. The FDG will also be used as a sampling device, taking material from the concentration polarisation region. The study of this phenomenon will enable real rejection ratios to be calculated and compared to existing models for the estimation of solute concentration at the membrane surface. The simultaneous measurement of both deposit thickness and permeate flux vs. time will also be useful in examining the establishment of Critical Flux regimes in membrane systems.

Chapter 7

Conclusions and Proposed Future Work

7.1. Conclusions

The aim of this study was to further understand the fouling and cleaning mechanisms of synthetic membranes used to filter an industrially relevant feed. The main focus of this study was the understanding of the fouling layer properties during pressure driven filtration. A relatively new technique known as Fluid Dynamic Gauging (FDG) was applied to examine the fouling layer thickness. This work comprised of four main themes with overlapping objectives: (i) the optimisation of Spent Sulphite Liquor fouling and cleaning conditions, (ii) the optimisation of molasses fouling and cleaning conditions, (iii) the investigation of the effect of a simple pre-treatment upon the membrane separation performance, and (iv) the application of the FDG in the study of polymeric membranes. The results presented in this study are summarised below.

7.1.1. Spent Sulphite Liquor Fouling and Cleaning Conditions

The fouling and cleaning optimisation of Spent Sulphite Liquor (SSL) filtration was studied in the cross flow rig with two different materials; Polysulphone (Ps*f*) and Fluoropolymer (FP) membranes. The fouling conditions were optimised by varying crossflow velocity (CFV), transmembrane pressure (TMP) and temperature. The results show that the rate of increase of flux with TMP became less apparent as pressure increased gradually to a high value for both membranes Ps*f* and FP. A limiting flux was seen at 3.0 bar. The increase in TMP caused an increase in the polarised layer thickness which acted as a secondary membrane. This increasing fouling layer which was formed was found to be increasingly more difficult to remove. Increasing the fouling temperature of the SSL on the Ps*f* and FP membranes showed increased initial permeate fluxes. As the fouling cycles reached steady state, the final fouling fluxes showed similar values for the 60 ºC and 70 ºC feed temperatures. The changes in viscosity of SSL did not affect the fouling process at the higher temperatures. The optimal fouling temperature for filtering SSL was found to be 60 ºC. The lower filtration temperature though can reduce the irreversible fouling resistance and increase both rinsable and concentration polarisation resistances. The optimised fouling conditions were found to

be: a TMP of 3.0 bar, a CFV of 1.89 ms^{-1} and a temperature of 60 ºC for 90 min. The standard rinsing and cleaning conditions were also optimised. The FP membrane overall had a superior performance over the Ps*f* membrane.

7.1.2. Molasses Fouling and Cleaning Conditions

The fouling and cleaning optimisation of molasses filtration was studied in a cross flow rig with three different membrane pore size Ps*f* membranes (0.5 μm, 0.9 μm, and 1.5 μm). The majority of the experiments were performed with the 1.5 μm Ps*f* membrane. The fouling conditions were optimised by varying concentration, CFV, TMP and temperature. The molasses was used at as low a dilution rate as possible, though it could not be used in the delivered form, as its viscosity was too high for pumping around the circuit and for effective separation. The highest possible dilution rate for filtration in this study produced flux values which were too low for a viable process, and a lower concentration resulted in a higher degree of cleanability. A 45 ºBrix solution was selected as a compromise, and a reasonable fouling flux performance was achieved. The molasses should be used at a high a temperature as possible, as the viscosity of the feed is particularly influential to the filtration process. The optimal temperature for the filtration of molasses was found to be 60 ºC; as there was no benefit of increasing the temperature to 70 ºC. The results showed that increasing the TMP increased the fouling flux until between ~2.5 and 3.0 bar, where the limiting flux effect occurred. After this pressure, the fouling fluxes began to decline slightly. It was therefore not advantageous to work at any higher pressures than 3.0 bar. The optimised fouling conditions were a TMP of 3.0 bar, a CFV of 1.89 ms^{-1} and a temperature of 60 ºC for 90 min.

Effective membrane cleaning protocols following molasses filtration to remove both cake and in-pore bound deposition required both alkali and acid cleaning steps. By optimising a two stage cleaning process, optimal TMP, temperature and concentrations were identified for the microfiltration of a 45 ºBrix molasses solution. The best cleaning regime from the range tested achieved a pure water flux recovery of 89 % using a NaOH concentration of 0.25 wt. % followed by a stage using 0.10 wt. % citric acid. The process conditions were the same for each stage (50 ºC, 30 min, 1.0 bar, and 1.89 ms^{-1}).

7.1.3. The Application of a Simple NaOH Pre-treatment

This study has investigated the fouling properties of SSL and molasses using ultrafiltration and microfiltration membranes after a simple NaOH pre-treatment was applied. The focus was to see if the use of a 0.50 wt. % NaOH pre-treatment could affect both the type of foulant species attaching to the membrane surface, and improve the separation performance.

The filtration of SSL was investigated over one, two and four operational cycles respectively. The use of a 20 kDa FP membrane to separate SSL resulted in the attachment of different fouling species depending upon the pre-treatment protocol used, as demonstrated by FTIR results. Zeta potential measurements, FTIR and electron microscopy demonstrated that both in-pore and surface fouling was present. The different pre-treatment protocols used did have an effect upon the subsequent separation and cleaning performance of the membranes. The deposits formed on the membranes subjected to conditioning with NaOH displayed some of the same characteristics as those deposits formed on membranes conditioned only with water, then subsequently cleaned using NaOH following fouling. The pre-treatment of polymeric membranes with dilute NaOH solutions thus appears to have a positive effect upon subsequent membrane filtration performance after fouling and cleaning for one cycle. Once the Protocol 1 and Protocol 2 membranes had been subjected to four fouling cycles, different species had attached to the membrane surface. The results presented show that Protocol 2 treated membranes had an improved pure water flux performance over Protocol 1 treated membranes for the first three cycles, although as the cycle number increased these improvements became less significant. After four fouling and cleaning cycles had been completed, NaOH preconditioning offered no significant improvement upon pre-treatment with water alone.

The pre-treatment protocol applied also resulted in the adhesion of different species when a molasses feed was treated using Ps*f* membranes. Protocols 1 and 2 resulted in the attachment of different species to the membrane, as shown by the resulting FTIR spectra. However, the functional groups in the cleaning agents partially masked the molasses foulant responses in the FTIR spectra, making data difficult to interpret. The peak height data suggest that different amounts of fouling had occurred on Ps*f*

membranes subjected to the different pre-treatment protocols. The fouling species in the molasses deposition displayed a slight negative charge, becoming slightly more negative with increasing pH. The zeta potential data indicated that the cleaning pre-treatment Protocol 2 (50 ºC water followed by NaOH) made the membranes more prone to in-pore fouling than those subjected to pre-treatment Protocol 1 (50 ºC only), but flux data indicated that the subsequent cleaning removed this in-pore fouling more easily than fouling occurring on membranes subjected to pre-treatment Protocol 1. The results obtained when filtering molasses also suggest that surface fouling plays a key role in the process.

The data collected indicated that for both membranes evaluated, the pre-treatment protocols did have some effect upon the subsequent separation and cleaning performance. These findings are significant, as they offer support to the recommendations made by some polymeric membrane manufacturers that conditioning protocols should include a NaOH step. However, in the SSL system examined, the effect of NaOH pre-treatment resulted in an improvement in the subsequent performance only over the first two or three complete filtration cycles. It is therefore necessary to study membrane systems over multiple fouling and cleaning cycles before a recommendation can be made.

7.1.4. Fluid Dynamic Gauging

FDG has been used to simultaneously track the thickness of cake and permeate flux *in situ* and real time. This study here has shown the application of FDG in both dead-end mode and cross flow filtration mode.

7.1.4.1. Dead End Filtration

Dead-end filtration was used to validate the application of using FDG for the measurements of fouling on polymeric membranes. The experimental results show that the FDG can be successfully applied to fouling layers on porous surfaces in dead-end filtration. The work here is consistent with previous findings of Chew *et al.*, (2007). The results however did show that the feed solutions in a dead-end filtration solution do not give a thick enough fouling layer and a reliably measureable flux. To improve the

accuracy of these results a thicker fouling layer would be required for the size of the nozzle, this could be achieved by increasing the value of H (pressure driving force).

7.1.4.2. Cross Flow Filtration

Fluid dynamic gauging was successfully used in the cross flow filtration system to simultaneously track the thickness of the fouled cake layer and permeate flux during deposition, rinsing and cleaning cycles. These initial experiments indicate that FDG can be applied to study deposition on permeable surfaces in cross flow microfiltration with some reliability. The work reported here is consistent with previous findings of Chew *et al.* (2007) for dead-end filtration and Lister *et al.* (2011) for cross flow filtration. FDG has been found to be a sensitive tool to variations in operating parameters for filtration. It has been shown that operating conditions have to be carefully chosen to minimize the effect of membrane fouling. A particular advantage of the FDG technique is its ability to determine the thickness of fouling layers where other techniques would find difficulty. For example, the layers formed in this study were opaque, and consequently the determination of the development of deposit thickness with time would have been immensely challenging using conventional optical microscopy techniques. The information provided by FDG should improve our understanding of the interaction between surface chemistry and surface physics during the membrane filtration of complex food based materials.

The FDG was used to investigate the effects of different cleaning options for the deposit removal on microfiltration membranes. The results elucidate the common industrial practice of cleaning with the permeate line closed to aid removal of cake deposits. Asymptotic fouling thicknesses of *ca.* 105 μm were developed after 30 minutes of filtration. Accordingly, flux declines were severe at *ca.* 93 %. Cleaning with the permeate line closed (PLC) is preferable to cleaning with the permeate line open (PLO). PLC operation leads to the complete removal of the deposit layer, and the recovery of 60 % of the flux (implying that there are still significant in-pore bound foulants present). However, PLO operation leads to only a 50 % flux recovery and an asymptotic deposit thickness of 10 μm.

7.1.5. Conclusions Summary

The main objectives of this work were outlined in Chapter 1 of this Thesis. This study has achieved these objectives. An understanding of the mechanisms involved in fouling and cleaning of microfiltration and ultrafiltration membranes used to filter molasses and SSL has been attained. The variables affecting permeate flux and quality were optimised and certain information concerning the synergistic effects between fouling and cleaning was gathered. The application of a simple pre-treatment was found to affect both the type of foulant species attaching to the membrane surface, and result in an altered separation performance. An improved understanding of the interaction between the surface chemistry and surface physics during membrane filtration of complex food based material will benefit both membrane manufactures and food industry based users.

The technique of Fluid Dynamic Gauging was incorporated into an existing system and validated to monitor the development of cake layers over time. The Fluid Dynamic Gauging was also used to optimise conditions and track the thickness of the cake layer during multiple fouling cycles and its removal rate during cleaning, as an aid to understanding removal mechanisms. The results show that FDG is a versatile and powerful technique for characterising the dynamics and mechanical behaviour of fouling layers on membrane surfaces.

7.2. Proposed Future Work

The work here could be extended in various directions, which will be discussed in this section. The main two topics, membrane pre-treatment and membrane Fluid Dynamic Gauging have been focused on.

7.2.1. Membrane Pre-treatment

This study explained the effects of multiple concentrations of NaOH during the fouling and cleaning properties on FP for the filtration of SSL and Ps*f* membranes for filtration of molasses. There are a number of areas of interest to advance this concept. These include: (i) the use of different cleaning chemicals, (ii) expanding this simple method to include different membranes and feeds, and (iii) applying the research of alcohol conditioning to the membranes and feeds used in this study.

The effect of pre-treatment on multiple fouling and cleaning cycles was only explored for the filtration of SSL due to time and equipment constraints. This could be extended for the filtration of molasses. As the results in this study showed that the effect of NaOH pre-treatment was different for a one cycle filtration and a seven cycle filtration. An extensive study of different membranes and feeds would be required before an overall recommendation on the application of this type of pre-treatment could be specified.

Conditioning with different alcohols has been found to affect the filtration behaviour of a membrane with respect to surface modification and permeate composition. Shukla and Cheryan (2002) investigated the performance of 18 different types of polymeric ultrafiltration membranes after conditioning with aqueous ethanol solutions. The conditioning method had a significant effect on solvent flux, membrane integrity and their pressure ratings. Too high a concentration of alcohol was found to cause pore degradation and significantly reduce the pressure rating of the membranes. This study was very useful as an insight into alcohol conditioning but didn't compare the work to an unconditioned membrane. This is important in terms of comparing fouling flux declines and rejection values. Zhao and Yuan (2006) investigated membrane pre-treatment using acetone, methanol and toluene on the performance of polyamide, polyimide and polydimethylsiloxane (PDMS) membranes. The pre-treatment had a significant effect of flux and membrane rejection. Kochan *et al.* (2009) extended this topic further to investigate the impact of different wetting agents (acetone, isopropyl alcohol and ethanol) on membrane filtration performance. The use of wetting agents was observed to improve the activation of smaller pores through the reduction of surface tension. However, it was found that wetting agents do not definitely make a positive contribution in terms of filtration enhancement. These studies are not exhaustive in terms of conditioning effects on fouling and multiple filtration cycles. In the literature to date, there is also a lack of research into the effect of alcohol conditioning on the surface and upon pore charge (Zeta-potential measurements). Investigating the effects of alcohol conditioning could be easily applied to the membranes and feeds used in this study.

Further information could be gathered using advanced forms of the analytical techniques implemented in this study. The streaming potential measurements in this

study were only performed for in pore analysis. It is also possible to measure the streaming potential along the membrane surface; this would provide further information on the fouling and cleaning behaviour in the filtration of SSL and molasses. Atomic force microscopy (AFM) was used in this study to measure the membranes surface roughness values. The AFM could also be used to measure the specific force interaction between known colloids and the membrane. A model foulant is absorbed onto the AFM tip producing a colloidal probe. The use of a colloidal probe is useful in measuring the behaviour of certain foulant on the membrane surface (Evans *et al*., 2008).

7.2.2. Fluid Dynamic Gauging

The FDG is still a relatively new lab-based measurement tool. Consequently, there is a large scope of concepts to still be investigated. This study could be simply extended by the inclusion of different membrane material and pore sizes. It would be interesting to extend the principles of this work into the ultrafiltration range. The use of different model fluids and real industrially relevant fluids could be applied. This could provide further evidence for the use of the FDG in membrane systems and further the development of the technique. The future uses and developments of FDG could also include: (i) acting as a sampling device, (ii) investigating the critical flux region, (iii) Computational fluid dynamic (CFD) studies, and (iv) rig and nozzle adaptation. The FDG could also be used as a method to evaluate the effect of particle sweeping, which could be a determining factor in deposit control. The FDG is currently a lab based tool, but also has considerable potential to be advanced as an inline industrial monitoring tool.

The FDG can be used as a sampling device, taking material from the concentration polarisation region. The study of this phenomenon will enable real rejection ratios to be calculated and compared to existing models for the estimation of solute concentration at the membrane surface. This requires using a feed with a well-defined concentration polarisation region and the slow withdrawal of samples through the gauge.

As the system in this study was unable to be performed in constant flux mode, evaluating the critical flux was not straight forward. The FDG could be applied to a

constant flux system and the simultaneous measurement of both deposit thickness and permeate flux vs. time will also be useful in examining the establishment of critical flux regimes in membrane systems.

The use of CFD can be a powerful analytical tool to enhance the performance of the FDG system. Combining CFD simulations with gauging experiments can be used to measure the strength of deposits on the membrane surface, thereby the force required to remove the foulant. The effect of gauging on the membrane filtration process can be modelled, looking at the flow patterns, local velocity profiles, pressure fields and shear stresses around the membrane surface. The predicted shear and normal stress distributions can be used as a guide for optimizing the design of the nozzle and system. This data will then be used for flux prediction in the cross flow filtration rig. The CFD models are advantageous as measuring these properties mentioned are difficult in real liquid systems. CFD studies have previously been performed by Chew *et al.* (2007) and Lister *et al.* (2011) for membrane systems. Chew *et al.* (2007) performed CFD studies on the fluid dynamics of FDG in the same dead-end formation used in this study. The work focused on the flow patterns and the stresses imposed on a porous surface. The stimulations were found to be in good agreement with the experimental data. Lister *et al.* (2011) used CFD to simulate the flow in a duct, in the gauge, and across the membrane to elucidate the flow patterns and stress imposed on the gauged surface. The experimental and CFD measurements were performed in the laminar region, and were in good agreement with each other. The results showed that the highest shear stresses are located under the rim of the nozzle, which was consistent with the work of Gu *et al.* (2009a) for an impermeable surface duct system. The studies to date for a FDG duct system have all been simulated in the laminar region. There is a need to increase the channel Reynolds number to simulate turbulent flow simulations in the system used in this study (a single channel is shown in Figure 7.1). This could be further extended to include a multiple channel simulation which would mimic the system used here completely.

The FDG apparatus used in this study was an adaptation of an existing membrane filtration rig. This enabled relatively high TMP, CFV, and temperature to be studied, but visualisation of the nozzle and fouling layers was impossible. To gain the full benefit of

the FDG tool a completely new system should be constructed. The design should include some aspect of visualisation. It could include one of the following ideas: (i) a clear lid, so the fluid flow could be monitored from above, (ii) an endoscope that could film the cake build up, (iii) a viewing window could be situated at the side wall of the duct if a one channel module was designed.

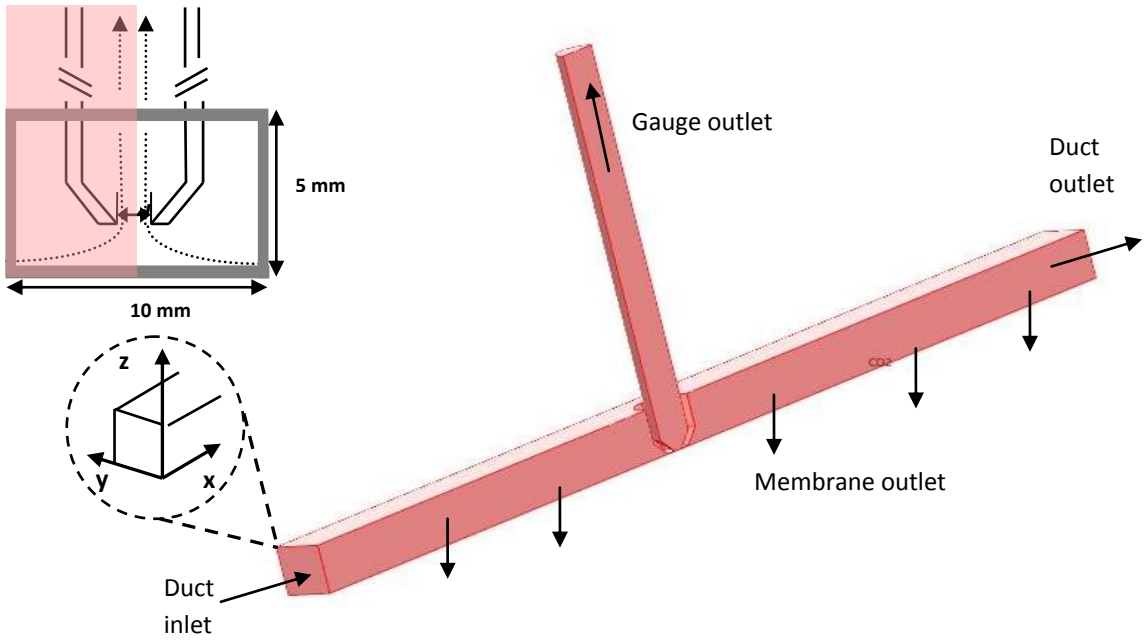

Figure 7.1. Simulation geometry of half the duct and gauge used in this study

A new design should include the option on multiple measurements. Gordon *et al.* (2010a) developed an automated scanning FDG probe (sFDG) which allowed the thickness of a sample layer to be monitored at several points during an experiment. This system worked in an open tank which allowed multiple locations to be gauged in parallel. For this concept to be transferred to a crossflow filtration module the sealing issue would have to addressed. A minimum of three ports should be included, ideally near the inlet, centre, and outlet. If the design included more than one channel, an option of gauging each channel should be considered.

The FDG used in this study had the following dimensions: d_t = 1 mm; d = 4 mm, 45º nozzle angle which produced a resolution of ± 5 μm. A new gauge with the dimensions half the size of this current one would be interesting to develop. The smaller nozzle could improve the resolution and decrease the minor effects of the gauge on the

filtration process. Peralta *et al.* (2011) investigated the effect of the external nozzle geometry on parameters affecting the gauged surface and developed a method that allows the optimisation of nozzle shape for a specific application. This method could be used to further enhance the performance of FDG in the filtration of molasses. Miniaturisation of the nozzle diameter could theoretically be carried out to a size where conventional fluid mechanics flow (Hagen-Poiseuille) breaks down, and micro-fluidics takes over. This would require micro fabrication techniques as the smallest hole that can be reproducibly drilled commonly is approximately 0.25 mm. However, fouling would be a serious issue with such a small diameter nozzle.

Chapter 8

References

Aimar, P. & Sanchez, V. 1986. A Novel Approach to Transfer Limiting Phenomena during Ultrafiltration of Macromolecules. *Industrial & Engineering Chemistry Fundamentals*, 25, 789-798.

Aimar, P. & Field, R. 1992. Limiting Flux in Membrane Separations - A Model Based on the Viscosity Dependency of the Mass-Transfer Coefficient. *Chemical Engineering Science*, 47, 579-586.

Aimar, P., Meireles, M., Bacchin, P., & Sanchez, V. 1994. Fouling and Concentration Polarization in Ultrafiltration and Microfiltration. Advanced Study Institute on Membrane Processes in Separation and Purification. Curia, Portugal, Kluwer Academic Publ.

Airey, D., Yao, S., Wu, J., Chen, V., Fane, A. G. & Pope, J. M. 1998. An Investigation of Concentration Polarization Phenomena in Membrane Filtration of Colloidal Silica Suspensions by NMR Micro-Imaging. *Journal of Membrane Science*, 145, 145-158.

Almécija M.C., Guadix, A., Martinez-Ferez, A., Gonzalez-Tello, P. & Guadix, E.M. 2009. A Flux Enhancing Pre-treatment for the Ultrafiltration of Acid Whey. *Desalination*, 246, 364-369.

Alfa Laval. 2009. FS61PP polymeric flat sheet membrane user instructions.

Altmann, J. & Ripperger, S. 1997. Particle Deposition and Layer Formation at the Crossflow Microfiltration. *Journal of Membrane Science*, 124, 119-128.

Bacchin P., Aimar, P. & Field, R.W. 2006. Review: Critical and Sustainable Fluxes: Theory, Experiments and Applications. *Journal of Membrane Science*, 261, 42-69.

Baker, R.W. 2004. Overview of Membrane Science and Technology, Membrane Technology and Application. 2nd Ed., John Wiley and Sons, New York.

Baikow, V. E. 1967. Manufacture and Refining of Raw Cane Sugar. 1st Ed., Elsevier Publishing Co., New York.

Bansal, B., Al-Ali, R., Mercadé-Prieto, R. & Chen, X.D. 2006. Rinsing and Cleaning of α-Lactalbumin Fouled MF Membranes. *Separation and Purification Technology*, 48, 202 – 207.

Barsinai, Y. L. & Wayman, M. 1976. Separation of Sugars and Lignin in Spent Sulfite Liquor by Hydrolysis and Ultrafiltration. *Tappi*, 59, 112-114.

Barros, S.T.D., Andrade, C.M.G., Mendes, E.S. & Peres, L. 2003. Study of Fouling Mechanism in Pineapple Juice Clarification by Ultrafiltration. *Journal of Membrane Science*, 215, 213-224.

Bartlett, M., Bird, M. R. & Howell, J. A. 1995. An Experimental Study for the Development of a Qualitative Membrane Cleaning Model, *Journal of Membrane Science*, 105, 147-157.

Bartlett, M. 1998. Chemical Cleaning of Fouled Membrane Systems. Doctoral Dissertation, Chemical Engineering Department, University of Bath.

Belfort, G., Davis, R. H. & Zydney, A. L. 1994. The Behaviour of Suspensions and Macromolecular Solutions in Cross-Flow Microfiltration. *Journal of Membrane Science*, 96, 1-58.

Bhattacharjee, C. & Bhattacharya, P. K. 1993. Flux Decline Analysis in Ultrafiltration of Kraft Black Liquor. *Journal of Membrane Science*, 82, 1-14.

Bhattacharya, P. K., Todi, R. K., Tiwari, A., Bhattacharjee, C., Bhattacharjee, S. & Datta, S. 2005. Studies on Ultrafiltration of Spent Sulphite Liquor using Various Membranes for the Recovery of Lignosulphonates. *Desalination*, 174, 287-297.

Bian, R., Yamamoto, K. & Watanabe, Y. 2000. The Effect of Shear Rate on Controlling the Concentration Polarization and Membrane Fouling. *Proceedings of the Conference on Membranes in Drinking and Industrial Water Production,* 1, 421 – 432.

Bird R. B., Stewart, W. E. & Lightfoot, E. N. 1960. Transport phenomena. 1st Ed., John Wiley and Sons, New York.

Bird, M. R. & Fryer, P.J. 1992. An Analytical Model for the Cleaning of Food Process Plant. *Food Engineering in a Computer Climate*, 126, 325-330.

Bird, M. R. & Bartlett, M. 2002. Measuring and Modelling Flux Recovery during the Chemical Cleaning of MF Membranes for the Processing of Whey Protein Concentrate. *Journal of Food Engineering*, 53, 143-152.

Bjørsvik, H. R. 1999. Fine Chemicals from Lignosulfonates. 1. Synthesis of Vanillin by Oxidation of Lignosulfonates. *Organic Process Research & Development,* 3, 330-340.

Blanpain, P., Hermia, J. & Lenoel, M. 1993. Mechanisms Governing Permeate Flux and Protein Rejection in the Microfiltration of Beer with a Cyclopore Membrane. *Journal of Membrane Science*, 84, 37-51.

Blanpain-Avet, P., Migdal, J.F. & Bénézech, T. 2004. The Effect of Multiple Fouling and Cleaning Cycles on a Tubular Ceramic Microfiltration Membrane Fouled with a Whey Protein Concentrate: Membrane Performance and Cleaning Efficiency. *Food and Bioproducts Processing*, 82, 231-243.

Bond, L.J., Greenberg, A.R., Mairal, A.P., Loest, G.W., Brewster, J.H. & Krantz, W.B. 1995. Real-Time Nondestructive Characterization of Membrane Compaction and Fouling. D.O. Thompson and D.E. Chimenti, Plenum Press, New York.

Bowen, W.R., Kingdon, R.S. & Sabuni, A.W. 1989. Electrically Enhanced Separation Processes - The Basis of in situ Intermittent Electrolytic Membrane Cleaning (IIEMC) and in situ Electrolytic Membrane Restoration (IEMR). *Journal of Membrane Science*, 40, 219-229.

Bowen, W. R., Calvo, J. I. & Hernandez, A. 1995. Steps of Membrane Blocking in Flux Decline during Protein Microfiltration. *Journal of Membrane Science*, 101, 153-165.

Bowen, W.R., Mongruel, A. & Williams, P.M. 1996. Prediction of the Rate of Cross-Flow Membrane Ultrafiltration: A Colloidal Interaction Approach. *Chemical Engineering Science*, 51, 4321-4333.

Bowen, W.R. & Doneva, T.A. 2000. Atomic Force Microscopy Studies of Membranes: Effect of Surface Roughness on Double-Layer Interactions and Particle Adhesion. *Journal of Colloid and Interface Science*, 229, 544-549.

Brans, G., Schroen, C., Van Der Sman, R. G. M. & Boom, R. M. 2004. Membrane Fractionation of Milk: State of the Art and Challenges. *Journal of Membrane Science*, 243, 263-272.

Bridge, S. P., Robbins, P. T., Paterson, W. R. & Wilson, D. I. 2001. A Pneumatic Gauging Sensor for Measuring the Thickness of Soft Films. *Proceedings of the Institution of Mechanical Engineers Part E-Journal of Process Mechanical Engineering*, 215, 19-27.

Britt, K.W. 1995. Handbook of Pulp and Paper Technology. 2nd Ed., Van Nostrand-Reinhold, New York.

Bryjak, M., Gancarz, I. & Poźniak, G. 2000. Plasma-Modified Porous Membranes. *Chem. Papers*, 54(6b), 496 – 501.

Capannelli, G., Bottino, A., Gekas, V. & Trägårdh, G. 1990. Protein Fouling Behaviour of Ultrafiltration Membranes Prepared with Varying Degrees of Hydrophilicity. *Process Biochemistry International*, 221 - 224.

Casey, J.P. 1980. Pulp and Paper: Chemistry and Chemical Technology,Vol.1. 3rd Ed., John Wiley and Sons, New York.

Chan, R. & Chen, V. 2004. Characterization of Protein Fouling on Membranes: Opportunities and Challenges. *Journal of Membrane Science,* 242, 169-188.

Chen, V. 1998. Performance of Partially Permeable Microfiltration Membranes under Low Fouling Conditions. *Journal of Membrane Science*, 147, 265-278.

Chen, J.P., Kim, S.L. & Ting, Y.P. 2003. Optimization of Membrane Physical and Chemical Cleaning by a Statistically Designed Approach. *Journal of Membrane Science*, 219, 27–45.

Chen, J. C., Li, Q. L. & Elimelech, M. 2004a. In Situ Monitoring Techniques for Concentration Polarization and Fouling Phenomena in Membrane Filtration. *Advances in Colloid and Interface Science*, 107, 83-108.

Chen, V., Li, H. & Fane, A. G. 2004b. Non-Invasive Observation of Synthetic Membrane Processes - A Review of Methods. *Journal of Membrane Science*, 241, 23-44.

Cheng, T.W. & Wu, J.G. 2001. Modified Boundary Layer Resistance Model for Membrane Ultrafiltration. *Journal of Science and Engineering*, 4, 111-117.

Cheryan, M. 1998. Ultrafiltration and Microfiltration Handbook. 2nd Ed., Technomic Publishing Company, Inc., Lancaster.

Chew, J. Y. M. 2004. Development of Fluid Dynamic Gauging for Cleaning Studies. Doctoral Dissertation, Department of Chemical Engineering, University of Cambridge.

Chew, J. Y. M., Paterson, W. R. & Wilson, D. I. 2004a. Fluid Dynamic Gauging for Measuring the Strength of Soft Deposits. *Journal of Food Engineering*, 65, 175-187.

Chew, J. Y. M., Cardoso, S. S. S., Paterson, W. R. & Wilson, D. I. 2004b. CFD Studies of Dynamic Gauging. *Chemical Engineering Science*, 59, 3381-3398.

Chew, J. Y. M., Paterson, W. R., Wilson, D. I., Höufling, V. & Augustin, W. 2005a. A Method for Measuring the Strength of Scale Deposits on Heat Transfer Surfaces. *Developments in Chemical Engineering and Mineral Processing*, 13, 21-30.

Chew, J. Y. M., Tonneijk, S.J., Paterson, W. R. & Wilson, D. I. 2005b. Mechanisms in the Solvent Cleaning of Emulsion Polymerization Reactor Surfaces. *Industrial & Engineering Chemistry Research*, 44, 4605-4616.

Chew, J. Y. M., Tonneijk, S.J., Paterson, W. R. & Wilson, D. I. 2006. Solvent-based Cleaning of Emulsion Polymerization Reactors. *Chemical Engineering Journal*, 177, 61-69.

Chew, Y. M. J., Paterson, W. R. & Wilson, D. I. 2007. Fluid Dynamic Gauging: A New Tool to Study Deposition on Porous Surfaces. *Journal of Membrane Science*, 296, 29-41.

Chew, J. Y. M., Paterson, W. R. & Wilson, D. I. 2010. Application of Fluid Dynamic Gauging and Optical Imaging to Membrane Fouling. *In: Fouling & Cleaning in Food Processing 2010.* Cambridge, UK: Department of Chemical Engineering, Cambridge.

Christoforou, C.C., Westermann-Clark, G.B. & Anderson, J.L. 1985. The Streaming Potential and Inadequacies of the Helmholtz Equation. *Journal of Colloid and Interface Science*, 106, 1-11.

Claussen, P. 1978. Membrane Filtration of SSL for By-Product Recovery and Pollution-Control. *Pulp & Paper-Canada*, 79, 41-45.

Coulson, J. M., Richardson, J. F., Backhurst, J. R. & Harker, J. H. 1997. Chemical Engineering: Particle Technology Separation Processes. Vol 2, Pergamon Press, Oxford.

Curtin, L.V. 1983. Molasses – General Considerations. Molasses in Animal Nutrition. National Feed Ingredients Association,West Des Moines, Iowa.

Dal-Cin, M.M., Mclellan, F., Striez, C.N., Tam, C.M., Tweddle, T.A. & Kumar, A. 1996. Membrane Performance with a Pulp Mill Effluent: Relative Contributions of Fouling Mechanisms. *Journal of Membrane Science*, 120, 273-283.

Daufin, G., Labbe, JP., Quemerais, A. & Michel, F. 1991. Fouling of an Inorganic Membrane during Ultrafiltration of Defatted Whey-Protein Concentrates. *Netherlands Milk and Dairy Journal*, 45, 259-272.

Decloux, M., Tatoud, L. & Mersad, A. 2000. Removal of Colorants and Polysaccharides from Raw Cane Sugar Remelts by Ultrafiltration. *Zuckerindustrie*, 125, 106-113.

Delaunay, D., Rabiller-Baudry, M., Paugam, L., Pihlajamäki, A. & Nyström, M. 2006. Physico-Chemical Characterisations of a UF Membrane Used in Dairy Application to Estimate Chemical Efficiency of Cleaning. *Desalination*, 200, 189–191.

Doyen, W., Adriansens, W., Molenberghs, B. & Leysen, R. 1996. A Comparison between Polysulfone, Zirconia and Organo-Mineral Membranes for use in Ultrafiltration. *Journal of Membrane Science*, 113, 247-258.

D'souza, N. M. & Mawson, A. J. 2005. Membrane Cleaning in the Dairy Industry: A Review. *Critical Reviews in Food Science and Nutrition*, 45, 125-134.

Eagles, W. P. & Wakeman, R. J. 2002. Interactions between Dissolved Material and the Fouling Layer during Microfiltration of a Model Beer Solution. *Journal of Membrane Science*, 206, 253-264.

Elimelech, M. & Bhattacharjee, S. 1998. A Novel Approach for Modelling Concentration Polarization in Crossflow Membrane Filtration based on the Equivalence of Osmotic Pressure Model and Filtration Theory. *Journal of Membrane Science*, 145, 223-241.

Evans, P. J. & Bird, M. R. 2006. Solute-Membrane Fouling Interactions during the Ultrafiltration of Black Tea Liquor. *Food and Bioproducts Processing*, 84, 292-301.

Evans, P. J. 2008. Membrane – Solute – Cleaning Agent Interaction during the Ultrafiltration of Black Tea Liquor. Doctoral Dissertation, Chemical Engineering Department, University of Bath.

Evans, P. J., Bird, M. R., Pihlajamäki, A. & Nyström, M. 2008. The Influence of Hydrophobicity, Roughness and Charge upon Ultrafiltration Membranes for Black Tea Liquor Clarification, *Journal of Membrane Science*, 313, 250-262.

Evans, P.J. & Bird, M.R. 2010. The Role of Black Tea Feed Conditions upon Ultrafiltration Performance during Membrane Fouling and Cleaning. *Journal of Food Process Engineering*, 33, 309-332.

Evtuguin, D.V., Quinta, T., Magina , S., Marques, A. P., Amado, F.M.L,& Prates, A. 2008. Study on the Chemical Composition of Lignosulphonates from Acidic Magnesium-Based Sulphite Pulping of *E. globulus*, [1]CICECO/Department of Chemistry, University of Aveiro

Fan L., Nguyen, T., Roddick, F.A. & Harris, J.L .2008. Low-Pressure Membrane Filtration of Secondary Effluent in Water Reuse: Pre-Treatment for Fouling Reduction. *Journal of Membrane Science*, 320, 135-142.

Fane, A. G. & Fell, C. J. D. 1987. A Review of Fouling and Fouling Control in Ultrafiltration. *Desalination*, 62, 117-136.

Field, R. & Aimar, P. 1993. Ideal Limiting Fluxes in Ultrafiltration. *Journal of Membrane Science*, 80, 107-115.

Field, R. W., Wu, D., Howell, J. A. & Gupta, B. B. 1995. Critical Flux Concept for Microfiltration Fouling. *Journal of Membrane Science*, 100, 259-272.

Fievet, P., Szynczyk, A. & Sbai, M. 2006. Tangential Streaming Potential as a Tool in the Characterisation of Microporous Membranes. *Desalination*, 199, 18-19.

Fryer, P.J. 1997. Thermal treatment of foods, in: P.J. Fryer, D.L. Pyle, C.D. Rielly (Eds.), *Chemical Engineering for the Food Industry*, Blakie Academic and Professional, London, 331 – 382.

Fontyn, M., Vantriet, K. & Bijsterbosch, B. H. 1991. Surface Spectroscopic Studies of Pristine and Fouled Membranes .1. Method Development and Pristine Membrane Characterization. *Colloids and Surfaces*, 54, 331-347.

Gabrus, E. & Szaniawska, D. 2008. Study on Fouling of Ceramic Membranes during Microfiltration of Yeast Suspensions. *Przemysl Chemiczny*, 87, 444-446.

Gale, G. E. 1995. A Thickness Measuring Device using Pneumatic Gauging to Detect the Sample. *Measurement Science & Technology*, 6, 1566-1571.

Gekas, V., Persson, K. M., Wahlgren, M. & Sivik, B. 1992. Contact Angles of Ultrafiltration Membranes and their Possible Correlation to Membrane Performance. *Journal of Membrane Science,* 72, 293-302.

Gesan, G., Daufin, G., Merin, U. & Labbe, J. 1995. Microfiltration Performance: Physicochemical Aspects of Whey Pre-Treatment. *Journal of Dairy Research,* 62, 269-279.

Gordon, P. W., Brooker, A. D. M., Chew, Y. M. J., Wilson, D. I. & York, D. W. 2010a. A Scanning Fluid Dynamic Gauging Technique for Probing Surface Layers. *Measurement Science and Technology*, 21, 1-10.

Gordon, P. W., Brooker, A. D. M., Chew, Y. M. J., Wilson, D. I. & York, D. W. 2010b. Studies into the Swelling of Gelatine Films using a Scanning Fluid Dynamic Gauge. *Food and Bioproducts Processing,* 88, 357-364.

Gowman, L.M. & Ethier, C.R. 1997. Concentration and Concentration Gradient Measurements in an Ultrafiltration Concentration Polarization Layer Part I: A Laser-Based Refractometric Experimental Technique. *Journal of Membrane Science,* 131, 95-105.

Gu, T., Chew, Y. M. J., Paterson, W. R. & Wilson, D. I. 2009a. Experimental and CFD Studies of Fluid Dynamic Gauging in Annular Flows. *AIChE Journal,* 55, 1937-1947.

Gu, T., Chew, Y. M. J., Paterson, W. R. & Wilson, D. I. 2009b. Experimental and CFD Studies of Fluid Dynamic Gauging in Duct Flows. *Chemical Engineering Science,* 64, 219-227.

Gu, T., Albert, F., Augustin, W., Chew, Y. M. J., Mayer, M., Paterson, W. R., Scholl, S.,Sheikh, I., Wang, K. & Wilson, D. I. 2011a. Application of Fluid Dynamic Gauging to Annular Test Apparatuses for Studying Fouling and Cleaning. *Experimental Thermal and Fluid Science,* 35, 509-520.

Gu, T., Albert, F., Augustin, W., Chew, Y. M. J., Paterson, W. R., Scholl, S., Sheikh, I., Wang, K. & Wilson, D. I. 2011b. Fluid Dynamic Gauging Applied to Annular Test Apparatuses for Fouling and Cleaning. *Heat Transfer Engineering,* 32, 339-348.

Güell, C., Ferrando, M. & López, F. 2009. Monitoring and Visualizing Membrane-Based Processes. Wiley-VCH, Tarragona, Spain.

Gyura, J.; Šereš, Z. & Eszterle, M. 2005. Influence of Operating Parameters on Separation of Green Syrup Colored Matter from Sugar Beet by Ultra- and Nanofiltration. *Journal of Food Engineering*, 66, 89-96.

Hamachi, M. & Mietton-Peuchot, M. 1999. Experimental Investigations of Cake Characteristics in Crossflow Microfiltration. *Chemical Engineering Science*, 54, 4023-4030.

Hamachi, M. & Mietton-Peuchot, M. 2001. Cake Thickness Measurement with an Optical Laser Sensor. *Chemical Engineering Research & Design,* 79, 151-155.

Hamachi, M. & Mietton-Peuchot, M. 2002. Analysis of Deposit Behaviour in Crossflow Microfiltration by Means of Thickness Measurement. *Chemical Engineering Journal,* 251-257.

Hamachi, M., Gupta, B.B. & Ben Aim, R. 2003. Ultrafiltration: A Means for Decolorization of Cane Sugar Solution. *Separation and Purification Technology*, 30, 229-239.

Hermia, J. 1982. Constant Pressure Blocking Filtration Laws-Application to Power Law Non-Newtonian Fluids. *Transactions of the Institution of Chemical Engineers,* 60**,** 183-187.

Hiemenz, P.C. 1997. Principles of Colloid and Surface Chemistry. 3rd Ed., Dekker, New York.

Hilal, N., Al-Khatib, L., Atkin, B.P., Kochkodan, V. & Potapchenko, N. 2003. Photochemical Modification of Membrane Surfaces for (Bio) Fouling Reduction: A Nano-Scale Study using AFM. *Desalination*, 158: 65–72.

Hilal, N., Ogunbiyi, O. O., Miles, N. J. & Nigmatullin, R. 2005. Methods Employed for Control of Fouling in MF and UF Membranes: A Comprehensive Review. *Separation Science and Technology*, 40, 1957-2005.

Hinková, A., Bubnik, Z., Kadlec, P., Pour, V. & Starhova, H. 2000. Membrane Filtration in the Sugar Industry. *In: 27th International Conference of the Slovak-Society-of Chemical-Engineering*, 27, 375-382.

Hinková, A., Bubnik, Z., Kadlec, P. & Pridal, J. 2002. Potentials of Separation Membranes in the Sugar Industry. *Separation and Purification Technology*, 26, 101-110.

Hobbs, C. Hong, S. & Taylor, J. 2006. Effect of Surface Roughness on Fouling of RO and NF Membranes during Filtration of a High Organic Surficial Groundwater. *Journal of Water Supply: Research and Technology*, 58, 559-570.

Hocking, M.B. 1997. Vanillin: Synthetic Flavoring from Spent Sulfite Liquor. *Journal of Chemical Education*, 74, 1055-1059.

Holser, R.A. 2008. Thermal Analysis of Glycerol Citrate/Starch Blends. *Journal of Applied Polymer Science*, 110, 1498–1501.

Hooper, R. J., Liu, W., Fryer, P. J., Paterson, W. R., Wilson, D. I. & Zhang, Z. 2006a. Comparative Studies of Fluid Dynamic Gauging and a Micromanipulation Probe for Strength Measurements. *Food and Bioproducts Processing*, 84, 353-358.

Hooper, R. J., Paterson, W. R. & Wilson, D. I. 2006b. Comparison of Whey Protein Model Foulants for Studying Cleaning of Milk Fouling Deposits. *Food and Bioproducts Processing*, 84, 329-337.

Huisman, I. 1998. Crossflow Microfiltration of Particle Suspensions. Doctoral Dissertation, Lund University.

Huisman, I. H., Trägårdh, G., Trägårdh, C. & Pihlajamäki, A. 1998. Determining the Zeta-Potential of Ceramic Microfiltration Membranes using the Electroviscous Effect. *Journal of Membrane. Science*, 147, 187-194.

Huisman, I. H., Prádanos, P. & Hernández, A. 2000. Electrokinetic Characterisation of Ultrafiltration Membranes by Streaming Potential, Electroviscous Effect, and Salt Retention. *Journal of Membrane Science*, 178, 55-64.

Hunter, R. J. 1981. Zeta Potential in Colloid Science: Principles and Applications. Academic Press, London.

Hwang, K.J., Wu, Y.S. & Lu, W.M.1996. The Surface Structure of Cake Formed by Uniform-Sized Rigid Spheroids in Cake Filtration. *Powder Technology*, 87, 161-168.

Jeżowska, A., Schipolowski, T. & Wozny, G. 2006. Influence of Simple Pre-Treatment Methods on Properties of Membrane Material. *Desalination*, 189, 43–52.

Jiraratananon, A. & Chanachai, A. 1996. A Study of Fouling in the Ultrafiltration of Passion Fruit Juice. *Journal of Membrane Science*, 111, 39-48.

Jones, S.A., Chew, Y.M.J., Bird, M.R., Wilson, D.I. 2010. The Application of Fluid Dynamic Gauging in the Investigation of Synthetic Membrane Fouling Phenomena. *Food and Bioproduct Process*, 88, 409 – 418.

Jones, S.A., Wilson, D.I., Chew, Y.M.J., Bird, M.R. 2012. Fluid Dynamic Gauging of Microfiltration Membranes Fouled with Sugar Beet Molasses. *Journal of Food Engineering*, 108, 22 – 29.

Jönsson, G. 1984. Boundary Layer Phenomena during Ultrafiltration of Dextran and Whey Protein Solutions. *Desalination*, 51, 61-77.

Jönsson, C. & Jönsson, A. S. 1995. Influence of the Membrane Material on the Adsorptive Fouling of Ultrafiltration Membranes. *Journal of Membrane Science*, 108, 79-87.

Jönsson, A. S. & Trägårdh, G. 1990. Fundamental Principles of Ultrafiltration. *Chemical Engineering and Processing*, 27, 67-81.

Jönsson, A. S. & Wimmerstedt, R. 1985. The Application of Membrane Technology in the Pulp and Paper-Industry. *Desalination*, 53, 181-196.

Kalhoinen, M., Pekkarinen, M., Manttari, M., Nuortila-Jokinen, J. & Nystrom, M. 2007. Comparison of the Performance of Two Different Regenerated Cellulose Ultrafiltration Membranes at High Filtration Pressure. *Journal of Membrane Science*, 294, 93-102.

Kane, D.R. & Middlemass, N.R. 1985. Cleaning Chemicals state of the knowledge in 1985. *Fouling and Cleaning in Food Processing*, 312.

Kaur, S., Kaler, R. S. S. & Aamarpali. 2002. Effect of Starch on the Rheology of Molasses. *Journal of Food Engineering*, 55, 319-322.

Khulbe, K.C., Feng, C.Y. & Matsuura, T. 2008. Synthetic Polymeric Membranes Characterization by Atomic Force Microscopy. Springer-Verlag, Berlin.

Kim, K.J., Fane, A.G., Fell, C.J.D. & Joy, D.C. 1992. Fouling Mechanisms of Membranes during Protein Ultrafiltration. *Journal of Membrane Science*, 68, 79-91.

Kim, K. J., Sun, P. S., Chen, V., Wiley, D. E. & Fane, A. G. 1993. The Cleaning of Ultrafiltration Membranes Fouled by Protein. *Journal of Membrane Science,* 80, 241-249.

Kim, K. J., Fane, A. G., Nystrom, M., Pihlajamaki, A., Bowen, W. R. & Mukhtar, H. 1996. Evaluation of Electroosmosis and Streaming Potential for Measurement of Electric Charges of Polymeric Membranes. *Journal of Membrane Science,* 116, 149-159.

Kim, A.S. & Hoek. E.M.V. 2002. Cake Structure in Dead-End Membrane Filtration: Monte Carlo Simulations. *Environmental Engineering Science,* 19, 373-386.

Kochan, J., Wintgens, T., Hochstrat, R. & Melin, T. 2009. Impact of Wetting Agents on the Filtration Performance of Polymeric Ultrafiltration Membranes. *Desalination*, 34-42.

Koltuniewicz, A. B., Field, R. W. & Arnot, T. C. 1995. Cross-Flow and Dead-End Microfiltration of Oily-Water Emulsion .1. Experimental-Study and Analysis of Flux Decline. *Journal of Membrane Science,* 102, 193-207.

Kulkarni, A., Mukherjee, D. & Gill, WN. 1994. Reprocessing Hydrofluoric-Acid Etching Solutions by Reverse-Osmosis. *Chemical Engineering Communications*, 129, 53-68.

Kumar, A. 2009. Bioseparation Engineering: A Comprehensive DSP Volumen. I K International Publishing House.

Laorko, A., Li, Z., Tongchitpakdee, S., Chantachum, S., & Youravong, W. 2010. Effect of Membrane Property and Operating Conditions on Phytochemical Properties and Permeate Flux during Clarification of Pineapple Juice. *Journal of Food Engineering,* 100, 514-521.

Lawrence, N. D., Perera, J. M., Iyer, M., Hickey, M. W. & Stevens, G. 2006. The Use of Streaming Potential Measurements to Study the Fouling and Cleaning of Ultrafiltration Membranes. *Separation and Purification Technology*, 48, 106-112.

Lee, DN. & Merson, R. 1976. Prefiltration of Cottage Cheese Whey to Reduce Fouling of Ultrafiltration Membranes. *Journal of Food Science*, 41, 403-140.

Li, H., Fane, A.G., Coster, H.G.L. & Vigneswaran, S. 1998. Direct Observation of Particle Deposition on the Membrane Surface During Crossflow Microfiltration. *Journal of Membrane Science*, 149, 83-97.

Li, H., Fane, A.G., Coster, H.G.L. & Vigneswaran, S. 2000. An assessment of depolarisation models of crossflow microfiltration by direct observation through the membrane. *Journal of Membrane Science,* 172, 135-147.

Li, J., Sanderson, R. D. & Jacobs, E. P. 2002. Non-Invasive Visualization of the Fouling of Microfiltration Membranes by Ultrasonic Time-Domain Reflectometry. *Journal of Membrane Science,* 201, 17-29.

Li, J. X., Hallbauer, D. K. & Sanderson, R. D. 2003. Direct Monitoring of Membrane Fouling and Cleaning during Ultrafiltration using a Non-Invasive Ultrasonic Technique. *Journal of Membrane Science,* 215, 33-52.

Li, J.-X., Sanderson, R. D. & Chai, G. Y. 2006. A Focused Ultrasonic Sensor for in situ Detection of Protein Fouling on Tubular Ultrafiltration Membranes. *Sensors and Actuators B: Chemical,* 114, 182-191.

Lin, J.C.T., Lee, D.J. & Huang, C. 2010. Membrane fouling mitigation: Membrane cleaning. *Separation Science and Technology*, 45, 858-872.

Lipnizki, F., Carter, M. & Tragardh, G. 2006. Applications of Membrane Processes in the Beet and Cane Sugar Production. *Zuckerindustrie*, 131, 28-38.

Lister V.Y., Lucas, C., Gordon, P.W., Chew, Y.M.J. & Wilson, D.I. 2011 Pressure Mode Fluid Dynamic Gauging for Studying Cake Build-Up in Crossflow Microfiltration. *Journal of Membrane Science,* 336, 1-2, 304 – 313.

Liu, C., Caothien, S. & Hayes, J. 2000. Membrane Chemical Cleaning: From Art to Science, *Scientific and Laboratory Services*, Pall Corporation.

Maartens, A., Swart, P. & Jacobs, E. P. 2000. Membrane Pre-treatment: A Method for Reducing Fouling by Natural Organic Matter. *Journal of Colloid and Interface Science,* 221, 137-142.

Maartens, A., Jacobs, E. P. & Swart, P. 2002. UF of Pulp and Paper Effluent: Membrane Fouling-Prevention and Cleaning. *Journal of Membrane Science,* 209, 81-92.

Madaeni, S.S., Saedi, S.H., Rahimpour, F. & Zereshki, S .2009. Optimization of Chemical Cleaning for Removal of Biofouling Layer. *Chemical Product and Process Modeling*, 4, 1-16.

Mairal, A. P., Greenberg, A. R., Krantz, W. B. & Bond, L. J. 1999. Real-Time Measurement of Inorganic Fouling of RO Desalination Membranes using Ultrasonic Time-Domain Reflectometry. *Journal of Membrane Science*, 159, 185-196.

Makardij, A., Chen, X. D. & Farid, M. M. 1999. Microfiltration and Ultrafiltration of Milk: Some Aspects of Fouling and Cleaning. *Food and Bioproducts Processing*, 77, 107-113.

Mänttari, M., Pihlajamäki, A. & Nyström, M. 2006. Effect of pH on Hydrophilicity and Charge and their Effect on the Filtration Efficiency of NF Membranes at Different pH. *Journal of Membrane Science,* 280, 311-320.

Marques, A. P., Evtuguin, D. V., Magina, S., Amado, F. M. L. & Prates, A. 2009a. Chemical Composition of Spent Liquors from Acidic Magnesium–Based Sulphite Pulping of Eucalyptus globulus. *Journal of Wood Chemistry and Technology*, 29, 322–336.

Marques, A. P., Evtuguin, D. V., Magina, S., Amado, F. M. L. & Prates, A. 2009b. Structure of Lignosulphonates from Acidic Magnesium-Based Sulphite Pulping of *Eucalyptus globulus*. *Journal of Wood Chemistry and Technology*, 29, 337-357.

Marselina, Y., Lifia, Le-Clech, P., Stuetz, R. M. & Chen, V. 2009. Characterisation of Membrane Fouling Deposition and Removal by Direct Observation Technique. *Journal of Membrane Science,* 341**,** 163-171.

Marshall, A. D., Munro, P. A. & Tragardh, G. 1993. The Effect of Protein Fouling in Microfiltration and Ultrafiltration on Permeate Flux, Protein Retention and Selectivity - A Literature-Review. *Desalination*, 91, 65-108.

Matzinos, P. & Alvarez, R. 2002. Effect of Ionic Strength on Rinsing and Alkaline Cleaning of Ultrafiltration Inorganic Membranes Fouled with Whey Proteins. *Journal of Membrane Science*, 208, 23-30.

McAlister, J.J., Smith, B.J. & Neto, J.A.B. 2000. The Presence of Calcium Oxalate Dihydrate (Weddellite) in Street Sediments from Niteroi, Brazil and its Health Implications. *Environ. Geochem. Health*., 22, 195-210.

McNulty, M. 1997. Sugarcane and the Everglades. *Journal of the American Society of Sugar Cane Technologists*, 9-12.

Mendret, J., Guigui, C., Schmitz, R. & Cabassud, C. 2007. An Optical Method for In Situ Characterization of Fouling During Filtration. *AIChE Journal*, 53, 2265-2274.

Mendret, J., Guigui, C., Schmitz, R. & Cabassud, C. 2009. In Situ Dynamic Characterisation of Fouling Under Different Pressure Conditions during Dead-End Filtration: Compressibility Properties of Particle Cakes. *Journal of Membrane Science,* 333, 20-29.

Mercadé- Prieto, R. & Chen, X.D. 2005. Caustic-Induced Gelation of Whey Deposits in the Alkali Cleaning of Membranes. *Journal of Membrane Science,* 254, 157 – 167.

Metsämuuronen, S., Howell, J. & Nyström, M. 2002. Critical Flux in Ultrafiltration of Myoglobin and Baker's Yeast. *Journal of Membrane Science,* 196, 13-25.

Metsämuuronen, S. 2003. Critical Flux and Fouling in Ultrafiltration of Proteins. Doctoral

Dissertation, Lappeenranta University of Technology.

Mikulasek, P. 1994. Methods to Reduce Concentration Polarization and Fouling in Membrane Filtration. *Collection of Czechoslovak Chemical Communications*, 59, 737-755.

Mousavi, S.M. & Moghadam, M.T. 2009. Separation of Sugar from Molasses by Ultrafiltration and Nanofiltration. *World Applied Sciences Journal*, 7, 632-636.

Mulder, M. 2000. Basic Principles of Membrane Technology. 2nd Ed., Kluwer Academic Publishers, Netherlands.

Muthukumaran, S., Kentish, S. E., Ashokkumar, M. & Stevens, G. W. 2005. Mechanisms for the Ultrasonic Enhancement of Dairy Whey Ultrafiltration. *Journal of Membrane Science*, 258, 106-114.

Muthukumaran, S., Kentish, S. E., Stevens, G. W., Ashokkumar, M. & Mawson, R. 2007. The Application of Ultrasound to Dairy Ultrafiltration: The Influence of Operating Conditions. *Journal of Food Engineering*, 81, 364-373.

Myrvold, B. O. 2008. A New Model for the Structure of Lignosulphonates Part 1. Behaviour in Dilute Solutions. *Industrial Crops and Products*, 27, 214-219.

Nigam, M.O., Bansal, N.B. & Chen, X.D. 2008. Fouling and Cleaning of Whey Protein Concentrate Fouled Ultrafiltration Membranes. *Desalination*, 218, 313-322.

Nordzucker. 2008. Personal Correspondence; Composition of Insoluble Solids in Molasses, Nakskov: Nordzucker.

Nyström, M., Pihlajamäki, A. & Ehsani, N. 1994. Characterization of Ultrafiltration Membranes by Simultaneous Streaming Potential and Flux Measurements. *Journal of Membrane Science*, 87, 245-256.

Nyström, M. & Zhu, H.H. 1997. Characterization of Cleaning Results using Combined Flux and Streaming Potential Methods. *Journal of Membrane Science*, 131, 195-205.

Okamoto, Y., Ohmori, K. & Glatz, C.E. 2001. Harvest Time Effects on Membrane Cake Resistance of Escherichia Coli Broth. *Journal of Membrane Science*, 190, 93-106.

Opong, W.S. & Zydney, A.L. 1991. Diffusive and Convective Protein Transport through Asymmetric Membranes. *AIChE Journal*, 37, 1497-1510.

Ousman, M. & Bennasar, M. 1995. Determination of Various Hydraulic Resistances during Crossflow Filtration of a Starch Grain Suspension through Inorganic Membranes. *Journal of Membrane Science*, 105, 1-21.

Peralta, J. M., Chew, Y. M. J. & Wilson, D. I. 2011. An Analytical Method for Selecting the Optimal Nozzle External Geometry for Fluid Dynamic Gauging. *Chemical Engineering Science*, 66, 3579-3591.

Pihlajamäki, A., Väisänen, P. & Nyström, M. 1996. Characterization of Clean and Fouled Polymeric Ultrafiltration Membranes by Fourier Transform IR Spectroscopy Attenuated Total Reflection. *Colloid Surfaces A: Physicochem. Eng. Aspects*, 138, 323-333.

Pihlajamäki, A. 1998. Electrochemical Characterisation of Filter Media Properties and their Exploitation in Enhanced Filtration. Doctoral Dissertation, Lappeenranta University of Technology.

Popović, S.S., Tekić, M.N. & Djurić, M.S. 2009. Kinetic Models for Alkali and Detergent Cleaning of Ceramic Tubular Membrane Fouled with Whey Proteins. *Journal of Food Engineering*, 94, 307 – 315.

Prádanos, P., Arribas, J. I. & Hernandez, A. 1995. Mass Transfer Coefficient and Retention of Pegs in Low Pressure Cross-Flow Ultrafiltration through Asymmetric Membranes. *Journal of Membrane Science*, 99, 1-20.

Puro, L., Manttari, M., Pihlajamaki, A. & Nystrom, M. 2006. Characterization of Modified Nanofiltration Membranes by Octanoic Acid Permeation and FTIR Analysis. *Chemical Engineering Research & Design*, 84, 87-96.

Rana, D., Matsuura, T., Narbaitz, R. M. & Feng, C. 2005. Development and Characterization of Novel Hydrophilic Surface Modifying Macromolecule for Polymeric Membranes. *Journal of Membrane Science*, 249, 103-112.

Restolha, J.A, Prates, A., de Pinho, & Afonso, M.D. 2009. Sugars and Lignosulphonates

Recovery from Eucalyptus Spent Sulphite Liquor by Membrane Processes. *Biomass and Bioenergy*, 33, 1558-1566.

Riedl, K., Girard, B. & Lencki, R.W. 1998a. Influence of Membrane Structure on Fouling Layer Morphology during Apple Juice Clarification. *Journal of Membrane Science,* 139, 155-166.

Riedl, K., Girard, B. & Lencki, R.W. 1998b. Interactions Responsible for Fouling Layer Formation during Apple Juice Microfiltration. *Journal of Agricultural and Food Chemistry*, 46, 2458–2464.

Ring, T.A. 2009. Comparison of Raman and ATR-FTIR Spectroscopy of Aqueous Sugar Solutions [Online], Salt Lake City: University of Utah, Available from: www.che.utah.edu/~ring/Sample%20Memo%20Report.doc.

Rogé, B., Bensouissi, A. & Mathlouthi, M. 2007. Effect of Calcium on White Sugar Turbidity. *Zuckerindustrie*, 132, 170-174.

Saikhwan, P., Geddert, T., Augustin, W., Scholl, S., Paterson, W. R. & Wilson, D. I. 2006. Effect of Surface Treatment on Cleaning of a Model Food Soil. *Surface & Coatings Technology*, 201, 943-951.

Saikhwan, P., Chew, J. Y. M., Paterson, W. R. & Wilson, D. I. 2007. Swelling and Its Suppression in the Cleaning of Polymer Fouling Layers. *Industrial & Engineering Chemistry Research*, 46, 4846-4855.

Saksena, S. & Zydney, A.L.1997. Influence of Protein-Protein Interactions on Bulk Mass Transport during Ultrafiltration. *Journal of Membrane Science*, 125, 93-108.

Sanderson, R.D., Li, J., & Jacobs, E. P. 2002. Non-invasive in situ visualisation of membrane fouling and cleaning processes in microfiltration by ultrasonic signal reflection. *Water Sa Special Edition: Wisa Biennial Conference 2002*, 78-85.

Saska, M. & De Lataillade, J. 1994. Concentration and Decolorization of Dilute Products from Cane Molasses Desugarization with Reverse Osmosis and Nanoflitration Membranes. *Sugar Industry Technologists Meeting*, 8-11 May 1994, Honolulu, Hawai.

Scott, K. & Hughes, R. 1996. Industrial Membrane Separation Technology. Blackie Academic & Professional, London.

Šereš, Z., Gyura, J., Filipovic, N. & Simovic, D.S. 2005. Application of Decolorization on Sugar Beet Pulp in Bread Production. *European Food Research and Technology*, 221, 54-60.

Šereš, Z., Gyura, J., Eszterle, M. & Djurić, M. 2006. Separation of Non-Sucrose Compounds from Syrup as a Part of the Sugar-Beet Production Process by Ultrafiltration with Ceramic Membranes. *European Food Research and Technology*, 223, 829-835.

Shimadzu. 2009. Measurement of Different Sugar based Samples like Sugar, Honey, Syrup with FTIR Technique, Duisburg: Shimadzu, (SCA_110_022).

Shirato, M., Aragaki, T. & Iritani, E. 1979. Blocking Filtration Laws for Filtration of Power-Law Non-Newtonian Fluids. *Journal of Chemical Engineering of Japan*, 12, 162-164.

Shorrock, C. J. & Bird, M. R. 1998. Membrane Cleaning: Chemically Enhanced Removal Of Deposits Formed During Yeast Cell Harvesting. *Food and Bioproducts Processing*, 76, 30-38.

Shorrock, C. J. 1999. Membrane Cleaning: Cleaning-in-place of a Microfiltration Membrane Fouled during Yeast Harvesting. Doctoral Dissertation, Chemical Engineering Department, University of Bath.

Shukla, R. & Cheryan, M. 2002. Performance of Ultrafiltration Membranes in Ethanol–Water Solutions: Effect of Membrane Conditioning. *Journal of Membrane Science,* 198, 75-85.

Silalahi, S.H.D., Leiknes, T., Ali, J. & Sanderson, R. 2009. Ultrasonic Time Domain Reflectometry for Investigation of Particle Size Effect in Oil Emulsion Separation with Crossflow Microfiltration. *Desalination*, 236, 143-151.

Smith, R. & Petela, E.A. 1994. Waste Minimisation in the Process Industry. *The Chemical Engineer*, 506, 1-21.

Song, L. 1998. A New Model for the Calculation of the Limiting Flux in Ultrafiltration. *Journal of Membrane Science*, 144, 173 - 185.

Sridhar, S. & Bhattacharya, P. K. 1991. Limiting Flux Phenomena in Ultrafiltration of Kraft Black Liquor. *Journal of Membrane Science*, 57, 187-206.

Steindl, R.J. 2001. Membrane Filtration Technology in the Cane Sugar Industry. *International Society of Sugar Cane Technologist*, 24, 3-14.

Steindl, R.J. & Rackemann, D.W. 2010. Membrane Filtration of Clarified Juice. *In: Procceddings of the 27th International Society of Sugar Cane Technologists Congress*, Veracruz, Mexico.

Tarabara, V. V., Koyuncu, I. & Wiesner, M. R. 2004. Effect of Hydrodynamics and Solution Ionic Strength on Permeate Flux in Cross-Flow Filtration: Direct Experimental Observation of Filter Cake Cross-Sections. *Journal of Membrane Science*, 241, 65-78.

Tarazaga, C.C., Campderros, M.E. & Padilla, A.P. 2006. Physical Cleaning by Means of Electric Field in the Ultrafiltration of a Biological Solution. *Journal of Membrane Science*, 278, 219-224.

Togrul, H. & Arslan, N. 2004. Mathematical Model for Prediction of Apparent Viscosity of Molasses. *Journal of Food Engineering*, 62, 281-289.

Todisco, S., Tallarico, P. & Gupta, B. B. 2002. Mass Transfer and Polyphenols Retention in the Clarification of Black Tea with Ceramic Membranes. *Innovative Food Science and Emerging Technologies*, 3, 255 - 262.

Toledo, R. T. 1991. Fundamentals of Food Processing and Engineering. 2nd Ed.,Van Nostrand Reinhold, New York.

Tracey, E. M. & Davis, R. H. 1994. Protein Fouling of Track-Etched Polycarbonate Microfiltration Membranes. *Journal of Colloid and Interface Science*, 167, 104-116.

Trägårdh, G. & Gekas, V. 1988. Membrane Technology in the Sugar Industry. *Desalination*, 69, 9-17.

Trägårdh, G. 1989. Membrane Cleaning, *Desalination*, 71, 325-335.

Tsapiuk, E. A., Bryk, M. T., Medvedev, M. I. & Kochkodan, V. M. 1989. Fractionation and Concentration of Lignosulfonates by Ultrafiltration. *Journal of Membrane Science*, 47, 107-130.

Tuladhar, T. R., Paterson, W. R., Macleod, N. & Wilson, D. I. 2000. Development of a Novel Non-Contact Proximity Gauge for Thickness Measurement of Soft Deposits and its Application in Fouling Studies. *Canadian Journal of Chemical Engineering*, 78, 935-947.

Tuladhar, T. R., Paterson, W. R. & Wilson, D. I. 2002a. Investigation of Alkaline Cleaning-In-Place of Whey Protein Deposits using Dynamic Gauging. *Food and Bioproducts Processing*, 80, 199-214.

Tuladhar, T. R., Paterson, W. R. & Wilson, D. I. 2002b. Thermal Conductivity of Whey Protein Films Undergoing Swelling - Measurement by Dynamic Gauging. *Food and Bioproducts Processing*, 80, 332-339.

Tuladhar, T. R., Paterson, W. R. & Wilson, D. I. 2003. Dynamic Gauging in Duct Flows. *Canadian Journal of Chemical Engineering*, 81, 279-284.

Tung, K.L, Li, Y.L., Wang, S., Nanda, D., Hu, C.C., Li, C.L., Lai, J.Y. & Huang, J. 2010. Performance and Effects of Polymeric Membranes on the Dead-End Microfiltration of Protein Solution during Filtration Cycles. *Journal of Membrane Science*, 352, 143-152.

Väisänen, P. 2004. Characterisation of Clean and Fouled Polymeric Membrane Materials. Doctoral Dissertation, Lappeenranta University of Technology

Väisänen, P., Bird, M. R. & Nystrom, M. 2002. Treatment of UF Membranes with Simple and Formulated Cleaning Agents. *Food and Bioproducts Processing*, 80, 98-108.

Vercellotti, J. R., Clarke, M. A., Godshall, M. A., Blanco, R. S., Patout, W. S. & Florence, R. A. 1998. Chemistry of Membrane Separation Processes in Sugar Industry Applications. *In: Annual Meeting of the Sugar-Industry-Technologists*, May 10-14 1998 Marseille, France, 736-745.

Vernhet, A. & Moutounet, M. 2002. Fouling of Organic Microfiltration Membranes by Wine Constituents: Importance, Relative Impact of Wine Polysaccharides and Polyphenols and Incidence of Membrane Properties. *Journal of Membrane Science*, 201, 103-122.

Vigneswaran, S. & Wong, YK. 1988. Detailed Investigation of Effects of Operating Parameters of Ultrafiltration using Laboratory-Scale Ultrafiltration Unit. *Desalination*, 70, 299-316.

Vrijenhoek, E.R., Hong, S. & Elimelech M. 2001. Influence of Membrane Surface Properties on Initial Rate of Colloidal Fouling of Reverse Osmosis and Nanofiltration Membranes. *Journal of Membrane Science*, 188, 115-128.

Wagner, J. 2001. Membrane Filtration Handbook: Practical Tips and Hints. 2nd Ed., Osmonics Inc, Minnetonka, USA.

Wallberg, O., Jonsson, A. S. & Wickstrom, P. 2001. Membrane Cleaning - A Case Study in a Sulphite Pulp Mill Bleach Plant. *Desalination*, 141, 259-268.

Wallberg, O., Jonsson, A. S. & Wimmerstedt, R. 2003. Fractionation and Concentration of Kraft Black Liquor Lignin with Ultrafiltration. *Desalination*, 154, 187-199.

Wang, Y., Kim, JH., Choo, KH., Lee, YS. & Lee, CH. 2000. Hydrophilic Modification of Polypropylene Microfiltration Membranes by Ozone-induced Graft Polymerization. *Journal of Membrane Science*, 169, 269–276.

Weis, A. & Bird, M. R. 2001. The Influence of Multiple Fouling and Cleaning Cycles upon the Membrane Processing of Lignosulphonates. *Food and Bioproducts Processing*, 79, 184-187.

Weis, A., Bird, M. R. & Nystrom, M. 2003. The Chemical Cleaning of Polymeric UF Membranes Fouled with Spent Sulphite Liquor over Multiple Operational Cycles. *Journal of Membrane Science*, 216, 67-79.

Weis, A. 2004. Fouling and Cleaning Synergy in Ultrafiltration Membrane System. Doctoral Dissertation, Chemical Engineering Department, University of Bath.

Weis, A., Bird, M. R., Nystrom, M. & Wright, C. 2005. The Influence of Morphology, Hydrophobicity and Charge upon the Long-Term Performance of Ultrafiltration Membranes Fouled with Spent Sulphite Liquor. *Desalination*, 175, 73-85.

Wijmans, J.G., Nakao, S., Van Den Berg, J.W.A., Troelstra, F.R., & Smolders, C.A. 1985. Hydrodynamic Resistance of 'Concentration Polarization Boundary Layers in Ultrafiltration. *Journal of Membrane Science*, 22, 117-135.

Wu, D., Howell, J.A. & Field, R.W. 1999. Critical Flux Measurement for Model Colloids. *Journal of Membrane Science*, 152, 89-98.

Wu, D. & Bird, M. R. 2007. The Fouling and Cleaning of Ultrafiltration Membranes During the Filtration of Model Tea Component Solutions. *Journal of Food Process Engineering*, 30, 293-323.

Yue, C.T., Li, S.Y., Ding, K.L. & Zhong, N.N. 2006.Thermodynamics and Kinetics of Reactions between C-1-C-3 Hydrocarbons and Calcium Sulphate in Deep Carbonate Reservoirs. *Journal of Geochemistry*, 40, 87-94.

Zhang, Y. P., Fane, A. G. & Law, A. W. K. 2010. Critical Flux and Particle Deposition of Fractal Flocs during Crossflow Microfiltration. *Journal of Membrane Science*, 353, 28-35.

Zhao, Y. & Yuan, Q. 2006. Effect of Membrane Pre-treatment on Performance of Solvent Resistant Nanofiltration Membranes in Methanol Solutions. *Journal of Membrane Science*, 280, 195-201.

Zhu, H. H. & Nystrom, M. 1998. Cleaning Results Characterized by Flux, Streaming Potential and FTIR Measurements. *Colloids and Surfaces a-Physicochemical and Engineering Aspects*, 138, 309-321.

Appendix A

Calibrations

A1: Displacement Measurement

The movement of the gauge was measured using the read out from the motor and the LVDT (Linear Variable Differential Transformer). The motor was 1 mm thread which was capable of 3200 steps, which each step equating to 0.3 µm. An LVDT was also used as a displacement measurement; the comparison of the two is in Table A.1.

Table A.1: Comparison of the two displacement methods used in the FDG measurements

Motor	LVDT	Actual Motor	Actual LVDT	Difference
-3200	4.9951	1.0000	0.9990	0.0010
-3000	4.6851	0.9375	0.9370	0.0005
-2500	3.916	0.7813	0.7832	-0.0020
-2000	3.1323	0.6250	0.6265	-0.0015
-1500	2.3633	0.4688	0.4727	-0.0039
-1000	1.582	0.3125	0.3164	-0.0039
-800	1.2646	0.2500	0.2529	-0.0029
-600	0.95459	0.1875	0.1909	-0.0034
-400	0.64697	0.1250	0.1294	-0.0044
-200	0.32471	0.0625	0.0649	-0.0024
0	0.014648	0.0000	0.0029	-0.0029
200	-0.29541	-0.0625	-0.0591	-0.0034
400	-0.60547	-0.1250	-0.1211	-0.0039
600	-0.91309	-0.1875	-0.1826	-0.0049
800	-1.2231	-0.2500	-0.2446	-0.0054
1000	-1.5283	-0.3125	-0.3057	-0.0068
1500	-2.3047	-0.4688	-0.4609	-0.0078
2000	-3.0811	-0.6250	-0.6162	-0.0088
2500	-3.8647	-0.7813	-0.7729	-0.0083
3000	-4.6387	-0.9375	-0.9277	-0.0098
3200	-4.9536	-1.0000	-0.9907	-0.0093
			Average:	0.0045
			SD:	0.0030
			Error:	**1.48** **%**

A2: Refractive Index

The molasses samples were measured in terms of ºBrix. The Brix value were gathered using an ABBÉ ‘60’ refractometer. This was measured by measuring the refractive index of the sample and relating it to the corresponding ºBrix (Figure A.2).

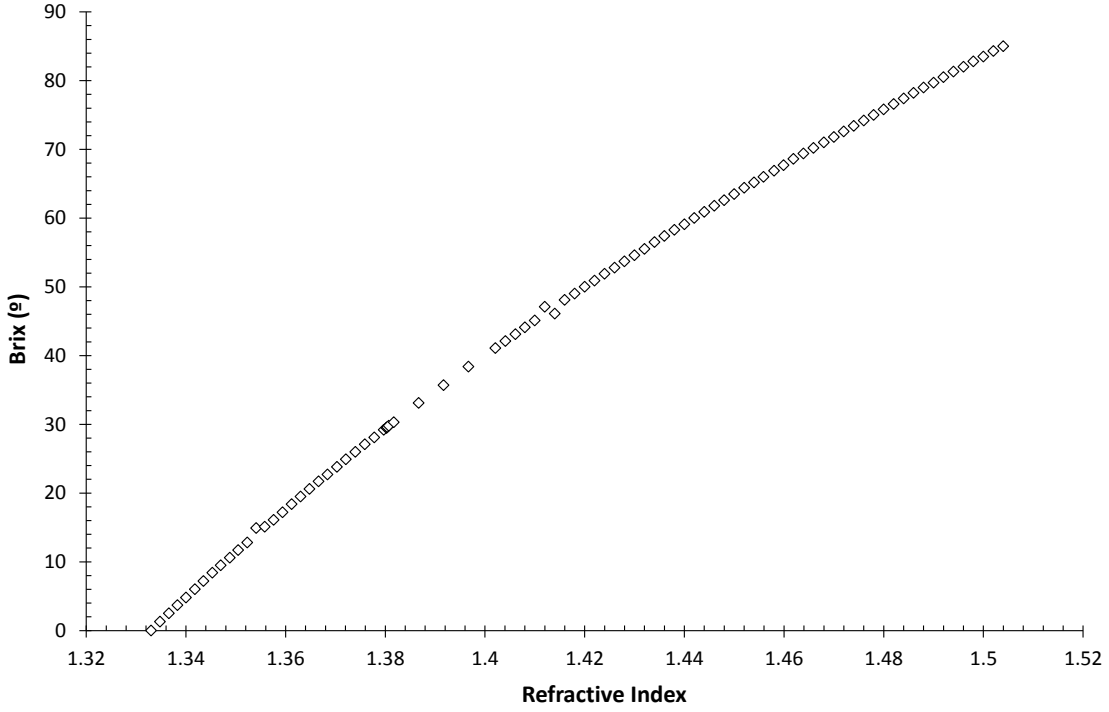

Figure A.1: Refractive index for varying Brix concentrations

Appendix B

Physical Properties

B1: Membrane Material

The operational conditions for the two different types of membrane material can be seen in Table B.1.

Table B.1: Recommended operating conditions (Alfa Laval, 2010)

	Polysulphone	Fluoropolymer
PRODUTCTION		
pH range	1 – 13	1 – 13
Pressure, bar	1 - 10	1 – 10
Temperature, °C	0 – 75	0 – 60
CLEANING		
pH range	1 – 13	1 – 13.5
Pressure, bar	1 - 5	1 – 5
Temperature, °C	1 – 75	1 - 65

B.2: Viscosity of Water and Cleaning Chemicals

The viscosity for water and the cleaning chemicals NaOH and citric acid used in this study are presented in Table B.2. The errors in these values are ± 0.0001.

Table B.2: Measured dynamic viscosities of water, NaOH and citric acid

Temp. (°C)	Water (Pa.s)	0.5 wt. % NaOH (Pa.s)	0.5 wt. % Citric Acid (Pa.s)
22	9.52E-04	9.28E-04	9.59E-04
50	5.47E-04	5.58E-04	5.52E-04
60	4.67E-04	4.54E-04	4.75E-04

B.3: SSL Viscosity

Using a Bohlin CVOR 200 rheometer the viscosity of SSL at the different filtration temperatures was recorded (Table B.3). The errors in these values are ± 0.0001.

Table B.3: Measured dynamic viscosities of 17.8 wt. % SSL

Temp. (°C)	SSL (Pa.s)
22	9.70E-04
50	5.52E-04
60	4.86E-04
70	4.12E-04

B.4: Molasses Viscosity

Using a Bohlin CVOR 200 rheometer the viscosity of molasses at the different filtration temperatures for 83 °Brix and 45 °Brix was recorded (Table B.4). The errors in these values are ± 0.0001.

Table B.4: Measured dynamic viscosities of 83 °Brix and 45 °Brix

Temp. (°C)	83 °Brix (Pa.s)	45 °Brix (Pa.s)
22	1.914	0.0015
40	0.878	0.00143
60	0.125	0.00136
70	0.062	0.00125

Appendix C

Sample Calculations

C.1: Linear Cross Flow Velocity and Reynolds Number

The Reynolds number is defined in Equation 9.1:

$$\mathrm{Re} = \frac{du\rho}{\mu} \qquad 9.1$$

where, d is the diameter of channel (m), u is the average linear velocity (ms^{-1}), ρ is the fluid density (kgm^{-3}), and μ is the fluid dynamic viscosity ($kgm^{-1}s^{-1}$).

The equivalent diameter (d_e) of the channel is used when the cross section is not circular. This can be found using the diagram and Equation 9.2:

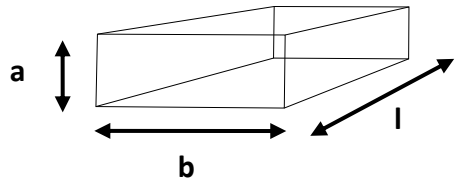

$$d_e = \frac{2ab}{a+b} \qquad 9.2$$

The linear velocity, u can be calculated using Equation 9.3.

$$u = \frac{Q}{abN} \quad = \left(\frac{m^3/s}{m^2} \right) \qquad 9.3$$

where, Q is the volumetric flowrate (m^3s^{-1}), and N is the number of channels. For a rectangular channel of height 0.001 m and width 0.007 m the effective diameter, d_e can be calculated using Equation 9.2.

$$d_e = \frac{2 \text{ x } 0.005 \text{ x } 0.01}{0.005 + 0.01} = 0.0067 \text{ m}$$

Using a flowrate of 6 Lm^{-1}:

$$u = \frac{6(60 \text{ x } 1000)}{0.001 + 0.007 \text{ x } 7} = 2.04 \text{ ms}^{-1}$$

The Reynolds number can be calculated using a 0.5 wt. % NaOH solution at 60 ºC, where ρ = 987.66 kgm^{-3} and μ = 4.54 x 10^{-4} $kgm^{-1}s^{-1}$:

$$\text{Re} = \frac{1.75\text{x}10^{-3} \text{ x } 2.04 \text{ x } 987.66}{4.54\text{x}10^{-4}} = 10332$$

C2: Flux measurement

Flux through a membrane is defined as the volume of fluid *V*, permeating the membrane in a given time *t*, through a known membrane area, A_m. The volume flux can be characterised by Equation 9.4.

$$J_v = \frac{\Delta V}{\Delta t A_m} \qquad 9.4$$

An example calculation is shown below where 100 g or 0.10 Litres (assuming permeate has the same density of water) of permeate (*V*) was collected in 5 seconds (*t*) through a membrane of area (A_m) 0.96 m^2:

$$J_v = \left(\frac{0.10}{5 \text{ x } 0.96} \right) \text{x } 3600 \quad = \quad 75 \text{ Lm}^{-2}\text{hr}^{-1}$$

C3: Resistance measurement

The membrane resistance (R_m) can be calculated by knowing the flux of permeate (J_v), the permeate fluid viscosity (μ_P) and the transmembrane pressure (ΔP), Equation 9.5.

$$R_m = \frac{\Delta P}{\mu_P \left(J_v\right)} \qquad 9.5$$

The membrane resistance was calculated either by the gradient of flux data or from individual flux points. Rearranging the equation above gives Equation 9.6.

$$J_m = \left(\frac{1}{R_m \mu_P}\right)\Delta P \qquad 9.6$$

The plotting of J_v vs. ΔP gives a gradient of $1/R_m\mu_p$, which enables the calculation of resistance (R).

C4: Effective Length Calculation

The effective length of the tube in the dead-end apparatus was determined by exploiting the siphon effect, by placing the tube in the tank with the nozzle removed, and at a high clearance from the surface (greater than 20 mm). The following steps were performed to calculate the effective length:

(i) Calculate mass flow rate:

$$\dot{m} = \frac{m}{t} \qquad 9.7$$

(ii) Calculate velocity for large and small tubing,

$$v = \frac{\dot{m}}{\rho A} \qquad 9.8$$

(iii) Calculate the Reynolds number for large and small tubing,

$$Re_t = \frac{4\dot{m}}{\pi \mu d_t} \quad 9.9$$

(iv) Calculate the Blasius coefficient,

$$f = 0.079 Re^{-0.25} \quad 9.10$$

(v) Calculate the total pressure of tubing,

$$\Delta P_{Tube} = \rho g H \quad 9.11$$

(vi) Calculate the pressure in the gauge section,

$$\Delta P_{Gauge} = \frac{32 \mu v l}{d_{tube}^2} \quad 9.12$$

(vii) Calculate the pressure in the additional tubing,

$$\Delta P_{length} = \Delta P_{Tube} - \Delta P_{Gauge} \quad 9.13$$

(viii) Calculate the effective length.

$$l_{eff} = \frac{2 \rho g H d_{tube}^4}{4 f \rho v^2} \quad 9.14$$

C5: Dead-end Thickness Calculation

The thickness calculations were made using data from the calibration profiles. An example calculation is shown below for the dead-end apparatus:

Data:

Diameter of nozzle throat, d_t	=	5.0 mm
Diameter of siphon tube, d_1	=	20.0 mm
Diameter of siphon tube, d_2	=	10.0 mm
Effective length of the tube 1, $l_{eff,1}$	=	420 mm
Effective length of the tube 2, $l_{eff,2}$	=	1800 mm

Experimental values:

Micrometer reading when nozzle tip touches membrane surface	=	10.00 mm
Micrometer reading at clearance *h* from deposit surface	=	12.80 mm
Hydrostatic head, H	=	20 mm
Water temperature	=	18 ˚C
Mass of discharge water collected, *m*	=	41.34 g
Time taken to collect sample, *t*	=	10.55 s

Mass flow rate:

(i) $\dot{m} = \frac{m}{t}$ = 3.92 gs^{-1}

Reynolds number:

(ii) $Re_t = \frac{4\dot{m}}{\pi \mu d_t}$ = 960

Pressure drop across siphon tube 1:

(iii) $\Delta p_{34,1} = \frac{128 \mu m l_{eff,1}}{\pi d_1^{\,4} \rho}$ = 0.43 Pa

Pressure drop across siphon tube 2:

(iv) $\Delta p_{34,2} = \frac{128 \mu m l_{eff,2}}{\pi d_2^{\,4} \rho}$ = 48.76 Pa

Total pressure drop across siphon tubes 1 and 2:

(v) $\Delta p_{34} = \Delta p_{34,1} + \Delta p_{34,2}$ = 0.43 + 48.76 = 49.19 Pa

The pressure drop across points 1 and 3 can now be calculated:

(vi) $\Delta p_{13} = \Delta p_{14} - \Delta p_{34}$ = ρgH – 49.19 = 136.79 Pa

Using all the data above the discharge coefficient (C_d) can now be calculated:

$$C_d = \frac{m_{actual}}{m_{ideal}} = \frac{m}{\frac{\pi d_t^{\,2}}{4}\sqrt{2\rho\Delta p_{13}}} = 0.48$$

The linear interpolation of the plot of C_d vs. h/d_t is then used to estimate h. With the knowledge of h_0 the deposit thickness (δ) is calculated:

$$\delta = h_0 - h$$

These steps are correct only if h/d_t is within the working range of the gauge ($h/d_t \leq 0.25$).

C6: Cross flow Thickness Calculation

The calculation for the discharge coefficient (C_d) and deposit thickness using the crossflow filtration apparatus is very similar as above. The steps include:

(i) Measurements of flowrate through the gauge, m

(ii) Measurement of differential pressure, $\Delta P_{14,}$ using a DP cell

(iii) Calculation of ΔP_{14}:

$$\Delta P_{13} = \Delta P_{14} - \Delta P_{34} = \Delta P_{14,measured} - \frac{32\mu u l_{eff}}{d^2}$$

(iv) These are then used to calculate, C_d:

$$C_d = \frac{m_{actual}}{m_{ideal}} = \frac{m}{\frac{\pi d_t^2}{4}\sqrt{2\rho\Delta p_{13}}}$$

(v) h/d_t is estimated through linear interpolation of a C_d vs. h/d_t plot with the corresponding conditions

(vi) h/d_t is then multiplied by d_t to give h, from which, δ, is given by h_0-h.

These steps are correct only if h/d_t is within the working range of the gauge ($h/d_t \leq 0.25$).

Appendix D

Error Analysis

D1: Flux Measurement

To ensure the reliability of the experimental data multiple measurements were performed at each stage. The membranes in this study are inhomogeneous hence they can produce flux variation. Therefore, the relative flux values were used to calculate the error values. The assumed error for flux data in the first part of the SSL and molasses measurements were determined based on two methods. Firstly the %error (absolute) for the largest different between the average and actual values is calculated. The second method, %error (statistical), was based on the standard deviation from the average value. An example set of data is shown in Table D.1a for SSL and Table D.1b for molasses.

The SSL data produced an error using method one of ± 5.76 %, using method two the error was ± 5.31 %. An error of ± 6 % was decided to be used for all flux data (except the pre-treatment work) to be statistically relevant; this is acceptable for the study of membrane fouling. In the pre-treatment work a different error value was used, calculated using the same methods described above. The Protocol 1 membranes produced an error of ± 4 % and Protocol 2 had an error value of ± 5 %.

The molasses data produced an error using method one of ± 6.64 %, using method two the error was ± 6.17 %. An error of ± 7 % was decided to be used for all flux data (except the pre-treatment work) to be statistically relevant; this is acceptable for the study of membrane fouling. In the pre-treatment work Protocol 1 produced an error of ± 3 % and Protocol 2 had an error of ± 4 %.

Table D.1a: Experimental flux data and error calculation for SSL filtration

Time	Time	Flux				Absolute Error					Statistical Error		
sec	min	Run 1	Run 2	Run 3	Average	Run 1	Run 2	Run 3	Largest	% Error	Average	SD	% Error
3000	50	0.152	0.172	0.169	0.164	0.012	0.008	0.004	0.012	7.557	0.164	0.011	6.648
3060	51	0.170	0.152	0.160	0.161	0.009	0.009	0.001	0.009	5.352	0.161	0.009	5.582
3120	52	0.169	0.145	0.180	0.165	0.004	0.019	0.015	0.019	11.770	0.165	0.018	10.743
3180	53	0.163	0.172	0.187	0.174	0.011	0.002	0.013	0.013	7.324	0.174	0.012	6.873
3240	54	0.163	0.158	0.169	0.163	0.000	0.005	0.005	0.005	3.259	0.163	0.005	3.237
3300	55	0.148	0.152	0.162	0.154	0.006	0.002	0.008	0.008	5.362	0.154	0.007	4.830
3360	56	0.163	0.166	0.175	0.168	0.005	0.002	0.007	0.007	4.084	0.168	0.006	3.612
3420	57	0.162	0.152	0.175	0.163	0.001	0.011	0.012	0.012	7.230	0.163	0.011	6.951
3480	58	0.169	0.155	0.169	0.164	0.005	0.009	0.004	0.009	5.564	0.164	0.008	4.819
3540	59	0.146	0.152	0.162	0.154	0.007	0.001	0.009	0.009	5.772	0.154	0.008	5.354
3600	60	0.158	0.172	0.175	0.168	0.010	0.004	0.006	0.010	6.184	0.168	0.009	5.398
3660	61	0.169	0.159	0.155	0.161	0.008	0.002	0.006	0.008	4.930	0.161	0.007	4.435
3720	62	0.152	0.159	0.162	0.158	0.006	0.001	0.005	0.006	3.718	0.158	0.005	3.414
3780	63	0.169	0.152	0.156	0.159	0.010	0.007	0.003	0.010	6.125	0.159	0.009	5.468
3840	64	0.158	0.139	0.172	0.156	0.001	0.017	0.016	0.016	10.237	0.156	0.017	10.746
3900	65	0.158	0.179	0.175	0.170	0.013	0.009	0.004	0.013	7.590	0.170	0.011	6.704
3960	66	0.166	0.166	0.160	0.164	0.002	0.002	0.004	0.004	2.313	0.164	0.003	2.004
4020	67	0.158	0.152	0.175	0.161	0.004	0.009	0.013	0.013	8.208	0.161	0.012	7.304
4080	68	0.169	0.152	0.162	0.161	0.008	0.009	0.001	0.009	5.603	0.161	0.008	5.240
4140	69	0.163	0.166	0.158	0.162	0.001	0.003	0.004	0.004	2.631	0.162	0.004	2.401
4200	70	0.163	0.168	0.162	0.165	0.001	0.003	0.002	0.003	2.102	0.165	0.003	1.834
4260	71	0.160	0.159	0.150	0.156	0.004	0.003	0.006	0.006	4.024	0.156	0.005	3.503
4320	72	0.158	0.145	0.169	0.157	0.000	0.012	0.011	0.012	7.513	0.157	0.012	7.396
4380	73	0.153	0.166	0.163	0.160	0.008	0.005	0.003	0.008	4.856	0.160	0.007	4.285
4440	74	0.163	0.149	0.162	0.158	0.005	0.009	0.004	0.009	5.820	0.158	0.008	5.046
4500	75	0.163	0.159	0.150	0.157	0.006	0.001	0.007	0.007	4.576	0.157	0.007	4.193
									Average:	**5.758**	**0.162**	**0.009**	**5.308**

Table D1b: Experimental flux data and error calculation for molasses filtration

Time	Time	Flux				Absolute Error					Statistical Error		
sec	min	Run 1	Run 2	Run 3	Average	Run 1	Run 2	Run 3	Largest	% Error	Average	SD	% Error
3000	50	0.064	0.060	0.062	0.062	0.002	0.002	0.000	0.002	3.073	0.062	0.002	3.07
3060	51	0.068	0.065	0.070	0.068	0.000	0.003	0.002	0.003	3.909	0.068	0.002	3.67
3120	52	0.073	0.060	0.066	0.066	0.007	0.006	0.000	0.007	9.800	0.066	0.006	9.52
3180	53	0.064	0.072	0.066	0.067	0.003	0.004	0.001	0.004	6.626	0.067	0.004	5.91
3240	54	0.064	0.066	0.058	0.063	0.001	0.003	0.004	0.004	7.049	0.063	0.004	6.27
3300	55	0.060	0.072	0.074	0.069	0.008	0.003	0.005	0.008	12.077	0.069	0.007	10.55
3360	56	0.062	0.068	0.066	0.065	0.003	0.003	0.001	0.003	4.040	0.065	0.003	4.70
3420	57	0.069	0.068	0.062	0.066	0.003	0.002	0.004	0.004	6.257	0.066	0.004	5.47
3480	58	0.062	0.060	0.070	0.064	0.002	0.004	0.006	0.006	9.096	0.064	0.005	7.98
3540	59	0.072	0.068	0.068	0.069	0.003	0.001	0.001	0.003	3.687	0.069	0.002	3.19
3600	60	0.069	0.067	0.071	0.069	0.000	0.002	0.002	0.002	2.899	0.069	0.002	2.90
3660	61	0.064	0.069	0.062	0.065	0.001	0.004	0.003	0.004	5.907	0.065	0.003	5.32
3720	62	0.064	0.060	0.071	0.065	0.001	0.005	0.006	0.006	8.929	0.065	0.005	8.27
3780	63	0.066	0.076	0.062	0.068	0.002	0.008	0.006	0.008	11.306	0.068	0.007	10.17
3840	64	0.069	0.064	0.074	0.069	0.000	0.005	0.005	0.005	6.950	0.069	0.005	6.93
3900	65	0.072	0.068	0.070	0.070	0.002	0.002	0.000	0.002	2.736	0.070	0.002	2.74
3960	66	0.066	0.072	0.068	0.069	0.003	0.003	0.001	0.003	4.700	0.069	0.003	4.32
4020	67	0.076	0.064	0.066	0.069	0.007	0.004	0.003	0.007	10.219	0.069	0.006	8.96
4080	68	0.068	0.064	0.062	0.065	0.003	0.001	0.003	0.003	3.935	0.065	0.003	4.51
4140	69	0.060	0.072	0.062	0.065	0.004	0.007	0.003	0.007	10.823	0.065	0.006	9.49
4200	70	0.072	0.076	0.070	0.072	0.001	0.003	0.003	0.003	4.400	0.072	0.003	4.03
4260	71	0.072	0.064	0.062	0.066	0.006	0.002	0.004	0.006	8.684	0.066	0.005	7.66
4320	72	0.060	0.072	0.070	0.067	0.007	0.004	0.003	0.007	10.413	0.067	0.006	9.13
4380	73	0.076	0.064	0.070	0.070	0.006	0.006	0.000	0.006	8.209	0.070	0.006	8.21
4440	74	0.069	0.067	0.071	0.069	0.000	0.002	0.002	0.002	2.668	0.069	0.002	2.93
4500	75	0.068	0.065	0.062	0.065	0.003	0.000	0.003	0.003	4.337	0.065	0.003	4.41
									Average:	**6.643**	**0.067**	**0.004**	**6.17**

D2: Gauging Experiments

The data in Figure 6.11 was used to calculate the error in the thickness experiments. The %error (statistical) was based on the standard deviation from the average value (Table D.2). This error margin of ± 5 μm has been deemed acceptable for the reliability of the FDG in this cross flow membrane filtration module.

Table D.2: Experimental thickness data and error calculation

T	Thickness (μm)			Average	SD	% Error
(Min)	Run 1	Run 2	Run 3	(μm)		
1	12	13	18	14	3.10	21.48
2	29	30	38	32	5.02	15.55
3	52	46	55	51	4.78	9.40
4	76	64	78	73	7.57	10.42
5	111	102	99	104	6.24	6.00
6	127	120	125	124	3.61	2.91
7	130	133	141	135	5.60	4.16
8	147	147	158	151	6.29	4.17
9	164	152	171	162	9.61	5.92
10	169	171	175	172	3.06	1.78
11	171	177	185	178	6.93	3.90
12	175	182	185	181	4.99	2.76
13	178	180	186	181	4.16	2.30
14	177	182	187	182	5.00	2.75
15	180	181	188	183	4.36	2.38
16	181	185	190	185	4.51	2.43
17	182	190	192	188	5.29	2.81
18	185	187	194	189	4.73	2.50
19	182	186	193	187	5.57	2.98
20	183	185	195	188	6.43	3.43
				Average	**5.34**	**5.40**